MULTIPLEXED LABEL-FREE ELECTRICAL DETECTION OF DNA AMPLIFICATION USING FIELD EFFECT TRANSISTORS

BY

CARLOS EDUARDO DUARTE-GUEVARA

DISSERTATION

Submitted in partial fulfillment of the requirements
for the degree of Doctor of Philosophy in Electrical and Computer Engineering
in the Graduate College of the
University of Illinois at Urbana-Champaign, 2016

Urbana, Illinois

Doctoral Committee:

Professor Rashid Bashir, Chair
Professor Brian Cunningham
Associate Professor Logan Liu
Professor Ilesanmi Adesida

ABSTRACT

The objective of this research project was to develop a miniaturized DNA amplification biosensor for the detection and identification of pathogenic bacteria. Using tailored loop-mediated isothermal amplification (LAMP) and field effect transistors, we developed a microchip platform for multiplexed screening of samples querying the presence of multiple pathogenicity genes. In our platform, ion-sensitive field effect transistors (ISFETs) detect the incorporation of nucleotides during LAMP by monitoring changes in the solution's acidity. Employing transistors as biosensors enables label-free detection of the reaction, simple multiplexing, and seamless integration with required electronics for data acquisition. These characteristics of the detection system and protocols that we developed will make genotyping analysis simple and readily available for different applications that would benefit from low cost, portability, and ease-of-use. Here, we present a series of studies performed in three experimental setups that are related to the multiplexed electrical detection of LAMP and culminate in a large ISFET sensor array microchip that monitors DNA amplification reactions. A first chip consisted of 30 nL silicon oxide wells that were prepared with dried nucleic acid primers for multiplexed on-chip amplification. This initial study demonstrated the high specificity and low limit of detection of on-chip parallel LAMP when used for the detection of *E.coli* O157, *S.enterica*, *L. monocytogenes*, and non O157 Shiga-toxin producing *E.coli* of the 'big six' group. Then, a second chip with novel individually addressable dual-gated ISFETs was fabricated in collaboration with Taiwan Semiconductor Manufacturing Company (TSMC). These devices were used to evaluate and optimize their pH sensing ability, develop methods to do label-free detection of LAMP, and study the sensor performance when biased with polypyrrole quasi-reference electrodes. The last platform, that demonstrates the impressive scalability of the semiconductor technology, is a chip with over a million ISFET sensors distributed

in a 7x7 mm^2 area. The use of on-chip decoding and routing circuits enables the parallel operation of 1024x1024 sensors in an array for massively multiplexed biosensing. In this platform we applied methods and systems developed previously to perform parallel electrical detection of foodborne pathogens by monitoring DNA amplification reactions in micro-chambers of 250 nL detecting down to 25 copies/reaction in less than 60 min. We demonstrate that the intrinsic redundancy of the high density ISFET array enabled clear identification of electrical signals resulting from the amplification reaction. This microchip for the detection of DNA and the related protocols on reaction miniaturization, parallelism, and electrical detection are poised to be the basis of new detection systems that bring the impressive advances of the semiconductor industry into biological applications.

To my family and friends whose support makes this work possible

ACKNOWLEDGMENTS

I would like to thank my advisor, Prof. Rashid Bashir, for giving me the opportunity to work in his group and in this project full of challenges and learning experiences. I also deeply appreciate his support, guidance and friendship. I want to thank my colleagues Dr. Eric Salm, Dr. Bobby Reddy Jr., and Dr. Vikhram Swaminathan for invaluable help and discussions that contributed to this project. I want to specially mention Dr. Yi-Shao Liu and J.C. Huang from Taiwan Semiconductor Manufacturing Company, whose efforts and guidance have made this project possible. I also acknowledge the assistance provided by the Micro and Nanotechnology Laboratory staff and the professors and students that are part of the Center for Food Safety Engineering in Purdue University.

This work is supported by a cooperative agreement with the Agricultural Research Service of the US Department of Agriculture (AG Sub Purdue 8000042759) and Taiwan Semiconductor Manufacturing Company (TSMC-2012-06536).

TABLE OF CONTENTS

LIST OF TABLES

LIST OF FIGURES

CHAPTER 1

INTRODUCTION

Recent developments in microelectromechanical systems (MEMS) and semiconductor technologies [1, 2, 3, 4], new business models for economies of scale [5, 6], and challenges faced by the health-care and regulatory industries [7, 8], are driving the development of new miniaturized biological sensors that promise to revolutionize diagnostics and screening methods. In the last decade microfluidic systems have left research environments to become commercial products, the semiconductor industry entered the biosensing market, and the 'dedicated-foundry' business model gave companies of multiple backgrounds access to high technology semiconductor manufacturing equipment. In this environment a few devices have already demonstrated that new technologies can positively impact biosensing applications. For instance, Abbott's I-stat (an impedance-based point-of-care molecular detector) is now being used in hospitals to reduce the time to result of assays making the patient screening more efficient [9], the FilmArray by Biofire (a microfluidic system for automated viral PCR screening) is used in low resource hospitals for fast screening of samples [10], and Genalysis (commercialized by U.K. based DNAe) has penetrated the cosmetic industry selling portable DNA test kits for personalized formulations [11]. These products have combined MEMS and electronic technologies to reduce the assay turnaround time, solve portability issues, or enable new applications.

Despite significant advances in point-of-care and on-site testing, portable systems that perform nucleic acid-based testing are currently in their infancy, have not entered important markets, and present significant opportunity for further development [12]. DNA-based methods such as polymerase chain reaction (PCR) are considered powerful assays for detection and identification of biological entities due to their outstanding specificity and selectivity. Development of platforms that allow untrained users to perform these assays in portable settings could significantly reduce the cost per test, shorten

time to results, and create new opportunities in a variety of environments that are currently not accessible to standard laboratory equipment. The ideal portable nucleic acid testing system would be inexpensive, fast, robust, and multiplexed. It also needs to be user friendly, minimizing hands-on work by operators and having an interface that integrates seamlessly with other electronics [13]. A few DNA analysis systems have attempted to fulfill all these requirements. Examples include valve-less microfluidics with customized photodiode arrays for the detection of an isothermal amplification reaction [14], droplet microfluidics and flow-through systems to minimize time and complexity of the equipment [15], and smartphones that are used for nucleic acid tests [16]. However, none of these systems have fulfilled all the mentioned ideal features or have not translated to successful commercial products. Whether it is lack of robustness or complex supportive/operative equipment, there is room for further improvement of the portable nucleic-acid amplification systems. The recent convergence of electronic devices and biological assays brings the opportunity to use 50 years of semiconductor technology research into the portable nucleic acid testing systems and fulfill all the desired features of a portable DNA analyzer.

In this work we present methods and systems for portable DNA amplification based on semiconductor devices. We created a microchip system for multiplexed genetic screening that monitors an isothermal DNA amplification reaction known as loop-mediated isothermal amplification (LAMP) using ion-sensitive field effect transistors (ISFETs). The selection of isothermal reactions and field effect sensing was made to fundamentally enhance portability while minimizing costs. LAMP is considered a better alternative over PCR for portable applications because it is simpler, less susceptible to inhibitors, and more specific [17]. On the other hand, ISFETs provide an alternative sensing method over the commonly used fluorescent dyes. The transistors can monitor pH changes intrinsic to the reaction without labels and are fabricated with well-established semiconductor manufacturing processes reducing cost and improving yields [18].

The microchip biosensor development was divided into three stages: reaction miniaturization, electrical detection, and multiplexed electrical detection. In the first stage we experimented with miniaturized LAMP reactions on silicon chips. A primer dehydration protocol consists in spotting primers prior to the introduction of sample in the chip enabling multiplexed assays

that are necessary for screening processes. We have studied and optimized this primer-dehydration protocol in silicon oxide wells and have demonstrated good sensitivity, specificity, and robustness for multiple pathogen targets. The second stage focused on doing electrical detection of the LAMP reactions. In collaboration with Taiwan Semiconductor Manufacturing Company (TSMC), we developed and studied transistor architectures that are compatible with reagents and temperatures that are required for the DNA amplification reaction. These sensors demonstrated the ability to sense the amplification reactions and were used to explore strategies to improve their sensitivity. The ISFETs fabricated by TSMC were operated in a complementary dual-gate mode to enhance their signal-to-noise ratio and were biased with multiple quasi-reference electrodes, including polypyrrole microelectrodes, to improve their stability and response to pH changes. The final development portion of the project couples the miniaturization and electrical detection stages to create a platform for label-free and multiplexed detection of LAMP reactions. The semiconductor devices developed in the second stage were replicated over a million times in an ISFET array that is partitioned by the silicon wells of the first stage. In the new integrated platform we repeated the protocols developed for parallel miniaturized reactions but changed the detection mechanism from fluorescence to semiconductor sensing. With ISFETs inside the reaction chambers and biased with local quasi-reference electrodes, the amplification signal is electrically transduced by the semiconductor sensors as current increments. In our platform thousands of transistors monitor independent reactions allowing the implementation of statistical filtering techniques that enhance the signal-to-noise ratio of the low and variable signals that are characteristic of the LAMP reactions. These three different stages are summarized in the block diagram of Figure 1.1 that also describes a last iterative step of evaluation and optimization.

The platform that we developed is fundamentally a tool for the detection of genes in a sample and it has many different applications ranging from forensic recognition, to genotyping, to microorganism identification. However we have focused on the detection of foodborne pathogens that are estimated to cause 37 million infections every year in the U.S. [19]. The detection of pathogens in food has been historically done with culturing techniques that suffer from very low turnaround times that result in infrequent testing and consequent high infection rates. In addition, the inclusion of new microorganisms in the

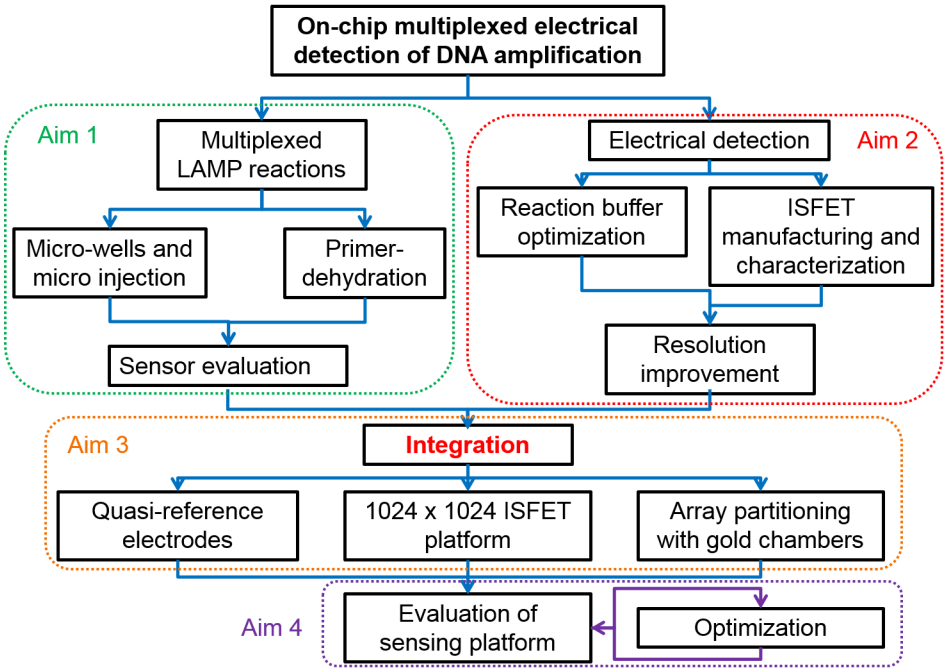

Figure 1.1: Block diagram of project stages and development sections

zero tolerance policy list in combination with heavy increments in food production and trade, are overwhelming the inspection services that need new faster methods to perform screening assays and assure food quality [20]. The ISFET and LAMP combination of our platform results in a portable, inexpensive, and easy to use bio-detection tool that can enhance the enforcing capabilities of the inspection services [21]. This portable nucleic acid testing system will enable multiple parties involved in food production and commercialization to detect pathogens, improve food quality controls, and reduce or eliminate recalls and food related illnesses. The significant impact of portable nucleic acid testing in food safety and strong collaborations with companies and other research laboratories that specialize in pathogen detection have motivated us to develop our system around foodborne pathogenic bacteria detection, but the system has also been easily adapted to other targets.

This document is divided into eight chapters including this introduction. Chapter 2 contains a literature review of other approaches for portable DNA analysis and related microfluidic, electrochemical, and electronic technologies. It also includes a revision of state of the art methods for foodborne pathogen detection. Chapter 3 describes protocols and methods used for on-

chip parallel detection of foodborne pathogens, detailing the silicon microwells fabrication, primer dehydration protocol, and a sensitivity evaluation. In chapter 4 there is a description of the dual-gated individually addressable ISFET that was developed in collaboration with TSMC. We present several experiments for characterization of the new structure and show that the dual-gate mode has an improved signal-to-noise for specific biasing conditions. Chapter 5 presents studies of on-chip quasi-reference electrodes for ISFETs. We show that an electrochemically deposited polypyrrole acts as a reliable reference for ISFET pH experiments with a performance comparable to that of Ag/AgCl electrodes. In chapter 6 we characterize a 1024x1024 dual-gated ISFET array that has been developed as a massively multiplexed biosensor and in chapter 7 we use this platform to perform parallel electrical detection of LAMP reactions in micro-chambers detailing data analysis techniques to improve signal-to-noise ratio. Finally chapter 8 presents conclusions and outlines possible future work to improve the detection system, use it for different applications, and create integrated solutions that exploit the advantages of semiconductor biosensing.

CHAPTER 2

BACKGROUND AND LITERATURE REVIEW

The studies presented in this dissertation aimed to further develop the field of portable biodetection and diagnosis using DNA amplification reactions. As background of that work, the first section of this chapter reviews the mechanisms of the polymerase chain reaction and other DNA amplification methods to provide a brief context of the complex biomolecular interactions that are used to detect microorganisms and molecules. The second section reviews multiple novel DNA analysis systems. These new systems have been built to replace the conventional thermocyclers and employ a variety of engineering and biochemical strategies to gain specific advantages. In the second section the multiple strategies for portable DNA analysis are classified based on particular features, benefits, and limitations. The final section of this chapter discusses the role of DNA amplification reactions in food safety. DNA analysis is used in multiple scenarios ranging from forensic testing to complex healthcare screening. However, as discussed in the introduction, the target application during our development was food safety. In the final section of this chapter we describe current protocols for the identification of pathogens in food samples, explain the use of DNA amplification in screening assays, and consider the advantages of portable DNA detection systems.

2.1 PCR and other DNA amplification methods

The development of the polymerase chain reaction in the 1980s changed the way we interact with and understand biological entities. This method that has been described in the past as 'molecular photocopying' has found multiple applications and its considered one of the biggest scientific advances in molecular biology. The technique was initially developed to increase the number of copies of a DNA sequence because analysis of isolated pieces is

nearly impossible. Later, lower costs of reagents, larger libraries of targets, and the development of robust assay development methods brought PCR to many other applications. For example, PCR was the fundamental tool that enabled the human genome project and it is a powerful technique in laboratories and clinics where it is used to identify microorganisms, diagnose genetic disorders, and conduct DNA fingerprinting tasks [22, 23]. PCR reactions are now performed in many laboratories around the world and represent an important market estimated at $ 9 billion [24].

PCR is a DNA multiplication reaction that is triggered only when a pair of shorter DNA strands, known as primers, hybridize to a matching template [22]. The DNA amplification process starts with the denaturation of the original copy or template DNA. The sample is heated to around 95 °C to break the hydrogen bonds holding the double helix and create two single strands. The sample is then cooled to an annealing temperature that ranges from 50 to 62 °C, at which point primers with the complementary sequence bind to the single-stranded DNA (ssDNA). At this point the sample is normally heated again to around 72 °C, a temperature that favors the polymerase activity and the synthesis of a new double-stranded DNA (dsDNA) from the primer-ssDNA pair formed in the annealing step. In this elongation cycle the polymerase identifies the unfulfilled 3' ends of the primer and creates a complementary strand by incorporating matching nucleotides that are included in the reaction mix. At the end of the process two identical dsDNA molecules have been formed. The 3 step process is summarized in Figure 2.1. The success of the PCR reaction lies in the fact that the polymerase does not lose activity after the three temperature steps that were described, allowing the iteration of cycles and exponential replication of DNA. The reaction is usually performed over 40 cycles potentially creating over a trillion dsDNA copies facilitating the detection of entities or the manipulation of the molecules.

Since its inception, many researchers have developed new technologies to improve the PCR reaction, enhancing specificity and sensitivity or reducing cost. For example, the gel-electrophoresis confirmation has been replaced with fluorescent techniques. The incorporation of intercalating dyes or the use of the taq-man probes has simplified the assays work-flow, improve its specificity, and enabled quantitative analysis [25]. Also, thermocycling machines have been optimized to minimize the reaction time while providing

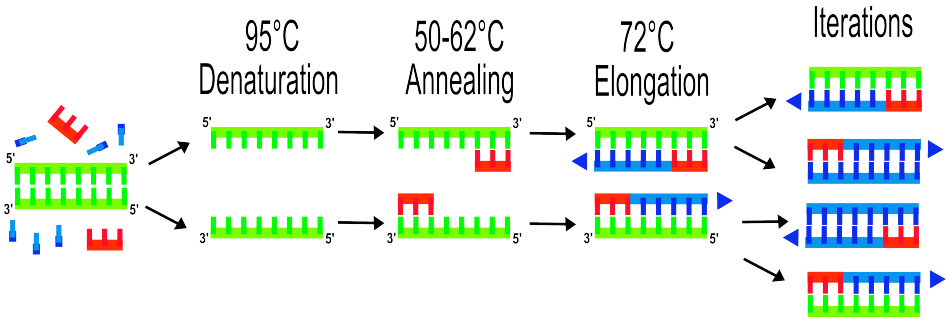

Figure 2.1: PCR DNA amplification process

optimized conditions to improve yields and minimize contamination [26]. In addition, other research has focused on the development of alternative amplification reactions that are inspired by PCR and have a similar working principle, but modify the amplification mechanism to gain certain advantages. The following subsections survey DNA amplification protocols that have been designed to operate robustly and with simpler equipment making them good alternatives for portable and on-chip amplification. Protocols like loop-mediated isothermal amplification (LAMP), rolling circle amplification (RCA), and Recombinase Polymerase Amplification (RPA), have simpler temperature profiles, higher yields, or more tolerance to inhibitors than the traditional PCR and are now established as alternative biomolecular assays.

2.1.1 Loop-mediated isothermal amplification (LAMP)

LAMP is a nucleic acid amplification method that uses an auto-cycling strand displacement DNA synthesis performed by the *Bacillus stearothermophilus* (*Bst*) polymerase [27]. LAMP has high specificity, sensitivity, and robustness and many researchers have contributed to its development in the last decade. In several reports LAMP has been used for the detection of pathogenic microorganisms and it was the selected method for the detection of pathogenic entities in our assays [28, 29, 30, 31].

Amplification Process

LAMP uses a displacement polymerase and a group of up to six primers designed to create DNA loops that initiate the exponential incorporation

of nucleotides [27]. The reaction takes place at around 65 °C when double-stranded DNA is in 'dynamic equilibrium.' At this stage primers can anneal to their complementary sequence in the template and the polymerase will perform initial replications. While the displacement polymerase elongates DNA, it releases a ssDNA that is then used to form more copies and create loop structures. After six steps of annealing, elongation and displacement, a structure with stem-loops at each end (dumbbell structure) is created (Figure 2.2). This structure is the starting element for isothermal amplification.

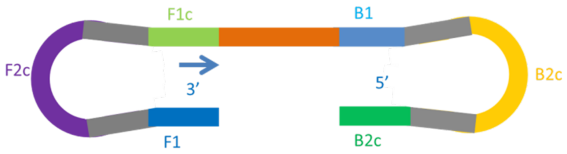

Figure 2.2: Dumbbell DNA structure that initiates LAMP amplification

The amplification with the dumbbell-like DNA structure as template creates loops of DNA made with copies of the original template when amplicons self-prime. Afterwards, inner primers anneal to the ssDNA region in the stem-loop and the polymerase will incorporate nucleotides, displacing and releasing the previously synthesized strand. The released strands then form new loop structures and the polymerase continues synthesizing DNA using self-structures as a template. Other primers in solution continue to create stem-loop structures and DNA synthesis keeps displacing dsDNA sustaining the amplification reaction active in an iterative process. The reaction will stop when concentration of free deoxyribonucleotides is too low, the concentration of dsDNA prevents proper annealing of primers, or the buffer capacity is reached. As a result of this 20-step process, variously sized DNA structures (made of concatenated inverted repeats of the target sequence) are formed. The process is described in (Figure 2.3) and detailed videos and schematics can be found on-line [32].

The fundamental innovation of LAMP is the clever design of primers sets that result in loop DNA structures for a continuous isothermal amplification. LAMP employs a group of four carefully selected inner (FIP and BIP) and outer (F3 and B3) primers. Two other primers, known as loop primers (LF and LB), can be included in the mix to enhance sensitivity and accelerate the reaction [33]. The selection of these six primers that are specific to a

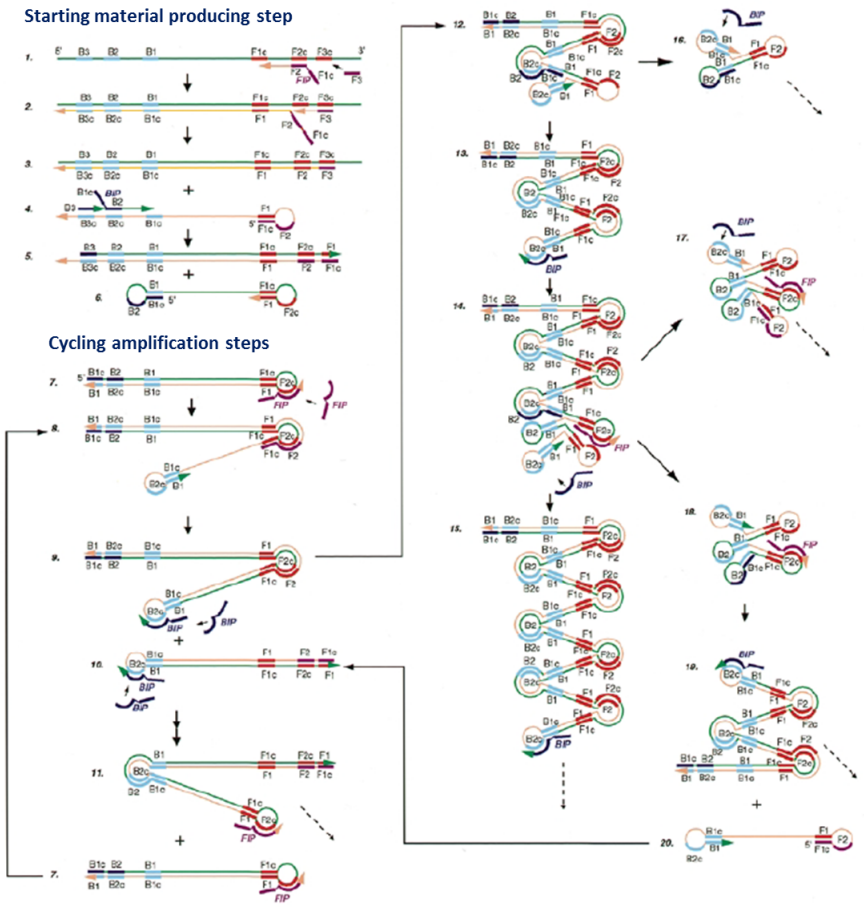

Figure 2.3: Schematic representation of LAMP reaction mechanism [27]

target gene and do not create primer dimers is a complex task that requires computer-assisted design.

Eiken Chemical, the company that invented and is commercializing LAMP products, made available to the public PrimerExplorer (http://primerexplorer.jp/e/). This is a software that takes user input of a text file with the target DNA sequence and outputs multiple primer sets that would amplify the provided sequence. Selection of the appropriate primer set is done by checking the specificity of primer sequences using sequence matching calculators and evaluating the CG content for stability. However, experimental trial and error are required to ultimately select an effective primer set, in some occasions discarding one or two loop primers to prevent dimerization or changing the buffering conditions to enhance specificity.

Key features

The complexity of the designed molecular interactions between DNA strands in LAMP is contrasted by the simplicity of the protocol that does not require complex laboratory instrumentation or elaborate methods for detection of the reaction products. The amplification protocol is isothermal and therefore simple heaters replace the expensive thermocyclers commonly used for PCR. Also, a high production of dsDNA is correlated with generous generation of pyrophosphates that allows turbidity assessment of the reaction or also enhances the signal of fluorescent indicators such as SYBR green.

Isothermality and visual assessment of amplification are the two main features of LAMP. But other important characteristics are low detection limit, high specificity (due to required annealing of 4 different primers to the target template), and short time to detection.

Overall, LAMP has been proposed as an ideal technique for nucleic acid amplification for point-of-care devices since it has less demanding equipment and better sensitivity and specificity than PCR and other amplification methods [34]. Advantages of LAMP are traded for more complex design of primers and more expensive reagents which explain the reaction's slow incorporation into standard biomolecular assays. However LAMP's clear benefits over PCR, especially for miniaturized systems, motivated us to use the isothermal reaction for on-chip detection of foodborne pathogens and label-free electrical detection using ISFETs.

2.1.2 Rolling Circle Amplification (RCA)

RCA is an isothermal process that uses special polymerases to generate copies of single stranded DNA. Displacement polymerases like '*Bst*', '*Phi29*', or '*Vent exo-*' allow continued nucleotide incorporation at nearly room temperature (37 °C) [35]. RCA is capable of achieving single molecule sensitivities [36] and can be performed on solid substrates [37], and precise design of probes and templates allows the amplification of customized functional sequences [38]. This amplification method has been effective for molecular diagnostics tasks, cell-free cloning, and the development of DNA origami structures [39].

For RCA the template has to be circular and the polymerase, usually *Phi29*, must have strong displacement activity. The overall process is described in Figure 2.4. It starts with the synthesis of the circular DNA template. A ligation enzyme (e.g. T4 DNA ligase, or CircLigase) is used to join ends of the sequence of interest (a). Then regular primers are annealed to the circular template and the displacement polymerase will start to generate long linear sequences of single stranded DNA(b). This amplification process will be continuous generating more single stranded DNA until the polymerase stops working or the mix runs out of nucleotides. However, in order to achieve exponential amplification it is possible to add complementary primers that anneal to the replicated DNA (e), introduce restriction enzymes and new ligation templates to generate more circle DNA sources (f), or incorporate nicking endonucleases that in conjunction with specially designed templates will generate more replication places (g). With these strategies it is possible to exponentially generate amplicons from the template DNA at nearly room temperature.

Although RCA is gaining popularity there are technical challenges that remain to be resolved before it is broadly utilized. First, RCA has a high tendency of primer dimers formation and nonspecific amplification on even optimized reaction conditions. At room temperature the likelihood of nonspecific DNA binding increases, augmenting the chances of undesired amplification. Even though some studies have demonstrated that the incorporation of proteins like *thermus thermophilus* SSB reduces formation of primer dimers [40], primer amplification still undermines RCA specificity. Second, the initial ligation is performed on single stranded DNA which requires additional

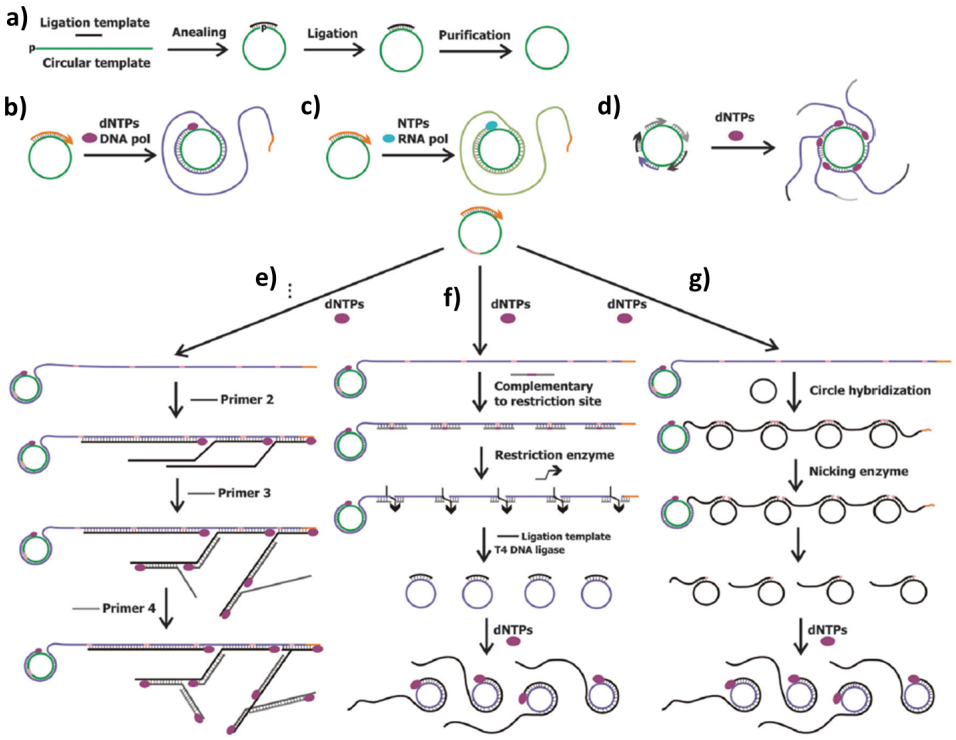

Figure 2.4: Schematics of RCA amplification process [35]

preparation steps. For ligation, it is necessary to denature the template, and then add and anneal with ligation enzymes. This results in an initial sequence of temperature profiles and additional reagents. Therefore, RCA is a promising technique that at nearly room temperature has multiple applications but preparatory steps and technical difficulties limit its actual application on portable DNA analyzers.

2.1.3 Recombinase Polymerase Amplification (RPA)

Recombinase polymerase amplification (RPA) is a room temperature isothermal method for replication of DNA. This protocol avoids thermal melting by utilizing a set of enzymes that invade and separate dsDNA to create space within the strands for a displacement polymerase that replicates the sequence. A schematic of the protocol is presented in Figure 2.5 [41, 42].

The key elements of this protocol are the 'nucleoprotein primers', a combination of a recombinase agent (RecA) with a DNA segment that has the desired complementary sequence and will invade the dsDNA. Inspired by the Zarling method [43], the use of nucleoprotein primers, labeled as RecA/ssDNA, will create spacers on the dsDNA forming D-loops. Then, a ssDNA binding protein (SSB) gets incorporated in the formed D-loop and the displacement polymerase finds a 3' end on which it can replicate the template sequence. If the process is mirrored in the opposite end of the template, the replication process will yield 2 new complementary strands like in PCR. In subsequent cycles of the process, the nucleoprotein primers will re-invade the new dsDNA and continue the replication process for an exponential amplification.

RPA is a new technique that has been slowly adopted by researchers. It has a couple of important limitations: First, the nucleoprotein primer is a complex entity, and specific design and efficient synthesis are critical to achieve a good performance. Up to this point Twistdx (http://www.twistdx.co.uk/) is offering kits for different foodborne pathogens and a few R&D kits for user developed assays. Several publications have reported RPA as a detection method reaction but the formulation of assays is cumbersome, making the protocol less versatile than other methods like PCR or LAMP. Instead of simply substituting primer sequences for specific targets, RPA assay de-

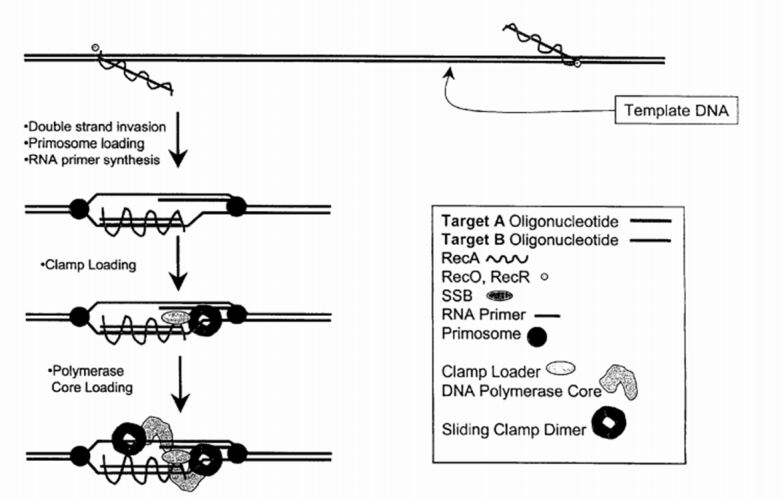

Figure 2.5: Schematics of the RPA amplification process that uses enzymatic activity to separate dsDNA [41]

velopment requires analysis of enzyme interaction demanding more careful developing efforts. Second, the enzyme cocktail that is required for this protocol is expensive and the cost per reaction is around $ 25 [44]. Even though this reaction is carried out at room temperature, assays with RPA report good specificity an low formation of primer dimers. Expansion of the available primers-protein complexes that start RPA and a larger customer base for better pricing might turn RPA into a powerful isothermal room temperature technique for on-chip DNA amplification.

2.2 Novel systems for DNA amplification analysis

Many companies produce reagents and equipment to conduct PCR reactions motivated by the large related market and the reaction's multiple applications. The largest laboratory equipment manufacturers sell PCR thermocyclers with different features and price-points. But classical thermocyclers that perform the temperature profiles and measure fluorescence are limited to laboratory settings. Therefore a new trend of portable PCR equipment is emerging and many companies have identified the potential of easy-to-use, portable, and inexpensive DNA amplification systems. Advances in MEMS, powerful batteries, and the appetite of the electronics industry to enter the

expanding field of molecular diagnosis have pushed the effort of portable PCR systems that aim to meet market needs that cannot be met with the standard laboratory equipment. Ideally, a portable DNA amplification system should have the following features [45]:

- Easy-to-use and automated. The system should be operable by untrained personnel and be designed to minimize human induced error.
- Portable. Handheld or with a small footprint, the system should be portable in order to relax facility requirements and allow on-site and point-of-care diagnosis.
- Multiplexed assays. Given the requirements of screening assays the system should be able to detect a broad range of genes and perform multiplexed detection assays.
- Good figures of merit. Despite the added features mentioned above, the system should sustain the same sensitivity, specificity, precision, and detection limit of current laboratory methods to be widely adopted.

Various research groups and companies have been working on systems that reduce assay complexity and facility requirements by creating portable DNA testing systems. As a result of these efforts, in the last few years portable DNA amplification systems have been reported and some of them commercialized. These new systems aim to exploit specific technological advances to achieve the features described above. Some systems rely on Peltier heating to quickly achieve the reaction temperatures in small handheld thermocyclers. Other devices use microfluidic circuits to simplify the assays, minimize reagent consumption, and enable parallel assays with minimal user input. Also, new systems substitute fluorescence detection with electrochemical methods to assess amplification and amplicon concentration. With these novel approaches, small and portable systems have been fabricated targeting multiple samples and objectives. In this section we will briefly review the reported systems that aim to allow portable, simple, and inexpensive nucleic acid testing through DNA amplification.

2.2.1 Handheld & low-cost thermocyclers

Targeting specific applications ranging from plant studies to high-school teaching, the market already offers a few low-cost portable systems that can run PCR reactions. Companies have identified the potential of portable DNA amplification and are currently commercializing small and inexpensive thermocyclers with some capability of fluorescent detection. For example, Ahram biosystems offers the Palm PCR Figure 2.6 (a). This is a hand-held device that can run PCR reactions of 20 μL doing up to 30 thermal cycles in less than half an hour using a lithium battery. Another related platform is the thermocycler designed by OpenPCR Figure 2.6 (b). Designed to achieve the lowest price tag, OpenPCR is a low cost PCR machine for the hobby and educational markets. This company has experimented with different materials to create the cheapest machines, and came up with a design that used Peltier heaters and a wood case to sell a system for $ 599. Finally, LavaAmp in Figure 2.6 (c) reduces the complexity of traditional PCR machines by replacing the heat block with a thermally driven flow mechanism that flows the sample through different temperature gradients [46]. They have created a 'pocket PCR' device that is powered with 4 regular AA batteries.

All the mentioned devices present interesting design concepts and marketing strategies. They have an innovative user interface, highly efficient power handling systems, and designs to minimize cost of manufacturing. However they do not provide an integrated solution and require preparatory steps or extra DNA detection assays (some of them still require gel electrophoresis for detection), making it difficult to use the portable PCR systems outside a laboratory.

2.2.2 Nested PCR in microfluidic pouch

Started in the University of Utah in the 1980s, Biofire is a company devoted to the development of new and more efficient screening apparatus. FilmArray is a microfluidic approach for multiplexed PCR in what they have named 'automated nested multiplex PCR system.' This system is composed of a polypropylene microfluidic pouch and instrumentation for PCR thermocycling and fluorescence detection.

The FilmArray system has customized pneumatic pumps to flow sam-

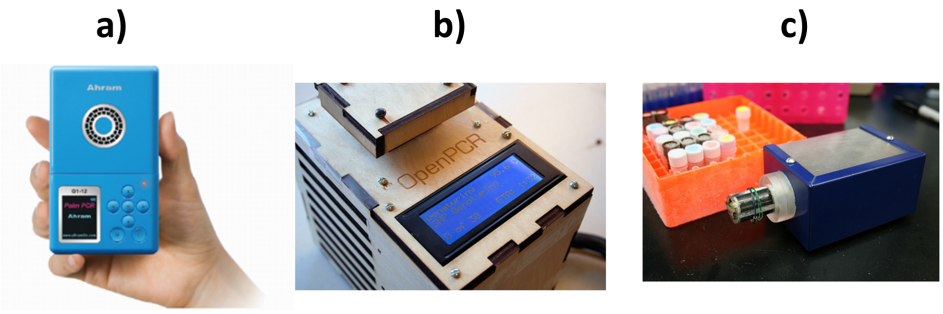

Figure 2.6: Portable PCR systems on the market including Palm PCR by Ahram Biosystems [47], the low cost OpenPCR system [48], and LavaAmp pocket PCR system [46]

ple, Peltier heaters to run reactions, and a LED/CMOS system that detects amplification. The pouch is the key innovation of this system and enables automated sample treatment in a series of fluidic steps. Figure 2.7 is a schematic with reservoirs, chambers and connections that are used for PCR amplification. When the sample is loaded on the pouch it gets mixed with lysing buffers that release DNA from target organisms. Then a first PCR amplification takes place in a chamber that has been loaded with multiple primers for an initial broad-range amplification. The amplified DNA is then divided in multiple chambers, each one with frozen reagents for specific amplification of target genes and intercalating dyes for fluorescent detection. The sequence of amplifications in the pouch provides automated genetic detection, from sample preparation to result or diagnosis.

Already in the market, FilmArray has demonstrated that the concept of preloaded primers is useful to reduce the hands-on time on a molecular analysis instrument. The pouch is stored in vacuum and up to 21 different target entities (i.e. bacteria or virus) could be identified in a single multiplexed assay. The company sells panels with reagents for respiratory, gastrointestinal, blood culture, and meningitis/encephalitis pathogenic targets [49]. The FilmArray system has a price-tag of around $ 40,000 and each microfluidic pouch that is good for one assay goes for around $ 100 [50]. Despite high hardware and consumables costs, when compared to standard equipment FilmArray is the most complete commercial solution for bench-top, fully automated, nucleic acid detection assays. The company has demonstrated that

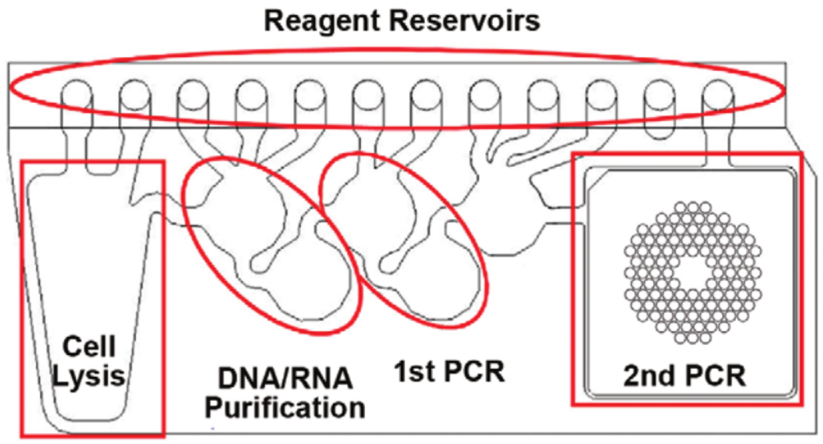

Figure 2.7: Schematic of FilmArray microfluidic pouch [10]

fully automated systems are useful both in low resource settings like African hospitals where poor laboratory facilities impede proper handling of samples, or regular laboratories where the work-load of trained personal needs to be reduced. The proven success of the automated system promotes the research of technologies that could drive down the cost of both system and equipment. Using label-free detection with field effect transistor could reduce the complexity of the system by eliminating required optics, and cut cost per assay by removing some of the consumed reagents and simplifying the pouch design.

2.2.3 Automation with vacuum-aided loading

Sony also contributed to the development of portable DNA amplification systems with a point-of-care system for detection of influenza. The system was comprised of a small laptop computer, a vacuum sealed glass/PDMS chip with spotted primers, and customized heaters and photo-detectors. The primers were designed for the amplification of pandemic influenza genes and consensus primers for influenza A, responding to the 2009 swine flu crisis that demonstrated the inability of authorities to detect and prevent infection outbreaks [51].

The system is cleverly designed to integrate fluidic handling and fluorescent querying. It also provided a simple user interface and data recording

with a small laptop. Sony's chip demonstrated a novel mechanism for sample loading that drives the fluid with a differential pressure between the vacuum sealed PDMS and atmosphere without pumps. After the sample is loaded, the control mini-PC sets temperatures to run DNA amplification using a Peltier heater. DNA amplification is observed with intercalating dyes like SYBR green and the fluorescence is detected through photodiodes that are aligned to each microfluidic chamber. The changes of the photodiode's electrical resistance / current indicate positive amplification.

The influenza detection tool supported by Sony targeted the market of fast and inexpensive screening to prevent disease spread. It integrated a system with a familiar user interface, on-chip handling of sample, and a simple but robust detection system through fluorescence photodiodes and vacuum-aided loading.

2.2.4 Multiplexed amplification in microfluidic chips

A similar microfluidic approach to the one from Sony was presented in 2012 by the Environmental Genomics Lab of Michigan State University [14]. Targeting low hardware cost, Gene-Z uses an ipod for operation and user interface in a DNA amplification system. It was presented as a prototype for point-of-care detection of bacterial pathogens and is composed of:

1. Microfluidics: Polyester micro-channels loaded with dried DNA primers for amplification.

2. Optical fiber array: For interrogation of fluorescence intensity during amplification.

3. Aluminum resistive heater: An aluminum block that serves as heat conductor and optical barrier between chambers.

4. Electronics for control and operation: Microprocessors and electronic modules to control temperature and communication with an Ipod touch.

With the described components, Gene-Z was able to detect the presence of up to 4 different entities in a single assay. The microfluidic chip has four arrays with 15 chambers each. Each chamber has a specific primer that was dried during the polymer fabrication. Having 4 separated arrays allows

testing of different samples and the inclusion of positive and negative controls in the same assay. No pumps are required to flow the sample because capillary forces push the liquid inside the different chambers. After the sample is loaded in the chambers the aluminum block is heated to trigger the reaction, LEDs connected to optical fibers excite the intercalating fluorophores, and fluorescence is recorded using a CCD sensor. A block diagram of the system is presented in Figure 2.8.

Gene-Z presents intelligent microfluidic and optical mechanisms to minimize hands-on work and allow multiplexed assays. However it also describes the challenges of using optical assessment when reactions are conducted in microfluidic channels. Good optical isolation between chambers was crucial to prevent cross-talk that leads to high noise and false positives. It was achieved by having a customized aluminum heating block as a barrier between chambers optically connected only with optical fibers. It demonstrates fundamental scalability limitations of optical sensors and motivates further research on electrical label- and optics-free approaches that simplifies hardware and enables higher multiplexing.

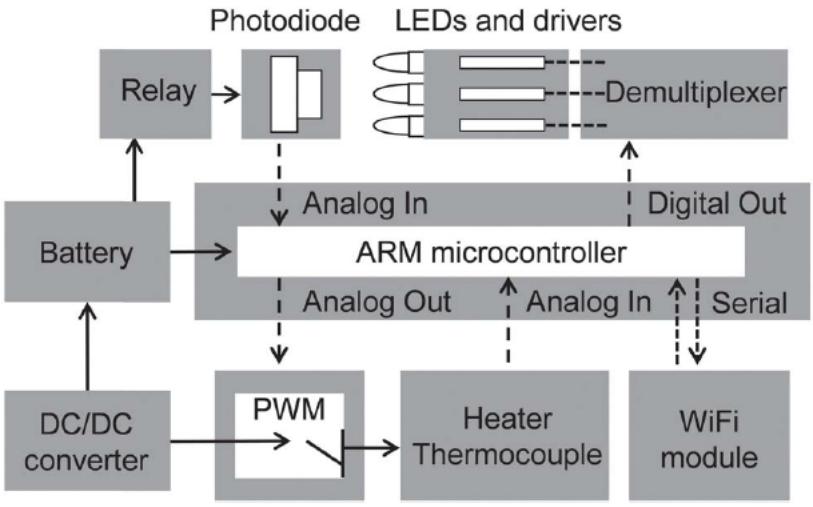

Figure 2.8: Block diagram of Gene-Z system [14]

Gene-Z has many of the elements desired in portable DNA testing systems. It is portable and multiplexed (allows loading of multiple samples), and reported characterization experiments demonstrated acceptable figures of sensitivity and specificity. However, because it uses fluorescence as means

of detection it has intrinsic limits on miniaturization and scalability.

2.2.5 Using smartphones for DNA analysis

Biological sensing can greatly benefit from smartphone attachments that turn these ubiquitous devices into pathogen detection systems. Nowadays smartphones have outstanding imaging and computing capabilities. They also are constantly connected to networks, are portable, and have simple and familiar user interfaces. These are the characteristics that are desired for a portable DNA analysis platform and therefore researchers have started to use smartphones as the core of their DNA amplification systems. Several authors have already incorporated smartphones into their biosensing systems for continued health monitoring, detection of molecular binding, and spectrographic analysis of biological samples [52, 53, 54]. There are clear benefits of using smartphones as biochemical sensors to meet demands of low-cost and portability. Using smartphones simplifies the development of portable DNA amplification systems with the ideal characteristics.

Based in Philadelphia, Biomeme is a company that is working on portable PCR systems that use an iphone to run DNA amplification reactions (http://www.biomeme.com/). The company has created a smartphone cradle, shown in Figure 2.9, with a compartment where up to five tubes with the reaction to be analyzed are loaded for analysis. The cradle aligns the phone's camera with the reaction tubes that are also placed in contact with heating coils and an air cooling mechanism. The cradle has been designed to be handheld and it is battery operated [55]. In addition to the smartphone cradle, Biomeme also sells testing kits with multiple pathogens of interest for agriculture, genetics, and water testing among other fields. The company has also created an ecosystem that mimics the developer/platform relationship of the popular app stores of Apple and Google attempting to incentivize development of more assays and expand the potential applications. By leveraging the smartphone as detector and user interface, Biomeme has quickly created a compact and cost-effective system for DNA testing and the proposed models for development of assays may yield a vibrant environment of biomolecular assay innovation.

Figure 2.9: Biomeme concept and promotional image [56]

2.2.6 Portable isothermal amplification systems

The isothermal amplification systems that we discussed in the previous section are fundamentally simpler and good candidates for portable applications. Multiple systems have started to use these alternative amplification methods in their portable devices to make them more robust or less expensive. Both the loop mediated isothermal amplification (LAMP) and the Recombinase Polymerase Amplification (RPA) are run in portable systems that can be fabricated at a reduced cost by discarding thermocyclers. So even though the systems still require optical elements for fluorescence, their heating mechanisms are simpler or even non-existent.

LAMP assays can be performed in the Genie series platforms fabricated by Optigene [21]. These are portable devices where 8 tube strips can be heated to the desired temperature for amplification while a dual-channel fluorescence detector monitors the reaction in two different wavelengths. The system has been designed for users who want to perform DNA assays in the field or remote settings and include features like GPS, wireless communication, long battery life, and built-in LCD display. In multiple publications Optigene platforms have been used to amplify different targets including Streptococcus [57], phytoplasmas [58], and necrotrophic fungus [59] demonstrating the

ability to specifically detect genes of interest. In addition, their studies performed in remote locations have revealed how portable DNA analysis platforms enable studies that cannot be performed with standard equipment and are useful for pathogenic control in plants and animals.

A similar system was built by the company that has developed RPA amplification. Twist DX not only offers the reagents and kits for this isothermal room temperature DNA amplification, but also sells equipment to run their reactions in a portable setup. The T-8 isothermal device can perform and monitor reactions in up to 8 standard PCR tubes. The machine includes magnetic stirring to automate the mixing processes that are required for RPA and it can be complemented with other systems and reagents that facilitate preparatory steps such as DNA extraction. The RPA process and the related equipment have been fabricated for the detection of bacterial pathogens [60], viral species [61], and plant pathogens [62]. In addition, researchers have exploited the fundamental advantage of having room temperature reactions by miniaturizing them in microfluidic systems [63]. A key challenge of the miniaturization of reactions that are triggered with temperature controls is the fast evaporation of small volumes. With RPA researchers have been able to perform miniaturized reaction in simple setups.

These two examples of portable DNA amplification systems that use alternative methods to PCR show the benefits of incorporating the new protocols to design devices. Simpler temperature profiles and greater amplicon yields relax the hardware and software requirements impacting the cost and complexity of the amplification system. With more researchers working on these alternative methods it is expected that multiple testing methods will be developed, increasing the user base of portable systems that employ these alternative protocols.

2.2.7 Electrochemical detection of amplification

The fluorescence methods that were developed for quantitative PCR (qPCR) are now commonly used for the detection of DNA amplification. The incorporation of intercalating dyes has been used not only for PCR but also for the alternative methods that have been described previously. However, the fluorescence detection of amplicons requires optical systems that can be cum-

bersome or difficult to miniaturize. Therefore electrochemical methods that detect the amplicon formation purely with electrical signals have been developed aiming to facilitate the miniaturization of the DNA testing systems. This is the case with approaches that detect charge from the reaction's by-products or that incorporate additional reagents to generate electrochemical signals upon amplification.

Prof. Toumazou from the imperial college of London pioneered the detection of DNA amplification using ion-sensitive field effect transistors (ISFETs). In his early work Toumazou et al. characterized the correlation between nucleotide incorporation and the pH of the solution. During the elongation step the polymerase adds a new base to the double stranded DNA in formation. The incorporation of a new nucleotide yields two by-products, a free pyrophosphate and a released hydrogen ion (Figure 2.10). Therefore using the pH sensitivity of ISFETs it was possible to electrically track the amplification reaction without the need of fluorescent labels or optics for fluorescence quantification [64, 65].

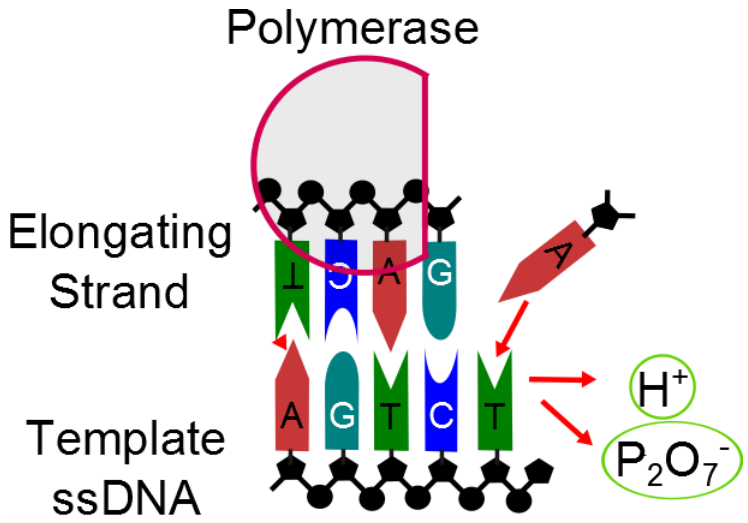

Figure 2.10: Schematic of nucleotide incorporation showing pyrophosphate and proton by-products

This technology is the essence of DNA Electronics, a company that has intellectual property rights over methods and systems for detection of DNA replications using ISFETs (http://dnae.co.uk/). The company has licensed its technology to DNA sequencing equipment manufacturers like Ion Torrent and Roche 454 but has also developed instruments for point-of-care DNA

testing. Their flag product is Genalysis, a three-part kit that is used for genotyping or detection of specific genes in a sample Figure 2.11. The first part of Genalysis is a sample preparation device that cleans saliva to have a usable template. The second part is a cartridge that stores the cleaned sample and allows transportation and has fluidic connection to the third component, a device with a USB connection where the sample is thermocycled; the ISFETs are interrogated as a function of reaction time, and data is transferred and displayed in the host computer [66].

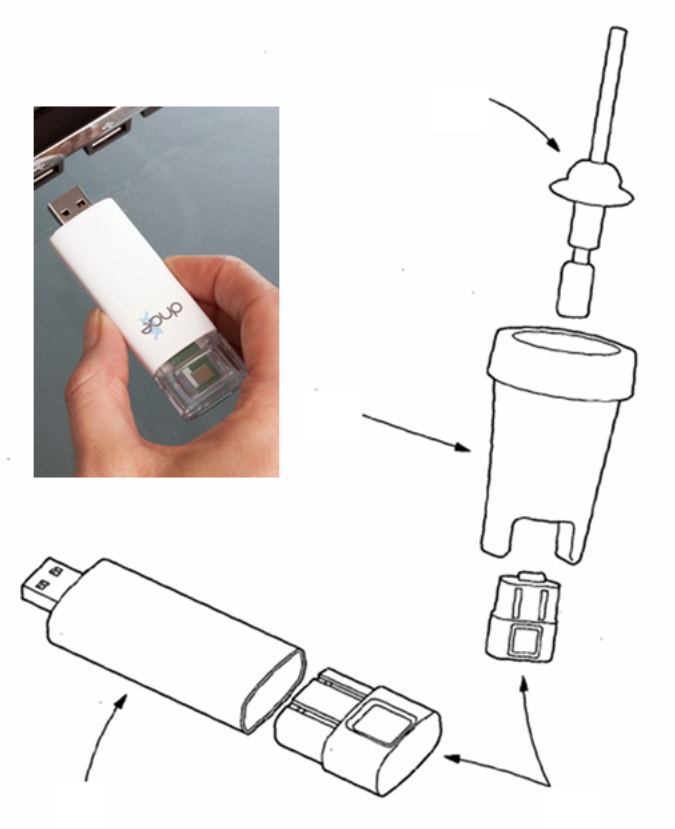

Figure 2.11: Concept of DNA electronics Genalysis kit sample prep and detection units [66]

DNA Electronics has tailored their system for near-patient testing of pharmacogenetically relevant single nucleotide polymorphisms (SNPs) for personalized medication prescription. Using SNP-specific primers, the Genalysis system is able to detect SNP variants in saliva in about 30 min. However,

the company has recently found a new niche market in personalized skin care products. A partnership with GENEU (http://www.geneu.com/) resulted in a cosmetic service that tests the DNA of customers to prescribe a personalized product for greater cosmetic benefits. The range of applications of Genalysis demonstrate that DNA amplification systems can be used in many different fields, and that portable and inexpensive DNA testing systems are useful in many scenarios.

Other electrochemical methods do not use by-products of the reactions to electrically detect the incorporation of nucleotides but add new reagents that mimic the fluorescence methods. The inclusion of molecules with high electrochemical activity like $Ru(bpy)_3^{3+}$ or $Os(bpy)_3^{3+}$, or DNA binding molecules like $Os[(bpy)2DPPZ]^{2+}$ and methylene blue, results in the electrochemical detection of the formation of dsDNA [67]. These molecules not only create redox pairs that enhance electrochemical activity in the solution but also interact with DNA. For example, nucleotides were modified with $Ru(bpy)_3^{3+}$ to report amplification. The free molecule acts as a redox mediator contributing to the electrochemical current, but once the nucleotide is incorporated into dsDNA its activity decreases and resulting current changes can be related to nucleotide incorporation [68]. Similarly molecules like methylene blue lose their electrochemical activity with higher concentration of dsDNA due to their affinity to double stranded DNA with mechanisms similar to those of intercalating dyes [69]. Finally, electrochemical taq-man probes have been reported to combine the added specificity of sequence specific taq reporters and electrochemical detection [70]. These methods have been incorporated in a PCR system known as ELICE (http://www.elice.fr/). The system creates a series of micro-chambers with printed electrodes to create cartridges for each reaction to monitor the reactions that have been modified with electrochemical labels for an optics-free system.

These electrochemical methods for the detection of DNA amplification fundamentally change the requirements of the monitoring device. The switch from optical to electrical signals opens possibilities of aggressive miniaturization and higher parallelism. In addition, bringing the molecular assay into the electrical domain enables the incorporation of electronic methods and devices into biological assays. This new combination can result in groundbreaking devices that achieve the desired portability, simplicity, robustness, and low cost that create the ideal portable DNA amplification system.

Table 2.1: List of new DNA amplification devices

Name	RXN	Detection	Prep	Multipl	Ref
GeneXpert	PCR	Fluorsc	Yes	No	[71]
Cobas Liat	PCR	Fluorsc	Yes	No	[72]
PalmPCR	PCR	Gel	No	Yes	[47]
LavaAmp	PCR	Gel	No	No	[46]
OpenPCR	PCR	Gel	No	Yes	[46]
FilmArray	nPCR	Fluorsc	Yes	Yes	[73]
NAT Sony	LAMP	Fluorsc	Yes	Yes	[51]
Gene Z	LAMP	Fluorsc	Yes	Yes	[14]
Genalysis	LAMP	ISFET	No	No	[74]
Elice	LAMP	Elec. Chem	No	Yes	[75]
Biomeme	PCR	Smartphone	No	Yes	[55]
Genie II	LAMP	Fluorsc	No	Yes	[59]
Twista T-8	RPA	Fluorsc	Yes	Yes	[42]
Phaseguided chip	RPA	Fluorsc	Yes	No	[76]
HNB-LAMP	LAMP	Naked eye	No	No	[77]
QuantumDx	PCR	Nanowire	Yes	Yes	[78]

2.2.8 Summary of novel DNA amplification systems

To summarize this section on novel DNA amplification methods and devices, Table 2.1 classifies multiple systems by DNA amplification reaction, detection mechanism, multiplexing ability, and sample preparation capacity. Abbreviations used in the table are:

- nPCR: Nested PCR
- Gel: Gel electrophoresis for the identification of amplicons
- Fluorc: Use of intercalating fluorescent dyes
- ISFET: Detection of amplification using ion-sensitive field effect transistors
- Elec.Chem: Electrochemical detection
- Prep: System includes means for on-site sample preparation
- Multipl: System supports multiplexed analysis of samples

The list in Table 2.1 is not comprehensive and many new companies and research groups are constantly reporting novel approaches. This dynamic research and commercial environment is the result of a large present and expected market for molecular diagnostics and microorganism identification. The new devices with special features can find niche applications and despite many the reported alternatives there is still room to improve the detection devices. The large number of research groups and companies interested in PCR shows how the reaction has reached a level of maturity that promotes its incursion in a myriad of new applications leveraging new engineering advancements.

2.3 Foodborne pathogenic bacteria and pathogenicity islands

Water and foodborne pathogenic bacteria destroy cells in the body or produce toxins that disrupt their normal physiology. The Center for Disease Control and Prevention (CDC) estimates that each year 1 in 6 Americans ($\sim$ 37 million people) is infected, around five thousand are hospitalized, and eighty patients die due to related complications [79]. Globally, foodborne bacterial infections are estimated to cause 1.5 million deaths and are responsible for over half of all food poisoning incidents [80]. In addition, most events are tracked to restaurants where food sources and processing are difficult to trace and control [81].

The Food Safety and Inspection Service (FSIS) is an agency of the United States Department of Agriculture in charge of regulating food products to prevent the distribution ofcontaminated goods. It has the authority to order recalls when infectious agents are detected and it is responsible for sample screening, implementation of controls, and monitoring adulterants in food. Currently FSIS normally uses a combination of microbial identification techniques for detection of pathogens that usually take several days [82]. The screening tests are performed in specialized laboratories and each state has a few, or even none, of these accredited institutions [83]. Few laboratories for pathogenic detection in food, and the increasing volume of food trades, result in a low sampling ratio (many products never get tested) and a long time to result. Therefore, alternative methods are actively pursued to im-

prove detection turnaround, cost and complexity to enable more parties to perform the screening task and expand food sampling. The backbone of the new screening protocols consists of biomolecular techniques such as PCR that detect and identify pathogens. The high specificity and sensitivity of molecular methods resulted in faster and more precise screening methods. Studies on bacteria recovered from infected patients had led to the identification of the pathogenicity islands for different microorganisms. For example, *E.coli* is pathogenic when it produces Shiga-toxin and has the ability to attach to enterocyte linings of the intestinal tract. Genes associated with the proteins responsible for toxins and attachment mechanisms are: shiga-toxin genes (stx1 or stx2), intimin (eae), intimin receptor (tir), and surface proteins (esp) [84]. Similar gene groups have been recognized for other common foodborne pathogens such as *L. monocytogenes* [85] and *S.enterica* [86]. These characteristic genes of pathogenic microorganisms led to the development of detection techniques based on DNA replication that have improved food screening methods.

2.3.1 Current standard for detection of foodborne pathogens and the role of portable tools

Figure 2.12 presents a typical flow chart of the protocol for detection of shiga-toxin producing *E.coli* in meat samples [87]. Similar protocols are employed to screen other samples and detect different pathogens like *S.typhi*, *L.monocytogenes*, or *C.jejuni* [88]. The process starts with incubation of the sample in specific enrichment broths to augment the bacteria count and simplify detection assays. Then PCR tests are used as an initial indicator of contamination and are followed by confirmation assays based in immunecapture or traditional plating techniques. In the best case scenario the full process takes a few days, requires specialized equipment and dedicated space, and it is performed by trained personnel. In this section we briefly describe the USDA protocol and identify how a portable and easy-to-use DNA amplification system will improve screening methods.

The FSIS guidebook for detection and isolation of pathogens describes equipment, quality control measurements, and consensus protocols to detect bacterial contaminants in food. The process begins with the homogenization

and filtering of at least 325 g of sample followed by a primary enrichment. An incubation of 15-22 hours will increase the colony forming units (CFU) count allowing PCR screening tests. This sample preparation and enrichment steps need to be also performed for positive and negative samples to assure quality of measurements. After the inoculation, an initial PCR test aims to detect the presence of pathogenicity genes related to the target pathogen (i.e. stx and eae for *E.coli*). If the detected genes match a pathogenicity island, the sample is tested for serotype specific genes, plated for culture confirmation, and inoculated in specific media for isolation. Bacterial cells are separated with immune-magnetic separation (IMS) that uses magnetic beads functionalized with antibodies to capture the detected pathogen. After magnetic beads specifically bind to the target pathogen, separation magnets isolate the agent of interest. Washing steps and acid treatments will eliminate background flora for a final incubation with only the suspected infectious agent.

Lysate from the isolated bacteria strand is used to confirm the pathogen presence and identity. In this final step, VIKTEK® and PCR assays are used as complementary detection techniques. VIKTEK® performs biochemical identification by observing agglutination of colonies that are cultured in sheep blood agar (SBA). PCR is used to amplify for a second time virulence genes, estimate concentration, and detect the presence of antigens specific to the suspected pathogen. If both biochemical and biomolecular assays are positive, the sample is considered contaminated and recall orders are issued.

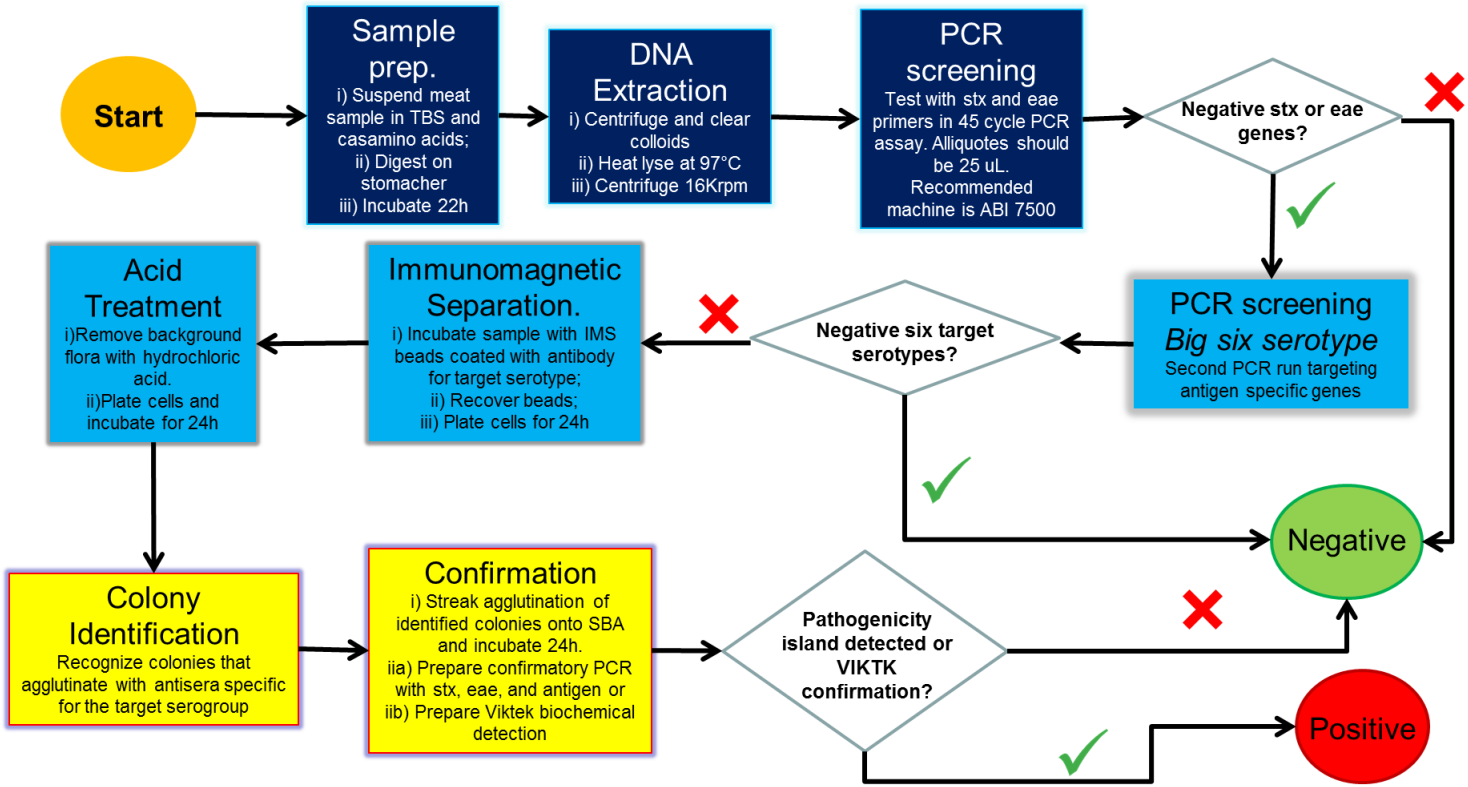

Figure 2.12: Flow diagram of USDA guideline for detection of foodborne pathogens

Portable DNA amplification systems will facilitate biomolecular assays that are used multiple times during the screening process. These new devices will simplify the creation of more control points in the food production chain and provide tools to perform fast and on-site molecular assays. However, they will not significantly improve the time to the detection. As the flow chart and other publications have discussed previously [89], most of the detection time is spent in the incubation and enrichment of samples. The DNA amplification systems cannot improve these sample enrichment steps because it requires bacterial concentrations that provide at least one pathogen in the 25 μL reaction that is normally analyzed. Other equipment and filtration strategies are designed specifically to improve bacterial growth steps and reduce the enrichment time. The use of lateral flow filtration [90] or dielectric concentration [91] has demonstrated that it can concentrate pathogens and significantly reduce enrichment periods. The portable DNA detection will need to pair with these other enrichment or concentration systems to create integrated solutions. When both the DNA screening equipment and sample preparation mechanisms are portable, the screening assays will be significantly improved. The flow chart in Figure 2.12 is not showing that the time to result is heavily affected by queue waiting and transportation times. With only a few laboratories handling samples in each state, the logistics to ship samples while sustaining judicial validity are complex and expensive. Therefore the portable systems can reduce the transportation cost and significantly increase the ratio of tested samples. Portable PCR systems are a crucial element to have portable detection of pathogens, but they will need to be complemented with other concentration and sample preparation techniques to provide full solutions that can be easily adopted by regulatory agencies or food producers.

CHAPTER 3

ON-CHIP PARALLEL DETECTION OF FOODBORNE PATHOGENS USING LAMP

An avenue to achieve all the desired features of portable DNA analysis systems is to incorporate semiconductor transducers as sensors of the reaction. The combination of semiconductor devices and isothermal amplification reactions promises to yield simple and powerful devices for nucleic acid testing that can be miniaturized for portable applications. In this chapter we report a study that used a microinjection system and silicon micro-wells to test protocols for multiplexed on-chip detection of bacterial foodborne pathogens using loop-mediated isothermal amplification (LAMP). After passivation of the silicon surface with Sigmacote (Sigma-Aldrich. St. Louis, MO), the microinjection system creates nano-droplet arrays on the wells where the amplification reaction takes place. Primers for amplification of virulence genes hlyA (*L. monocytogenes*), stx2 (*E. coli* O157), and invA (*S.enterica*) are dried in the micro-wells prior to the injection of a primer-less LAMP mix [92, 93, 29]. This technique allows parallel screening of multiple pathogens in a single assay. In this chapter we also report characterization experiments to quantify sensitivity, specificity and robustness of on-chip LAMP amplification.

3.1 LAMP assays in silicon oxide micro-wells

3.1.1 Fabrication of micro-wells

Figure 3.1 (a) shows cross-sectional schematics of the fabrication of silicon wells. Undoped silicon wafers (University Wafers, South Boston, MA) are used as the substrate. After a short piranha clean (1:1 H_2O_2-H_2SO_4, 8 mins) a 160 nm layer of silicon oxide is thermally grown at 800 °C for 20 min (Lindberg/Tempress Model 8500). AZ1518 photoresist (AZ Electronic

Materials, Branchburg, NJ) is spin-coated to form a 2 μm layer on the unpolished side of the wafer, followed by an 8 min soft-bake on a hotplate at 110 °C. The process is repeated on the polished side of the wafer where the photoresist is patterned using a Quintel aligner with a high resolution transparency mask (FineLine Imaging, Colorado Springs, CO) defining the wells openings. Exposed regions are developed in MIF AZ300 (AZ Electronic Materials, Branchburg, NJ) for 2 min and exposed silicon oxide is etched in 10:1 buffered oxide etchant (VWR, Chicago, IL) for 10 min. The photoresist is stripped in Remover PG (MicroChem, Newton, MA) warmed to 70 °C for 30 min, leaving a hard silicon oxide mask in the polished side of the wafer and a protective oxide layer on the wafer's back side. Then, the patterned wafer is immersed in hot TMAH bath 80 °C (1:1 TMAH: DI) for 18 hours to anisotropically etch inverted square pyramids. To prevent inhibitory effects on biomolecules, a 10 nm layer of silicon oxide is then thermally grown (2 min, 800 °C). Finally, a photoresist protective layer is spin-coated and soft-baked before the wafer is diced into 1x1 cm chips. Figure 3.1 (b) shows a chip with 6x6 arrays of silicon wells and Figure 3.1 (c) presents a scanning electron micrograph of a well's cross-section.

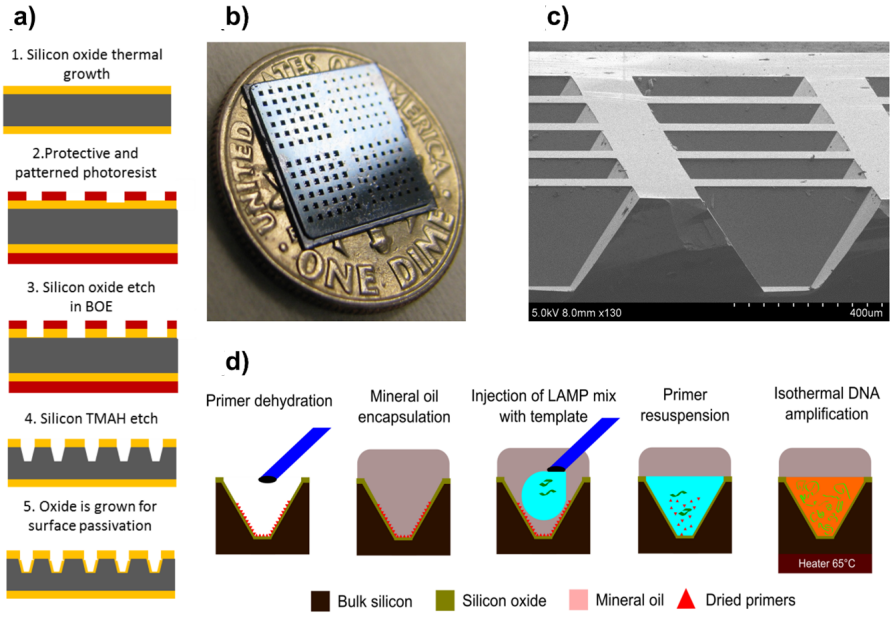

Figure 3.1: Silicon oxide micro-well chip and experimental protocol

3.1.2 Micro-injection operation

Experiments were performed using a microinjector IM-300 (Narishige Scientific Instrument Lab. Tokyo, JP). This systems was used for dehydration of primer mix and injection of the primer-less LAMP solution in the silicon micro-wells. An Eppendorf VacuTip (Eppendorf. Hamburg, De) with an internal diameter of 15 μm is connected to the microinjector output and is loaded with $\sim$ 1 μL of reagents. Reagents in the tip are dispensed for 20 ms at 60 psi to form droplets of around 30 nL. The tip position is controlled with a 3D micromanipulator (MCL-D331) from World Precision Systems, Sarasota, FL. After the initial alignment to two reference points, a Matlab script (MatWorks, Natick, MA) coordinates the position system and the microinjector to fill the array of wells.

3.1.3 Micro-wells silanization

Silicon and silicon-based materials undermine polymerase activity and inhibit nucleic acid amplification [94, 95]. To prevent inhibition of amplification, the silicon wells were passivated with Sigmacote to create a silane layer that neutralized surface adsorption of biomolecules [96]. Sigmacote is a solution of chlorinated organopolysiloxane in heptane; it reacts with the surface silanol groups and binds covalently to the substrate. To deposit the silane, the silicon wells chip is submerged for 5 min in Sigmacote followed by isopropanol and DI water rinses to remove any excess.

3.1.4 Primer-less LAMP reaction mix

For each experiment, 30 μL of primer-less LAMP solution was prepared with the following components: Betaine (800 mM), mix of dNTPs (1.4 mM), isothermal buffer (1x, New England Biolabs, Ipswich, MA), magnesium sulfate (8 mM), *bacillus stearothermophilus* (*Bst*), 2.0 WarmStart polymerase (0.64 unit/μL), Evagreen fluorescent dye (20 μM), and Template DNA (variable concentrations). Instead of the wild-type *Bst* we used *Bst* 2.0 WarmStart polymerase (New England Biolabs, Ipswich, MA). This is an 'in-silico' designed homologue developed as a robust alternative with higher thermal stability and salt tolerance (New England Biolabs, 2012). The template for

amplification is genomic DNA extracted from overnight *E.coli* O157:H7 and *L. monocytogenes* cultures in bovine-brain heart infusion (Sigma-Aldrich. St. Louis, MO) reaching estimated concentrations of 10^9 CFU/ml for *E.coli* and 10^8 CFU/ml for *L.monocytogenes*. After incubation, 1 ml of cultured bacteria is centrifuged at 8600 RCF for 3 min to pellet the bacteria. Bacterial cells are re-suspended in nuclease-free water (Invitrogen, Grand Island, NY) and heat-lysed at 95 °C for 15 min in at 300 RPM in a Thermomixer R (Eppendorf. Hamburg, De). A final centrifugation is performed at 12400 RCF for 10 min, which pellets undesired cell debris, leaving template DNA in the supernate.

3.1.5 Primers dehydration

The primer sequences used for amplification of pathogenic genes of bacterial targets are listed in Table 3.1. The primer mix was prepared with custom DNA oligomers (Integrated DNA technologies, Coralville, IA) and mixed in the following concentrations: FIP/BIP (19 μM), F3/B3 (2.4 μM), and LF/LB (9.6 μM). Primers are spotted in the wells after chip silanization using the microinjector with a 10 ms pulse to dispense around 15 nL. The dispensed volume quickly dries at room temperature, leaving dehydrated primers in wells prior to mineral oil encapsulation. For multiplexed screening experiments, each well was prepared with a specific primers.

3.1.6 On-chip amplification experiments

A schematic illustrating the detection experiment sequence is presented in Figure 3.1 (d). Silanized chips with dehydrated primers are covered with mineral oil to prevent evaporation of droplets during amplification. The microinjector is then used to load silicon wells with 30 nL of the primer-less LAMP solution that includes the target template. Next, the chip is heated to 65 °C with an mK1000 heated stage (Instec, Boulder, CO). Fluorescence changes related to greater dsDNA concentration are observed on a Nikon Eclipse FN-1 fluorescence microscope (Nikon Instruments Inc. Melville, NY) that captures images every minute.

Table 3.1: LAMP primers used in this study. Target genes were stx2 & eae for *E.coli*, hlyA for *L.monocytogenes*, and invA for *S.enterica*.

Target (Gene)	**Primer**	**Sequence (5'-3')**	**Source**
E.coli	F3	GAGATATCGACCCCTCTTG	[14]
(stx2)	B3	AATCTGAAAAACGGTAGAAAGT	
	FIP	TCCACAGCAAAATAACTGCCCA	
		ACATATATCTCAGGGGACCA	
	BIP	GATGTCTATCAGGCGCGTTTTGC	
		CGTATTAACGAACCCGG	
	LF	TGT GGTTAATAACAGACACCGATG	
	LB	ACCATCTTCGTCTGATTATTGAGC	
E.coli	F3	AGCTCTAACAATGTACAGCT	[93]
(eaeA)	B3	AGTTGCAGTTCCTGAAACA	
	FIP	GTCTTATCCGCCGTAAAGTCCG	
		CCGTTCTGTCGAATGGTC	
	BIP	CTAAAGCGGATAACGCCGATACCC	
		AGGGACATTAGCCTGAG	
	LF	CCCAACCTGGTCGACAACTT	
	LB	ATTACTTATACCGCGACGGTGAA	
L. monocytogenes	F3	TTGCGCAACAAACTGAAGC	[92]
(hlyA)	B3	GCTTTTACGAGAGCACCTGG	
	FIP	CGTGTTTCTTTTCGATTGGCGTCT	
		TTTTTTCATCCATGGCACCACC	
	BIP	CCACGGAGATGCAGTGACAAATGTT	
		TTGGATTTCTTCTTTTTCTCCACAAC	
	LF	TAGGACTTGCAGGCGGAGATG	
	LB	GCCAAGAAAAGGTTACAAAGATGG	
S.enterica	F3	CGGCCCGATTTTCTCTGG	[29]
(invA)	B3	CGGCAATAGCGTCACCTT	
	FIP	GCGCGGCATCCGCATCAATA	
		TGCCCGGTAAACAGATGAGT	
	BIP	GCGAACGGCGAAGCGTACTG	
		TCGCACCGTCAAAGGAAC	
	LF	GGCCTTCAAATCGGCATCAAT	
	LB	GAAAGGGAAAGCCAGCTTTACG	

3.1.7 Analysis of fluorescence images

Fluorescence images are analyzed in ImageJ (http://rsb.info.nih.gov/ij/). Each well's fluorescence was individually measured using Raw Integrated density 'RawIntDen', the stack-measurement plugin, and the rectangular selection. Data is imported to Matlab where data for each well is normalized to the first recorded value. A well is considered to exhibit positive amplification when its intensity increases by 20%, significantly above the noise level observed in negative controls. The threshold is defined as the reaction time to achieve the 20% increment.

3.2 Evaluation of on-chip LAMP

3.2.1 Primers rehydration and assay reproducibility

To evaluate DNA amplification on silicon oxide micro-wells after silanization and primer dehydration initial experiments aimed to confirm that primers resuspend in the injected LAMP solution and then anneal to target template for amplification. In addition, we were interested in measuring intra-chip amplification efficiency and the rate of false negatives and positives. Figure 3.2 shows an experiment where primers for *E.coli* O157 were dehydrated in all 36 wells of the array. After mineral oil encapsulation the primer-less LAMP solution, with template extracted from a 10^9 CFU/ml culture, was spotted in the bottom 18 wells. The top 18 wells were spotted with a solution without template (the template was replaced with DI water) to create on-chip negative controls.

The initial and final fluorescence images are presented in Figure 3.2 (a) and 3.2 (b). Real-time fluorescence intensity curves for all wells are shown in Figure 3.2 (c). Figure 3.2 (d) shows the fluorescence increase for negative and positive controls and the average threshold time (time when fluorescence increased by 20%) for the positive control samples. The real-time data shows that amplification was observed in all wells where the injected solution contained *E.Coli* O157 template. The coefficients of variation for threshold times and fluorescence increments in positive controls were 25% and 4% respectively. The variation is higher than that observed in other reports using

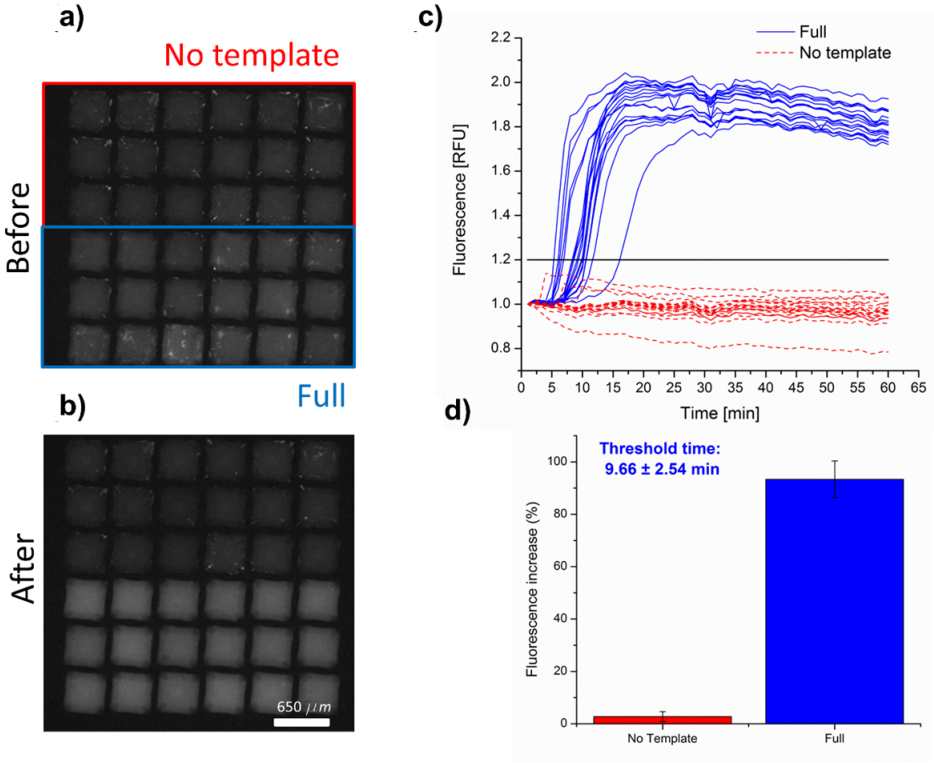

Figure 3.2: Amplification of stx2 gene of *E.coli* O157 after primer dehydration

similar primer dehydration strategies (Stedtfeld, 2012). Volume inconsistencies on smaller samples and stronger interaction between molecules and the chip with high surface to volume ratios may explain the higher observed intra-chip amplification variability. The false negative ratio (defined as the rate of wells where amplification was expected but not observed over the total number of positive control wells) is zero at this concentration. Furthermore, none of the negative controls presented amplification, for zero false positives and full specificity. These results indicate that primers in the prepared chip will rehydrate when LAMP reagents are injected and participate in specific amplification for the detection of pathogens.

3.2.2 Sensitivity of on-chip reactions

The concentration of template used in the LAMP solution was serially diluted and then spotted on the silicon wells to evaluate the detection limit of LAMP with dehydrated primers in a silicon chip. Figure 3.3 shows the threshold time and false negative ratio for experiments with multiple template concentrations of *E.Coli* O157 and stx2 dehydrated primers. The number of CFU per reaction is computed from the measured plated CFU/ml and scaled to 30nL of the reaction volume. The lowest detected concentration was 10^5 CFU/ml which translates to 3 CFU/reaction. The false negative ratio increases as the template concentration decreases and it approaches 1/2 for experiments performed with the minimum detectable bacterial concentration. However, we observed amplification in most of the wells in experiments with low template concentration demonstrating an acceptable detection limit. This agrees with other reports that show the ability of LAMP to detect single copies in miniaturized platforms [97].

A hypothesis for the higher number of false negatives is an incomplete surface passivation by the Sigmacote treatment. According to the Poisson distribution the probability of having at least one copy in each well at the lowest concentration of 3 CFU/reaction is 95%, effectively assuring that each well will have at least one template for amplification. However the few copies present in the well could be adsorbed by silicon oxide areas with poor coverage by the silane. The probability of having all template molecules inactive during the reaction due to exposed silicon increases at lower concentrations.

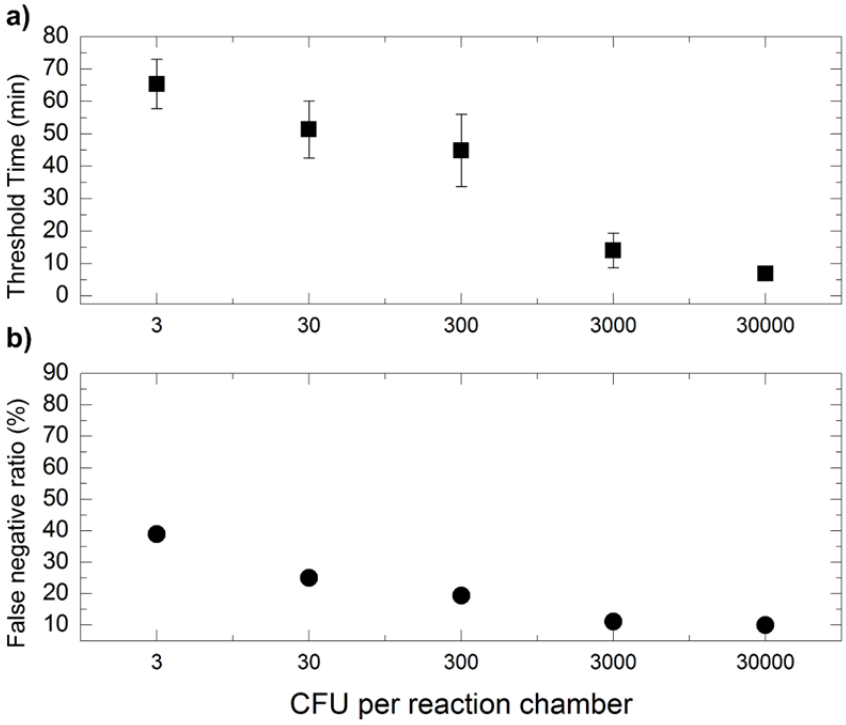

Figure 3.3: Sensitivity experiments on silicon oxide wells

The Sigmacote treatment was selected for this study due to its simplicity, but further studies using other passivation and deposition methods that improve coverage and uniformity may lead to single copy amplification for on-chip digital LAMP [98].

3.2.3 Concurrent screening of multiple pathogens

On-chip LAMP amplification after primer dehydration is sensitive and reproducible. However, the main advantage of this technique is that it enables multiplexed screening in one single assay when primers for multiple pathogens are dried in the same chip. There are 31 identified foodborne pathogens that cause hospitalizations in the United States and it is necessary to screen for all those pathogens to assure that food is not contaminated. Therefore, it is very desirable that a screening method is capable of multiplexed detection of several pathogens in a single assay to avoid labor-intensive protocols.

For experiments shown in Figure 3.4 primers for *S.enterica* invA, *L. monocytogenes* hlyA and *E.coli* O157 stx2 were dehydrated in different positions of the array. In Figure 3.4 (a) the two left columns had primers for hlyA (*L.monocytogenes*), the middle columns for invA (*S.enterica*) and the right columns for stx2 (*E.coli* O157). After primer dehydration and mineral oil encapsulation, a primer-less LAMP solution with template extracted from culture of 10^8 CFU/ml *L. monocytogenes* was injected in the top 30 wells. The bottom row was set as a negative control injecting a primer-less solution without template. The same experiment was executed with a different chip using a primer-less LAMP solution with template from 10^8 CFU/ml *E.coli* O157culture.

Figure 3.4 (d) and 3.4 (e) show that the method is specific and amplification is observed only in the wells where the template and primers match. Figure 3.4 (d) shows data from an experiment with *L.monocytogenes* template. We observed that only wells with dried primers for *L.monocytogenes* hlyA amplified. On the other hand in Figure 3.4 (e), experiment with *E.coli* template, only wells with primers for *E.coli* stx2 amplified. Data from the two experiments is summarized in Figure 3.4 (c). The plot shows the average increase in fluorescence for each group of wells with common primers in experiment 1 (with *L.monocytogenes* template) and experiment 2 (with *E.coli*

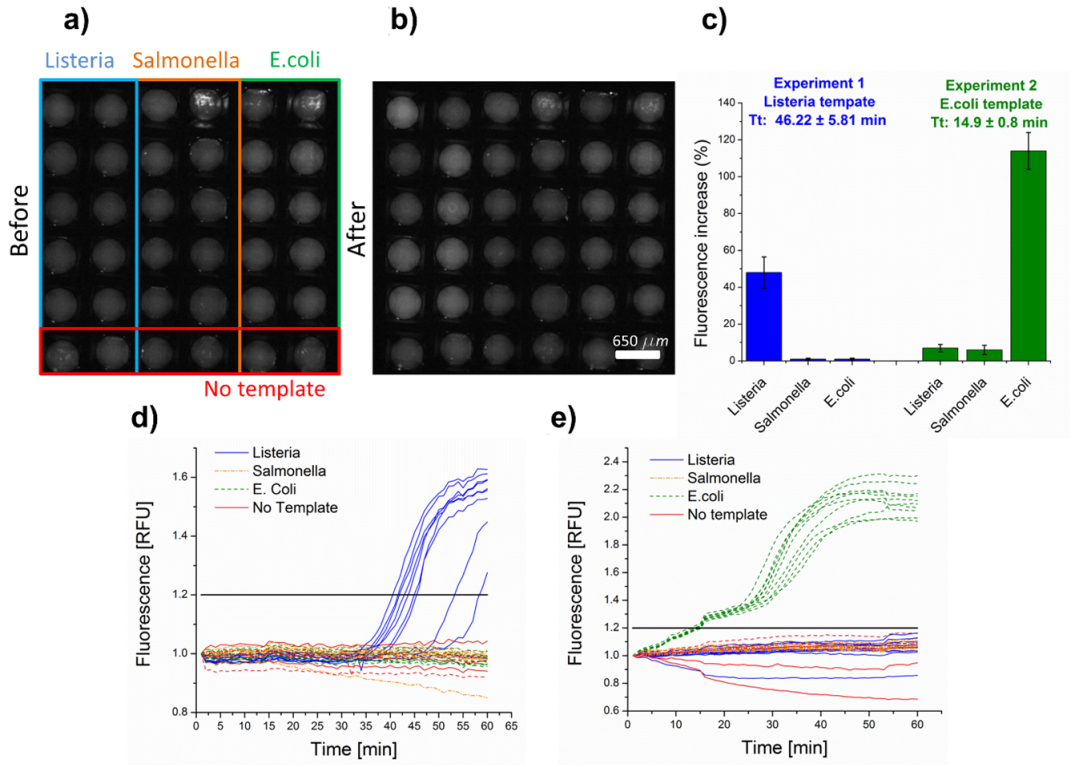

Figure 3.4: Multiplexed on-chip identification of foodborne pathogens

template). Only the wells where primers find a complementary had increased fluorescence intensity after amplification demonstrating specific amplification. The variability in fluorescence signals and threshold times between *E. coli* O157 and *L. monocytogenes* experiments could be due to different primer efficiency. It has been shown previously that the LAMP reaction speed is a function of the primer length, GC content, melting temperature, free energy of hybridization, and especially 3'- and 5'- ends availability [99]. Given that the concentration of template and the DNA extraction protocol is the same in both experiments, the variability of threshold time and fluorescence increase can be attributed to a difference in primer activity and affinity.

3.2.4 Amplification with raw lysate template

Successful development of portable DNA testing requires simplified systems that allow inexpensive and simple miniaturization. The DNA extraction step, done regularly for LAMP and PCR experiments, is performed to remove cellular components that could potentially inhibit the polymerase activity or the assay specificity (Headman and Radstrom, 2013). However, this step involves reagents and laboratory equipment that increase the overall process complexity. For the experiment presented in Figure 3.5, *E.coli* O157 stx2 primers were dehydrated in all wells. After mineral oil encapsulation, 3 primer-less solutions were spotted. In Figure 3.5 (a) the LAMP solution injected in the left columns contained extracted DNA from a 10^8 CFU/ml culture of *E.coli*. In the middle columns, the template is raw lysate (no centrifugation steps after lysis) from the same culture, and in the right columns LAMP solution has no template (as negative control). Figure 3.5 (c) shows real time fluorescence intensity of each well. Figure 3.5 (d) quantifies fluorescence intensity and threshold time, indicating that wells where the template is raw lysate have lower amplification efficiency. The detection times are slightly longer and fluorescence changes are smaller in the raw template samples when compared to the ones with extracted DNA. These results are consistent with expectations of reduced yield from non-purified template. In addition, we observed a false negative in one of the 'raw-lysate' wells while all wells for extracted DNA template amplified. From this experiment it is possible to conclude that amplification can be carried out without DNA extraction but

with lower amplification efficiency and a slightly higher probability of false negatives. However, the use of larger arrays would mitigate robustness issues that arise from the raw lysate template. With more wells the probability of observing amplification statistically increases and compensates for possible false negatives.

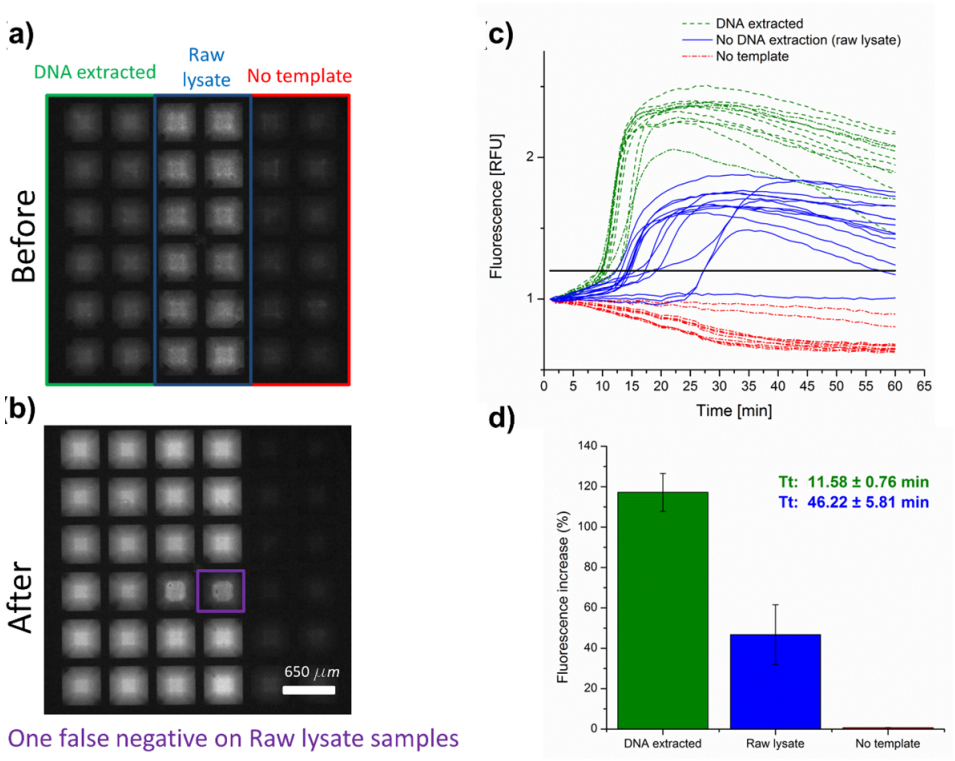

Figure 3.5: On-chip amplification without DNA extraction

3.2.5 Dehydrated primers shelf life

Spotting of primers on a microchip for multiplexed detection must be done using laboratory equipment like the microinjector or ink-jet printers [100]. The multiple solutions that are dispensed (one per target pathogen) and alignment to the chip demand highly specialized equipment. Therefore, it is important to know for how long the primers can be stored after dehydration, without losing affinity to the complimentary sequence and ability to generate the loop structures for LAMP amplification. Primers for *E.coli* O157 stx2

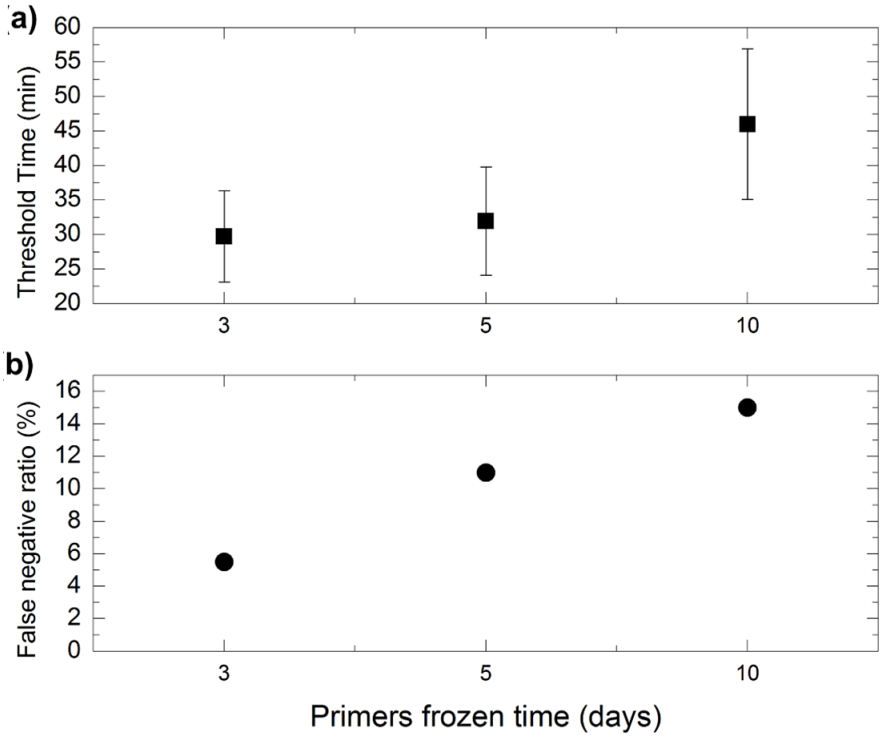

Figure 3.6: Frozen on-chip dried primers shelf life

were dehydrated in silicon wells and then refrigerated at $-20\,^{\circ}\mathrm{C}$ for 1, 3, and 10 days. These chips were then used for *E.coli* O157 detection experiments using template extracted from a 10^8 CFU/ml culture. Once again the threshold time and the false negative ratio were recorded. Figure 3.6 shows that primers can be used for amplification after having been frozen for up to 10 days. However, after 10 days of refrigeration the threshold time and the false negative ratio are higher, indicating that frozen primers lose their ability to anneal with complementary sequences and create structures required for LAMP with storage time. Previous studies have shown a progressive degradation of dehydrated DNA. The molecule loses molecular weight and supercoil content as a function of time [101, 102] explaining the observed performance loss.

3.3 On-chip detection of non O157 shiga-toxin producing *E.Coli*

Shiga toxin-producing *E.coli* (STEC) strains are virulent agents responsible for thousands of illnesses in the United States [103]. The most common and notorious STEC serotype is O157:H7; however, other serotypes, such as the O104:H4 strand that was responsible for the May 2011 HUS outbreak in Germany [104], account for one third of STEC-related illnesses. Beginning in June of 2012, the U.S. Department of Agriculture initiated a zero tolerance policy for six non-O157 STEC groups (the 'big six') that cause over 70% of total non-O157 illnesses. In order to detect these 6 serotypes (O26, O45, O103, O111, O121, and O145) the food safety and inspection service has outlined a detection protocol that requires two steps of quantitative PCR (qPCR). The new requirements make the screening process more expensive and labor intensive [105]. Utilizing the methods described in this chapter for on-chip amplification it is possible to reduce complexity and cost of the 'big six' detection and identification process.

Using the array of silicon oxide micro-wells described in previous sections of this chapter, and the same primer dehydration technique that was used to target *E.coli*, *L.monocytogenes* and *S.enterica*, we have demonstrated parallel detection and identification of the 'big six' group serotypes. Simply by changing the primers that are dehydrated we can use the same materials and

protocols to detect and identify the non-O157 STECs.

Figure 3.7 (a) shows the layout for primer dehydration in the 6x6 silicon micro-well array. In each column a primer targeting a specific serotype is dehydrated [105] and later the rest of the LAMP reaction is microinjected. The first row of wells is reserved for a no-template control microinjection that is used to discard false positives due to primer-dimer amplification. The rest of the wells are filled with a LAMP reaction containing the sample that will be analyzed. Therefore, as shown in Figure 3.7 (b), for each primer there are 5 replicates along with one negative control for a truly multiplexed DNA interrogation.

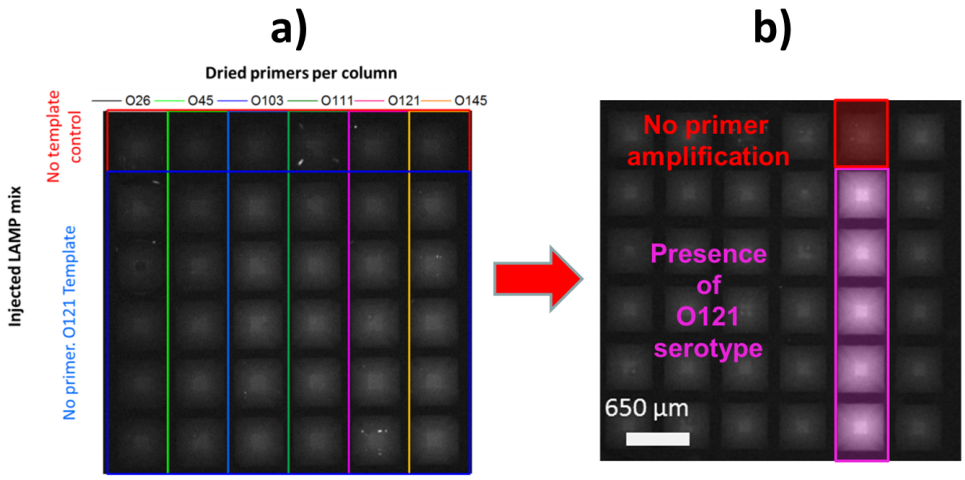

Figure 3.7: Chip layout and amplification demonstration for 'big-six' non O157 Shiga-toxin producing *E.coli*

All six different pathogens were used as templates for specificity experiments. Results are summarized in Figure 3.8, showing that despite variations in threshold voltages and final fluorescence intensity, in all 6 cases only wells where there is matching primer and template presented amplification. In Figure 3.9 we present titration experiments where the template concentration per reaction is decreased. Similarly to results presented for other pathogens, as the template concentration decreases the threshold time and number of false negatives increase. However, the sensitivity is still down to a few copies per well.

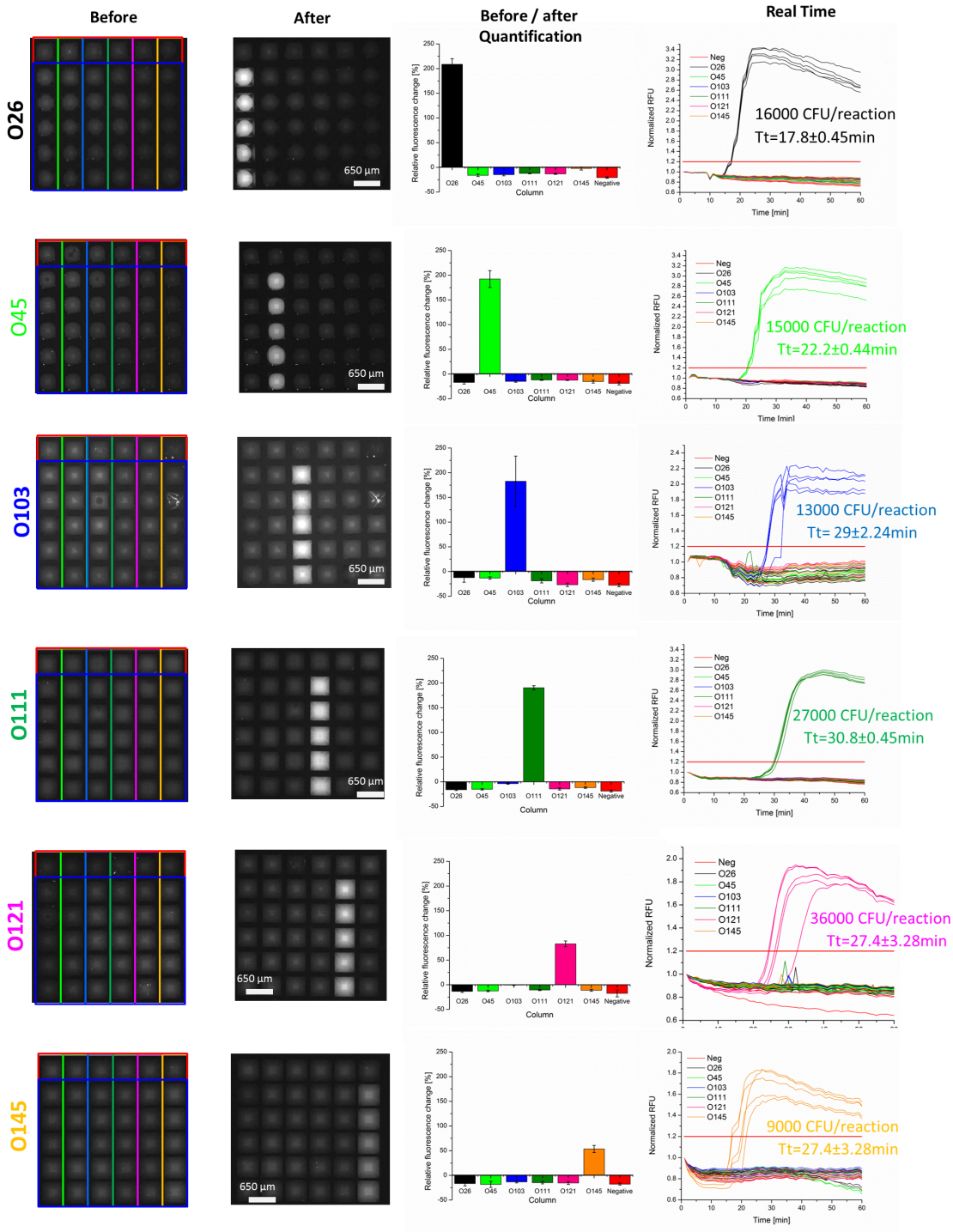

Figure 3.8: Specificity experiments for the 'big-six' non O157 Shiga-toxin *E.coli*

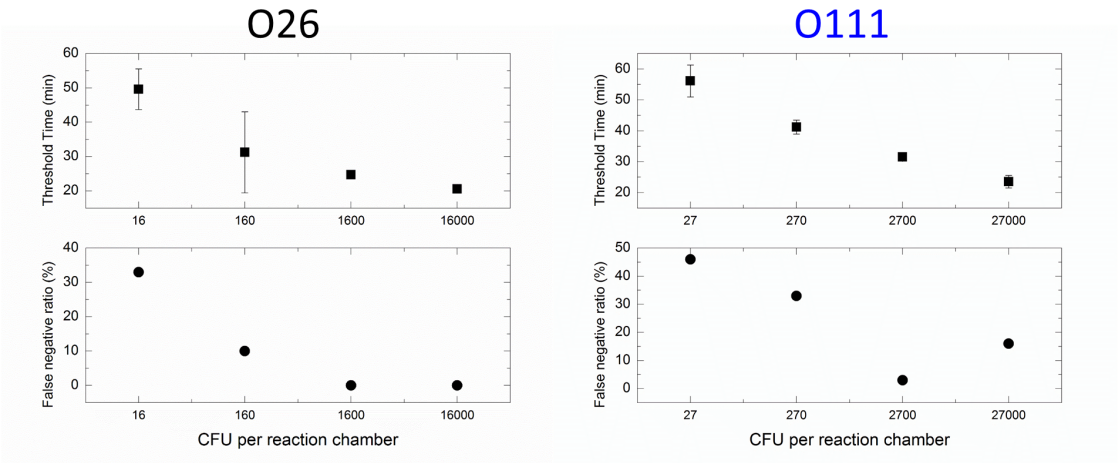

Figure 3.9: Sensitivity studies of on-chip amplification for 2 serotypes of the 'big-six' STECs

3.4 Summary of on-chip LAMP amplification

For portable DNA-based diagnostic tools it is necessary to simplify the instrumentation that is required to perform assays to enable simple, inexpensive, and miniaturized detection. Isothermal amplification strategies like LAMP do not require temperature controllers needed in conventional strategies like PCR simplifying protocols and devices to run the reaction [51]. In addition, semiconductor devices can be used to electrically monitor amplification reactions without the need for optics that measure fluorescence [106], locally heat samples to reaction temperatures removing bulky heaters [107], and lyse cells through electroporation to locally extract DNA [108]. Therefore, it is possible to develop a simplified portable nucleic acid diagnostic system incorporating both LAMP and semiconductors.

This chapter describes protocols to conduct LAMP reactions on a silicon oxide well array. The silicon surface had to be passivated with a silane treatment to prevent adsorption of biomolecules, and primers were dehydrated prior to running the assay to enable multiplexed screening. We demonstrated that on-chip amplification is reproducible, sensitive down to a few copies/reaction, and specific allowing multiplexed identification of pathogens in a single assay. In addition, our experiments indicate that it is possible to perform amplification without DNA extraction protocols and that dehydrated primers

can be frozen for up to 10 days for future detection experiments. Overall, our results indicate that LAMP can be reliably performed in silicon wells, enabling further integration of bio-molecular assays and semiconductor technologies for portable genetic based diagnosis.

CHAPTER 4

DETECTION OF LAMP REACTIONS WITH DG-ISFETS OPTIMALLY BIASED

Ion-sensitive field effect transistors (ISFETs) have become effective transducers of biochemical reactions into electrical signals [109, 2]. In an ISFET, the gate region is exposed to an electrolyte, making the drain-source current sensitive to charged molecules and chemical reactions in the solution [110]. These devices promise to enable parallel, label-free, inexpensive, and portable diagnostic tools by translating advances of the semiconductor industry to health-care and biological applications [111]. Different studies have applied the concept of electrical biosensing through field effect and capacitive coupling for different purposes. Silicon nanowire transistors have been used for the detection of proteins and nucleic acids in low concentrations [112, 113, 114], carbon nanotubes and graphene FETs are being used as gas and molecular sensors [115, 116], and ISFETs made with metal oxides and polymers are used to monitor biological activity [117, 118, 119]. The potential advantage of having label-free, multiplexed, and miniaturized sensors incentivizes research in ISFETs and its multiple variations [120, 121]. The portable DNA amplification system that we are developing leverages these advantages of FET biosensing. In this chapter we describe a dual-gate ISFET that has been fabricated to detect pH changes triggered by LAMP reactions. We describe the fabrication of the semiconductor device, optimization of its operation, and the label-free detection of nucleotide incorporation.

4.1 Sensitivity above Nernst limit in DG-ISFETs and benefits of individual gates

Detection of biomolecules at low concentrations and analysis of biomolecular reactions that give small signals have driven research toward signal enhancement techniques for ISFET sensing. Researchers have labeled analytes with

particles or enzymes [122, 123], utilized surface treatments to the sensor's active layer to control wettability [124], and used complementary electrokinetic structures [125], all to enhance the biological signals and enable more sensitive electrical measurements. For studies where the measured variable is the solution's acidity, a number of publications demonstrated the use of coupled transistors for signal enhancement. Couples of sensors connected in parallel yield a 'super-Nernstian' pH sensitivity that exceeds the 59 mV/pH limit defined by the Nernst equation [126]. This method is particularly relevant for semiconductor DNA sequencing [127], label-free gene detection [128], or electrochemical diagnostics [129], where accurate measurement of small pH changes is important to reduce error rates, lower detection limits, and improve throughput. Our group has reported coupling of nanowire and nanoplate transistors with different W/L ratios to amplify pH signals [130], but the most common and notable coupling mechanism is the dual-gated field effect transistor (DG-FET)[131, 132, 133]. Transistors fabricated from silicon-on-insulator (SOI) wafers have a top gate that is formed by depositing a dielectric on the active silicon layer, and a back-gate where the dielectric is the SOI's buried oxide. When the active silicon is considerably thicker than the maximum depletion layer, there is no charge coupling between gates, and the bottom and top transistors can be treated as independent parallel devices [134]. When the top and bottom transistors are coupled in a dual-gate mode operation, their geometrical and electrical properties will produce an amplification of the pH sensitivity [135].

A new process developed by Taiwan Semiconductor Manufacturing Company (TSMC) resulted in double-gated ISFETs that have individually addressable back-gates, overcoming limitations of the single back node of standard SOI fabrication. In a regular SOI process all transistors have a common back-gate that is biased through the bulk silicon. Having a common back-gate prevents tailored biasing of individual transistors that is important to operate in optimum conditions [136]. In addition, the buried oxide quality and its variations across the wafer produce DGFETs with non-uniform electrical characteristics which undermine scalability and optimization [137, 138, 139]. These limitations can be overcome with a new structure of dual-gate ISFETs with individually addressable or 'true' back-gates fabricated by TSMC in a 0.18 μm SOI technology. The new transistor is made in a two-stage process. First, the transistor is formed as a standard SOI

metal-oxide-semiconductor FET (MOSFET). Then, the SOI wafer is flipped upside down and is attached to a new substrate. After removing the bulk silicon from the original SOI wafer, an opening is formed through the buried oxide to expose the back of the silicon, and a hafnium oxide film is deposited to form the ISFET's sensing layer. The resulting device then has two gates, the fluid-gate biased with a reference electrode in solution and the back-gate which is the a standard foundry fabricated MOSFET. A schematic illustrating a cross section of the new device is presented in Figure 4.1. The full fabrication is performed in a standard semiconductor foundry leveraging high-quality materials and automated processes of CMOS manufacturing that enable traceable reliability with very high yields at a low cost. Furthermore, the devices have been integrated with control and read-out circuitry making the full process amenable for immediate commercialization.

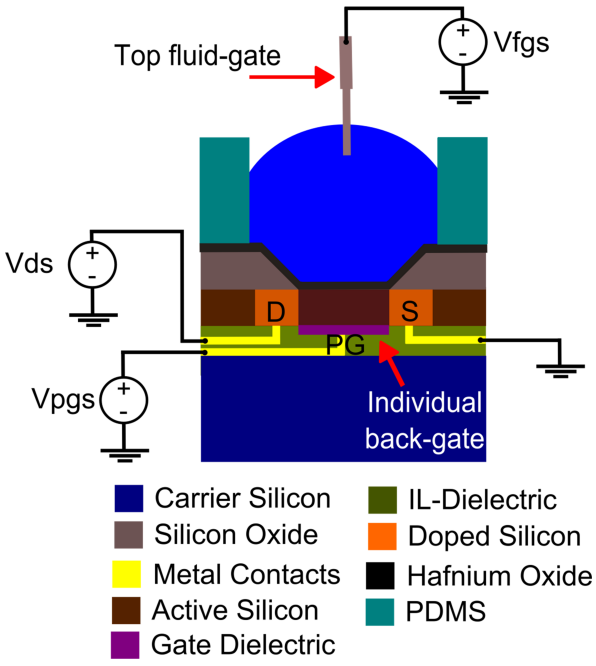

Figure 4.1: Schematic of the fabricated dual-gated ISFET

Besides enabling true back-gates, the new architecture improves electri-

cal robustness and enables higher transistor density. Electrical interconnects (metals 1 and onwards in a foundry process) are well isolated from the fluid with the original SOI buried oxide preventing leakage current from the metal leads to the fluid, which can be a crippling problem for thin deposited dielectric layers [131]. In addition, the new structure does not have a floating sensing gate preventing accumulation of charges and reducing the probability of sudden threshold voltage changes due to electrostatic discharge [140, 141]. This novel device architecture also simplifies routing and increases possible transistor density because interconnect leads are in a different layer from the sensing regions. Figure 4.2 compares the cell footprint of single-gate transistors with the new structure. Since node connections are in a different layer and the extended gate is not used in the new structure, the true dual-gate transistors only occupy $\sim 25\%$ of the area of the single-gate device which will impact transistor count. For sensing purposes, the new devices enable a tailored dual-gated operation that allows improvement of the signal-to-noise ratio (SNR). For defined pH ranges, increments in sensitivity overcome average noise resulting in enhanced pH resolution. This characteristic is used to improve the sensor accuracy and decrease detection times when monitoring biological reactions. Using a loop mediated isothermal DNA amplification [27], we demonstrate that these devices enhance signals of biological reactions when operated in dual-gate mode enabling more accurate control and assessment. Due to the increased resolution of the configuration, the dual-gate mode yields a larger output signal in shorter detection times.

4.2 Individually addressable DG ISFETs and tailored LAMP reactions

4.2.1 DG ISFET fabrication

The proposed dual-gate ISFET is manufactured on SOI wafers and was totally fabricated at TSMC. Using standard complementary metal-oxide-semiconductor (CMOS) processing, the transistors are formed in the device layer. At this initial instance devices are composed of a gate dielectric made of thermal silicon dioxide, a poly-silicon gate, and source drain regions formed

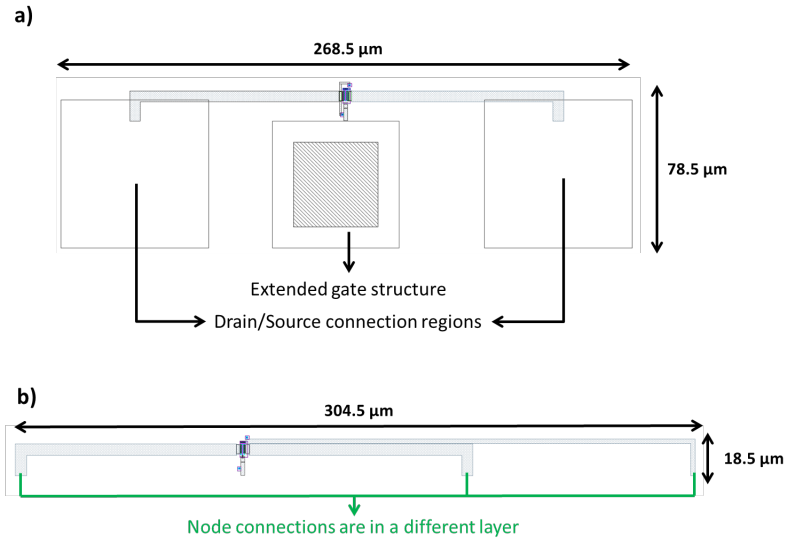

Figure 4.2: Image from the GSDII (Graphic Database system) file of the cell layout for single- and dual-gate

in a well with opposite doping. The formation of transistors is followed by deposition and patterning of multi-layer interconnects (MLI) on the device substrate that create electrical connections to source, drain, and gate. The MLI structures comprise aluminum / copper conductive lines and tungsten vias, and are isolated with silicon dioxide inter-layer dielectric (ILD).

Following the MLI definition, a silicon handling wafer is bonded to the front side (exposed MLI and ILD layers) of the device substrate and the wafer is flipped upside down. The bulk silicon layer of the original SOI wafer is then removed using a chemical mechanical polish (CMP) process that uses the buried silicon oxide as an etch-stop layer. The now exposed buried oxide is etched in specific regions using standard photolithography and a wet etch to create windows that expose the back of the active silicon layer between the drain and source regions. It is then necessary to form the top-gate dielectric that will act as the sensing interface between the transistor and electrolyte. A seed layer of silicon dioxide followed by a thicker layer of hafnium oxide serves as the fluid-gate dielectric and sensing interface. The micro-fabrication process culminates with etching steps that reveal the connection pads for device probing. Cross-sectional schematics of a summarized fabrication process are presented in the supplementary material (Figure 4.3).

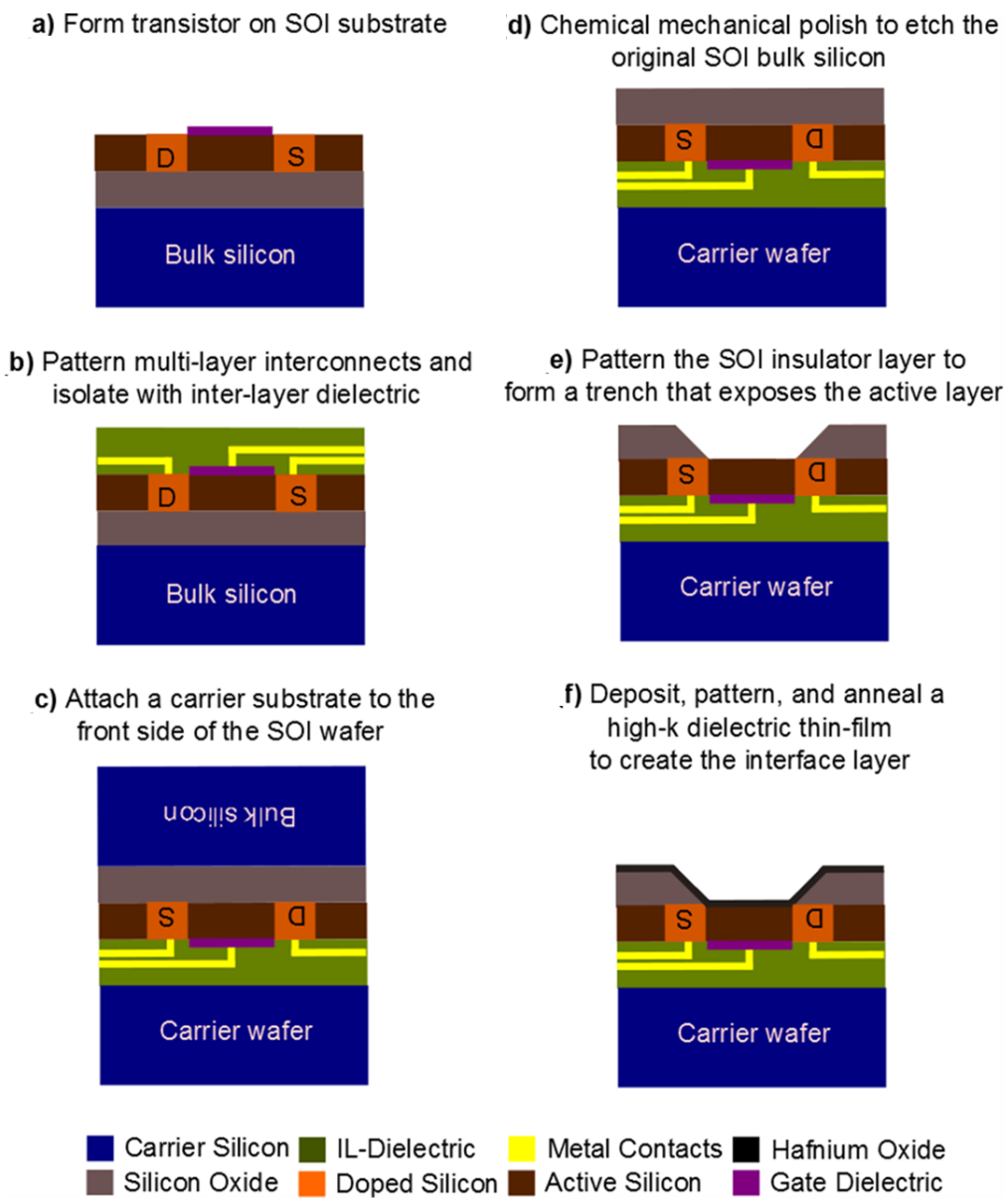

Figure 4.3: Cross-sectional schematics of the fabrication process of true DG ISFETs

4.2.2 Device measurements on Keithley 4200 scs

The electrical characterization of the fabricated dual-gated ISFETs was performed in a Keithley 4200 SCS with a filter factor of 1, Delay factor of 1.3, and an automatic settling of the A/D aperture. These are the parameters of the 'Quiet' acquisition mode and different settings will change the measurement's noise. The device was probed in the configuration described in schematic of Figure 4.1, having independent SMUs for fluid-gate, back-gate, and drain nodes, with all potentials referenced to a grounded source. A polydimethylsiloxane (PDMS) well is plasma-bonded to the front side of the transistor to act as a reservoir of the electrolyte that is biased with a leak-free reference electrode (Warner Instruments, Hamden, CT) connected to one of the SMUs to sweep or fix the fluid potential. The well is filled with a 10 mM PBS solution at different pH values or LAMP solution, Vds is set at 100 mV, and the two gates have specific biases depending the desired operation mode.

4.2.3 pH Sensitivity quantification method

The pH sensitivity is evaluated for both the dual- and single-gate modes measuring changes of the surface potential as a function of pH. Solutions of 10 mM PBS are titrated with HCl and NaOH, and measured with an Orion 3 star pH meter (Thermo Scientific, Pittsburgh PA) to have five electrolytes of known pH. As will be discussed later in the results section, the dual-gate amplification mode limits the range of pH that can be measured. Therefore the five testing electrolytes have pH values in the 6-9 range.

The prepared PBS solutions are manually pipetted in the PDMS well. After 5 min of stabilization, transfer characteristics are obtained in both the single- and dual-gate modes. For single-gate measurements, the MOS transistor is turned off by applying a negative potential to the back-gate and the electrolyte potential is swept (0 to 2 V). For the dual-gate mode the top transistor is turned on applying an inversion bias while the back-gate is swept (-1 to 1 V). The drain current vs. gate voltage transfer characteristic is measured five times. The solution is then changed to the following pH value, and the procedure is repeated.

Table 4.1: Primers mix targeting wzy gene of Shiga-toxin producing *E.coli* serotype O111

Pathogen (Gene)	**Primer**	**Sequence (5'-3')**	**Source**
E.coli O111 (wzy)	F3	AAGGCGTAACTTTTTTTGAAC	[105]
	B3	TCATGAGGGTCATTAGGAATT	
	FIP	TCACCAAGCTGTGAAACCAAA CTACAGCAAGTAATATTGAACGT	
	BIP	TCCATGGTATGGGGACATTAAATTT TGATGGAAGTCCATATAACGT	
	LB	CTTAAATAACGGCGGACAAT	

4.2.4 Pseudo real-time DNA amplification reaction

To test the benefits of the improved sensitivity and resolution, the dual-gate ISFETs were used to monitor a LAMP reaction. For each measurement, 100 μL of LAMP solution was prepared with the following components: 800 mM of betaine (Sigma-Aldrich. St. Louis, MO), 1.4 mM of dNTP mix (New England BioLabs, Ipswich, MA), 5 mM of magnesium sulfate (Sigma-Aldrich), 0.1x isothermal buffer, 50 mM potassium chloride, 0.64 unit/mL of *bacillus stearothermophilus* (*Bst*) 2.0 WarmStart polymerase (New England BioLabs), and 20 μM EvaGreen (Biotium, Hayward, CA). Additionally, the LAMP solution contains the primers for the wzy gene of Shiga toxin-producing *E.coli* (STEC) O111 specified in Table 4.1 with the following concentrations: 1.9 μM FIP/BIP, 0.24 μM F3/B3, and 0.96 μM Loop-B primers [142, 105]. The positive samples had DNA extracted from an STEC O111 18 h culture (Plating count of $9.1x10^8$ CFU/ml) while the negative controls had no template DNA.

For a pseudo real-time study, identical LAMP solutions are heated to 63 °C for different time intervals in a Thermomixer R (Eppendorf. Hamburg, De). The solutions are cooled down in an ice bath for 1 min to stop the amplification reaction before electrical and optical measurements to quantify amplification are performed. Changes of the solution pH are measured with an Orion 3 star meter, fluorescence changes related to increased binding sites for the intercalating dye are observed on a Nikon Eclipse FN-1 microscope (Nikon Instruments Inc. Melville, NY), and the transistor threshold voltage is obtained from transfer characteristics taken for the dual- and single-gate

modes. All three measurements are performed for each time interval for both negative and positive samples.

4.2.5 Sensitivity, resolution, and statistical analysis

The reported sensitivity is the derivative of the surface potential to pH function. For the single-gate mode, as it is usually done with ISFETs, the sensitivity is the slope 'b' of the linear regression $f(x) = a + bx$ to the pH response, where f(x) is the surface potential and 'x' the pH value. Therefore the sensitivity remains constant for the different pH points. However, for the dual-gate operation the surface potential to pH function is approximated with an exponential fit and an asymptotic regression $f(x) = a - b * c^x$. The derivative of the model $f'(x) = -bc^x ln(c)$ is the sensitivity function that is evaluated for different pH values.

The pH resolution is defined as the ratio of noise over sensitivity [135]. Then, resolution in pH units is calculated as $\Delta pH_{min} = \sigma\psi_s/S$, where $\sigma\psi_s$ is the standard deviation of the measured surface potential and 'S' is the sensitivity quantified as it was described above.

Finally, to compare the performance of dual- and single-gate operation modes for monitoring DNA amplification, a two tail paired P-value was calculated comparing surface potential changes in positive samples with the respective negative controls. The potential changes compared are accumulated with reaction time, differentiating only initial measurements for P-value at 5 min and comparing the total number of points for the 60 min P-value. The P-value threshold is set at 0.01 that translates into a 'very strong presumption' against a null hypothesis of having two identical samples.

4.3 Characterization of DG ISFET performance

4.3.1 Electrical characteristics

Figures 4.1 and 4.4 present the device structure and basic electrical characterization. The schematic in Figure 4.1 describes the layers that compose the transistors including the attached PDMS well and the leak-free reference electrode. The nomenclatures for potentials are: Vds for drain-source,

Vpgs for the back-gate, and Vfgs for the fluid-gate. Figure 4.4 (a) shows the IdsVpgs transfer characteristics of the double-gate operation sweeping the back-gate from -1 to 1V and having several Vfgs. The same information is plotted in the contour heat map (Figure 4.4 (b)) that summarizes the dependence of the drain current as a function of the fluid and back-gate biases. In Figure 4.4 (c) and (d) Vds is swept from 0 to 2 V for different gate biases showing typical resistive FET characteristics for the isolated top and bottom transistors. To isolate the transistors, the opposite gate is biased so it does not contribute to the drain current. This means that for back-gate transistor testing (Figure 4.4 (c)) the fluid-gate is set to Vfgs = 0 V and for fluid-gate testing (Figure 4.4 (d)) the back-gate is set to a slight negative potential of Vpgs= -0.4 V. Figure 4.4 (b) shows that at 0 V the conductivity of the bottom transistor is at tens of nano-amps implying that at 0 V there are already inversion carriers in the back-gate side. Therefore, a negative potential is applied to the back-gate for completely shutting off the bottom current isolating the fluid-gate transistor.

Overall the back-gate has better electrical characteristics than the fluid-gate side of the DGFET. The on/off ratio and saturation current are higher, while sub-threshold swing and threshold voltage are lower for the back-gate side. Electrical characterization of top- and back-gates of multiple devices is presented in Figure 4.5. Measurements and extracted distributions show that noise and threshold variations are low at the back-gate but their variability is larger for the fluid-gate. This is expected since the gate dielectric on the back-gate side experiences highly optimized annealing steps that reduce oxide charge while the fluid-gate's high-k dielectric is difficult to properly anneal at the end of processing. Furthermore, the fluid-gate is biased through the electrolyte where the capacitive coupling has a greater variability than in the back-gate [143]. Despite having the mentioned short-comings, the fluid-gate transistors have a near Nernstian sensitivity and high repeatability (mean threshold variation was only 10mV in a stress test of 50 consecutive Id-Vg sweeps) for pH sensing.

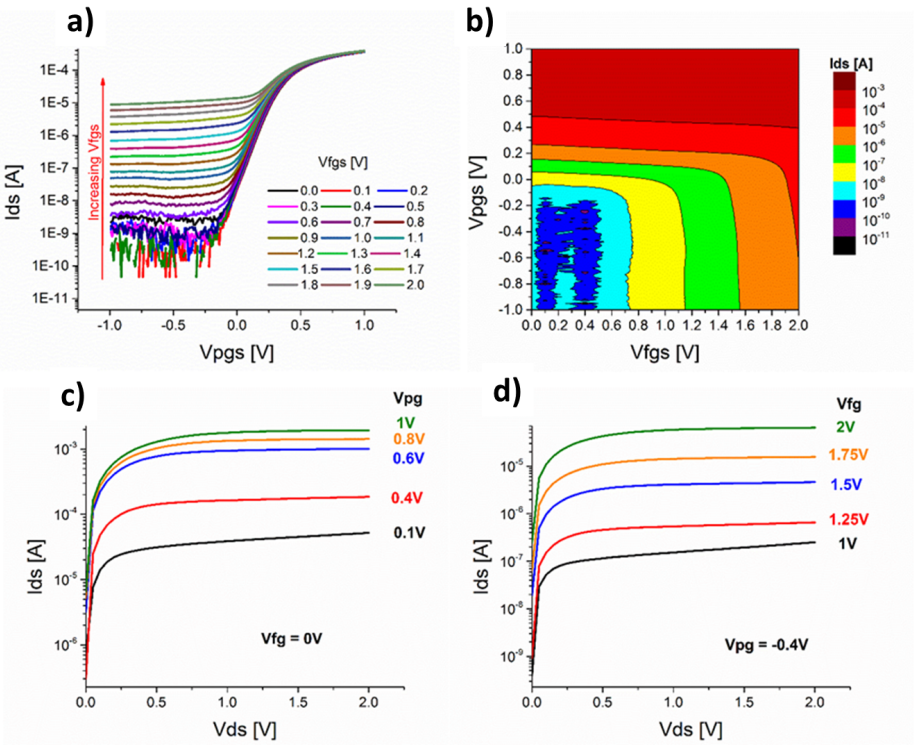

Figure 4.4: Electrical characterization of the transistor for fluid- and back-gate operations

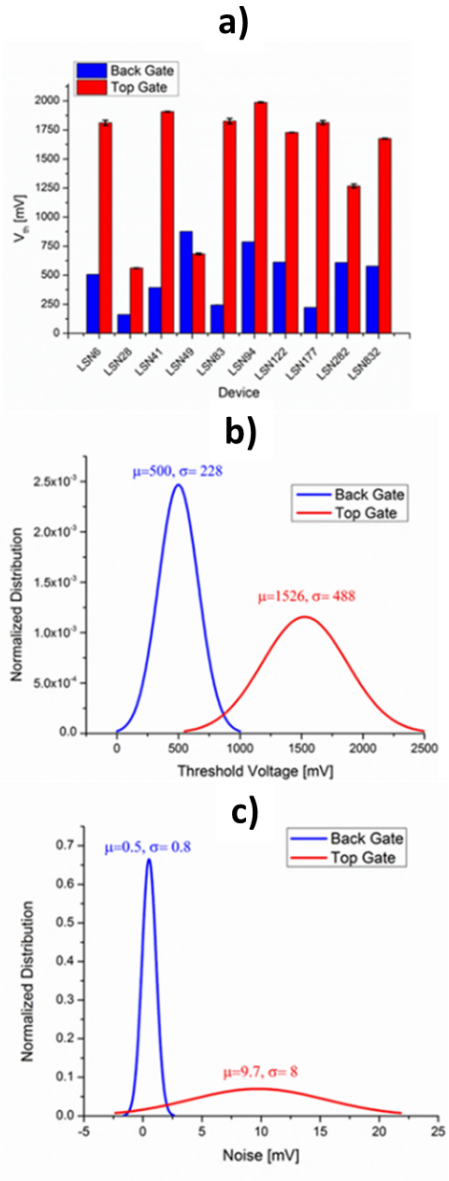

Figure 4.5: Electrical characterization of top- and back-gate for 10 different transistors in a stress test of 50 consecutive Id-Vg plots

4.3.2 Response to pH changes

Sensitivity to pH changes was measured for dual- and single-gate modes as surface potential changes. For the fluid-gate mode, the electrolyte potential is swept while the back-gate has a slight negative potential. On the other hand, in dual-gate operation the fluid potential is set to create an inversion channel in the front side of the DGFET while the back-gate is swept. Figure 4.6 (a) shows the single-gate Ids-Vfgs transfer characteristics for electrolytes with different pH values. The inset magnifies the region of voltages for a threshold current of 5 μA. Similarly, Figure 4.6 (b) shows the Ids-Vpgs transfer characteristics for the dual-gate mode and an inset with magnification at threshold voltages. Figures 4.6 (c) and 4.6 (d) show the surface potential changes as a function of pH with pH 7.32 as the origin or reference acidity. Each point in the figure is the average of five measurements and error bars are one standard deviation their standard deviation. The insets in Figures 4.6 (c) and 4.6 (d) are schematics illustrating that in the single-gate mode only the front side transistor is inverted (Figure 4.6 (c)) while in the dual-gate mode both sides are conducting (Figure 4.6 (d)).

Figure 4.6 (c) shows the typical linear response of the ISFET surface potential to pH changes, demonstrating a sensitivity of 52.9 mV/pH. On the other hand, Figure 4.6 (d) shows a nonlinear response to pH for the dual-gate operation. The nonlinear behavior is due to the relation between sensitivity to pH changes and the drain current ratio of the coupled transistors $[\Delta I_{top}/\Delta I_{bottom}]$. Since for a fixed electrolyte potential the current ratio is a function of pH, the sensitivity is also a function of the solution's acidity. For instance, at a fixed potential, higher pH values will reduce the drain current in an N-type ISFET. Higher pH values are correlated with higher OH^- concentrations which will reduce the number of inversion carriers in an N-type ISFET modifying the ratio of bottom / top transistor currents and in consequence changing pH sensitivity.

In addition, the surface potential to pH relation in the dual-gate mode shows an asymptotic behavior (Figure 4.6 (d)). As the pH increases, the top transistor current decreases and the back-gate side is forced to contribute more current to achieve the threshold that is used to extract the surface potential. The MOS side of the device is not sensitive to the electrolyte pH, so the device loses sensitivity as the bottom transistor becomes the dominant

source of drain current. Since at large pH values the top current is minimal, most of the drain current is coming from the bottom transistor, and therefore the sensitivity approaches zero explaining the asymptotic trend.

Figure 4.6 (d) also shows that the dual-gate mode has sensitivities above the Nernstian limit for certain range of pH values. For example, the sensitivity (or derivative of the asymptotic model) at pH 7.32 is 107.65 mV/pH and it increases for more acidic electrolytes. However, a greater sensitivity is also accompanied by larger noise. This is observed in Figure 4.6 (d) by the larger error bars for lower pH values. Therefore the ideal signal-to-noise is constrained to a window of pH values that is limited in one side by low sensitivities and in the other by large noise.

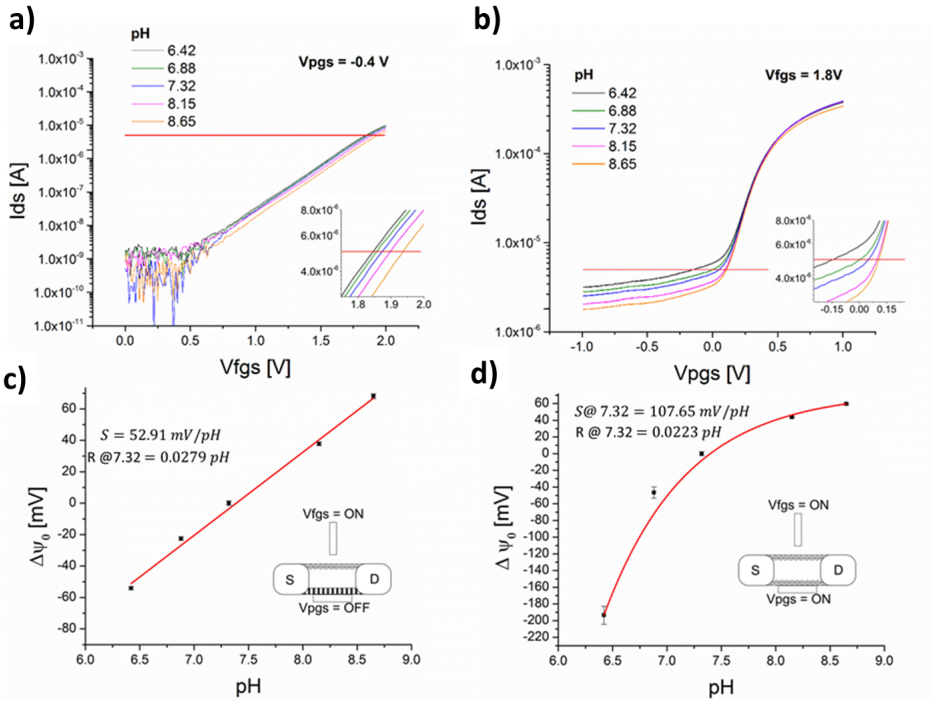

Figure 4.6: Measurement of transistor response to pH changes

4.3.3 Tailoring of biasing conditions

The amplification of sensitivity does not necessarily improve resolution because larger sensitivities are accompanied by increased noise. Therefore, to

enhance the signal-to-noise ratio it is necessary to optimize the biasing condition to find operation points where the noise sources are not being amplified as much as the sensitivity gains [135]. Figure 4.7 presents the results of a resolution optimization experiment. Figure 4.7 (a) illustrates the dual-gate mode surface potential to pH relationship for the same device under small differences of fluid-gate bias. Variations on the fluid bias modify the magnitude of drain current in the front transistor changing the current ratio and the pH sensitivity. Figure 4.7 (b) quantifies the sensitivity and resolution at pH 7.32 for the different fluid biases (Table 4.2 presents the constants of the extracted models). As expected, the sensitivity increases with increments in Vfgs since the top transistor contributes more to the threshold current. However it is interesting to note that the optimal resolution is observed for Vfgs = 1.775 V. With this biasing we obtain the best resolution of the five screened fluid biases. Figure 4.8 plots sensitivity, noise, and resolution as a function of the electrolyte pH comparing the single-gate and the tailored dual-gate modes. With Vfgs = 1.775 V and for a specific pH range, gains in sensitivity are greater than noise increments. The sensitivity and resolution of the single-gate mode are also plotted in Figure 4.3 to compare the performance of both operations for electrolytes with different pH. When compared to the single-gate mode, the dual-gate mode exhibits an improvement in signal-to-noise of a factor of $\sim$2X for the 7.32 pH (from $\sim$0.03 to 0.015 resolvable pH units). Similar exercises could be performed for other pH values to improve resolution for other electrolytes. Depending on experimental conditions like starting pH and expected pH change, the fluid-gate bias can be tailored to have optimal sensitivity and resolution.

To test the robustness and repeatability of the amplification method, the same pH characterization was done for 5 different transistors in both single- and dual-gate operation (Figure 4.9). In all devices there is a pH range of improved resolution when operated in the tailored dual-gate mode. However, the magnitude and range of the sensitivity enhancement vary between transistors. Our measurements indicate that the resolution improves by 20.3% on average when compared with the single-gate operation but the standard deviation is 19.1%. Variance in the top-gate threshold voltage and noise (as it is shown in Figure 4.5) may explain the lack of uniformity of the dual-gate resolution enhancement. However, the best resolution achieved with the tailored dual-gate operation is superior to that required for DNA sequenc-

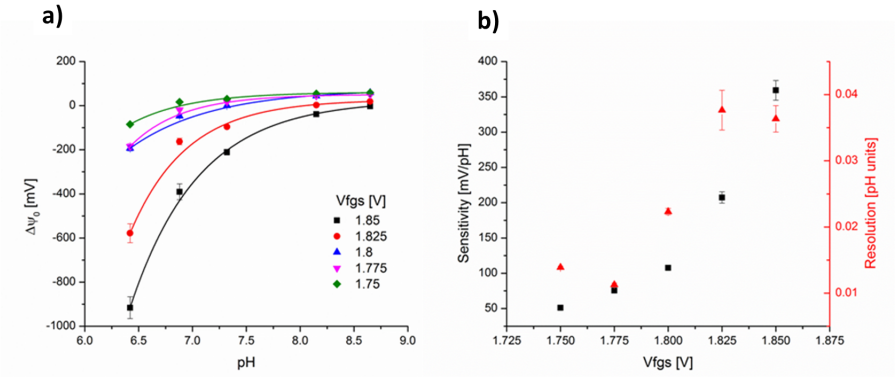

Figure 4.7: Tailoring fluid-gate bias to enhance resolution in the dual-gate mode

Table 4.2: Extracted asymptotic models of surface potential vs. electrolyte pH for the dual-gate amplification

Vfg [V]	**Extracted model f(x)** **Sensitivity S(x)**	R^2
1.75	$f = 128.8 - 1.97x10^7 * 0.16^x$ $S = -1.97x10^7 * 0.16^x ln(0.16)$	0.99
1.775	$f = 118.8 - 1.49x10^8 * 0.12^x$ $S = -1.49x10^8 * 0.12^x ln(0.12)$	0.96
1.8	$f = 141.4 - 1.24x10^6 * 0.27^x$ $S = -1.24x10^6 * 0.27^x ln(0.27)$	0.96
1.825	$f = 95.04 - 1.28x10^8 * 0.14^x$ $S = -1.28x10^8 * 0.14^x ln(0.14)$	0.97
1.85	$f = 93.07 - 2.34x10^7 * 0.20^x$ $S = -2.34x10^7 * 0.20^x ln(0.20)$	0.95

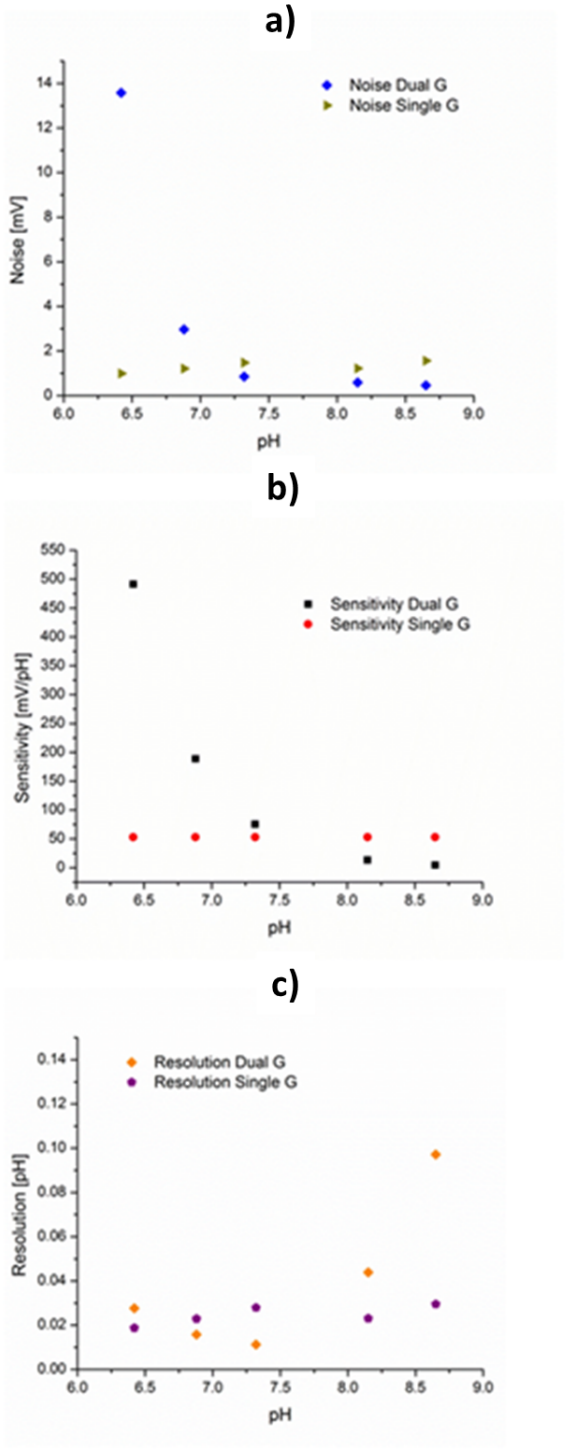

Figure 4.8: Comparison of single and tailored dual-gate operation pH response as a function of measured electrolyte

ing [127] and comparable to the inherently more sensitive nanowires [144]. Comparison of our results with other dual-gate approaches is complicated because, as Rajan et al. mentioned, noise analysis has only been recently adopted by the FET-biosensor and the reported sensitivity increments are not necessarily resolution improvements.

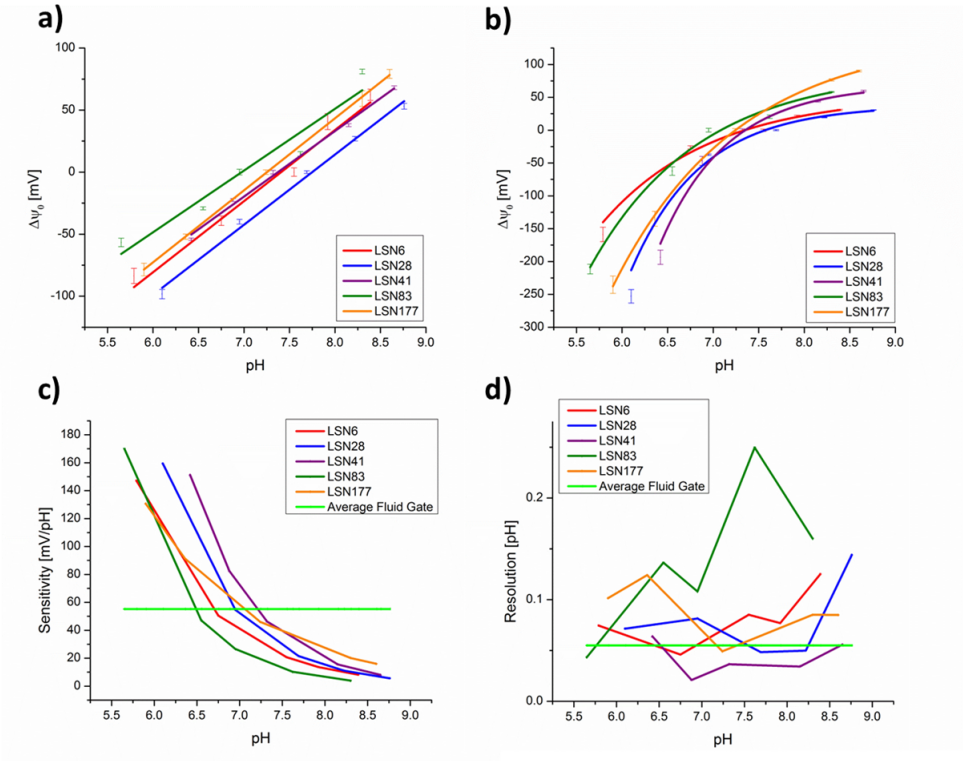

Figure 4.9: pH sensitivity characterization of multiple DGFET transistors

4.3.4 Label-free detection of LAMP reactions

Improved sensitivity and resolution enable more precise monitoring of biological reactions. To illustrate this principle, we compared the response of dual- and single-gate modes when monitoring pH changes of DNA amplification reactions. The incorporation of dNTPs into a growing DNA strand causes the release of hydrogen ions and pyrophosphates [127, 145]. This process has been thoroughly studied as a label-free sensing method of amplification and

has been used for DNA sequencing [6] and detection of specific mutations [65].

Experiments in Figure 4.10 show pseudo real-time amplification of the wzy gene of O111 STEC using loop-mediated isothermal amplification (LAMP). Starting in 2011, the US department of agriculture initiated a zero tolerance policy for a group of 6 non O157 STECs [146]. The O111 serotype is part of this so-called 'big six group' and has caused multiple outbreaks thereby becoming an important target for food safety control [147, 148]. Our lab has investigated detection methods for the 'big six' strands and the O111 type was used to evaluate and compare the performance of the single- and dual-gate operation of the fabricated ISFETs for monitoring a LAMP amplificaiton.

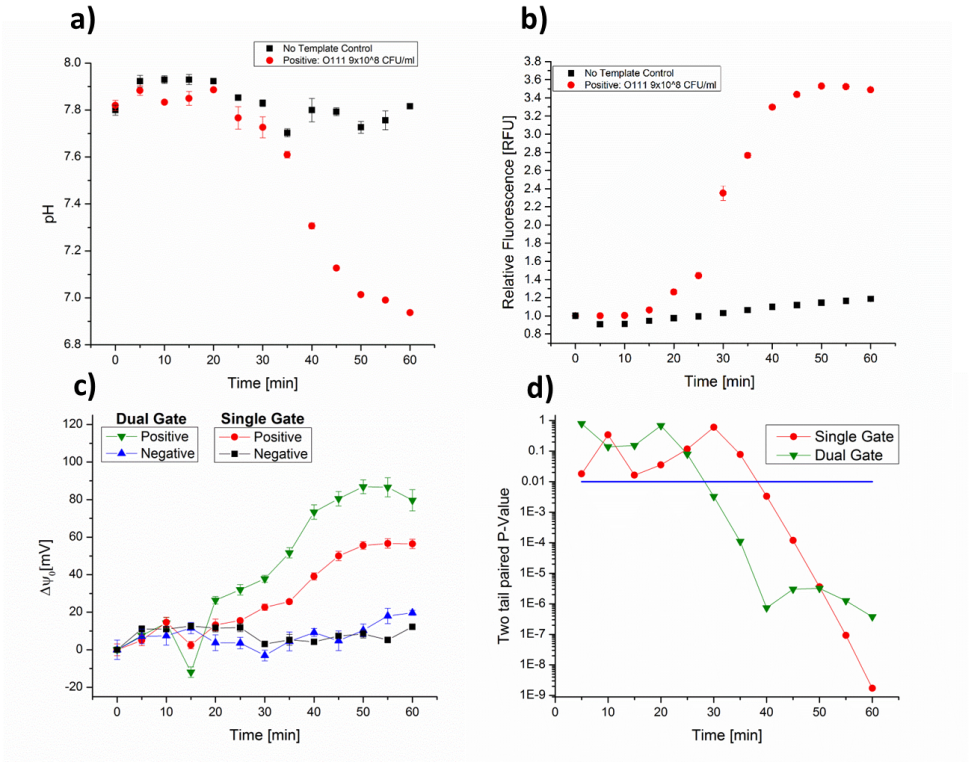

Figure 4.10: Pseudo real-time monitoring of LAMP DNA amplification of the wzy gene of O111 STEC

DNA amplification and simultaneous measurement of the transistor sur-

face potential presented challenges that hinder the comparison of dual- and single-gate modes. First, the heated stage that is used for on-chip amplification (mK1000 heated stage from Instec, Boulder, CO) introduces noise that obscures the small pH signals coming from the amplification reaction. Second, when performed on the silicon materials the DNA amplification reactions have lower yields due to non-specific adsorption of molecules that reduce the measured signal [149, 150]. Third, even though the solution is capped with mineral oil, the evaporation through the PDMS well causes a concentration of products that increases experimental noise. Therefore, a pseudo real-time LAMP (described in the methods sections) is performed to have a controlled experiment to evaluate the benefits of dual-gate ISFETs for reaction sensing.

Figure 4.10 (a) shows the measured LAMP solution pH as a function of time, Figure 4.10 (b) shows relative fluorescence for positive and negative samples (Figure 4.11 shows the fluorescence images), and Figure 4.10 (c) shows the surface potential change for dual- and single-gate modes as a function of time. Figures 4.10 (a) and 4.10 (b) show that solutions where amplification is expected turn more acidic and increase fluorescence intensity with reaction time. On the other hand, Figure 4.10 (c) shows that the surface potential is maintained relatively constant for negative solutions while measurements of positive solutions induce surface potential changes as a function of time. This means that the surface potential responds to pH changes induced by nucleotide incorporation which occurs only in LAMP samples with template DNA. The larger sensitivity of the dual-gate mode, which is achieved by tailoring the top and bottom current ratio of the device at the beginning of the experiment, produces surface potential changes that are larger than the ones in single-gate operation. This translates into a faster detection time because the dual-gate mode enables the differentiation of negative and positive samples faster than the single-gate operation. Figure 4.10 (d) shows the two tailored P-value calculated to compare negative and positive solutions for the dual and single-gate modes. The threshold is set at 0.01 or in other words when the null hypothesis of having two equal samples is rejected with 99% confidence. The P-value shows that the dual-gate operation allows us to establish statistical conclusions about 10 min faster than with the single-gate operation.

This result demonstrates the benefits of having an amplified sensitivity

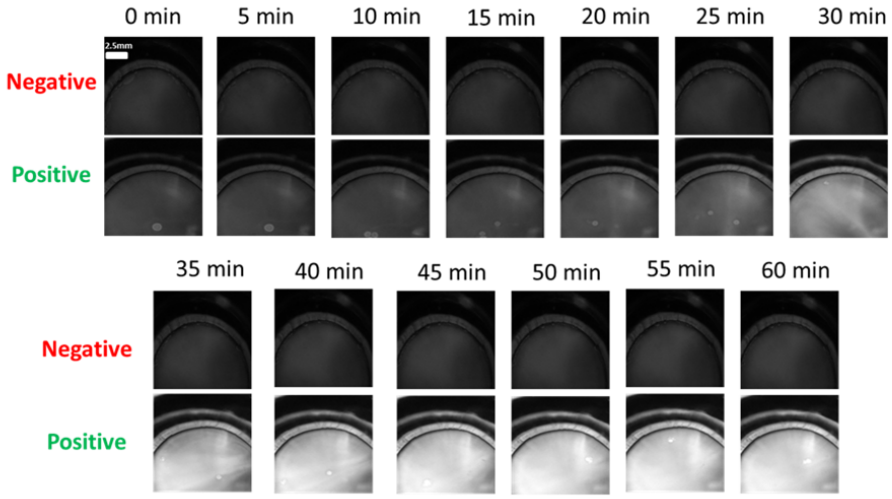

Figure 4.11: Progression of fluorescence images of positive and negative samples imaged on the chip during LAMP

especially in high-noise environments or protocols. For the pseudo real-time measurements, the dominant source of noise is not coming from the device itself but the measurement protocol and setup. Each time point is a different solution that was measured individually. This means that for each measurement there are small experimental changes like probe contact resistance, position of the reference electrode, and temperature changes that will introduce experimental noise to the surface potential measurement. In fact, these experimental variations become the dominant source of noise. The noise in experiments for pH characteristics (Figure 4.6) was in the order of 4 mV while the one for the DNA amplification experiment is about 12-19 mV. The experimental noise is not being amplified by the dual-gate operation and therefore a higher resolution is achieved with amplified sensitivity. Go et al. had similar predictions and observations when modeling dual-gate operation [130, 135]. If the sensor signal-to-noise ratio is limited by extrinsic sources of noise, the dual-gate offers superior resolution since the sensitivity increases without significant noise amplification. Go et al. also discussed the role of instrumentation noise and here we observe a similar extrinsic noise source which is the experimental procedure. In this case, the increased sensitivity amplifies the signal from the pH amplification without significant noise increments, and in consequence, differentiation of negative and positive samples is

faster for the dual-gate operation. This demonstrates that the signal amplification of the dual-gate operation allows improved monitoring of reactions, especially in noisy environments, enabling observation of smaller pH signals or reducing the reaction time needed to achieve conclusions. These attributes of the dual-gate mode are especially desirable for point-of-care and on-site applications. Diagnostic assessments that are performed outside a controlled environment (i.e. not in a standard laboratory) are required to operate under more aggressive extrinsic sources of noise and with low-precision instrumentation [151]. Then, for these applications the dominant source of noise will not be amplified in the dual-gate operation enabling greater resolution improvements. In addition, the improved detection time of the dual-gate operation enables a faster turnaround diagnosis that is essential for portable applications where subsequent actions are contingent on diagnosis [152]. Therefore, it is in the portable applications where true dual-gated ISFETs can provide greater SNR amplification improving the device performance. However, data in Figures 4.10 (c) and 4.10 (d) also demonstrates that the increased sensitivity is accompanied by a loss of linearity and a consequent reduction in dynamic range. After 40 min, the dual-gate response changes the trend of improved signal-to-noise suggesting that the new pH of the LAMP solution is outside the operation range where the dual-gate mode has improved resolution. Therefore, gains in sensitivity and resolution are offset by reductions in dynamic range and linearity of response.

4.4 Advantages of DG ISFETs for biological sensing and further optimization

We have presented a dual-gated ISFET with a true back-gate where the coupling of front and back transistors enables pH sensitivity amplification and enhanced resolution for determined biasing conditions and ranges. A novel fabrication process results in devices with standard MOSFET in the back-gate transistor and a high-K dielectric to interface the electrolyte. The devices are made in a conventional semiconductor foundry, making the fabrication process and the device structure suitable for rapid scalability and seamless incorporation of other electronic components. These transistors were operated in single- and dual-gate modes for pH measurements and bi-

ological reaction monitoring. The single-gate mode operation has the same linear pH response characteristics of regular ISFETs, but when operated in dual-gate mode the sensor response to pH becomes asymptotic due to the dynamic current ratios for different pH values. We show that for certain pH range, the dual-gate sensitivity is amplified more than the noise, yielding a higher signal-to-noise and enhanced resolution. Furthermore, we demonstrate that the operation point can be tailored by manipulating the fluid bias to minimize the resolution for a specific pH range and application.

We used the fabricated ISFETs to monitor a LAMP DNA amplification reaction in single- and dual-gate modes. The pH changes related to incorporation of nucleotides change the surface potential of the transistor enabling electrical label-free detection of DNA replication that is better monitored with the dual-gate operation. For the presented experiment, the noise is dominated by an extrinsic source and the greater sensitivity of the dual-gate mode yields an improved resolution that reduces the detection time which is established when the negative and positive samples are clearly differentiated. This new device and the dual-gate operation can be used as an electrochemical transducer for biological sensors that enable signal enhancement for better monitoring of reactions. The new structure has particular potential for applications targeting point-of-care diagnosis that are subject to noisy environments and require a fast turnaround. Future work will aim to maximize the resolution improvement and the pH range of operation of the dual-gated ISFETS by optimizing W/L ratio and top/bottom capacitances, and using arrays of devices to monitor the reactions.

CHAPTER 5

ON-CHIP QUASI-REFERENCE ELECTRODES WITH ELECTRODEPOSITED POLYPYRROLE

One of the main advantages of incorporating semiconductor technology to biological reactions is the opportunity to easily scale and multiplex reactions. The scalable nature of micro-fabrication processes and simple adaptation of integrated circuitry for parallel reading creates a simple path for a large number of reactions in a single chip. Field effect biosensors can improve processes where multiple reactions are run in parallel like drug discovery assays or pathogen/molecule screenings. There are still important challenges to be solved before transistors are used as transducers in multiple isolated reactions. For ion-sensitive field effect transistor (ISFET) the electrolyte needs to be referenced to set the electrolyte potential that forms a conduction layer on the silicon. Figure 5.1 shows a band diagram for ISFET transistors. The potential set by the reference electrode determines the electrolyte Fermi-level (E_f) and therefore the band bending in the silicon/insulator interface [153]. Conventional reference electrodes are bulky, fragile, and too big for applications where the electrolyte volume is small. Several researchers have proposed tackling this issue using planar micro-reference electrodes or a reference field effect transistor (REFET). However, these approaches are limited by poor robustness, high cost, or complex integration with other microfabrication processes. In this chapter we study quasi-reference electrodes and describe a simple method to create robust on-chip quasi-reference electrodes by electrodepositing polypyrrole on micro-patterned metal leads.

5.1 The challenge of electrolyte referencing

An important difficulty that has prevented the broad incorporation of ISFETs into biosensing systems is the practical limitation of the conventional reference electrodes that are required to operate the sensors [154]. Com-

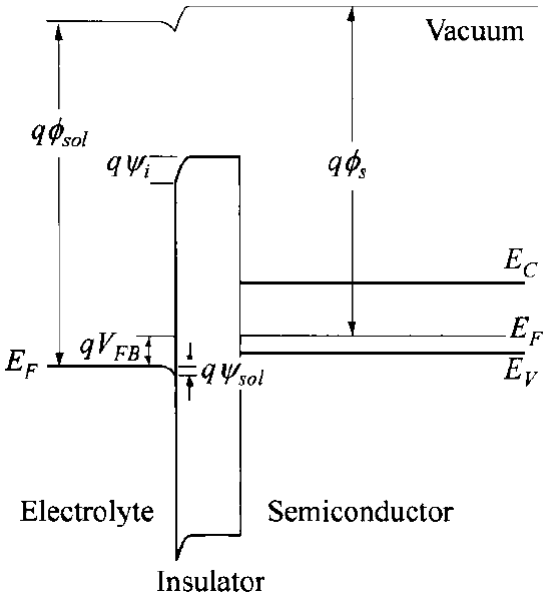

Figure 5.1: ISFET band diagram showing the effect of the electrolyte potential [153]

monly used Ag/AgCl reference electrodes are too big, fragile, and expensive for applications that use small volumes (e.g. droplets) or target portable/disposable devices [155]. To the replace Ag/AgCl reference electrodes, various micro-fabricated electrodes have been reported in the past [156]. For example, a combination of thin-film metal deposition and agar gel saturated with KCl was used to mimic Ag/AgCl electrochemical referencing mechanisms on a miniature solid-state planar electrode [157, 158]. Also, platinum has been treated with hydrogen gas, Nafion, and perfluorosulfonic acid polymer, to create reference electrodes for miniaturized electrochemical cells [159, 160]. In addition, greater miniaturization has been achieved with microscopic quasi-reference electrodes (a reference that does not have an established potential but varies predictably under certain conditions) [161] that have been fabricated with iridium oxide [162] and with polyvinyl chloride (PVC) as a passivation layer [163]. Despite good reported stability and reliability, these miniaturized reference electrodes are undermined by complex and expensive fabrication protocols that involve several micro-machining steps, complicated chemical processes, the use of expensive precious metals and reagents, or incompatibility with other processes involved in silicon transistor fabrication.

Therefore, due to a combination of complexity, cost, and process compatibility issues, it is unlikely that these previous approaches for miniaturization of reference electrodes will be successful alternatives to bias FET-based biosensors.

This chapter describes the fabrication of stable on-chip quasi-reference electrodes through the electrodeposition of polypyrrole (PPy) on patterned metals. The PPy coating process involves cyclic voltammetry to polymerize pyrrole on a metal electrode. The deposition method and the polymer characteristics were originally described by Bard et al., who reported PPy polymerization on platinum and stainless steel wires [164]. This technique has been adopted by many others to create quasi-reference electrodes for electrochemical experiments with small or localized volumes such as scanning electrochemical microscopy [165, 166]. We used a similar technique to create on-chip quasi-reference electrodes with photolithography patterned metals and evaluated their robustness and pH stability using open circuit potential measurements. Our results indicate that with the on-chip PPy electrodes random potential fluctuations are less than 1 mV, drift is typically between 1-2 mV/h, and potential changes due to pH variations are normally below 5 mV/pH. Other results demonstrate that the PPy deposition process is compatible with CMOS processes, and that operation of ISFETs with on-chip PPy is robust and sensitive. The electrodeposition of PPy was carried out both on precious (platinum, gold, and palladium) and non-precious metal microelectrodes (iron and nickel), demonstrating that the polymerization can be performed on metals that are currently used in a standard semiconductor foundry. Also, the PPy quasi-reference electrodes were fabricated on foundry ISFET chips and used to bias ISFETs during pH sensing experiments. The sensing performance of the transistors biased with on-chip PPy is similar to that obtained when the transistor is biased with Ag/AgCl. The similar results obtained with these two kinds of electrodes indicate that the high stability and low pH response of the PPy quasi-reference translates to the ISFET system, allowing robust operation of the transistor as pH sensor with a microreference.

5.2 Fabrication and evaluation methods of polypyrrole-coated microelectrodes

5.2.1 Electropolymerization of PPy

Partially oxidized PPy has been deposited in the past on platinum and stainless steel wires through a cyclic voltammetry deposition process for the formation of quasi-reference electrodes [164]. This technique is frequently used to form electrodes for scanning electrochemical microscopy assays [167]. We used a similar method to deposit the PPy on patterned metal leads to form on-chip quasi-reference electrodes. Figure 5.2 (a) shows a schematic of the three-electrode cell for PPy polymerization and deposition in patterned metal microelectrodes. A polydimethylsiloxane (PDMS) well is bonded to the silicon substrate, the on-chip metal is electrically contacted with a micromanipulator probe, a graphite rod is inserted in the solution, and a Ag/AgCl reference electrode (BASi, West Lafayette, IN) is bridged with a pipette tip filled with Agar gel and 0.1 M $NaClO_4$ for minimization of a liquid junction potential between the organic solvent and the aqueous filling solution in the reference electrode. The well is then filled with 400 μL of acetonitrile containing 10 mM pyrrole and 100 mM of Tetrabutylammonium hexafluorophosphate (all chemicals from Sigma-Aldrich). Figure 5.3 presents a photograph of the electrochemical cell used in the PPy polymerization on the microelectrode.

The three electrodes are connected to a Reference 600^{TM} potentiostat (Gamry Instruments, Warminster, PA) that performs cyclic voltammetry (CV), sweeping the potential from -0.6 to 1.2 V at a 0.1 V/s rate and an start/end potentials of 0.4 V. The CV process is repeated for the desired number of cycles, depositing the polymer on the working electrode. In every iteration, pyrrole is polymerized and a dark film of partially oxidized polypyrrole $PPy/PPy^{+}PF_{-}^{\pm}$ is formed on the exposed microelectrode.

5.2.2 Physical characterization deposited PPy

The polypyrrole film deposited in electrodes was characterized using profilometer and goniometer measurements, optical and SEM imaging, and X-

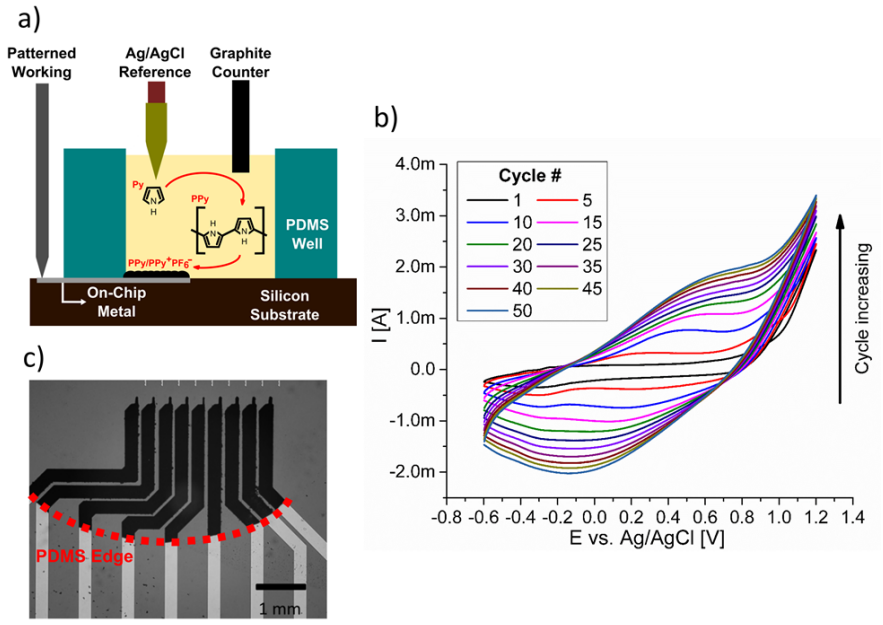

Figure 5.2: Electrodeposition of PPy on on-chip microelectrodes

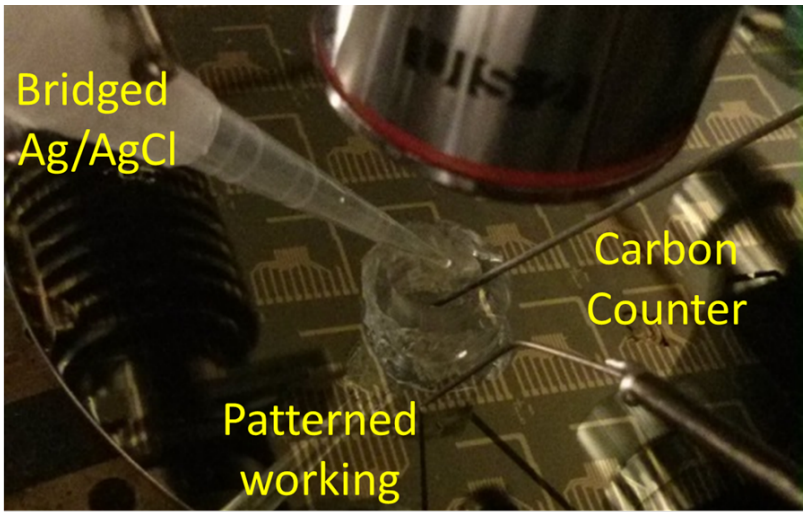

Figure 5.3: Photograph of the 3 electrode cell that was used for fabrication of the on-chip PPy quasi-reference electrodes

ray diffraction (XRD) analysis. The reported membrane thickness is the total indicator runout (TIR) obtained in a step-high profilometer measurement and the total height of the roughness profile (Rt parameter) is retrieved after applying 2CR filting to the acquired data. To assess hydrophilicity of the membranes, contact angle measurements were performed on larger electrodes to accommodate 3 μL DI-water droplets. In addition, bright field and SEM images of electrodes were taken after different numbers of PPy coating cycles to evaluate the growth of polymeric membrane. The area of the PPy electrode is estimated with the number of dark pixels in the bright field images quantified with ImageJ. Finally, to evaluate the structural composition of the deposited PPy film, XRD patterns of the electrodeposited polymer were obtained in a continuous scan from 5 ° to 105 ° in a PANalytical/ Philips X'pert MRD system.

5.2.3 Potentiostat open circuit potential measurements

Open circuit potential (OCP) measurements were taken to evaluate stability and response to pH changes of the fabricated on-chip electrodes. For stability experiments, the PDMS reservoir was filled with a 10 mM KCl solution, the Ag/AgCl (unbridged) electrode was used as the reference, and the on-chip metal was set as the working electrode. The potentiostat was programed to take OCP measurements every half second for one hour after the initial 10 min of stabilization, and each experiment was done 3 times. For the pH response analysis, the KCl solution in the PDMS reservoir was spiked with 10 mM HCl or NaOH during the OCP measurement and the pH value was calibrated with an InLab ® ultra-micro pH electrode (Mettler-Toledo, Columbus, OH). After the injection, the potential is allowed to stabilize for 10 min and the last 50 s of measurements are averaged to obtain the OCP value for each pH. A pH range of 5.5-8.5 was selected for sensitivity characterization experiments in order to model the behavior of electrodes in regular physiological buffers and a typical reaction mix of biomolecular assays such as DNA amplification [163].

The OCP measurements without pH changes are used to quantify stability, repeatability, and drift of the microelectrodes. Stability is the potential variation during a one hour experiment, and is determined by taking the

standard deviation of all measurements in an experiment. Repeatability is the variation across the different experiments and is calculated using the average of the standard deviations of measurements in three experiments. The drift measures the changes in potential as a function of time and is the difference of the recorded potentials at the beginning and the end of the experiment. Lastly, the reported pH sensitivity is the absolute value of the slope in a linear regression of the OCP vs. pH data

5.2.4 Extended-gate ISFET fabrication

ISFET devices were fabricated by Taiwan Semiconductor Manufacturing Company (Hsinchu, Taiwan) with a standard semiconductor process performed on silicon-on-insulator wafers. A complementary metal-oxide-semiconductor (CMOS) process forms the transistor in the device silicon layer. This process is followed by a metallization layer that defines contacts to drain/source nodes and a metallic extended gate that will act as the sensing region. Then, the top inter-layer dielectric is deposited and selectively dry-etched to create openings that reveal the metallic extended gate. The ISFETs are finalized with the deposition of atomic layer deposition (ALD) hafnium oxide over the entire wafer, creating the dielectric sensing membrane on top of the extended gate. The use of hafnium oxide as the sensing layer on ISFET pH sensors has been reported in the past. Our group demonstrated that ISFETs made with HfO_2 had a sensitivity of 56 mV/pH, with high linearity, over a range between pH 4-10 [168]. Other publications have also reported the use of HfO_2 as the sensing layer in ISFETs for larger ranges (pH 2-12) [169], and extended-gate transistors that use high-K dielectrics report high sensitivity and linearity [170]. In Figure 5.4 we present pH dependent transistor transfer curves of ISFETs to characterize performance of HfO_2 ISFETs used is this study.

5.2.5 Method to measure semiconductor sensors

To operate ISFETs, source, drain, and gate nodes of the transistors are connected to independent source measure units (SMUs) of a Keithley 4200scs (Keithley, Columbus, OH), and a PDMS well is plasma-bonded to the chip to

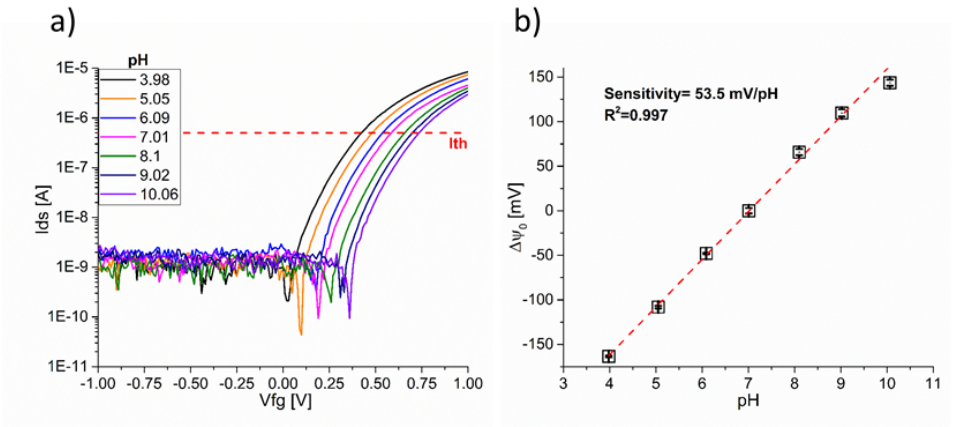

Figure 5.4: pH response of hafnium oxide ISFET using a leak-free Ag/AgCl reference electrode

hold the electrolyte solutions. The fluid-gate is swept from -1 to 1 V to obtain transfer characteristic curves that are used to extract threshold voltages using a constant-current extraction method defining $I_{th} = 300nA * \frac{W}{L}$, where $\frac{W}{L}$ is the transistor's aspect ratio [171]. In stability tests, the threshold voltage is measured every minute for an hour to quantify stability and drift. For pH sensitivity experiments, the electrolyte in the PDMS reservoir is titrated with 10 mM NaOH or HCl, and the resulting changes in the threshold voltage are correlated with surface potential to obtain the ISFET pH sensitivity. Testing buffers were selected in the range of pH 6-8 to model the sensor performance in physiological buffers, the master mix of molecular reactions such as PCR or LAMP, or solutions used in protein binding assays [18].

5.3 Assessment of polypyrrole microelectrodes for electrolyte biasing

5.3.1 Physical properties of deposited PPy

The electrodeposition of PPy in the patterned microelectrodes was carried out in the three-electrode electrochemical cell that is illustrated in Figure 5.2 (a). Cyclic voltammetry between working and counter electrodes referenced to a bridged Ag/AgCl creates a dark film of partially oxidized PPy in the

electrodes that is exposed to fluid. Voltammograms from a typical CV deposition process are presented in Figure 5.2 (b), which shows the expected shape of CV curves and larger peak/valley currents as the PPy film grows [164, 172]. Figure 5.2 (c) shows PPy-coated platinum microelectrodes on an oxidized wafer. Each electrode was set as the working electrode in independent polymerizations, showing that the process is repeatable and will cover the full electrode that is exposed to the acetonitrile solution.

Figure 5.5 presents results of PPy film characterization analysis. Profilometer measurements were carried out on electrodes with different deposition cycles to assess the evolution of the PPy film thickness and roughness. Figure 5.5 (a) shows that the film quickly grows to a few microns in the initial cycles and proceeds to grow linearly in subsequent iterations, reaching around 25 μm at the end of the 50^{th} cycle. A similar trend is observed in the roughness of the growing film. Figure 5.5 (b) shows that a thicker layer is correlated with a rougher electrode, indicating uneven growth of the PPy layer. In addition, Figure 5.5 (d) shows that more cycles result in more hydrophilic electrodes. The well-known enhancement relationship between roughness and wettability [173] explains the observed trend of lower contact angles as the hydrophilic PPy layer becomes rougher. The high wettability of the PPy electrodes will simplify their use for applications that use small volumes or droplets. Contact between an on-chip electrode and small volumes can be cumbersome with other approaches that use hydrophobic membranes and therefore would require structures for volume confinement [174].

Figures 5.5 (e) and 5.5 (f) are bright field and SEM images of electrodes with different CV deposition cycles. They reveal the uneven and isotropic growth of the polymer layer. The bright field images show that electrodes with more PPy have a larger area and an irregular shape. Figure 5.5 (c) presents the quantified relative growth of the electrode area as a function of the number of polymerization cycles. It shows that during the initial cycles the measured area is equivalent to the patterned electrode indicating that the PPy film grows mostly perpendicular to the substrate. However, in later cycles the PPy layers grow stacked on top of each other resulting in the observed isotropic growth. Figure 5.5 (f) zooms in on the left portion of the electrode array (for 0, 10, and 50 cycles) and clearly shows that the PPy film becomes thicker and rougher as it grows. The isotropic growth and variability of the deposition process will limit the spatial resolution of the

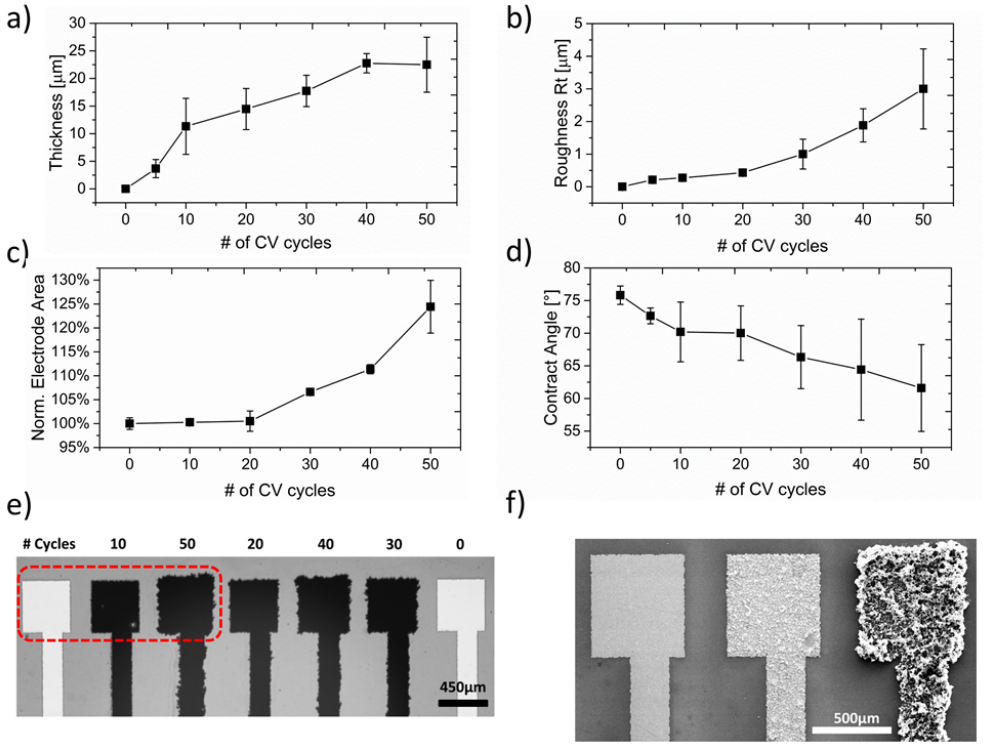

Figure 5.5: Characterization of the deposited PPy film

PPy electrodes. The horizontal growth of the polymer (parallel to the chip) may cause undesired shorts between patterned electrodes and PPy coating of regions adjacent to electrodes. Therefore, the design of photolithography masks for the lift-off process must take into account this lateral growth and provide adequate spacing between electrodes and on-chip features to prevent shorts or undesired PPy coating during the electropolymerization. In addition, Figure 5.6 shows X-ray diffraction patterns for PPy films deposited on platinum and nickel patterned electrodes. In both cases we observed expected peaks from metal and substrate in addition to peaks at around 24 °C. These peaks arise from the π-bonds interaction of the PPy chains and correspond to a 'd' spacing of 0.38 [175]. These results indicate that the on-chip electrodeposition yields a normal PPy film that can be used in the electrochemical operations.

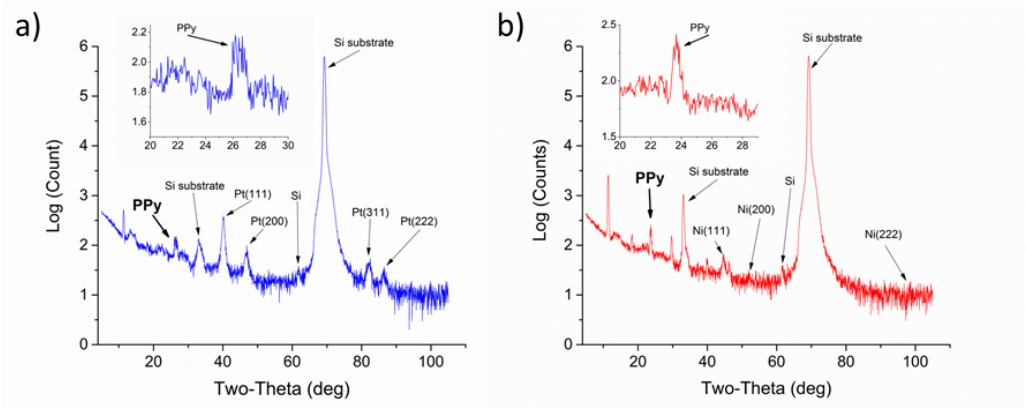

Figure 5.6: X-ray diffraction pattern of the deposited PPy

5.3.2 Stability of PPy microelectrodes

The stability of on-chip microelectrodes fabricated with different metals, with and without the PPy film, was quantified with open circuit potential (OCP) measurements against a standard Ag/AgCl reference electrode. For each experiment, OCP measurements were collected for one hour because biochemical reactions that are monitored with ISFETs, such as DNA amplification [176] or protein binding [177], normally occur within that time frame. Figure 5.7 (a) shows the measured OCP as a function of time for platinum and gold electrodes with and without PPy. The same figure also shows an OCP stability measurement between two Ag/AgCl electrodes that is used as a benchmark. Data in Figure 5.5 (a) is presented in the form of 'bands' where the thickness is correlated to repeatability of OCP measurements. Each time point for all 5 datasets represents 3 averaged experiments at the same time point with the calculated standard deviation plotted as the error bar. The error bars, which are in close proximity because measurements were taken every half second, create the effect of a thick band. Therefore, the thickness of each band is a representation of the electrode repeatability, and variations in the profile represent the electrode stability. Comparative quantifications of stability and drift are in Figure 5.7 (b) and 5.7 (c). The PPy coating makes the electrodes more stable, reducing the variability by around one order of magnitude, and substantially reduce drift. The best results were obtained with PPy coated platinum that has stability and drift comparable to the commercial Ag/AgCl electrode. Although the commercial reference electrode is

better than those fabricated with polypyrrole, their stability and possibilities for miniaturization make the PPy electrodes an interesting alternative to the conventional reference electrodes for ISFET operation.

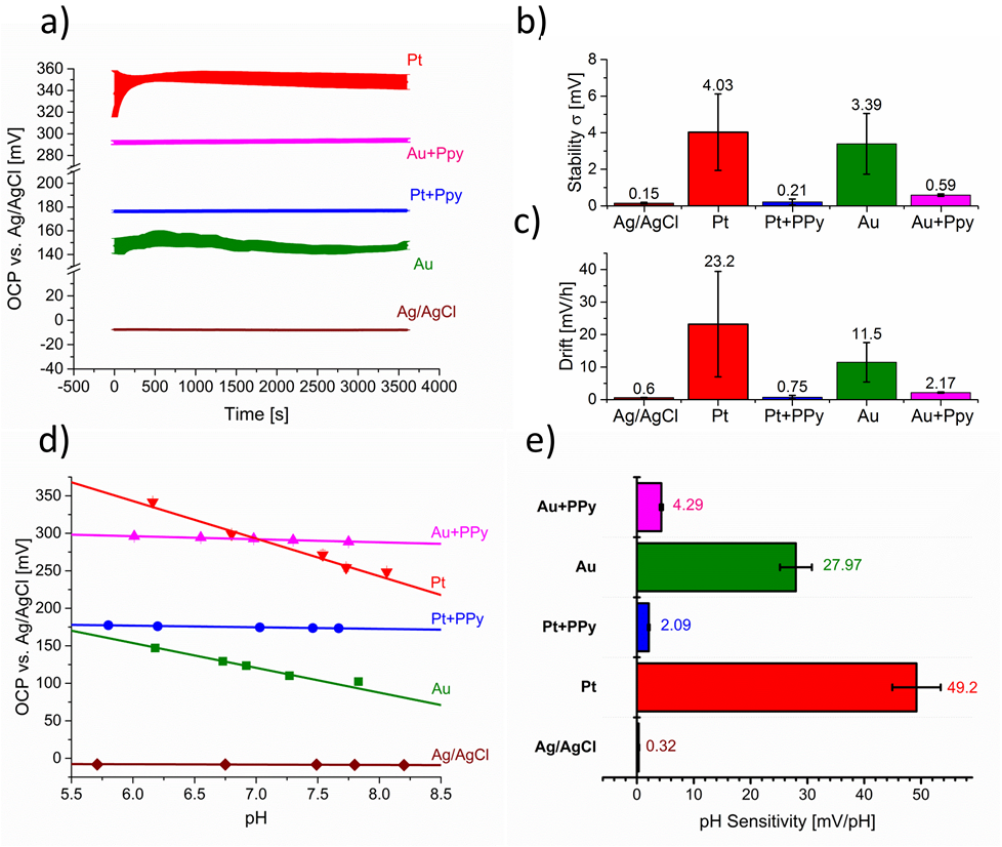

Figure 5.7: Open circuit potential (OCP) measurements of electrode stability and pH sensitivity

5.3.3 Quasi-reference electrode pH sensitivity

Besides providing a stable potential during the experiment, a reference electrode needs to sustain a constant voltage despite changes in the electrolyte [155]. Figure 5.7 (d) presents the pH sensitivity of gold, platinum, and Ag/AgCl electrodes measured by tracking the OCP as a function of the solution's acidity. Individual plots for each experiment with a different scale that show details of the pH response for each electrode are in the supplementary Figure 5.8. The ideal reference electrode response to pH changes is the one observed for the Ag/AgCl reference electrode. With this electrode,

despite electrolyte pH variations, the OCP potentials are within 1 mV, resulting in a very low pH sensitivity. This is a consequence of the Nernst equation for the Ag/AgCl electrode that is independent of H^+ ions. Experiments with other electrodes show potential variations as a function of pH. The deprotonation and protonation of the electrode's surface are a function of the solution's pH and affect the electrode-localized potential, resulting in pH-dependent OCP [178]. Other publications have reported similar trends and sensitivity quantification of metal electrodes to pH changes [179]. However, electrodes coated with the PPy film are substantially less sensitive to pH changes than their bare metal counter parts. The partially oxidized PPy film deposited on the on-chip electrodes is posed by the half reaction $PPy/PPy^+ + e \longleftrightarrow PPy + A^-$ that allows exchange of ions to sustain a stable potential [164]. The pH titration experiments are summarized in Figure 5.7 (e), which compares pH sensitivity of different electrodes. Potentials measured with platinum electrodes are known to have high pH dependence [163], but after the PPy polymerization the pH sensitivity is reduced by more than 10 times. A similar pH sensitivity reduction is observed for the gold electrode. The PPy layer brings new ion dynamics that result in low pH sensitivities that are significantly smaller than in bare metal electrodes and are required to reference an ISFET.

5.3.4 Referencing electrodes made with non-precious metals

Lack of compatibility with semiconductor processes and high manufacturing costs explain why previously reported strategies to create on-chip reference electrodes have not been fully adopted for ISFET operation [180]. The PPy deposition process has been widely reported in gold and platinum wires, but to reduce cost and enable simpler implementation it is necessary to perform the electrodeposition process in regular metals used in the CMOS process. The electrodeposition of PPy has been also carried out on a stainless steel wire [164] and others have reported deposition on aluminum at the expense of modifying the electrolyte solution, adding polishing steps, and using electron transfer mediation techniques [181]. To facilitate adaptation of the PPy reference microelectrodes to other standardized fabrication techniques, we attempted the same simple PPy deposition process, used in gold

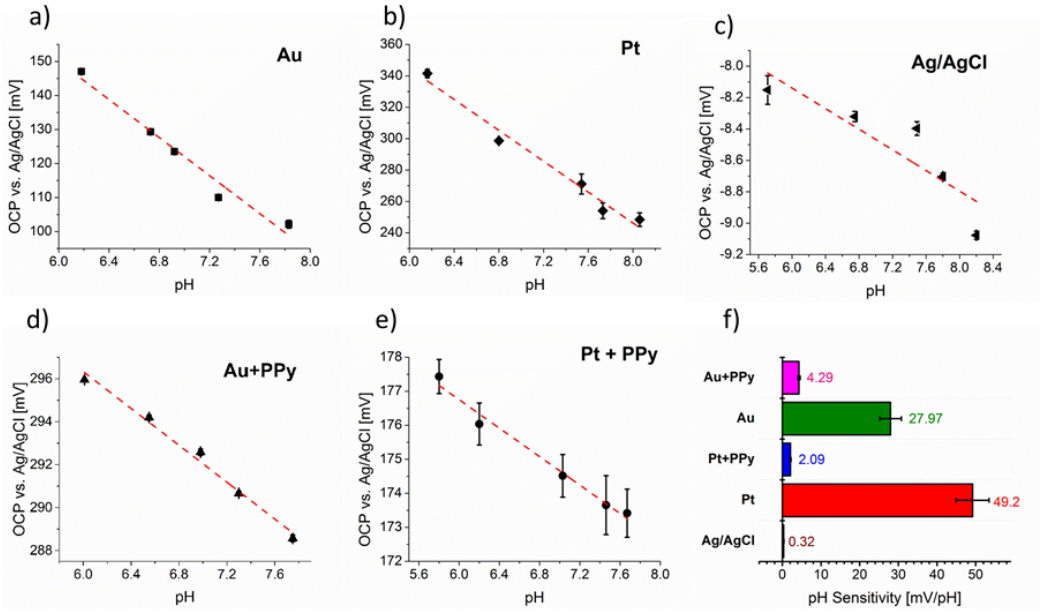

Figure 5.8: pH sensitivity of on-chip electrodes with and without PPy, and a Ag/AgCl benchmark

and platinum, in metals compatible with CMOS microfabrication steps and evaluated their performance. The PPy polymerization was also performed on palladium on-chip microelectrodes. Although it is an expensive precious metal, palladium has been used to improve reliability and thermal stability of contact electrodes in MOSFETs and can be incorporated in the CMOS semiconductor processes [182]. Results are presented in Figure 5.9, which shows normal cyclic voltammograms during the deposition process, stable OCP measurements, and a substantial reduction in the pH sensitivity. The next polymerization experiment was performed in iron microelectrodes. The previous polymerization of the PPy layer in steel suggested that iron, which is not currently used for CMOS processes but is an inexpensive commodity material, could be used as a microelectrode in the deposition process. Figure 5.10 shows that despite irregular cyclic voltammograms and unexpected reduction of peak currents during the CV process, the deposition of PPy drastically improves stability and pH sensitivity of the electrode. This shows that the PPy coated iron is a stable quasi-reference electrode with performance equivalent to that of the PPy electrodes that use precious metals.

The CV polymerization experiments were also performed with metals that

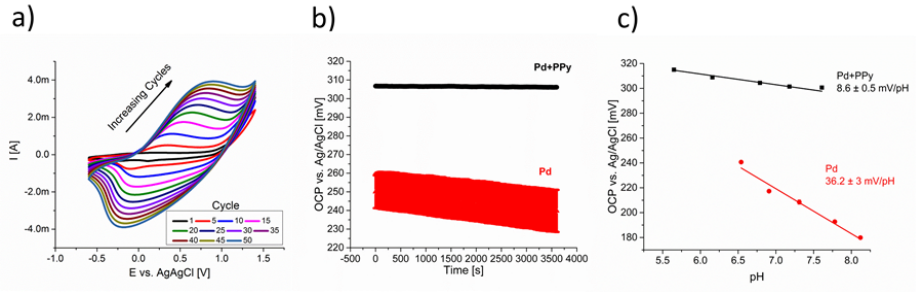

Figure 5.9: Deposition on palladium microelectrodes and electrical characterization

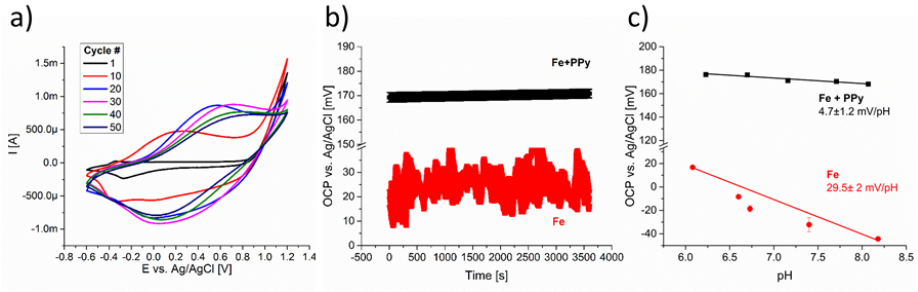

Figure 5.10: Deposition on iron microelectrodes and electrical characterization

are commonly used in semiconductor foundries. Electrodeposition of PPy on metals that are currently used for metallization layers in the CMOS manufacturing process would facilitate the inclusion of these electrodes in the foundry fabrication process to create on-chip quasi-reference electrodes. In this case, electrodes could be easily created in a new metal layer in the surface of the chip that would be coated with PPy using the cyclic voltammetry electrodeposition, with no need of additional masks or lithography steps. With the same deposition protocol described above we were able to deposit the PPy film on nickel microelectrodes but not on copper, titanium, or aluminum. Although nickel is not used for metal leads in the CMOS process, it is commonly used to create low-resistance nickel-silicide contacts that interface silicon and metal layers in the source and drain nodes [183]. Figure 5.11 (a) presents the deposition voltammograms on nickel, showing the expected trend of greater peak currents as the layer grows. These curves also show a secondary process around -0.2 V in reduction. Nevertheless, that process is eliminated in the later cycles, and the final voltammograms are similar to those observed in the deposition on precious metals. Figure 5.11 (b) presents the stability measurements and Figure 5.11 (c) shows the pH sensitivity results for both bare nickel and nickel coated with the PPy layer. Once again, quantification of the stability and pH sensitivity demonstrate that the PPy layer significantly reduces potential variations and the response to pH changes of the nickel electrode, demonstrating that once the polymeric film is deposited it will dominate the electrochemical exchange.

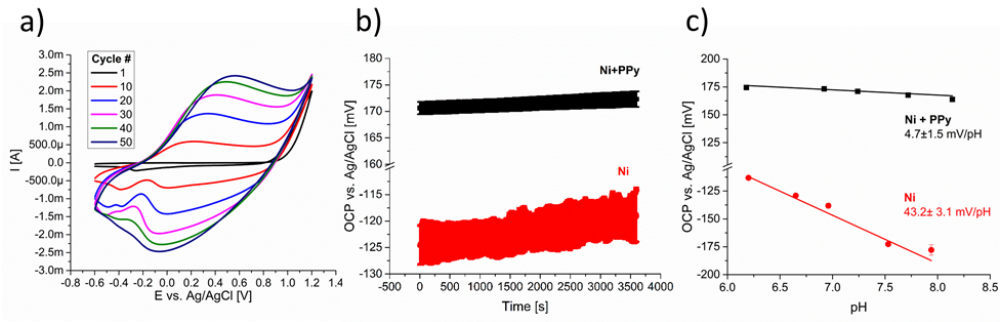

Figure 5.11: Polymerization of PPy on nickel electrodes and electrical performance evaluation

The electrodeposition of PPy in the other metals typically used in semiconductor foundries suffered from low metal reduction potentials that resulted in

the dissolution of the metal thin-film during the CV process, or high resistivity of metals and metal oxides that prevented PPy film formation. Previous publications have described other approaches to deposit PPy on these metals [181, 184, 185]. Nevertheless, those methods were not pursued because they include additional steps that would complicate the deposition process, undermining desired CMOS compatibility and protocol simplicity. The results of the attempted electrodepositions on copper, aluminum and titanium, are presented in Figures 5.12- 5.14.

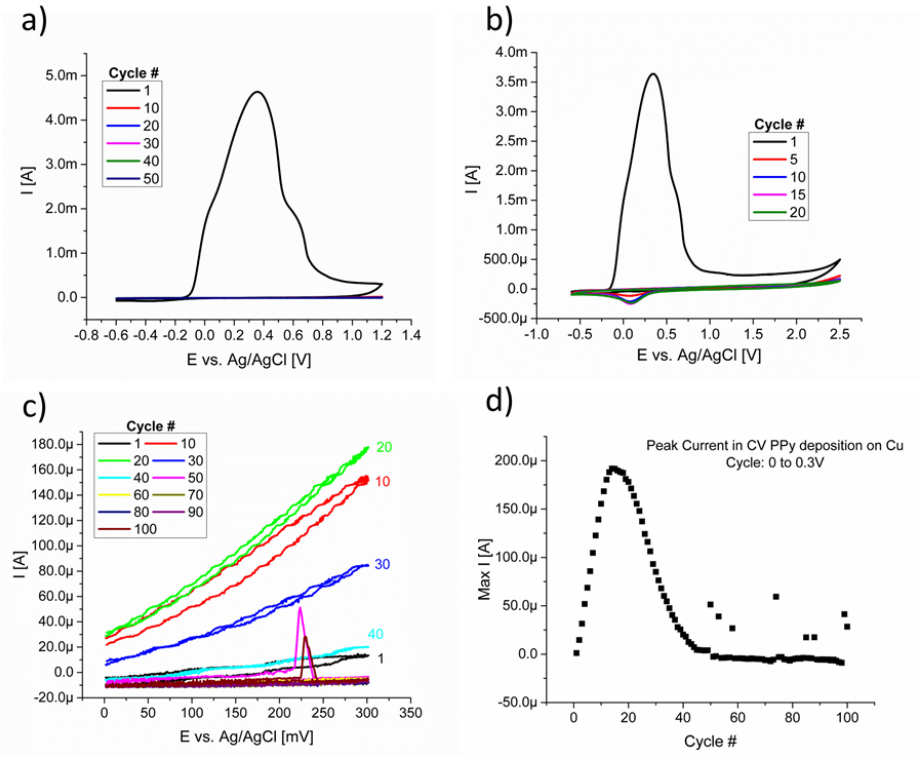

Figure 5.12: Attempted deposition of PPy on copper

Table 5.1 summarizes the stability and pH sensitivity data for all the electrodes where PPy polymerization was successful, including data for their bare metal counter parts. For all metals, the metal/PPy electrodes presented better stability, improved repeatability, lower drift, and reduced pH response. It is important to note that pH sensing with bare metal electrodes was in general unreliable and only linear within short pH ranges. However, the pH sensitivity evaluation through linear regressions of OCP vs. pH data created a standard metric that enabled comparisons between electrodes and demon-

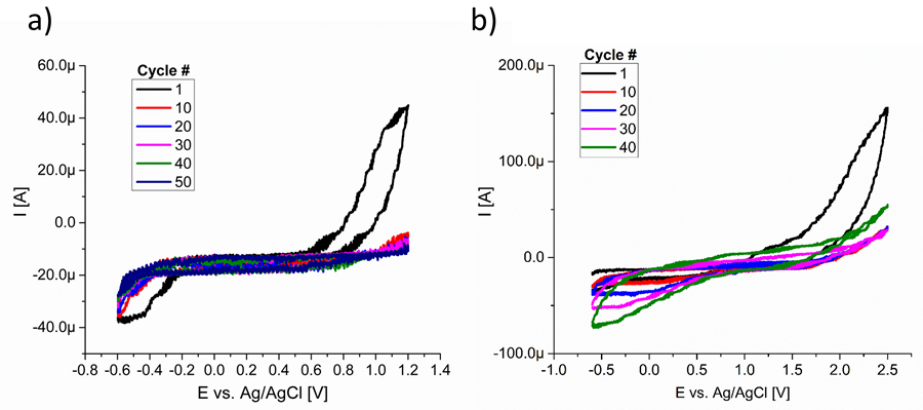

Figure 5.13: Attempted deposition of PPy on titanium

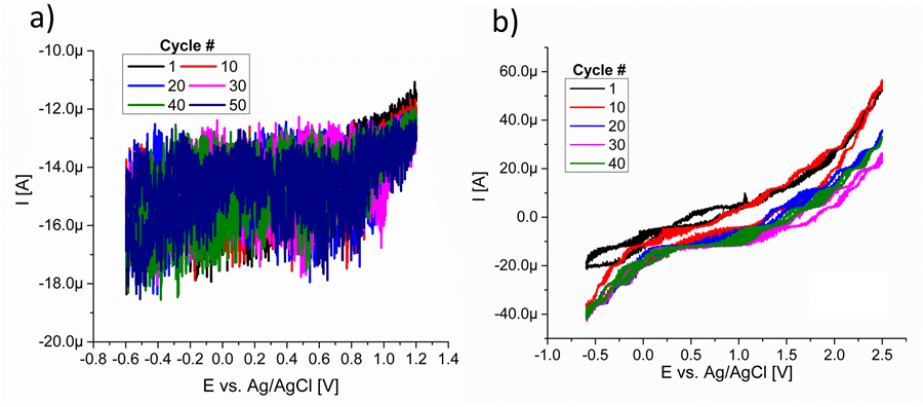

Figure 5.14: Attempted deposition of PPy on aluminum

Table 5.1: Summary of stability, repeatability, drift, and pH sensitivity of electrodes made with different metals and with/without the deposited PPy film

Electrode	Stability [mV]	Repeatability [mV]	Drift [mV/h]	pH sensitivity [mV/pH]
Platinum	4.03 +/- 2.09	6.10 +/- 1.82	23.2 +/- 16.2	49.2 +/- 4.25
Platinum+PPy	0.21 +/- 0.16	0.67 +/- 0.17	0.75 +/- 0.53	2.09 +/- 0.16
Gold	3.38 +/- 1.66	4.22 +/- 1.19	11.5 +/- 6.07	27.97 +/- 2.81
Gold+PPy	0.59 +/- 0.06	1.63 +/- 0.05	2.17 +/- 0.18	4.29 +/- 0.28
Palladium	3.32 +/- 0.42	10.7 +/- 0.42	10.6 +/- 0.52	36.2 +/- 3.5
Palladium+PPy	0.21 +/- 0.12	0.48 +/- 0.13	0.92 +/- 0.43	8.61 +/- 0.57
Nickel	1.72 +/- 0.35	3.64 +/- 0.4	7.12 +/- 1.5	43.19 +/- 3.12
Nickel+PPy	0.51 +/- 0.10	1.28 +/- 0.08	1.73 +/- 0.36	4.7 +/- 1.56
Iron	6.91 +/- 1.11	5.37 +/- 2.8	35.8 +/- 7.25	29.5 +/- 2.03
Iron+PPy	0.44 +/- 0.06	1.87 +/- 0.05	1.57 +/- 0.26	4.71 +/- 1.23

strated a clear reduction of the pH sensitivity with PPy electrodes. The main conclusion to be drawn from Table 5.1 and from the different OCP experiments is that patterned microelectrodes coated with PPy are more stable and less sensitive to pH changes than the metal-only electrodes. Therefore, PPy electrodes are better candidates for on-chip quasi-reference electrodes to operate ISFETs.

5.3.5 Operation of ISFET with PPy electrodes

Platinum microelectrodes were patterned on ISFET chips with standard lift-off. The same electrochemical cell used for other PPy depositions on electrodes (Figure 5.2 (a)) was used for the ISFET chip. A PDMS well is bonded to the top of the die with ISFETS and is filled with the acetonitrile solution. Then, the graphite counter and the bridged Ag/AgCl electrodes are placed inside the well. The deposition cyclic voltammograms are similar to the others reported previously but have lower current peaks because the electrodes on the ISFET chip have a smaller area than the testing structures (Figures 5.18). On the same chip, platinum leads were coated with PPy but others were left exposed for comparative measurements. The result is presented in Figures 5.15 (a), which shows an extended gate ISFET surrounded by a PPy electrode and an exposed platinum electrode close to the sensing

area.

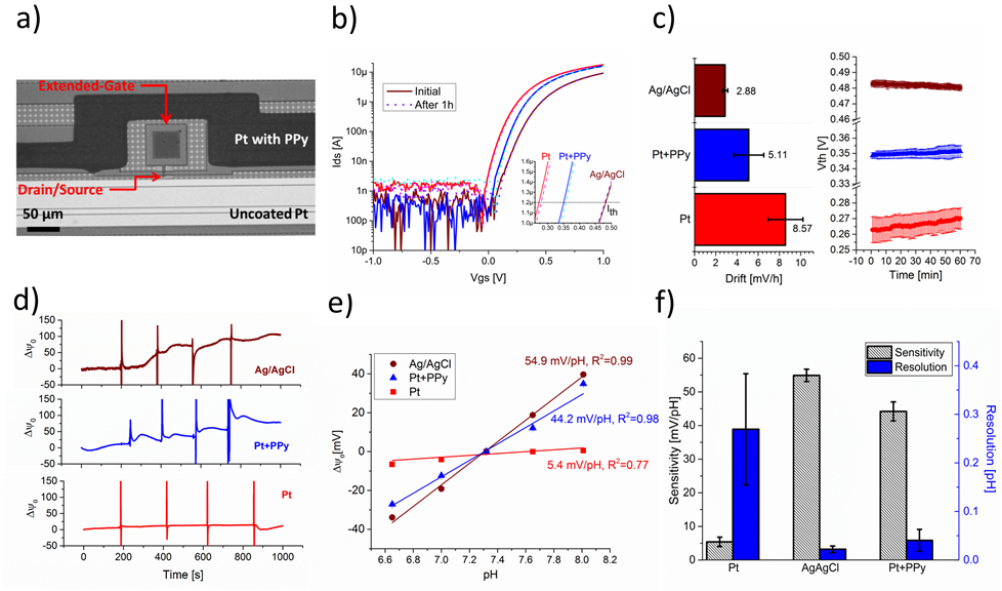

Figure 5.15: Evaluation of ISFET operation with PPy microelectrodes

After the polymerization process, the acetonitrile solution is switched to a 10 mM KCl solution for stability and pH experiments. To modulate drain current, the transistor's fluid-gate is biased with the on-chip electrodes (platinum and PPy) and also with a commercial Ag/AgCl reference electrode. Transfer characteristics of the transistor are presented in Figure 5.15 (b)), where the inset zooms in the region of threshold current to obtain Vth. Operation with the 3 electrodes yielded standard transfer characteristics similar to those from other devices with the same fabrication process. The stability of the transistor is evaluated by measuring transfer characteristics every minute for an hour with each electrode in 3 separate experiments. The extracted threshold voltage as a function of time is plotted in Figure 5.15 (c)), along with bars that quantify the threshold voltage drift. As expected, the best stability results are obtained with the commercial Ag/AgCl electrode, the worst with the bare platinum electrode, and intermediate results with the PPy electrode. It is clear that the potential applied to the transistor is more stable and repeatable when the patterned platinum is coated with PPy. Also, the voltage variations and drift are greater in the ISFET experiment than in OCP measurements. This indicates that new noise sources related to the ISFET operation, such as thermal voltage fluctuations or stochastic

electrochemical interactions in the gate oxide [186], diminish the transistor's voltage stability.

Evaluation of the ISFET pH sensitivity was performed by measuring threshold voltage variations due to pH changes and correlating them with the change in the oxide surface potential. The same evaluation was performed by biasing the solution with the platinum, PPy, and Ag/AgCl electrodes to compare ISFET pH sensing performance. Figure 5.15 (d)) shows the extracted surface potential as a function of time while the electrolyte pH is changed by titrating NaOH and the full pH-dependent transfer curves are presented in Figure 5.16. Even though there is a clear pH response with the Ag/AgCl and PPy electrodes, the high pH sensitivity of the platinum electrode counteracts the ISFET response reducing the recorded surface potential changes in the ISFET. This same behavior has been reported previously and constitutes a strong argument against using platinum electrodes as quasi-reference electrodes for pH monitoring with ISFETs [163]. The quantification of the pH sensitivity is presented in Figure 5.15 (e)), which plots normalized changes in surface potential as a function of the electrolyte pH for the three electrodes. The linear regressions quantify sensitivity and show that the ISFET has sensitivity close to the Nernstian limit when operated with Ag/AgCl, a lower but similar response with the PPy electrode, and very low sensitivity with the platinum electrode. This quantification underscores the importance of minimum pH response of the quasi-reference electrodes. Good ISFET operation is achieved when only the transistor's surface potential changes as a function of the electrolyte pH. Otherwise, other secondary interactions between potentials can undercut pH sensitivity and the ISFET performance. Figure 5.15 (f)) compares the pH sensitivity and resolution of ISFETs biased with the different electrodes. The pH resolution is defined as the ratio of noise to sensitivity $\Delta pH_{min} = \sigma\psi_s/S$ where $\sigma\psi_s$ is the average of potential fluctuations in each pH measurement (noise), and S is the extracted sensitivity. From this plot we conclude that ISFET pH sensitivity can be greatly improved by coating the microelectrode with the PPy layer. The greater stability and lower dependence of the PPy/electrolyte potential to pH changes result in the ability to sense smaller pH fluctuations (of around 0.04 pH units), which would translate into faster response times and lower detection limits in the biochemical assays. Therefore, the addition of the PPy layer turns patterned microelectrodes into a robust reference for ISFET operation.

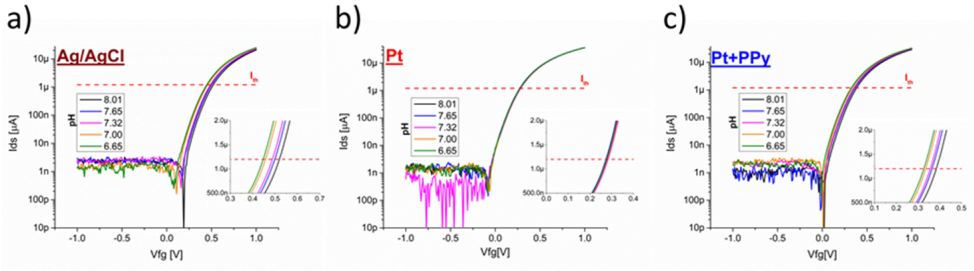

Figure 5.16: pH-dependent transfer curves of ISFET biased with different reference electrodes

A similar pH sensing evaluation was performed for ISFETs operated with nickel-based electrodes. Cyclic voltammograms of the PPy deposition on nickel microelectrodes are presented in Figure 5.18 that shows expected shapes but low current. Figure 5.17 presents measured sensitivity and stability of an ISFET biased with a Ni+PPy electrode and compares it with results obtained using a bare Ni microelectrode. Figure 5.17 (a) shows pH-dependent transfer curves when the ISFET is operated with a Ni+PPy electrode. As shown in Figure 5.17 (b), the sensitivity quantification yielded a surface potential change of 39 mV/pH. This is significantly larger than the 15 mV/pH obtained with bare Ni. In addition, the Ni+PPy electrodes are more stable than the bare Ni counterpart. Figure 5.17 (c) shows the ISFET threshold voltage as a function of time during one hour, demonstrating that measurements performed with Ni+PPy electrodes are more repeatable and have lower noise levels. Comparative measurements of pH resolution and total drift are presented in Figure 5.17 (d) that summarizes the characteristics of Ni+PPy electrodes. The fine pH resolution and low threshold voltage drift of the ISFET biased with Ni+PPy are consistent with the low pH dependence and high stability observed for coated nickel electrodes in OCP measurements. With both Ni and Pt the electrodeposition of PPy on the patterned electrodes created a robust reference that translates into higher sensitivities and lower noise levels.

The PPy electrodes are well-suited to be efficient on-chip quasi-reference electrodes for ISFET fabrication and operation. The stability and lack of pH response of the PPy electrodes is complemented with a simple and in-

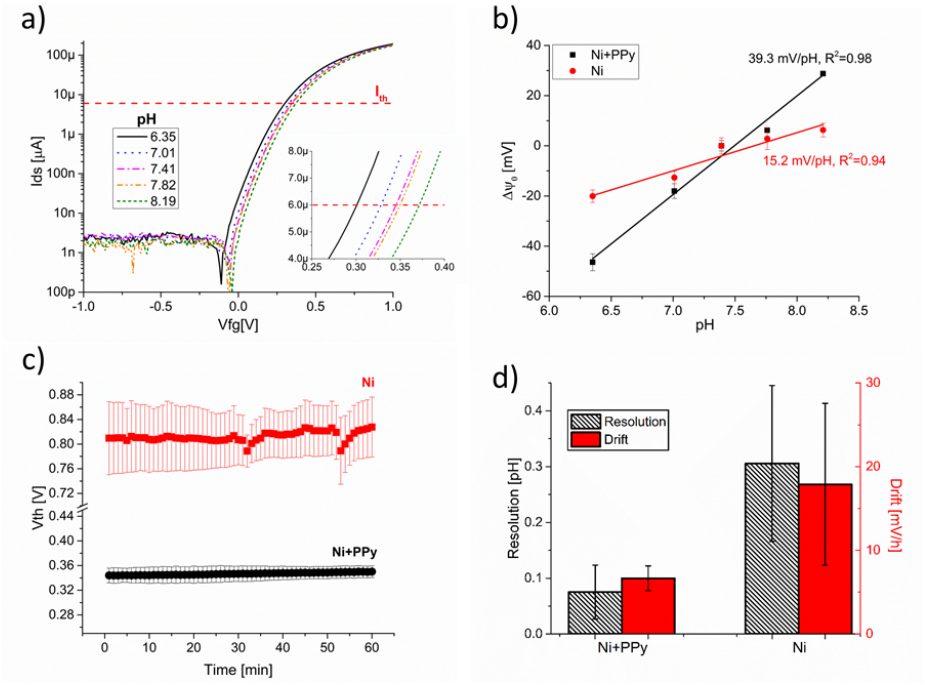

Figure 5.17: ISFET pH sensitivity and stability when biased with PPy coated and un-coated nickel electrodes

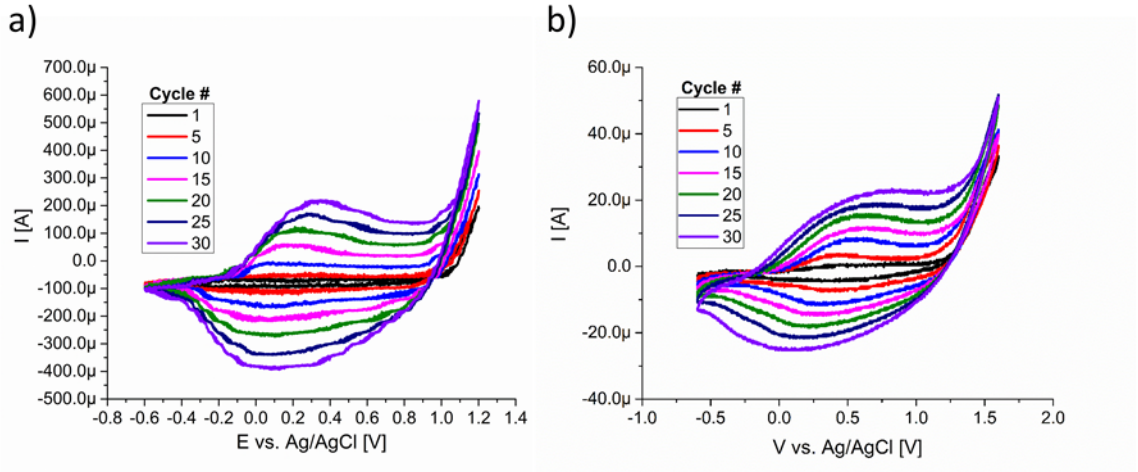

Figure 5.18: Results of the CV deposition process on a platinum and nickel microelectrodes

expensive manufacturing process. The electrodeposition method has several advantages when compared to other reported alternatives. First, it does not require photolithography and etching steps that are used for other on-chip solid-state reference electrodes. Second, the iteration of CV cycles assures that all the exposed metal will be covered by the polymer, minimizing performance degradation caused by fabrication defects. Third, unlike other processes that print electrodes, the polymerization of PPy can be easily scaled to create quasi-reference microelectrodes in a parallel deposition process by setting up multiple nodes as the working electrode. In addition, deposition of PPy does not involve chemical surface modifications that may harm the FET's sensing hafnium oxide layer, and the materials required for the process are inexpensive, especially when non-precious metals are used for patterning the microelectrode. These advantages of the PPy electrodes make them good candidates for fabrication of ISFETs with on-chip quasi-reference electrodes made directly in semiconductor foundries.

The PPy electrodes will enable the use of ISFETS to perform and monitor biochemical reactions that take place in small droplets, creating new opportunities for FET-based biological sensing. There are several advantages for performing reactions in small volumes that can be exploited using the microscopic ISFETs. Besides the obvious reduction of reagent consumption, performing reactions in small volumes enables high-throughput screening assays, results in better sensitivity and quantification, and permits fast and low energy thermocycling [107]. Therefore, the robust PPy electrodes solve the issue of droplet electrolyte referencing. They will allow the integration of FETs and droplet reactions creating a path for multiplexed, inexpensive, label-free, and portable biological sensing.

5.4 Polypyrrole electrodes performance overview and low-cost fabrication

In this chapter, we presented a robust and low-cost method to create on-chip quasi-reference electrodes to bias ISFET sensors. Simple cyclic voltammetry deposition of polypyrrole on patterned electrodes yielded robust quasi-reference electrodes that have stability and pH response similar to the conventional Ag/AgCl. We characterized the deposited polypyrrole film on the mi-

croelectrodes by studying its deposition process and performed open circuit potential measurements to evaluate its electrical characteristics. We showed the isotropic growth of micrometer polypyrrole layers on the patterned microelectrodes and demonstrated that these quasi-reference electrodes are stable within 1 mV, have a drift of only 1- 2 mV/h, and present a low pH response of around 5 mV/pH. These characteristics are substantially better than the ones obtained with bare metal electrodes and translate into robust ISFET operation with close to Nernstian sensitivity and good pH resolution. Furthermore, we polymerized PPy in different metals demonstrating that the technique can be expanded to non-precious metals like nickel, showing a clear path for integration of these quasi-reference electrodes to the semiconductor foundry fabrication processes.

On-chip reference electrodes are smaller, more robust, less expensive, and simpler to package than the common glass packed reference electrodes. The polypyrrole on-chip electrodes that we studied have all those desirable characteristics with the added bonuses of simple fabrication, low cost, and facile integration with other process of a semiconductor foundry. We believe that these new on-chip electrodes will allow novel applications of ISFET sensing by enabling the use of smaller electrolyte volumes and simplifying implementation of portable applications.

CHAPTER 6

OVER ONE MILLION ISFET ARRAY BIOSENSOR

The multiplexing ability of ISFETs (and other electronic-based biosensors) has been identified previously as one of the key benefits of electrical biodetection methods. However, only a few studies have developed platforms that use large parallelism for new spatial and temporal monitoring applications. For example, large arrays of nano-capacitors are used to perform electrical impedance spectroscopy (EIS) analysis of cell cultures to monitor the dynamic attachment of cancer cell lines in real time with sub-micrometer resolution [187, 188]. Also, a platform of 64 pixels of ISFETs is being developed to monitor extracellular pH and cellular behavior by configuring ISFET sensors as CMOS inverters and switches [189], and large arrays of foundry-fabricated ISFETs have been used for the detection of DNA binding events and urea by-products [190]. These platforms are the basis for new approaches of high-throughput screening that leverage the high scalability of the CMOS processes to create parallel sensors that monitor multiple reactions or study the spatial and temporal behavior of biological entities [191]. They have demonstrated that the incorporation of electronics into biosensing applications creates new tools with promising biomolecular applications and clear advantages over traditional methods. This chapter presents a novel massively multiplexed ISFET biosensing platform with enhanced capabilities over those published in the past. A dual-gated ISFET array of 1024 x 1024 transistors, distributed in a 7x7 mm^2 area, was fabricated with a 0.18 μm SOI process, having a high-K hafnium oxide sensing layer, and individually addressable MOS back-gates. The ISFET platform was thoroughly characterized, obtaining standard metrics of electrical performance and evaluating the sensitivity to pH changes as the measurement of responsiveness to changes in the electrolyte. In addition, we show that the massive amount of sensors in the array simplifies the development of statistically significant assays and enables the incorporation of redundancy techniques to improve

the measurement accuracy.

6.1 ISFET array fabrication and operation

6.1.1 Fabrication of sensing array and on-chip circuits

The array of dual-gated ISFETS (DG-ISFET) is fabricated at TSMC foundries without any required post-processing steps and a detailed step-by-step flow chart was provided in Chapter 4. MOSFET transistors are fabricated with a standard CMOS process on the device layer of an SOI wafer. This initial set of transistors defines the back-gate of future ISFET sensors and creates the logic transistors that make multiplexers, decoders, and selection elements required for row and column addressing. To test the reliability of the decoding circuits, selector transistors in the diagonal across the chip are disconnected creating 'dummy' pixels within the array becoming an embedded control that tests the correct addressing of sensors in the array (Figure 6.2 (b)). After the initial standard CMOS fabrication the top of the SOI wafer is bonded to a carrier wafer, the full structure is flipped upside down, and the SOI handling silicon is etched with a chemical mechanical polish (CMP) revealing the SOI buried oxide. The buried oxide is dry-etched in the sensor area and hafnium oxide is ALD-deposited over the entire wafer creating the ISFET sensing membrane. A schematic of the resulting transistor structure is presented in Figure 6.1 (a).

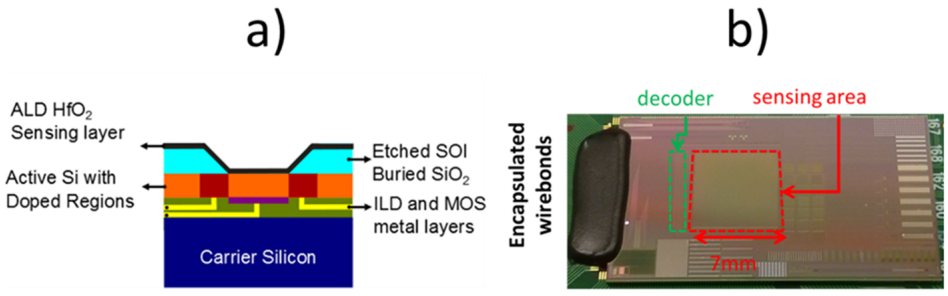

Figure 6.1: DG ISFET schematic and chip photograph

The finalized chip is mounted on a PGA 256 pin printed-circuit board

(PCB) and 48 contact pads are wire bonded to the board for electric access to the silicon die. The pads are used to supply voltage to the array, access the FET's drain/source/gate nodes, and specify the address of the selected transistor. The wire bonds are then encapsulated with an epoxy matrix, a crucial step to improve robustness of connections during bio-detection assays. A finalized chip is presented in Figure 6.1 (b), indicating the ISFET array sensing area, the position of the logic transistors used for row and column addressing, and the wire bonded pads.

6.1.2 IC tester to interrogate a million sensors

For pH experiments a 600 μL PDMS well is bonded to the chip without covering the sensing area. The chip (now mounted in the PCB) is then connected to a 256 PGA socket (Integrated Service Technology, Hsinchu, TW) that establishes connections between the silicon die and a PXI logic IC tester with trigger (PE16A/S) and reading cards (PEMU32) respectively (OpenATE, Hsinchu, TW) that are synchronized with a Spectrum transient recorder (Spectrum, Grosshansdorf, DE) with all three cards housed in a NI PXI-1033 chassis (National Instruments, Austin, TX). The trigger card of the IC tester supplies voltages to the decoding circuit to select the desired transistor and sets biasing conditions while a transimpedance amplifier routes the ISFET drain current to reading circuits that record serial measurements at intervals of about 0.11 ms. The full process is coordinated with a customized MTS3 software (OpenATE) and the output is presented in the form of comma separated values files.

6.1.3 Protocols for pH measurements on array

Five 10 mM PBS solutions of different pH are prepared by titrating HCl and NaOH in specific concentrations. The resulting pH of these calibration solutions is measured with an Orion 3 star pH meter (Thermo Scientific, Pittsburgh, PA) and used to evaluate the ISFET pH sensitivity. The solutions are manually pipetted in the PDMS well, the sensors are allowed to stabilize for 10 min, and a leak-free Ag/AgCl reference electrode (Warner Instruments, Hamden, CT) is immersed to set the electrolyte potential. The

drain current of each transistor is obtained for a specific biasing condition creating a drain current map for a given gating voltage. The PBS solution is swapped for the next pH and potential changes induced by protonation and deprotonation of the sensing layer are observed as current changes [163].

6.1.4 Analysis of IC tester output for sensor evaluation

Data collected in the IC tester is compiled with Matlab scripts that average drain current measurements (each transistor is interrogated up to 15 times) and arrange data in a two-dimensional matrix for each measurement. The pH sensitivity is determined by taking the derivative of the electrolyte pH vs. I_{ds} relationship both for the full ISFET array and single sensors. The I_{ds} pH sensitivity is then converted to the traditional surface potential sensitivity by multiplying current variations with the transistor's transconductance, that is obtained from transfer characteristics, using the relation $S_{I_ds} = g_m * S_{V_g}$ in the triode region [192]. With sensitivity values it is possible to determine the sensor's pH resolution (minimum detectable pH change) by dividing ISFET noise over sensitivity $pH_{(min)} = \sigma/S$, having the noise of the system equivalent to the standard deviation of the drain current measurements [193].

6.2 Assessment of ISFET array performance and data analysis strategies

6.2.1 FET transfer characteristics

Figures 6.2 and 6.3 show the transfer characteristics of transistors in the array plotting the drain-source current as a function of the fluid- and back-gate potentials. Figure 6.2 shows the transfer characteristics when the back-gates (BG) are swept from 0 to 1 V with a drain voltage of 2 V and 0 V in the fluid-gate. Each transistor has an individual BG that is set to a specific potential and the resulting current is recorded. Figure 6.2 (a) is a 3D plot of the matrix presenting the multiple I_{ds} for each sensor as a result of different Vg_{BG} tensions. Figures 6.2 (b) shows a heat map that presents the top-view of the 6.2 (a) plot. It shows the drain-current in the

array when Vg_{BG} is set at 0.75 V and reveals the 'dummy diagonal' that is used to assure the reliability and proper status of the decoding circuits that are used for row and column addressing. Finally, Figure 6.2 (c) presents the quantification and the transfer function with error bars showing the standard deviation of all the pixels in the array excluding the dummy pixels in the diagonal. Results presented in Figure 6.2 demonstrate standard transistor characteristics, overall $g_m = 0.05\frac{uA}{mV}$, and low variations across the chip. The drain current seems to saturate at large voltages. This is caused by the fact that the acquisition card protection circuits truncate larger volumes resulting in an apparent saturation.

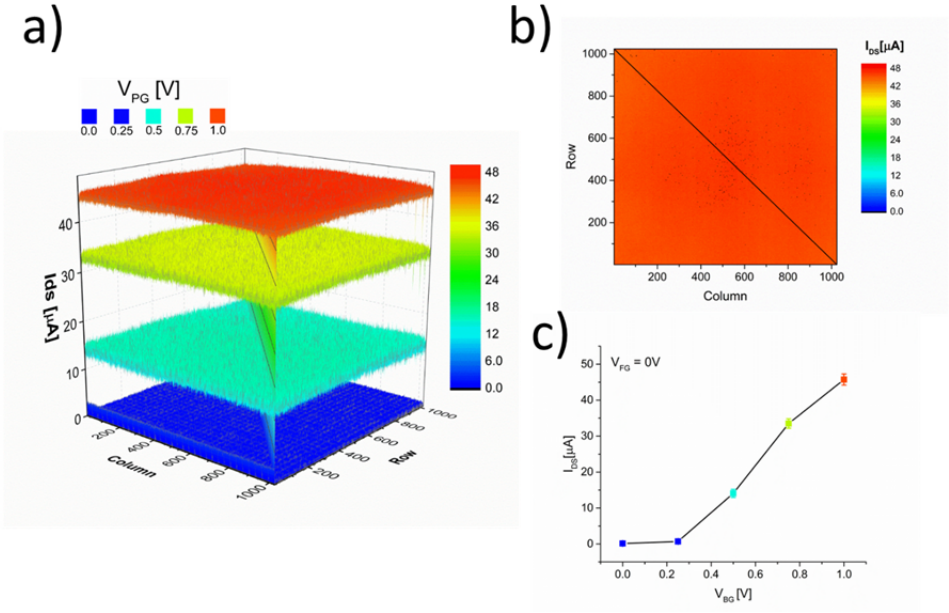

Figure 6.2: Array transfer characteristics of ISFET back-gate

Similar measurements are performed to characterize the fluid-gate (FG) using a reference electrode that biases the electrolyte potential and all the transistors of the array. Figure 6.3 (a) shows the I_{ds} heat-map when the FG is set at 2.5 V, BG at 0 V, and the drain-source at 2 V. Similarly to Figure 6.2 (b) the dummy-diagonal is used as an embedded control of the decoding circuits. The transfer characteristic of I_{ds} as a function of the electrolyte potential (Vg_{FG}) is shown in Figure 6.3 (b) that presents a standard transfer characteristic with an overall transconductance $g_m = 0.01\frac{uA}{mV}$.

The comparison of Figures 6.2 and 6.3 demonstrates a behavior previously

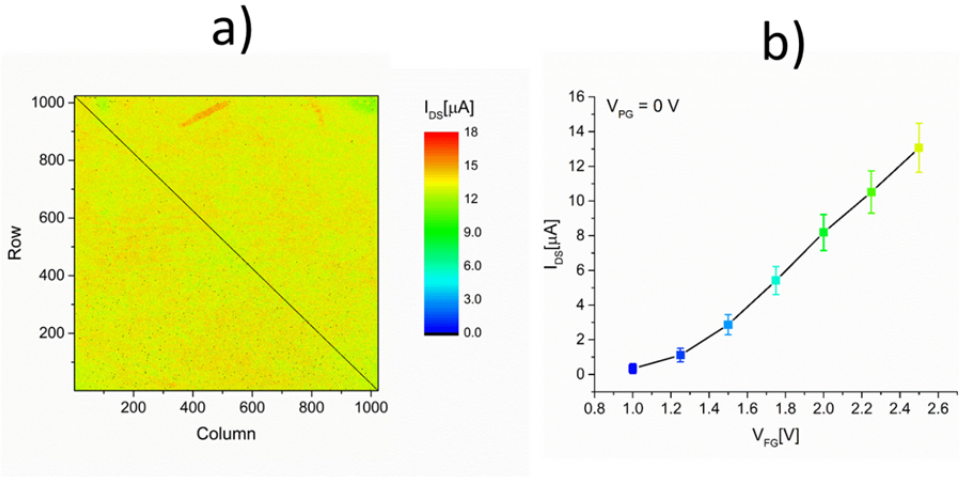

Figure 6.3: Array transfer characteristics of ISFET fluid-gate

observed in similar DG-ISFET structures [176]. The stability, uniformity, and gate potential response of the back-gate are significantly better than that observed in the fluid-gate. This is attributed to greater variations in the fabrication process of the high-K dielectric that acts as sensing membrane and dielectric on the fluid-gate. While the silicon oxide that is used in the back-gate is subject to optimized annealing processes and tightly controlled conditions, the ALD deposition is intrinsically more variable and its deposition at the end of the fabrication process limits restoration processes. Despite nonidealities and variations across the 7x7 mm^2 area, devices present standard transfer characteristics for FET devices, the large number of sensors facilitates the acquisition of data, and the use of adjacent pixels to normalize response or detect uncommon behaviors will result in more robust biosensing.

6.2.2 Array response to electrolyte changes

The sensitivity to pH changes of the transistors is commonly used as a performance metric of ISFET sensors. We evaluated the ISFET array pH sensitivity by modifying the electrolyte's pH as described in the methods section. Figure 6.4 (a) shows the pH-dependent drain current heat maps obtained

from the ISFET sensors when the electrolyte is biased at a constant 2 V but the pH is changed. Decrements in pH cause the protonation of the sensing membrane which results in surface potential increments that are transduced as a greater current in NMOS devices [130]. The opposite occurs when the pH of the electrolyte increases and deprotonation events will modify the ISFET's current. The overall response to pH changes is observed in the drain current quantification of Figure 6.4 (b) that reveals lower drain currents as the pH of the electrolyte increases. The error bars represent the standard deviation of all the ISFET drain currents recorded in the array, a total of 1,048.576 data points. Figure 6.4 (c) presents similar information but in terms of surface potential changes by translating the drain current into surface potential changes via each ISFET trans-conductance obtained from the front-gate sweep (figure 6.3). Table 6.1 summarizes electrical and sensing characteristics of the ISFET platform.

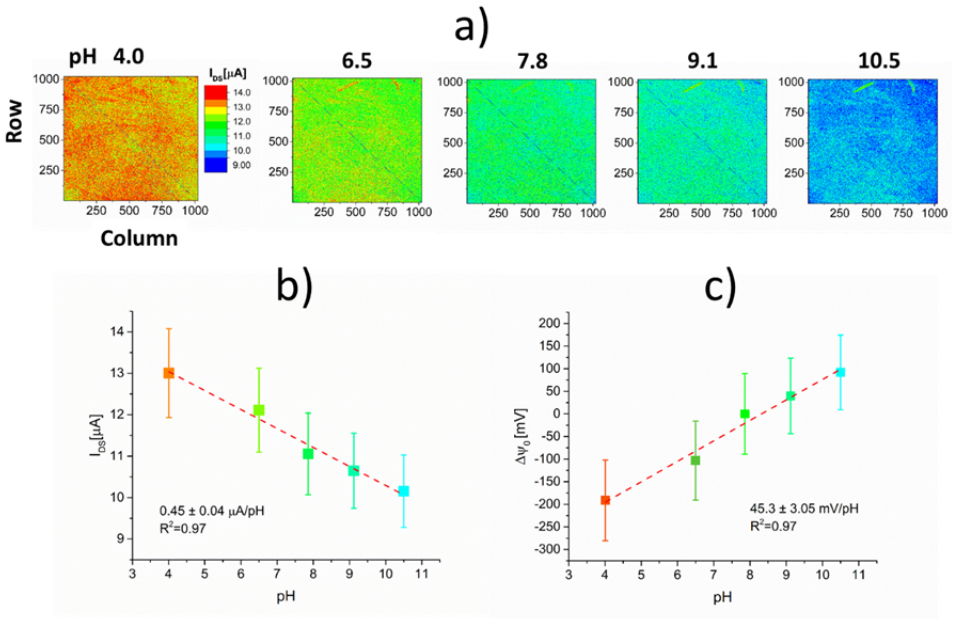

Figure 6.4: ISFET array pH sensitivity

The pH sensitivity analysis reveals an overall response of 45 mV/pH and significant variations across the drain currents recorded in the array. Hafnium oxide has been used in the past as the sensing layer for ISFETs with near Nernstian sensitivity but in our array we observe a slightly lower response

Table 6.1: ISFET sensor array specifications

Specification	**Value**
Technology	0.18μm
Number of ISFETs	1048576
Sensing Membrane	HfO_2
Sampling Rate [ms]	0.11 ± 0.028
pH sensitivity [mV/pH]	45.8 ± 5.4
pH resolution [pH_{min}]	0.25 ± 0.09
Dynamic Range [pH]	4-10

[193]. When inspected in detail, the drain current maps show areas that are pinned to a specific value that reduce the overall sensitivity and contribute to large deviation between devices in the array. Three factors affect the pH response in these regions. First, contamination and defects in the sensing membrane would prevent sound electrochemical exchange in the dielectric resulting in lower and diverse sensitivities. Second, selector pixels introduce a pH insensitive current into the reading. The on-chip circuitry for row and column addressing of the devices uses selector pixels connected in series to select specific drain-source nodes. Poor performance of these selector transistors of the decoding circuitry will minimize pH response and enhance deviations. Finally, in an area of 7x7 mm^2, variations in the electrolyte and the referencing potential are probable and will result in lower sensitivities, increased noise, and topographical variations. Defects in the sensing membrane, non-idealities in the selector circuits, and lack of uniformity in electrolyte and biasing conditions explain the variations and non-ideal sensitives observed in the pH characterization. Therefore, a more robust analysis can be done in a pixel by pixel analysis that normalizes the response of each sensor.

6.2.3 Pixel-normalized analysis

A pixel-normalized pH sensitivity and resolution analysis is presented in Figure 6.5. Figure 6.5 (a) shows a sensitivity heat map that color-codes the surface potential variations as a function of the electrolyte's pH. It clearly shows spatial sensitivity variations in the array, confirming that the nature of current variability is related with processing, circuitry, or biasing defects that locally affect the sensing membrane. The distribution of sensitivities

for the million different ISFETs in the array is presented in Figure 6.5 (b). It presents a slightly negatively skewed normal distribution with a mean 'μ' of 45.8 mV/pH and standard deviation 'σ' of 5.4 mV/pH. Similar figures are presented in panels (c) and (d) of Figure 6.5, that show the heat map of each sensor's resolution (minimum detectable pH change) and the corresponding distribution. As described in the methods section, the resolution is calculated as the ratio between the ISFET's noise and sensitivity. Therefore the resulting resolution distribution is mirrored from sensitivity, a positively skewed normal distribution with a mean μ of 0.25 pH and standard deviation of 0.1 pH. The ample sample size available with the ISFET array reveals important aspects of the sensor behavior when analyzed as a population. The skewed characteristic of the distributions is explained by the non-idealities discussed above and also the rigid upper physical limit of the Nernst equation that sets a maximum sensitivity of 59 mV/pH [194]. The defects in the HfO_2 membrane and readout circuitry cause variations in sensitivity, but those variations cannot overcome the intrinsic sensitivity limitations of the maximum electrochemical response. Therefore the non-idealities in the platform reduce the sensitivity of devices but never increase it above the Nernst limit resulting in the skewed distributions that we observe.

6.2.4 Filtering based on performance metrics

A key advantage of having multiple equivalent sensors in a single platform is the ability to discard elements based on performance metrics or compression techniques. These methods are common practice for platforms with many sensing elements such as piezo-sensor arrays [195], CMOS imaging systems [196, 197], or gas detection clusters [198]. They have been developed to minimize noise, optimize use of bandwidth, or increase sampling and transfer rates. With over a million different ISFET elements in our platform, it is possible to apply this concepts in the biosensing platform taking advantage of the massively multiplexed sensing ability.

For ISFETs, the key metric of performance is the sensor's pH resolution. The resolution metric takes into account both sensitivity and noise, resulting in a signal-to-noise ratio metric that accurately reflects the ability of the sensor to detect biochemical events[144]. Using the pixel-normalized reso-

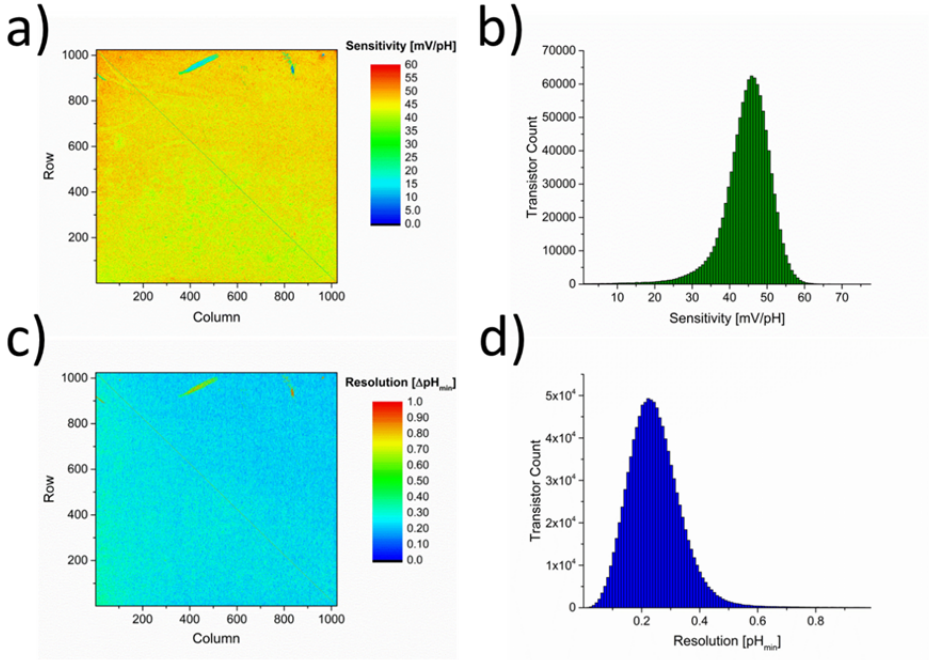

Figure 6.5: Pixel-normalized analysis of sensitivity and resolution

lution calculations presented in Figure 6.5, we filtered the data based on a performance metric of 0.25 pH resolution. Devices with larger resolution than the one selected would have a low sensitivity or high noise which indicate issues with the sensing membrane or readout circuitry. Figure 6.6 (a) shows a binary map of the array with rejected and accepted ISFETs under the resolution metric that discarded 40% of the sensors. The map shows how areas of the array that had poor sensitivity are discarded and also evidence a spatial division between accepted and rejected elements, indicating that an important source of performance variation is processing conditions of the fluid-gate. After discarding elements the overall pH sensitivity is recalculated. Results are presented in Figures 6.6 (b) and 6.6 (c) that show not only an increased gross pH sensitivity but lower variations across the accepted devices. The performance of the ISFET biosensing platform improved by discarding elements of the array based on an individual performance metrics demonstrating the power of redundant measurements with a massively multiplexed system.

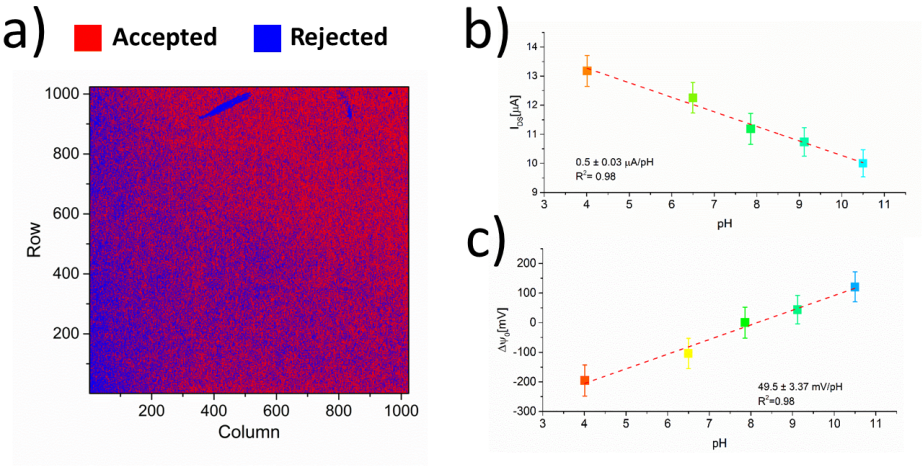

Figure 6.6: Selection of pixels based on performance metrics

6.2.5 ISFET array drift

Electrical characteristics of ISFETs are known to be subject to sudden changes due to temperature effects, hysteresis, and drift [199]. Different techniques have been studied to correct these events and improve the stability of the sensors [200, 201]. However, minimizing these undermining effects by optimizing quality of manufacturing steps and materials is an alternative that has demonstrated success in the past [202]. The ISFET sensing array has been carefully studied and developed to optimize robustness of the measurements. Even though spatial variations are observed in different devices, the performance of these foundry-fabricated sensors is highly robust. Figure 6.7 presents a drift analysis of the ISFET array by sampling drain current at constant biasing conditions every hour during a 6 hour period. The results demonstrate that both the fluid-gate and back gate of the transistors are stable during this time frame. As expected, there is greater variability in the fluid-gate samples due to the manufacturing differences that have been discussed previously, but measurements taken in both gates show highly stable conditions that would facilitate monitoring of reactions that cause potential changes as a function of time.

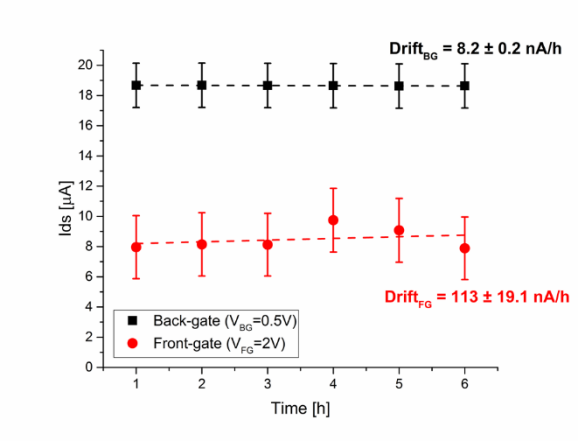

Figure 6.7: Array drift analysis for the fluid and back gates

6.2.6 Temporal and spatial redundancy

At a sampling of rate of less than a millisecond per measurement and over a million devices, the ISFET platform that we have developed makes it easy to quickly take redundant measurements both in time and space. The ability to perform massively redundant measurements can be used to improve the signal-to-noise ratio by generating many data points that reveal the true value of the measured variable and its related distribution [203]. This technique has been used in the past to eliminate or reduce the effect of outlier events and to improve the accuracy of comparisons between data sets by minimizing variability under the assumption of normal distributions [204, 205]. In our platform the redundancy can be obtained by sampling many times per sensor (time redundancy) or by using many sensors to monitor the same reaction (spatial redundancy). Figure 6.8 (a) shows the effect of sampling the same group of sensors multiple times. It shows how the sample standard deviation decreases as a function of the number of samples taken. Even though the reduction in standard deviation in the group is small, it demonstrates a solid trend that this strategy would minimize the effect of drift and randomize events creating a more robust measurement. In Figure 6.8 (b) we present the effect of increasing the number of sensors that monitor a reaction. It shows that the sample-to-sample variation decreases dramatically as more sensors are used to monitor a single reaction and enable better comparisons between samples by reducing the influence of sensors with abnormal behaviors. Figure 6.8 (b) shows that significant variation decrements are observed up to

around 100 sensors but the improvement is small with more sensors. This trend indicates that after a certain number of sensors, spatial related effects (such as the spatial variations that have been observed in the other heat maps) affect the sample noise resulting in a stable sample-to-sample variation. The two redundancy strategies show how redundant techniques can be employed to handle measurements in noisy environments and the power of a massively parallel ISFET platform with integrated circuitry for fast data acquisition. The intrinsic variability of the fabrication process of ISFETs and the variations of the biochemical events that are investigated with FET biosensors can be managed by using iterative and redundant measurements that improve accuracy and simplify quantitative conclusions on the detection of entities and differences in the response between target and control samples.

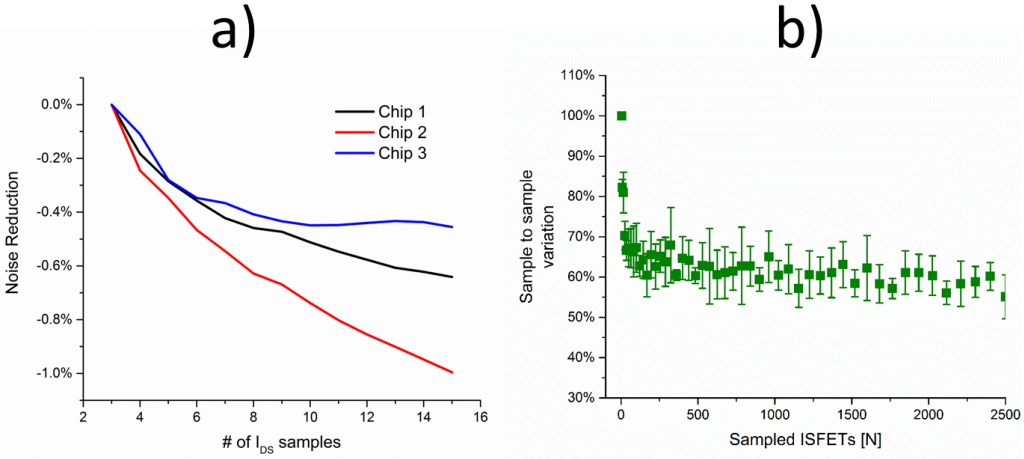

Figure 6.8: Spatial and temporal strategies to minimize noise and improve resolution

6.3 Summary of the ISFET array evaluation and future biosensing applications

This chapter describes a massively multiplexed dual-gated ISFET sensing platform with over one million devices organized in a 1024 x 1024 array of 7x7 mm^2. The transistors are addressed with an on-chip row and column decoding circuit that quickly obtains I_{ds} measurements for each sensor scan-

ning the full array in around 90 s. We presented transfer characteristics of a typical sensing array, evaluated its pH sensitivity, and estimated the minimum pH change that the sensors can resolve. This characterization revealed distributions of the ISFET sensors and spatial variations in the array. We identified factors that affect performance and uniformity of the sensing events and propose filtering techniques based on performance metrics to improve robustness, sensitivity, and ultimately resolution of the ISFET sensors. In addition, we tested the ISFET platform stability by measuring its drift over a period of six hours and observed the advantages of performing spatial and temporal redundant measurements to reduce variations within a group of sensors and to minimize the sample-to-sample variations.

With the 1024x1024 ISFET platform we have developed a tool that exploits the intrinsic advantages of semiconductor biosensors creating a miniaturized, inexpensive, and massively multiplexed tool for label-free detection reactions. With the sensing power of over one million sensors we foresee new instruments and applications in clinical diagnostics, point-of-care biosensing, environmental control, and drug discovery. The massive parallelism and low cost that have revolutionized digital applications can now be applied to biological problems, improving research and diagnostic tools that ultimately advance healthcare and our understanding of biology.

CHAPTER 7

MULTIPLEXED LABEL-FREE LAMP DETECTION OF FOODBORNE PATHOGENS

An emerging approach for portable detection of DNA amplification reactions leverages advances in the semiconductor industry to minimize cost and size of detection tools while enhancing their robustness and level of automation [18]. After more than 50 years of exponential improvements, the semiconductor industry nowadays can easily fabricate transistors at fractions of a penny and pack millions in a microscopic area [206]. This ability in combination with recent research on ionic and molecular sensing with field effect transistors has created a pathway to incorporate semiconductor devices in bio-sensing applications [207]. The use of inexpensive and highly dense transistor chips has already demonstrated that it can minimize the cost and size of DNA sequencing tools [6] and point-of-care devices [208], and similar approaches can result in novel biosensing systems for food safety. In this chapter we describe an integrated device where primer dehydration techniques are coupled with ISFET electrochemical sensing to achieve on-chip multiplexed detection of foodborne pathogens through LAMP reactions. The massively parallel dual-gated ion-sensitive field effect transistor (DG-ISFET) array of 1024x1024 sensors described in Chapter 6 was used to electrically detect nucleotide incorporation. The DG-ISFET array is divided in several independent micro-chambers with anisotropically etched gold-coated silicon wells that are bonded to the sensing area. The gold-coated silicon acts both as the confinement element to create independent reactions and a pseudo-reference electrode to bias the electrolyte and gate the transistors. With this setup ISFETs are monitoring multiple independent 250 nL reactions, the transistors are used to recognize pH changes that result from LAMP, and parallel assays are easily performed using microinjection and primer dehydration techniques described in Chapter 3. Each one of the formed micro-chambers in the partitioned ISFET chip was prepared with specific primer groups that target a pathogenic gene and will report the presence of bacterial pathogens in a process that is briefly

summarized in the schematic of Figure 7.1 (b). The results that we report describe the electrical and pH sensing performance of the ISFET array with the gold-coated chambers, differential electrical signals recorded by ISFETs from chambers with and without reaction, and techniques to improve the signal-to-noise ratio based on redundancy techniques and filtering strategies. In addition, this chapter presents experiments of concurrent electrical detection of *Escherichia coli* and *Salmonella typhimurium* using the described platform and evaluates the effect of lower bacterial concentration to estimate the protocol and tool limit of detection.

7.1 Partitioned ISFET array for parallel LAMP detection

7.1.1 Description of ISFET array and fabrication of gold-coated chambers

The DG-ISFET array is fabricated in collaboration with Taiwan Semiconductor Manufacturing Company with a CMOS compatible process that has been described in detail in Chapters 4 and 6.

To partition the ISFET array and create the micro-chambers for multiplexed detection gold-coated silicon wells were fabricated at the Micro and Nanotechnology Laboratory cleanrooms at UIUC. Standard silicon wafers (University Wafers, Boston, MA) are thinned down with a cycle of oxidation and hydrofluoric etch to achieve a thickness of around 200 μm. The wafer is left with 80 nm of silicon oxide that is patterned with standard SPR220 photolithography (MicroChem, Westboroguh, MA) and 10:1 BOE etch (Avantor, Center Valley, PA) to reveal the silicon that will be etched to form the micro-chambers. After the silicon oxide is patterned the photoresist is stripped of the wafer with Remover PG (MicroChem) and then immersed in a 1:1 TMAH (Sigma-Aldrich, St. Louis, MO) bath for 36 h heated to 80 °C. The etched process creates inverted square pyramids that carve through the wafer creating an array of chambers. After etching, 20 nm of Ti and 80 nm Au are deposited on the wafer with an E-beam evaporator (CHA Industries, Freemont, CA) so the silicon wells act also as a pseudo-reference electrode

[209, 210]. Finally, to assemble the ISFET array chip with the gold-coated silicon micro-chambers a layer of uncured Sylgard PDMS (Dow Corning, Midland, MI) is spin coated on the back of diced gold-coated chips that are then aligned with the 7x7 mm^2 ISFET sensing area and baked at 60 °C for 3 h. The resulting sensing chip is presented in Figure 7.1 (a).

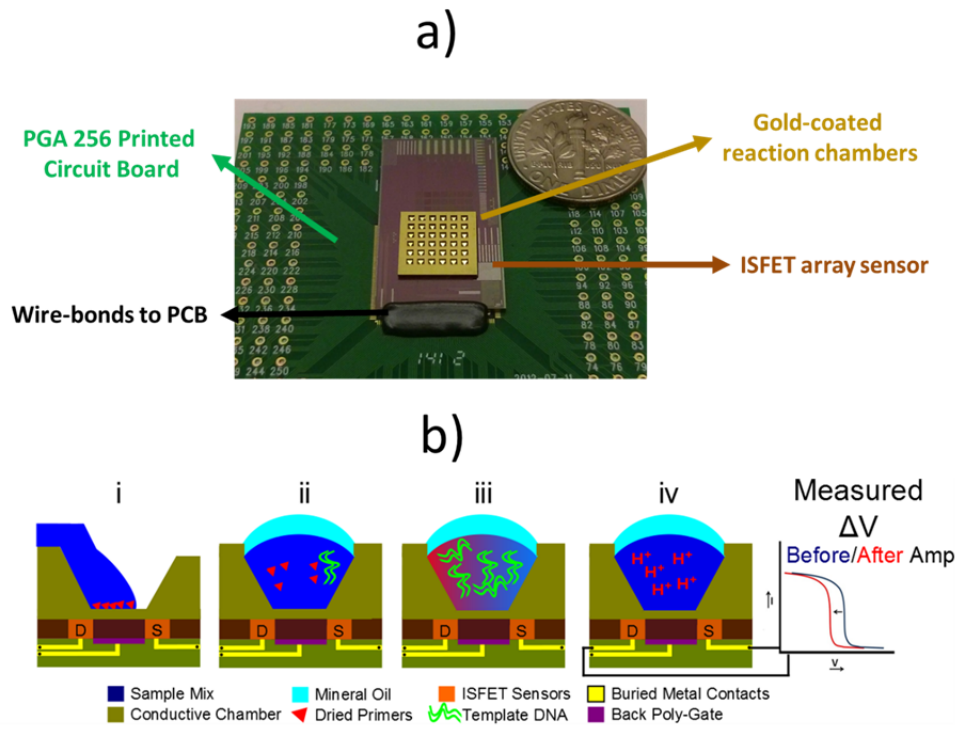

Figure 7.1: Photograph of assembled chip and parallel LAMP detection assay schematics

7.1.2 Response to pH changes of partitioned array

The pH of 10 mM phosphate buffered saline (PBS) is modified by diluting hydrochloric acid and sodium hydroxide until a desired pH calibration value is obtained. Solutions are adjusted with an Orion 3 start pH meter (Thermo Scientific, Pittsburgh, PA) and injected into the reaction chambers with a microinjector IM-300 (Narishige Scientific Instrument Lab., Tokyo, JP). With the droplets of the calibration pH solution inside the micro-chambers the chip

is connected to the testing station, the gold is biased to the desired fluid-gate potential with the micromanipulator, and the drain current of each element in the array is recorded. Subsequent measurements are obtained by swapping the PBS solution for one with a different pH, and current changes are correlated with surface charge in the hafnium oxide layer indicating the surface potential sensitivity to pH changes.

7.1.3 LAMP reaction mix and primer dehydration

The LAMP reactions for the detection of pathogenic genes of *E.coli* and *S.typhi* are divided into 3 different stages: chip priming, electrical profiling prior the reaction, and drain-current measurements after the reaction. The process is described in the schematic of Figure 7.1 (b) that shows primer dehydration and sample injection, primer resuspension and annealing to target sequence, DNA amplification, and electrical detection of pH changes. In the chip priming stage a primer mix for the selected pathogen is dispensed and air-dried inside the micro-chambers. The sequences of primers for the amplification of eae (*E.coli*) and invA (*S.typhi*) are specified in Table 7.1. They are prepared from customized oligos (iDT DNA, Coralville, IA) in concentrations of 19 μM for FIP/BIP pair, 9.6 μM for loop primers LF/LB, 2.4 μM for F3/B3. After the primers are dehydrated a primer-less LAMP reaction mix that has been optimized to trigger pH changes [163] is injected in all the reaction chambers. The LAMP reaction mix consisted of 0.1X isothermal amplification buffer, 1.3 mM of dNTP mix, 5 mM of magnesium sulfate, 6 units of Warmstart Bst 2.0 polymerase (all four from New England Biolobs, Ipswich, MA), 800 mM betaine, 55 mM KCl (Sigma-Aldrich), and 1x EvaGreen (Biotium, Hayward, CA) . The template DNA is extracted from bacteria cultures, *E.coli* O157:H7 in brain-heart infusion medium or *S.typhi* in Lysogeny broth (Fisher Scientific, Pittsburgh, PA), grown overnight in a 34 °C incubator. For DNA extraction bacterial cells are centrifuged at 8600 rcf for 3 min and re-suspended in DI water, lysed at 95 °C, and cell debris is removed with a fast centrifugation (12500 rcf for 10 min) leaving template DNA in the supernate.

In the second stage of the detection protocol, the primer-less LAMP solution is microinjected in the reaction chambers and immediately covered with

Table 7.1: LAMP primers targeting eae and invA for the detection of *E.coli* O157 and *S.typhi*

Target Gene	Primer set	Sequence (5'-3')	Source
eae	F3	TGACTAAAATGTCCCCGG	[93]
	B3	CGTTCCATAATGTTGTAACCAG	
	FIP	GAAGCTGGCTACCGAGACTC-CCAAAAGCAACATGACCGA	
	BIP	GCGATCTCTGAACGGCGATT-CGTATTAACGAACCCGG	
	LF	TGT GGTTAATAACAGACACCGATG	
	LB	ACGCGAAAGATACCGCTCT	
invA	F3	CGGCCCGATTTTCTCTGG	[29]
	B3	CGGCAATAGCGTCACCTT	
	FIP	GCGCGGCATCCGCATCAATA-TGCCCGGTAAACAGATGAGT	
	BIP	GCGAACGGCGAAGCGTACTG-TCGCACCGTCAAAGGAAC	
	LF	GGCCTTCAAATCGGCATCAAT	
	LB	GAAAGGGAAAGCCAGCTTTACG	

mineral oil to prevent evaporation during the heating stages. Fluorescence intensity of the reaction chambers is obtained with a Nikon Eclipse FN-1 microscope (Nikon Instruments Inc. Melville, NY) and electrical characteristics of ISFETs are obtained with the IC tester obtaining an optical and electrical characteristic prior the amplification reactions. The chip is then taken to an oven at 60 °C to trigger LAMP.

Finally after the chip is heated up in a convection Isotemp oven (Fisher Scientific) to 60 °C for 60 min, the fluorescence intensity and electrical characteristics are measured again. Differences between before and after states and differential signals with negative controls will reveal DNA amplification in chambers where the primer set found a matching template indicating the presence of a specific pathogen.

7.1.4 Drain current maps and filtering techniques

For every reported I_{ds} measurement each sensor in the array was interrogated 5 times. The reported I_{ds} is the average of the 5 measurements and the

standard deviation is considered the experimental noise. The pH sensitivity is obtained with the linear regression of the drain-current to pH function and surface potential changes can be obtained by correlating current changes to fluid-biasing conditions via the sensors transconductance $S_{I_{ds}} = g_m * S_{V_g}$ [192]. The resolution is estimated by dividing the measured experimental noise with the recorded sensitivity [193]. This ratio would indicate the minimum pH shift that is electrically detectable with the particular FET.

The inclusion of EVA green into the reaction mix enables the fluorescent confirmation of DNA amplification products. Increments in the fluorescence intensity are related to a greater concentration of dsDNA in the standard method to monitor amplification and a related pathogenic presence for qPCR and qLAMP. The fluorescence images are analyzed using ImageJ (http://rsb.info.nih.gov/ij/) to estimate intensity with mean gray values. Increments in the recorded mean grey value indicate successful replication of target DNA and are computed as relative intensity changes. The results also show the subtraction of before and after images that are performed with the image calculator tools of ImageJ to highlight fluorescence intensity changes caused by the amplified dsDNA.

Electrical detection of DNA amplification reactions is obtained by comparing the measured drain current in monitoring ISFETs before and after the reaction takes place inside the micro-chambers. Matlab scripts let the user select the micro-chamber to be analyzed, create histograms and obtain other statistical metrics of the recorded current in the selected chamber. For a pixel-normalized evaluation, the drain-current matrices before and after the reaction are subtracted creating a differential matrix that describes current and potential changes that occurred during the amplification reaction. Given that thousands of ISFETs are monitoring a single reaction, the collected drain current and differential data sets can be filtered to obtain an improved signal-to-noise ratio. Groups of sensors can be discarded from the measurement to improve clarity of the recorded signals using performance-based filters and statistical detection of abnormal or outlier elements. First, the resolution of ISFETs was used as the performance metric to accept or reject individual sensors. Sensors with poor sensitivity or large experimental noise can be identified with a resolution metric that is used to discard elements. A second filtering technique is based on statistical tests that reveal elements outside the normal expected distribution. The Grubbs test

and its iterative form of the Extreme Studentized Deviate (ESD) test have been used in the past to filter data sensor arrays or networks [211, 212]. We use the same algorithms to discard points outside the normal distribution to enhance differences between populations of currents of different reaction chambers and obtain clear signals of amplification. Unless specified in the results section, the performance filter is set to have a threshold of maximum resolution of 0.5 pH units while the ESD test is done using a discard probability threshold α of 0.05 and a maximum number of iterations equivalent to half of the total number of points in the data set (N/2).

7.2 Biosensing in the partitioned ISFET

7.2.1 Chip electrical characterization

Figure 7.2 presents transfer characteristics of fluid and back-gate of ISFETs in the sensing array presenting typical I-V curves, a 3D map of measured drain currents as a function of gate voltage, and drain-current color coded maps of the 1024x1024 array. Figure 7.2 (a) shows how the full array responds to changes in the back-gate potential while Figure 7.2 (d) shows that only sensors in the bottom of the reaction chambers respond to the fluid-gate bias that is established with the gold-coated silicon. Similar information is presented in the heat-maps of Figures 7.2 (b) and 7.2 (d) that color code the current in each sensor. In Figure 7.2 (b) the position of reaction chambers has a correlation to the measured drain current induced by the back-gate, an effect that has been previously identified as charge coupling between gates in DG-ISFETs but that has no significant influence on pH monitoring [213]. Figure 7.2 (d) on the other side presents a clear shape of each reaction chamber's bottom (the irregular shapes are related to PDMS reflow during the bonding step). Only ISFETs exposed to the electrolyte are affected by the fluid-gate potential resulting in the sectioned heat map with most of the ISFETS in the array having negligible current. Finally Figures 7.2 (c) and 7.2 (e) present standard Id Vg plots for the bottom and fluid gates showing standard transfer curves. These plots show a lower threshold voltage for the back-gate and a saturation current at high gate voltages for both bottom and fluid gates. Lower and more uniform threshold voltages have been previ-

ously observed in the back-gate of DG-ISFETs due to better controlled and optimized fabrication processes in the MOS gates [176]. On the other hand, the drain-current saturation and the resulting lack of linearity are caused by protection circuits in the PXI reading card that truncate high currents above a threshold.

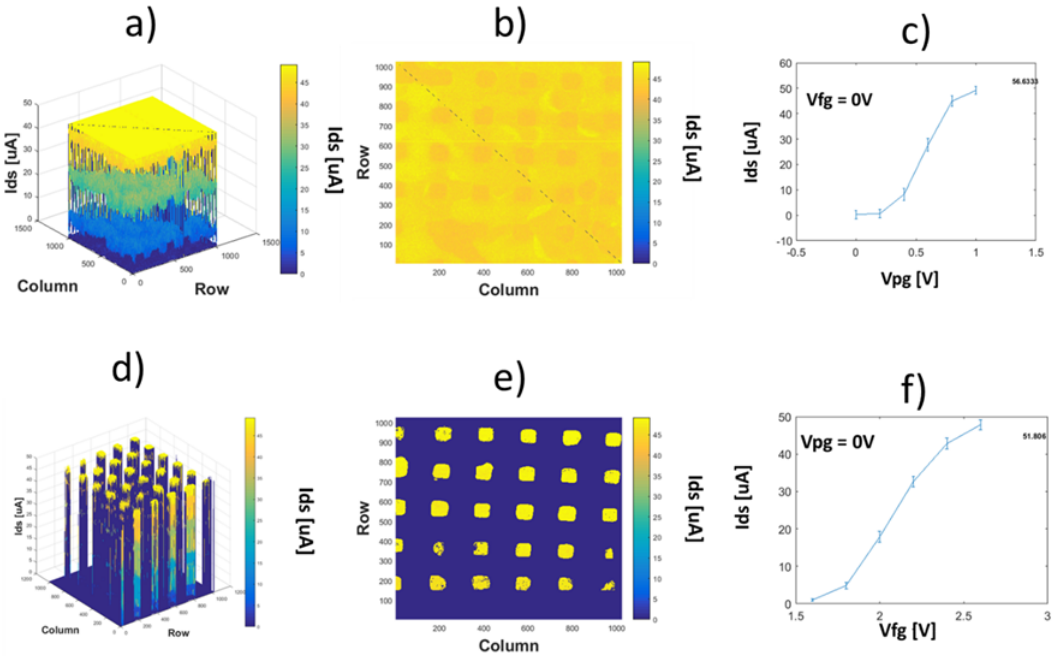

Figure 7.2: Electrical characterization of the ISFET array with gold-coated chambers for confinement and electrolyte biasing

7.2.2 pH sensitivity in independent chambers

More acidic electrolytes cause the protonation of the hafnium oxide layer, increasing the surface potential, and in consequence augmenting the NMOS transistor drain current. That trend is observed in Figure 7.3 (a) that shows how I_{ds} decreases with pH increments. Data presented in Figure 7.3 (a) is the average of all the transistors that are exposed to fluid in the array and the error bars represent the standard deviations across all the devices. This error is high, but it indicates not ISFET variability but rather spatial variations across the chip that can be reduced by normalizing each pixel value. A pixel

to pixel sensitivity analysis is presented in Figure 7.3 (b) that presents a color coded map of the sensitivity for each pixel. The linear regression of surface potential vs. pH in each sensor independently is reported as the sensitivity. A similar plot is presented in Figure 7.3 (c) that presents the sensor estimated resolution that relates sensitivity and noise for each device. Sensors that are not in contact with fluid and therefore not affected by the fluid-gate have no sensitivity to pH changes and therefore infinite resolution that is truncated at value of 1 for visualization purposes. Histograms of both sensitivity and resolution of sensing ISFETs are presented in Figures 7.3 (d) and 7.3 (e). The sensitivity histogram shows a normal distribution skewed to the left with a mean sensitivity of 32 ± 4.9 mV/pH. The sensitivity distribution is skewed because some sensors have a decreased response due to variable conditions in the sensing layer that have an upper limit set by the Nernst relation. The measured sensitivity is far from the ideal Nernst limit, but it is explained by the potential induced by the quasi reference electrode. Unlike standard Ag/AgCl reference electrodes the gold surface has a small but significant reactivity to bulk pH changes that decreases the ISFET sensitivity [193]. On the other hand the resolution mean is of 0.51 ± 0.13 pH units with a normal distribution this time skewed to the right. This behavior is explained by the inverse relation between sensitivity and resolution that translates poor sensitivities into a high resolution metric.

Multiplexing ability to detect pH changes in the ISFET array is exemplified in Figure 7.4 (a) that shows a drain current map of the array when chambers grouped in columns had an electrolyte of different pH value. From left to right in the array, increasing pH values are correlated with lower currents. Quantification of the drain current recorded for each group of wells is presented in Figure 7.4 (b) that shows a similar trend and slope to those obtained for the full chip experiments of Figure 7.3 with a linear regression that indicates a pH sensitivity of around 2 μA/pH. Error bars in Figure 7.4 (b) again represent variations between the thousands of ISFETs in each group of chambers and pixel-normalized analysis will result in lower variations. The experiment shows that it is possible to identify electrolytes of different pH value in reaction chambers by tracking the associated drain current of transistors inside the chamber. This ability allows multiplexed monitoring of reactions for parallel screening assays.

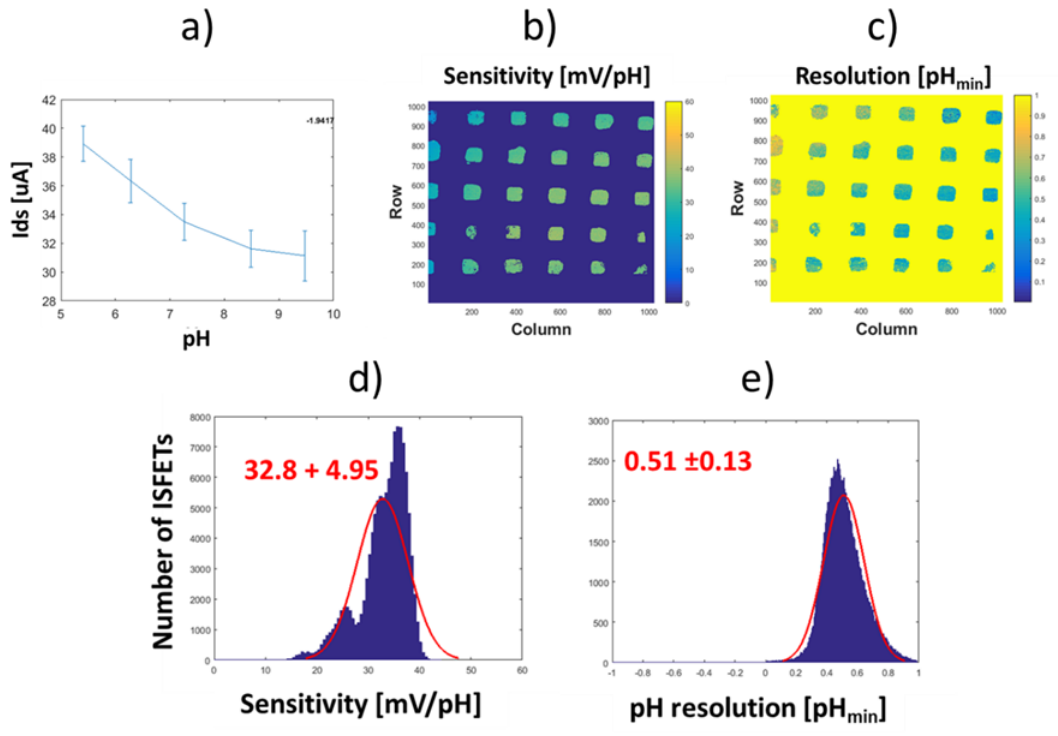

Figure 7.3: pH sensitivity of ISFET array with gold-coated chambers

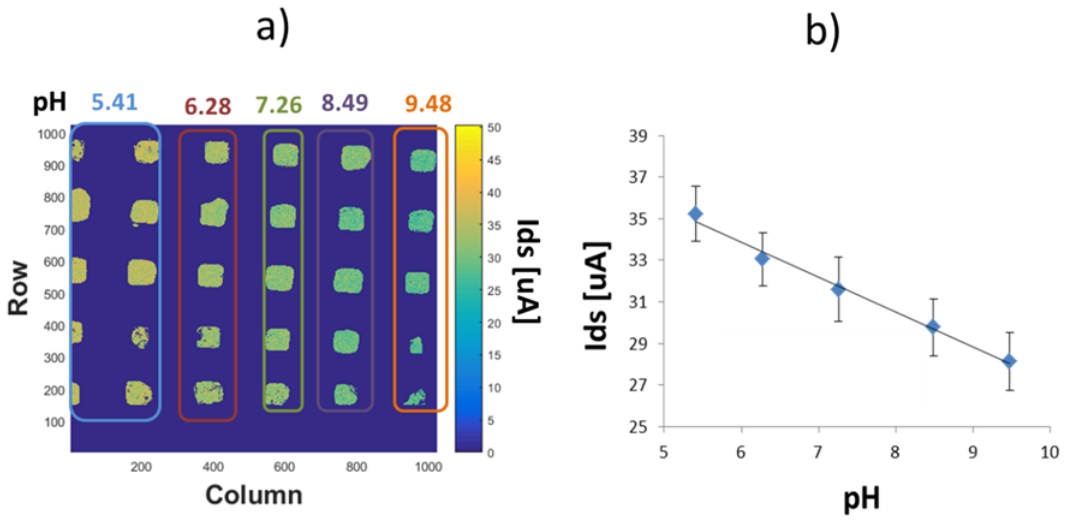

Figure 7.4: Parallel pH measurements on the ISFET array

7.2.3 Detection of LAMP reactions on ISFET platform

We divided chambers in the array into positive and negative assays having half of the chambers with full reactions and the second half with reactions without primers to test the ability of the ISFET array to detect the proton by-products of LAMP reactions. No amplification and no pH change are expected from control chambers without primers (negatives) while amplification is anticipated in the chambers with full (positive) reactions. Figure 7.5 shows fluorescence and drain-current measurements before and after the amplification reaction. The fluorescence detection is used as an optical confirmation of DNA amplification using the intercalating dyes to support conclusions. Figure 7.5 (a) shows the full array with 36 chambers prepared with methods described previously and also delineates the division between positive and negative samples. A similar map is presented in Figure 7.5 (d) that shows the drain current map dividing the different sensing regions in positive and negative samples. The electrical map is missing one column of negative reactions that are outside the ISFET sensing area. Using uncured PDMS to bond the gold-coated chambers with the ISFET array provides a good seal to hold the reactions during amplification but requires a single-attempt alignment that is difficult, and misalignments can leave chambers outside the sensing region.

After heating the chip for 60 min at 60 °C, the 'after' measurements presented in Figures 7.5 (b) and 7.5 (e) were taken. These measurements show increments in fluorescence intensity for the positive samples and a lower intensity in negative samples. Amplified dsDNA in positive reactions increases the number of binding points for the intercalating dye increasing measured fluorescence while the lack of amplification in negative chambers in conjunction with partial photo-bleach of fluorescent molecules results in a diminished fluorescence. The electrical measurements reveal that in both positive and negative samples the drain current increased. However increments in the positive chambers are higher by approximately 1.8 μA than those in the negative samples indicating that despite overall variations across the chip related to drift and noise, the sensors are detecting changes caused by the DNA amplification reactions. Comparative fluorescence and electrical quantification are presented in Figures 7.5 (c) and 7.5 (e).

Whereas the fluorescence increment in positive reaction chambers clearly

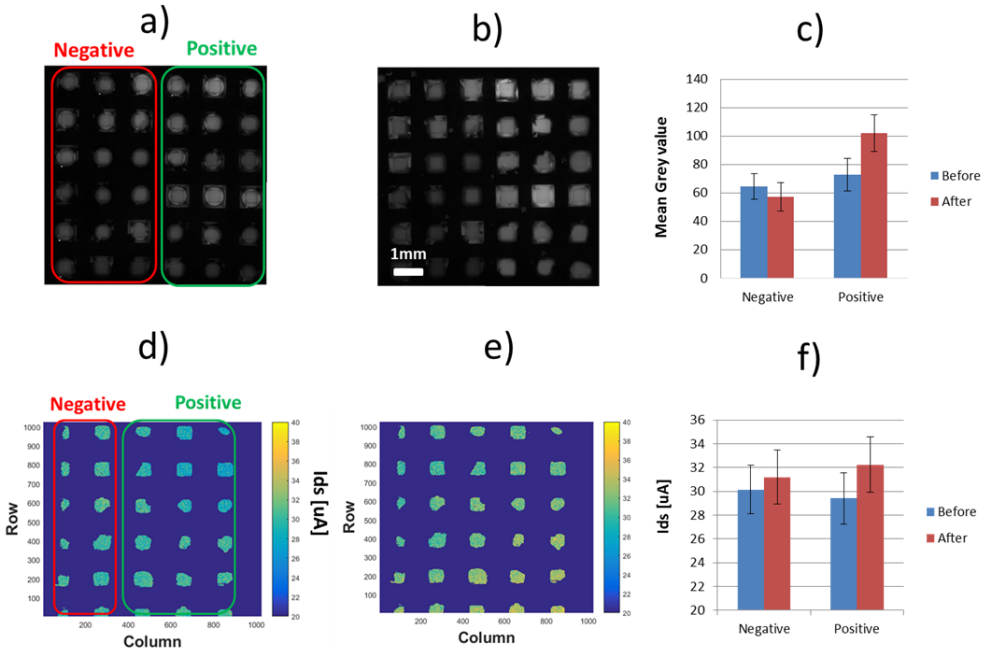

Figure 7.5: Optical and electrical measurements before and after DNA amplification in a chip of 36 wells

differentiates amplification, the signal is more obscure in the electrical measurements where standard deviations are higher and means are closer. The electrical measurements reveal two important features. First the full chip, including reactions chambers with no amplification, presented current changes. This is the result of ISFET drift, change in biasing conditions, and common electrolyte changes during the reaction [199]. A second important characteristic is the high variations between ISFETs monitoring a single reaction. As has been observed during the electrical characterization and pH sensitivity analysis, ISFETs present a normalized distribution and associated standard deviation that are correlated with spatial variations. From plot 7.5 (e) it is clear that the associated standard deviation is high compared to the signal obtained from the amplification reaction. This result demonstrates the importance of having strong sensing capabilities and high quality and quantity of sensors to obtain the highest possible signal-to-noise ratio that enables a robust differentiation of the LAMP by-products. The incorporation of negative controls will simplify the rejection of common noise and drift, and the employment of filtering techniques that detect and discard sensors with ab-

normal behaviors will decrease the variability of the current measurements and facilitate the detection of LAMP-related signals. These two strategies will enable statistically significant differentiation between positive and negative samples.

7.2.4 Statistical and performance filtering techniques

High variability among sensors reduces the signal-to-noise of the amplification reactions and obscure results from the amplification assays. However the massive sensing ability of our ISFET platform results in redundant measurements that enable the use of filtering and statistical outlier detection techniques that allow discarding sensors with poor performance or abnormal behaviors. The elimination of elements with high noise or with current values that fall away from the normal distribution will result in improved signals to facilitate the electrical detection of LAMP amplification.

Performance based filtering rejects sensors with poor response to pH changes under the metric of resolution. The ISFET resolution combines the pH sensitivity and stability of the sensor creating a comprehensive evaluation parameter. Therefore we have selected the resolution of ISFETs to discard ones with poor performance. Figure 7.6 (a) shows the ISFET drain current difference matrix, calculated by subtracting after and before measurements of the experiment presented in Figure 7.5. The sequence of images in Figure 7.6 (c) shows the same map but without sensors discarded based on a resolution higher than the established threshold. Current maps in Figure 7.6 (c) show that most of the sensors monitoring reactions in the array have a resolution better than 0.5; however, as the performance metric is more strict (0.4 to 0.1 pH) the number of accepted sensors decreases and a resolution threshold of 0.1 would discard most of the sensing ISFETs. The image sequence also reveals that the discarded sensors tend to be clustered in specific regions of the array. This indicates that there is a correlation between the sensor performance and its position in the array suggesting spatial fabrication variations in the sensing membrane or the reading circuitry. The relation between the selected resolution metric and number of sensors monitoring the reaction is presented in Figure 7.6 (b).

A second filtering strategy uses statistical analysis of data to detect ab-

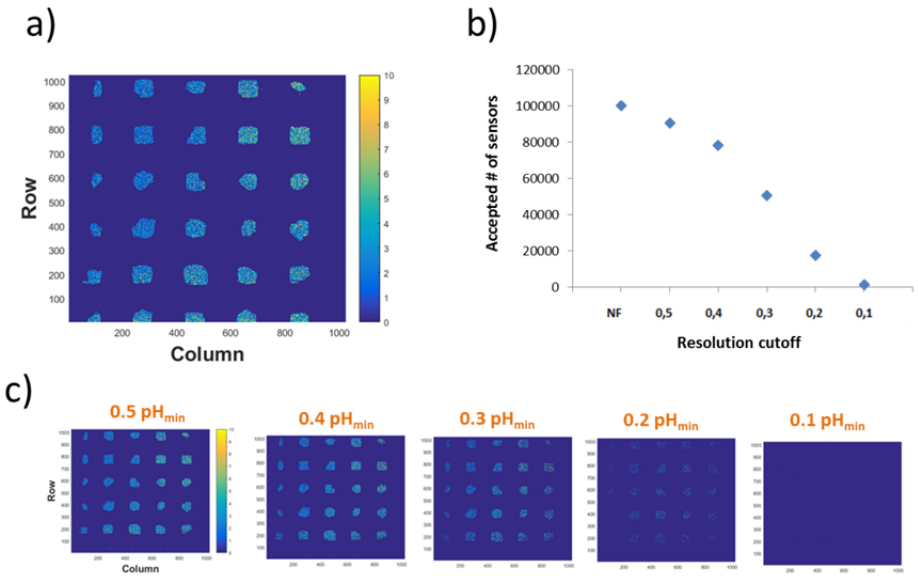

Figure 7.6: Resolution based performance filtering

normal populations. The Grubbs test is an algorithm that is used evaluate whether or not a data point falls out of a normal distribution [212]. It involves the identification of elements' maximum distance to the mean, an estimation of a related t-distribution, and evaluation of a critical value that takes into account a user-defined rejection probability. The same process can be iterated over a data set with the Extreme Studentized Deviate (ESD) test, eliminating unrepresentative elements in the array that fall outside the expected normal distribution to reduce variations in the drain current populations obtained from ISFETs. This process is described in Figure 7.7 (a) that summarizes the detection and elimination process in a flow diagram. To demonstrate the effect of applying the ESD technique into a recorded drain-current data set, Figure 7.7 (b) and 7.7 (c) present original and ESD tested distributions. The full data set in Figure 7.7 (b) presents a normal distribution skewed to lower current. After applying the ESD algorithm with $\alpha = 0.05$ and $r = N/2$, the current distribution is changed to the one presented in Figure 7.7 (c). The clear cutoff boundaries are obtained by having strict probability tolerances and the high likelihood of deletion. Under those parameters around 30,000 sensors out of the original 108,028 are discarded because they have a current outside the estimated distribution. This process

statistically reduces variability (the standard deviation of the distribution is reduced by around 50%) and enhances the signals that are caused by the DNA amplification reaction.

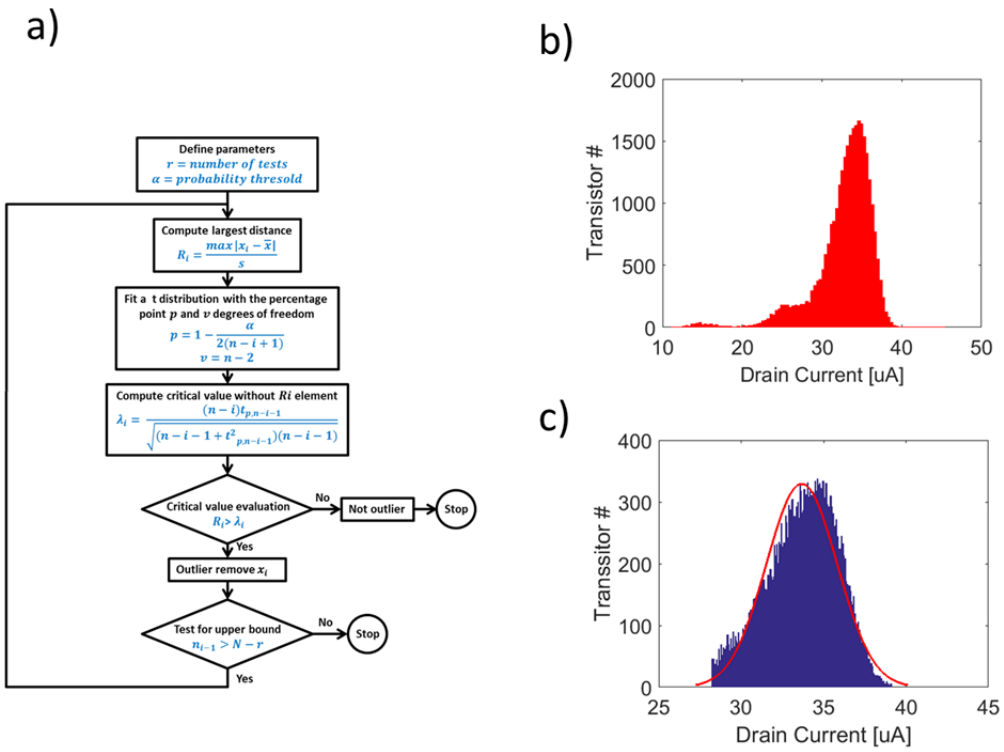

Figure 7.7: Statistical filtering analysis of a drain current distribution

The redundancy that provides the 1024x1024 ISFET array in combination with performance and statistical filters allows monitoring pH in reaction chambers with a high signal-to-noise ratio. The validity of the analysis is not changed as long as the filtering techniques are equally applied to all sampled sensors in the array. The use of the described techniques results in narrower distributions with clear signals recovered from the noisy environment inherent to the ISFET sensors and the amplification protocols. In addition, these statistical processes can be easily performed with minimal computing power and could be incorporated into the standard detection protocols leveraging the massive multiplexing of the ISFET array to clearly identify differences in populations and the seamless integration with other circuitry and data processing elements.

7.2.5 Multiplexed detection of foodborne pathogens

Using the techniques described in previous sections (primer dehydration, monitoring of the ISFET current, and data filtering), we have performed assays that show the multiplexing ability of the ISFET platform for the detection of foodborne pathogens. Figure 7.8 presents results from an experiment where the ISFET array was divided into three regions. A control region (on the right) had no primers, and it is used as reference ISFETs to subtract common noise in differential measurements. A second group was prepared with primers to amplify the invA gene for *S.typhi* detection and the third and final group had primers for the amplification of the eae gene of shiga-toxin producing *E.coli*. The LAMP reaction mix injected after primer dehydration contained templated DNA extracted from an overnight culture of *S.typhi* in LB. After setting up the reaction fluorescence, electrical images were taken to record the status of reaction chambers prior the reaction. Before and after fluorescence images are summarized in Figure 7.8 (a) that shows the differential image calculated with imageJ, and the bar plot in Figure 7.8 (b) evaluates increments in fluorescence by calculating relative fluorescence intensity changes. Similarly, the before and after current maps are condensed in Figure 7.8 (c), that shows the difference map of the two measurements, and the current distributions of the filtered difference data for each group of chambers, filtered with a resolution threshold of 0.5pH and ESD inputs of $\alpha = 0.05$ and $r = N/2$, is presented in Figure 7.8 (d).

The differential fluorescence image shows that only wells prepared with primers for the amplification of the invA gene ended up with a larger concentration of dsDNA. Only in this group of wells does the template find a matching primer set that triggers the amplification reaction. On the other hand, the electrical difference map shows changes in all reaction chambers but a greater change in chambers where amplification took place indicating that the pH change affects the surface potential and threshold voltage of the devices. These differences are clear once the current distributions of each group of chambers are filtered with the techniques described previously. When the negative control is compared to the wells with eae primer, there is no difference (P value of 0.81) indicating that current changes in the wells prepared for *E.coli* detection are common noise and not related to the amplification reaction. On the other hand, the current from ISFETs in reaction

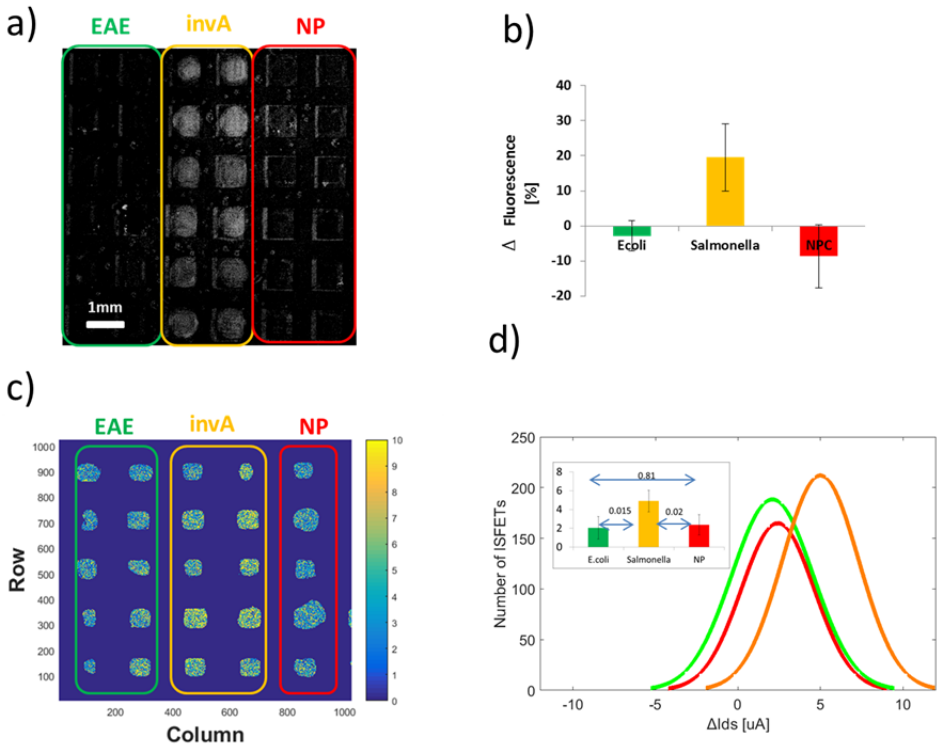

Figure 7.8: Multiplexed electrical detection of foodborne pathogens in ISFET array chip

chambers with the invA primer is significantly different from the negative control (P value of 0.02) which indicates that the differential signal is related to the DNA amplification reaction that was fluorescently confirmed. The differential signal of approximately 2 μA is expected given that the pH change in positive reactions oscillates between 0.8 and 1.2 pH units [65]. The same methods of primer dehydration and pH monitoring with ISFETs could be expanded to create panels of multiple relevant targets in the miniaturized system, resulting in minimal hands-on work during detection assays [73].

7.2.6 Titration of template DNA (LOD)

The sensitivity of the ISFET array platform was evaluated by titrating the concentration of DNA template obtained from the bacterial cultures. For the assay presented in Figure 7.9 all chambers were prepared with a single primer set (eae) for the detection of the gene for STECs. After the dehydration stage, a reaction mix with known template concentration was injected in each chamber. Chambers were grouped by columns having the highest concentration in the left-most column, with an equivalent of 250,000 copies / reaction, logarithmic dilutions in neighboring columns, and no template for the last column that acts as reference. Figure 7.9 (a) shows the fluorescence differential image of before and after the reaction also indicating the CFU / ml equivalent concentration in the chip. It shows a clear fluorescence increment in all reaction chambers with the exemption of the negative control. Normalized increments are quantified in Figure 7.9 (b). The fluorescence significantly increases in the reaction chambers where amplification is expected but there is no increment in the control chambers. Furthermore, Figure 7.9 (b) shows that the reaction is able to replicate DNA when the template concentration is as low as 25 copies/reaction. Similar results were observed in the electrical measurements. Figure 7.9 (c) shows the differential drain current in before and after measurements in a color coded map with the reaction chambers divided by groups based on the concentration of template DNA used in the injection step. In Figure 7.9 (d) changes of drain current in the ISFETs monitoring the reaction groups are quantified after applying the filtering strategies that have been described previously. It shows that in all ISFETs there were current changes but increments were higher in the

chambers where the amplification reaction took place. The greater current changes in those chambers are related to the pH changes triggered by the amplification reaction that does not occur in the control chambers.

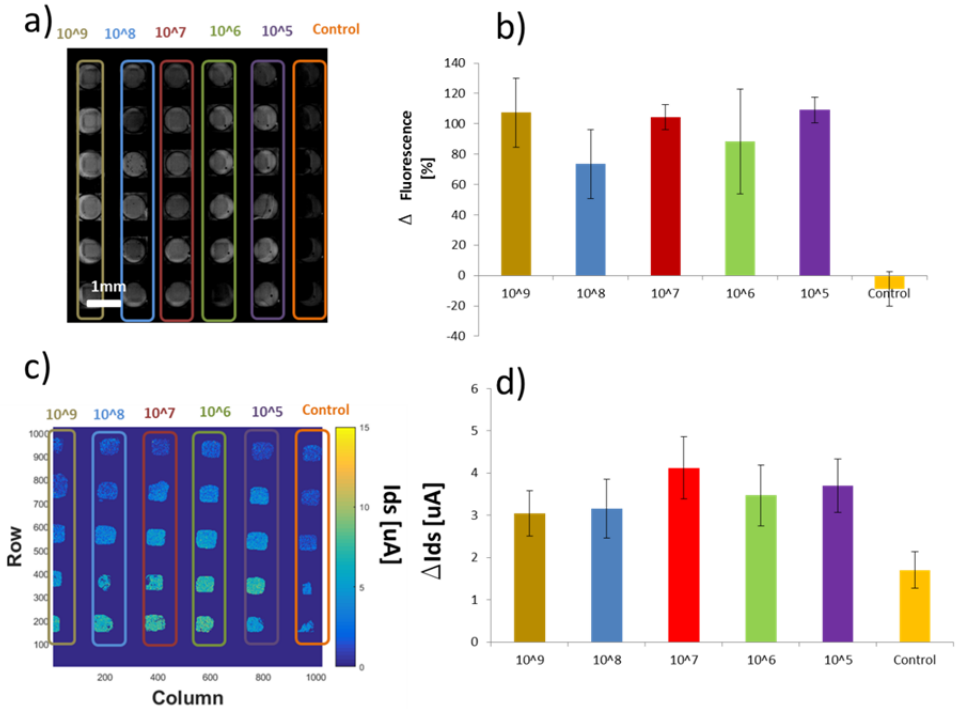

Figure 7.9: Sensitivity evaluation of LAMP reaction on the ISFET array divided in groups of chambers with different template concentration

The quantifications presented as bar plots in Figure 7.9 show that the magnitude of end-point fluorescence and drain current signals are independent from the starting concentration. This effect is explained by plateau stage of the amplification reactions that terminates LAMP regardless of the initial concentration. There are three main mechanisms behind the plateau stage of PCR and LAMP: The reactions run out of material to increase the number of amplicons, a very high concentration of created dsDNA prevents proper annealing of primers, or by-products change the buffering conditions and impede the normal polymerase elongation [214, 215]. For the case of pH-LAMP reactions, changes in the buffering conditions that affect the polymerase behavior are likely to be the dominating cause of the plateau stage. In pH LAMP, the composition of the amplification reaction is modified by reducing the concentration of buffering agents to enhance the pH signals from

the incorporation of nucleotides. The reduction of the buffer concentration facilitates electrical monitoring of the reaction but limits the ability of the polymerase to continue amplification when the by-products change the reaction mix characteristics. Under nominal conditions (e.g. 65 °C, 8.8 pH) the Bst polymerase incorporates 10 nmol of dNTP in 30 min, but if these conditions are changed the polymerase activity decreases and large variations will result in negligible activity causing the amplification stagnation [216]. With the minimized buffering conditions the reaction mix's pH steps out of the working range faster than in regular reactions reaching the plateau state due to polymerase inactivity. In Figure 7.9, the plateau effect is evident in both the fluorescence and electrical measurements. Besides the saturation of current and fluorescence signals, another relevant result is a demonstrated sensitivity of 25 copies/reaction. Further optimization of the reaction composition and the preparation of the chambers with passivation agents such as silanes can further reduce the limit of detection to a few copies/reaction chamber by limiting inhibitory effects present in small volumes [217].

7.3 On-chip multiplexed electrical detection of LAMP in the future of biodetection

We have performed multiplexed electrical detection of LAMP reactions using a massive parallel array of ISFETs divided with gold-coated silicon microchambers. The ISFET sensors in the array have typical drain current to gate voltage relations with the exception of a saturation current at high biases that is caused by protection circuits of the IC tester. ISFETs being referenced with the gold pseudo-reference electrode presented an average sensitivity of 32 mV/pH (equivalent to $\sim$2 μA/pH) with an estimated resolution of 0.5 pH units with both metrics being described by skewed normal distributions. That pH sensing ability of the sensors was used to detect by-products of modified LAMP amplification reactions. LAMP reactions with low buffer concentration enhance pH signals related to nucleotide incorporation [163] and a primer dehydration technique allows the concurrent detection of multiple genes in a single assay [142]. With these techniques thirty independent reactions were set up on the ISFET array and monitored with fluorescent and electrical methods. As expected, in chambers where the dried primer finds

the target gene the fluorescence intensity and drain current increase indicating greater concentrations of dsDNA and the generation of protons during elongation. The large quantity of individual ISFETs that monitor each reaction in our platform allows the use of statistical and performance filtering methods to clearly identify LAMP-triggered surface potential changes despite low and noisy signals. These methods are used in a parallel foodborne pathogen detection experiment where *S.typhi* and *E.coli* are detected in a single assay. An electrical signal of $\sim$2.5 μA drain current increment is obtained from chambers with matching primer set and template. The inclusion of negative controls as references enables the simple subtraction of common noise and reveals changes due to the amplification and in consequence the presence of a specific pathogenic. Finally we evaluate the sensitivity of the platform by titrating the concentration of template DNA. It was possible to detect concentrations of 25 particles / reaction, which represents an equivalent to 10^5 CFU / ml but lower detection limits should be obtained with surface treatments and optimization of the reaction conditions that augment the efficiency of the reaction and eliminate inhibitory effects.

The current and upcoming challenges in food safety demand better pathogen detection tools that enhance the enforcing ability of regulatory agencies. Tighter food quality controls and faster outbreak reaction protocols are only possible with contamination sensors that sustain performance of current methods but are portable, inexpensive, and easy to use. The platform that we describe in this chapter is aligned with these targets thanks to its small size, minimal cost, and simple detection of biological entities through DNA amplification. By combining sensitive molecular diagnosis techniques and semiconductor sensors we created a multiplexed, robust, and simple platform that can be used for many bio-detection applications creating the core of a biosensing tool. However the success of this approach depends on novel sample preparation techniques. Even though LAMP has been demonstrated to be more robust than other DNA amplification techniques and it can be performed with minimal sample preparation [218], fully integrated detection systems for foodborne pathogens require the incorporation of concentration, partitioning, and mixing stages [219]. Such integrated devices that miniaturize and automate all processes for pathogen detection will promote screening tests in food samples and enhance control over the food chain. Food safety can greatly benefit from the advances in MEMS and semiconductor fields

to create new tools that solve problems of low sampling rates, poor detection times, and expensive bio-detection to improve the quality of the food products.

CHAPTER 8

CONCLUSIONS AND RECOMMENDATIONS FOR FUTURE WORK

It has been almost 25 years since Dr. Kary Mullis was awarded the Nobel Prize for the development of the polymerase chain reaction. The ability to specifically replicate DNA has had a profound impact in the way we understand microorganisms and interact with them [22]. In this dissertation we explored methods to miniaturize the equipment required to conduct DNA amplification with the goal of enabling more entities to use this reaction in multiple settings. Our approach was to utilize semiconductor devices to detect amplification by-products. With field effect transistors as the core element of our biosensor we reduced cost, minimized size, and improved the robustness of a portable DNA amplification system. We have created a microchip for the multiplexed electrical detection of DNA amplification reactions and during the development of our system tackled multiple challenges related to the miniaturization of a biochemical reaction and its integration with semiconductor devices. The prototype resulting from our work shows the basis of novel DNA amplification systems based on the ubiquitous and nanoscopic field effect transistors.

This project had the goal of creating small portable pathogen detection devices. It started by miniaturizing the DNA amplification reaction so it could be performed on silicon devices. In the initial stage we learned the importance of passivation layers to enhance compatibility between biomolecules and silicon, and developed methods to perform multiplexed assays using a primer dehydration technique [142]. Then, in collaboration with Taiwan Semiconductor Manufacturing Company, we created a field effect transistor structure that could be exposed to fluid and had strong pH sensitivity. With this device we were able to electrically detect the reaction by-products utilizing the same principle that Ion Torrent uses in their popular sequencer [220]. The electrical signals that we obtained from the reaction by-products are intrinsically small and optimization exercises to improve the signal-to-noise

ratio were required to clearly identify the electrochemical signatures of the nucleotide incorporations. The optimization was done in three fronts. First, the reaction components were modified to enhance pH changes[176]. Second, the transistors were operated in a dual-gate mode to enhance resolution and facilitate the detection of pH changes [193]. And third, we studied the effect of multiple electrolyte biasing techniques designed to minimize variations in the reference electrode to focus potential changes in the transistor's sensing membrane. The optimization effort improved our understanding of the relationship between the sensors and the amplification reaction and served as a pathway to expand the sensing platform into a massive array of sensors that leverage the ability of the semiconductor industry to easily replicate structures with the top-down fabrication paradigm.

In the final stage of the project we fabricated a sensing platform with over one million sensors, showing the scalability potential of semiconductor devices. We utilized all the methods developed in the previous projects to create a platform of multiplexed electrical detection of DNA amplification reactions. The three elements of reagent dehydration, electrical sensing, and pseudo-reference of an electrolyte were incorporated in a single platform to perform an electrical measurement of biochemical reactions designed to detect the presence of pathogenic entities. The developed platform demonstrated the power of semiconductor devices when used for biological applications. Having transistors as biosensors not only reduces size, cost, and complexity of the biological assays but also provides sensing redundancy that enables the utilization of statistical methods to improve the quality of the signal recorded from the reaction. Millions of sensors distributed in an area about the size of a finger nail used as biosensors show what could be the next generation of biological assays. New tools will feature small and inexpensive devices that allow untrained users to perform complex biological assays by leveraging technology of the revolutionary semiconductor industry [18].

The platform that we have developed has been designed as the core of new biological sensors. The ability to perform and monitor multiple DNA amplification reactions on a microchip with dried primers to promote automation can create new kinds of biological sensing tools that take advantage of the low cost, small size, and seamless integration with electronics of the transistor biosensors. However, this core element will need to be complemented with other support systems to create devices that provide complete biosens-

ing solutions for entities interested in pathogens detection. The next few sections delineate possible future work that could lead to complete platforms fabricated in large commercializable scales.

8.1 Methods for automated loading

In this work we conducted our on-chip reactions in nanoliter chambers. The miniaturized reaction chambers are treated and loaded with a microinjection system that provides fine control of droplet size, low dead volumes, and the possibility to automate fluid dispensing. However microinjection equipment is large and expensive. It would severely undermine the portability and cost of the DNA amplification system. Therefore new alternatives for loading and sensor preparation techniques must be pursued. The combination of microfluidic systems and microarray printing services would yield inexpensive and efficient sensor preparation and sample partition. There were two tasks performed with the micro-injector: primer dehydration and sample loading. The first task could be performed with inkjet printing tools that have a very accurate control of the position and volume of dispensed fluids [221]. The primer dehydration that is critical for multiplexed assay could be performed with these commercially available tools developed to create micro-arrays [222]. In addition, the use of more sophisticated mechanisms developed in this industry can enable the dehydration of more reagents required for the reaction like dNTPs, buffers, and salts. The second task of sample loading must be performed with small and simple devices that can be part of the chip so the detection assays can be performed in a portable setting. We have explored the use of PDMS microfluidic devices to partition the sample in the reaction chambers. The microfluidic 'greek-key' presented in Figure 8.1 and other structures utilized in digital PCR assays could be replicated in our system to load the chambers with the reaction mix with minimal equipment [223, 224]. By utilizing commercial tools to dry reagents in the chip and microfluidic components to partition the sample to be analyzed it will be possible to overcome the use of the micro-injector and have a truly portable system.

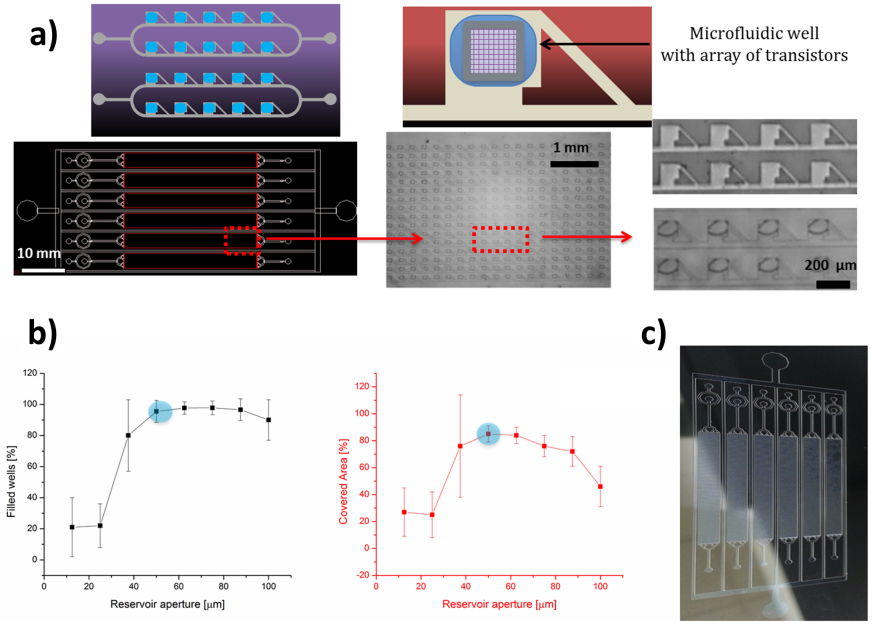

Figure 8.1: Microfluidic Greek-Key. Studies for sample partitioning showing schematics and microscope images of microfluidic partition with greek-key, optimization of reservoir aperture, and photograph of full microfluidic chip.

8.2 On-chip cost effective reference electrodes

Chapter 5 of this work described studies for on-chip reference electrodes and their effect on the ion-sensitive field effect transistor pH performance. In those studies we developed protocols to coat different metals with polypyrrole to significantly improve their referencing ability. However due to fabrication constraints in the one million sensor array we were not able to apply these techniques for the integrated version. In order to use the PPy techniques in the ISFET array it will be necessary to modify the polymer deposition protocols to prevent damage to the sensing structures. Improved compatibility between the polymerization process and the ISFET array can be obtained by designing electrode layouts that minimize interference with the decoding circuit, changing the solvent utilized during electrochemical deposition, or modifying the cyclic voltammetry protocol to minimize stress in the fluidic devices. Working on new fabrication methods to allow the deposition of polypyrrole electrodes in the ISFET array will be a complex iterative processes but it will result in better devices with three specific advantages over

the gold-coated chambers reported in this dissertation. First, the pH signal will be larger with polypyrrole electrodes facilitating the identification of the amplification by-products to distinguish positive and negative samples. Second, on-chip electrodes would allow a higher density of independent reactions. The gold coated chambers that were utilized to partition samples in the array sacrifice many transistors that are not exposed to fluid. With on chip electrodes a more precise partition could be obtained potentially increasing the number of reactions that can be performed and improving multiplexing ability. Finally, our studies demonstrated that the polypyrrole deposition can be performed on non-precious metals such as nickel and iron reducing the fabrication cost while improving performance. These advantages of utilizing polypyrrole on-chip electrodes motivate further optimization of polymerization protocols to exploit the advantages of the semiconductor biosensors. The photograph of Figure 8.2 shows the ISFET array chip with on-chip electrodes for polypyrrole deposition studies.

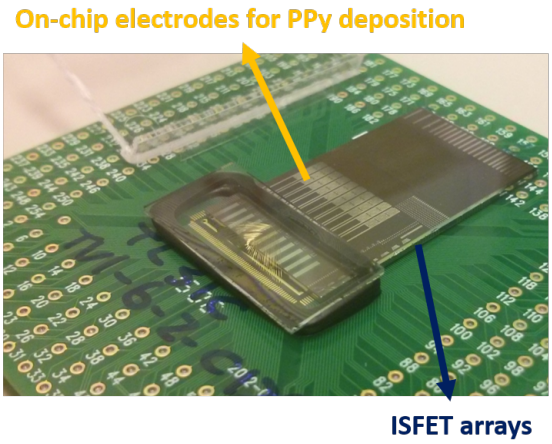

Figure 8.2: ISFET array with on-chip electrodes for PPy deposition

8.3 Embedded heaters and fast thermocycling

The loop-mediated isothermal amplification that we use for the detection of pathogens is triggered at $60 - 65\,^{\circ}\mathrm{C}$. In the experiments reported in this work we utilized external heating sources to drive the amplification reaction. However, creating heating structures embedded in the silicon chip will result

in more portable devices, allow real time analysis, and reduce the detection time. Our collaborators in TSMC have created grids of polysilicon that can be used as resistive heaters embedded in the silicon chip [190]. Cross section and top-view schematics of the heaters are presented in Figure 8.3 that also shows an adjacent diode that is used as temperature control. With these heaters it will be possible to perform real time analysis to do quantitative detection reactions and conduct very fast PCR, two tasks difficult to do with external heaters.

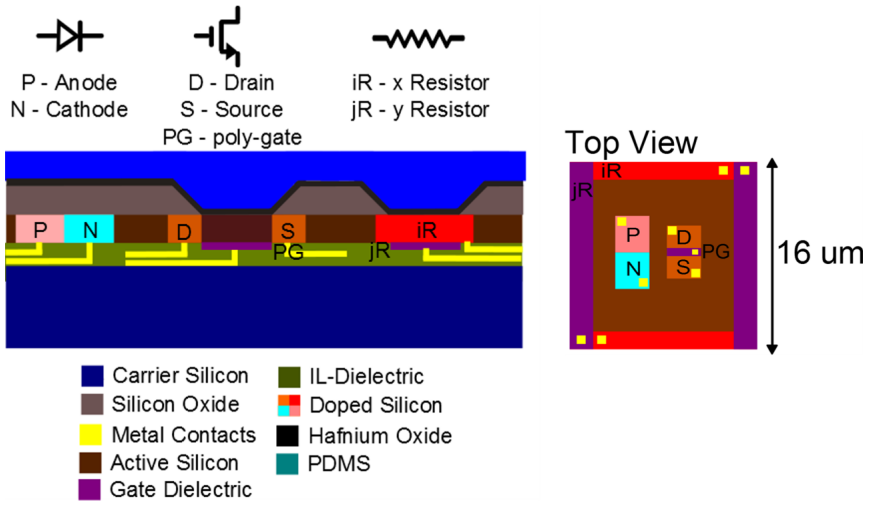

Figure 8.3: Cross section and top view schematics of embedded heaters on the silicon chip

Quantitative analysis of LAMP reaction requires real-time monitoring of the by-products to assess the time to threshold that is correlated with the initial target concentration. This real-time detection of the electrical by-products was not possible with external heating sources. External sources introduce noise into the electrical measurement obscuring the signal from the reaction. They are also difficult to incorporate in the measurement setup diminishing the system robustness and repeatability of the experiments. On the other hand, on-chip heating elements are simple, small, and provide great control over the temperature profile. Also, the polysilicon grid on the chips enables highly localized heating of small volumes. By reducing the thermal mass it will be possible to perform very rapid thermocycling accelerating the PCR reaction. Characterization experiments presented in Figure 8.4

demonstrate the faster response of on-chip heaters. Panels (a) and (b) show the heating / cooling response while panel (c) shows that the platform could potentially complete the 3 temperatures of PCR in less than 500 ms. The on-chip heaters will expand the functionality of the ISFET platform for DNA amplification reactions.

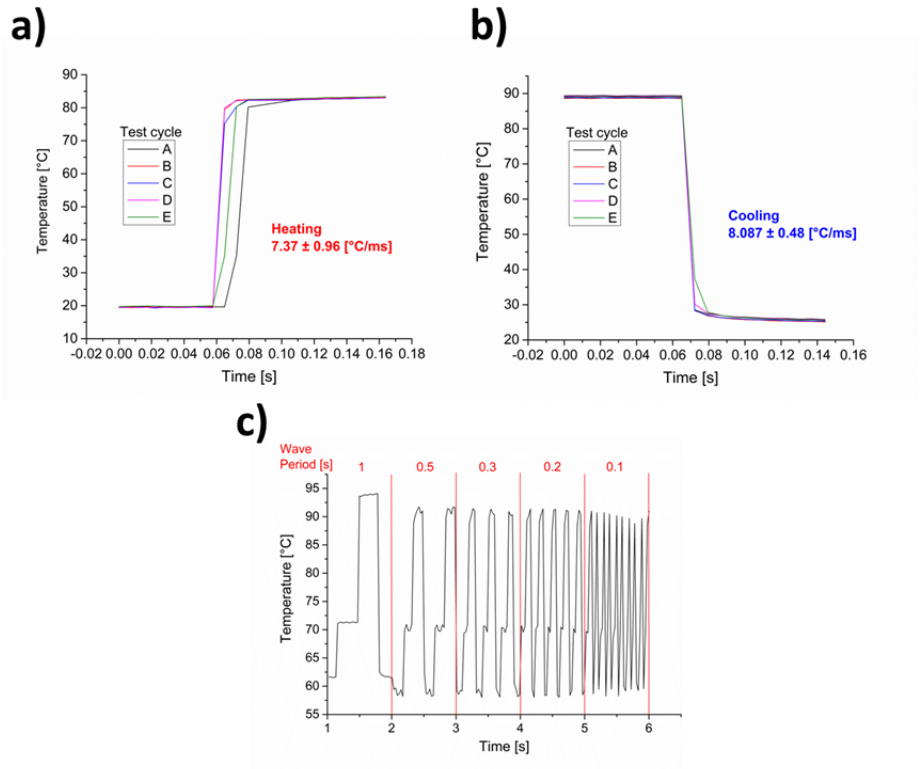

Figure 8.4: Characterization of on-chip polysilicon heaters

8.4 Path towards integrated solutions

The use of microfluidic and electrochemical approaches for pathogenic detection in the system that we have developed has multiple advantages. It allows the development of label-free assays, enables portability and automation, and reduces cost of reagents and equipment. However it has two important intrinsic limitations. The first one is related to the quality and composition of the

sample to be analyzed. In order to use microfluidics it is important to have clear samples that can be flown through the fluidic network. The samples that are typical for pathogen detection are usually complex and with many colloids in solution. These samples cannot be flown through microfluidics and need to be cleared and filtered before the miniaturized devices can be utilized. Second, the sampled volume that can be handled in the microscopic devices is low. The amount of sample that can be screened in a microfluidic device is intrinsically small. Therefore it is required to have samples with analytes in a concentration high enough to have at least one analyte in the sampled volume. These two challenges can be mastered if the detection system is integrated with sample preparation or concentration devices.

Other researchers and collaborators have been working in other platforms that focus on preparing/cleaning the sample and concentrating the target analyte. Examples include the lateral flow concentration elements [90], immobilized gangliosides [225], or DNA aptamer capture [226]. These systems are complementary to the portable DNA amplification system and a unified system will create a complete solution that could be easily adopted by parties interested in detecting pathogens from complex samples. The integration process between platforms should be dictated by a target application that specifies sample quantity, quality, and required limit of detection in the design of the complete system. After many years of development of novel methods for bacterial detection, it seems that the combination of multiple technologies will be the key to address the challenges of pathogenic detection and microorganism identification.

APPENDIX A

ON-CHIP RT-LAMP FOR VIRAL DETECTION

The ISFET platform for LAMP reactions was developed to detect foodborne pathogenic bacteria and improve current food safety inspections. However the same platform can be used for other applications that can also benefit from specific, low cost, and rapid diagnosis tools. In this appendix we briefly document work on the use of the same platform for the detection of HIV virus demonstrating that the DNA amplification methods can be used in different scenarios. A reverse transcription LAMP (RT-LAMP) assay was developed with primers designed to target the HIV p24 gene in viruses [227]. The assay has demonstrated robust detection of HIV directly in blood and it is a good candidate for portable detection. Carrying out this method on-chip can simplify the detection procedures allowing more frequent screenings in multiple settings. Here we present the use of on-chip LAMP to detect down to 30 copies/reaction of HIV cDNA from a human sample.

A.1 Formulation of the RT-LAMP

The LAMP reaction mix consisted of HIV viral cDNA sample in different concentrations, a P24 primer mix, Betaine (800 mM), dNTP mix (1.4 mM), isothermal amplification buffer (1x, New England Biolabs, MA), magnesium sulfate (8 mM), *Bst* 2.0 WarmStart polymerase (0.64 units/μl, New England Biolabs), Eva Green fluorescent dye (20 μM, Biotium, CA), and DI water. The sample of HIV viral DNA was prepared using the PureLink purification kit and the ProtoScript First Strand cDNA reverse transcription kit. The p24 primer sequences were obtained from previous literature. One control reaction with no viral DNA, and three others with 30, 3,000 and 300,000 copies of cDNA per reaction were prepared in order to test sensitivity. Reaction mixes were then microinjected into the silicon micro-wells. The top row

has the control reaction mix without template and the other three solutions are injected in the described groups of 10 wells (Figure A.1 (a)). The chip was heated to 65 °C and imaged with a fluorescence microscope every minute for 60 min with the same protocol described in Chapter 3.

A.2 On-Chip amplification of p24 gene

Figure A.1 (a) illustrates the placement of 30 nL reaction droplets inside individual wells in the silicon dioxide microarray creating 36 individual nano reactions in the 4x4 mm chip. Figure A.1 (b) shows fluorescence images of the LAMP reaction progression. Groups of pixels with the different concentrations achieve the fluorescence threshold at 11, 15, and 18 min. These different threshold times are expected for each concentration and are used to build the standard curve presented in Figure A.1 (c). In Figure A.1 (d) the threhsold time is plotted against the equivalent virus/reaction concentration. The linear regression shows an R^2 value of 0.985 indicating a robust sensitivity and a limit of detection of 30 particles/reaction.

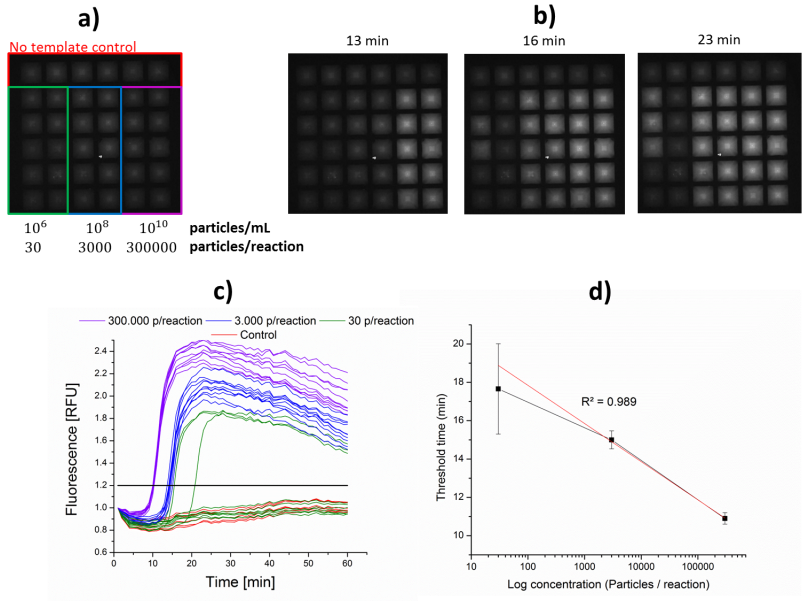

Figure A.1: On-chip amplification of HIV p24 with different viral concentration in columns of the array

These preliminary experiments on detection of viruses show the ability

to use the same platform that has been described in the main chapters to detect targets other than bacterial pathogens. In recent publications the same protocols were used for the detection of viruses using a smartphone [218]. These new approaches incorporate microfluidic mechanisms for sample preparation and smartphone-based fluorescence imaging of the amplificaiton reactions to create a small and portable detection unit, showing that on-chip detection in micro-chambers can be integrated with other miniaturized systems to create integrated solutions. This experience has demonstrated that the methods developed for on-chip amplification can be tailored for multiple applications simply by changing the primer set and will allow the detection of different pathogenic entities based on their genetic composition.

APPENDIX B

ISFET ARRAY SENSOR TESTER AND SOFTWARE

This appendix describes the operation of the IC tester and software that are used to interrogate the elements of the array. The testing setup is shown in Figure B.1. It is composed of a PCB with a 256 socket where the wire bonded device is connected, a power source supplying -15 V and +15 V to the transimpedance amplifier, and a NI PXI IC testing rack with excitation and reading cards.

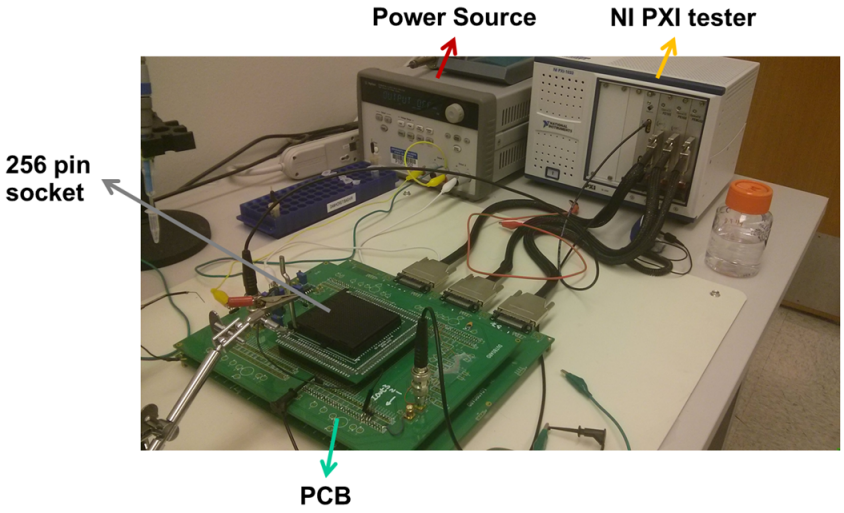

Figure B.1: Testing setup for ISFET array measurement

The user would connect the chip to the 256 PGA socket, then turn on the power supply, and start the MST3 software. Do not connect the chip while the circuit is powered to prevent electrostatic discharge damage. The MTS3 software will open the launcher and panel control windows shown in Figure B.2. The user will then open the desired project with the scripts to test the specific array. C scripts have been created by OpenATE (Hsinchu, Taiwan) and coordinate excitation and reading of the IC testing cards. With

the appropriate project loaded the user will click Utility and TP build to open the editor shown in Figure B.3 (a). In this window the user will define the excitation voltages, number of cycles performed in the array, and lead time between cycles.

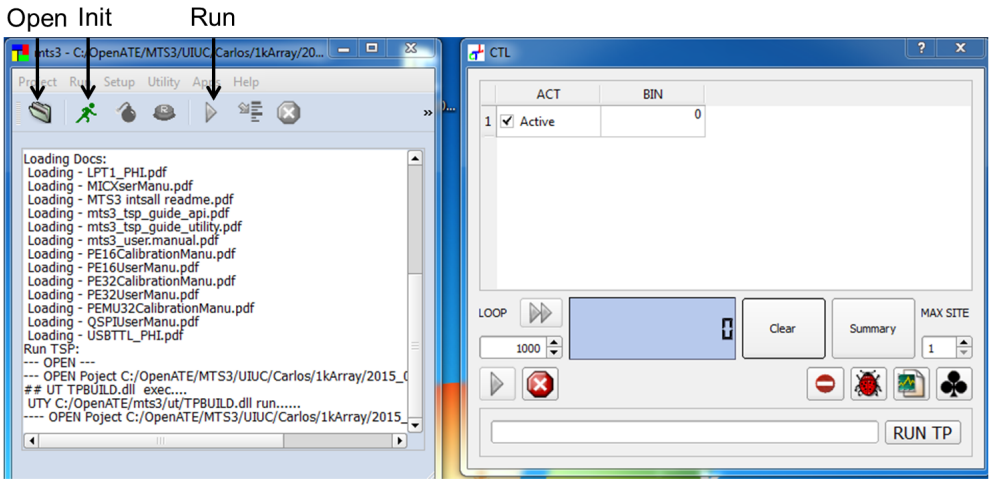

Figure B.2: Launcher and panel control of MTS3 software

After operation variables are defined the user should click on the 'Test' tab to open the window shown in Figure B.3 (b). Here the chip ID with any other relevant experimental information can be described in the $chip_id$ variable. The user should then save and compile the project with icons in the tool bar, and go back to the launcher to initialize and run the code (green man and play button in the tool bar). The program will then execute the measurements and output a csv file with voltages that are related to the drain current in each transistor.

a)

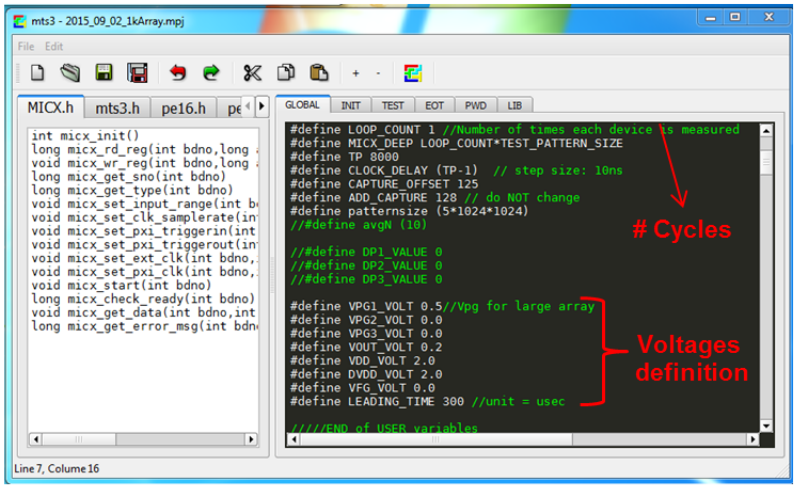

b)

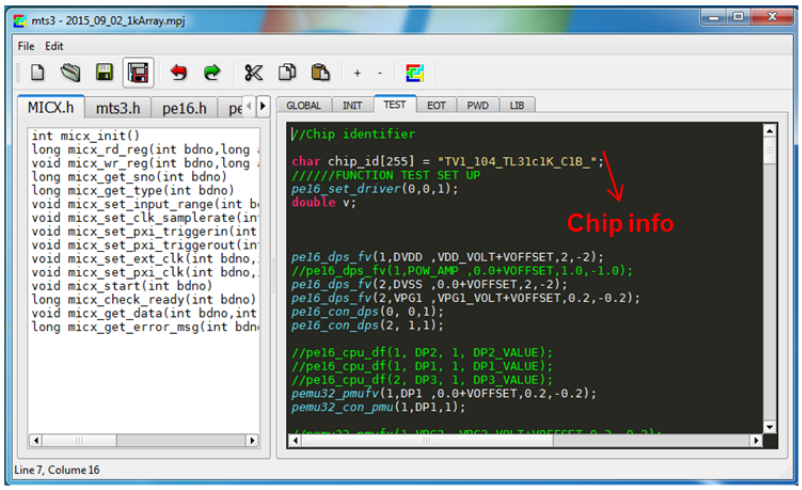

Figure B.3: MTS3 editing windows to define voltages and chip ID

APPENDIX C

SELECTED MATLAB SCRIPTS AND ROUTINES

This appendix specify short subroutines in Matlab used for data analysis or collection. Complete code can be found in our group's website (libna.mntl.illinois.edu).

C.1 Micromanipulator control

```
%Initialize communication with Agilent E3647A to trigger
    injection.
FG_E3647A_init
%set Agilent at 5 so there is no injection (Negative logic)
FG_E3647A_set_voltage(5,0.5);



%This gets data from text boxes
speed = str2num(get(handles.edit_speed,'String'));
zinj= str2num(get(handles.edit_zinj,'String'));
zrel= str2num(get(handles.edit_zrel,'String'));
deltax= str2num(get(handles.edit_x,'String'));
deltay=str2num(get(handles.edit_y,'String'));
columns= str2num(get(handles.edit_columns,'String'));
rows=str2num(get(handles.edit_rows,'String'));
delay=str2num(get(handles.edit_pause,'String'));
tiltpositive = get(handles.checkbox_tilt,'Value');
alignx = str2num(get(handles.static_AlignX,'String'))
aligny = str2num(get(handles.static_AlignY,'String'))

correctx = (alignx-deltax*(columns-1))/(columns-1);
correcty = (aligny-deltay*(rows-1))/(rows-1);
```

```
25
%Send message for alignment in 0,0,0.
27 set(handles.static_status,'String','Align to 0,0,0. Press
    enter in console')
%dummy=input('Align the surface of 1x1 so motor micrometers
    at: x=3 y=3 z= 20, switch to auto and enter');
29 %Initiate communication
if (exist('obj_MCLxyz','var')==0)
31     MCLxyz_init;
end
33 %Set origin

35 MCLxyz_set_position(0,0,0)
%Set speed (faster gives issues on communication and stuck
    motors)
37 MCXxyz_joystick_off(speed)
%Raise tip to injection point
39 MCLxyz_goto_abs(0,0,zinj)
set(handles.static_status,'String','Ready for injection?
    Press enter in console')
41 %dummy=input('Enter if ready for injection');
set(handles.static_status,'String','Inject every beep')
43 %Cycle depending on number of droplets. Every time a row is
    finished will
%change row.
45 c =1;
r=1;
47 movex=deltax+correctx;
movey=deltay+correcty;
49

for (i=1:columns*rows)
51     if (get(handles.pushbutton_start,'UserData') ==2)
         set(handles.static_status,'String','STOP. Program
    was stopped')
53     else
         %Change row columns status
55       set(handles.static_column,'String',c);
         set(handles.static_row,'String',r);
57       %Inject
         beep;
59       FG_E3647A_set_voltage(0,0.5);
         pause(delay)
61       FG_E3647A_set_voltage(5,0.5);
```

```
        %Release
        MCLxyz_goto_abs(0,0,zrel)
        pause(delay)
        %Go to next position
        if (mod(i,columns)==0)
            MCLxyz_goto_abs(-(deltax+correctx)*(columns-1)
    ,-(correcty*(columns-1)),zrel)
            MCLxyz_set_position(0,0,zinj)
            MCLxyz_goto_abs(correctx,deltay+correcty,zinj)
            r=r+1;
        else
            MCLxyz_goto_abs(deltax+correctx,correcty,zinj)
            c=c+1;
        end
        MCLxyz_set_position(0,0,zinj)
    end
end

set(handles.static_status,'String','Array done. Press enter
    in console')
dummy=input('Array done. Press enter when ready to clear');
MCLxyz_goto_abs(5000,5000,-30000)
FG_E3647A_close
MCLxyz_close;
```

C.2 Auto shutter control

```
%Initialize serial communication with shutter
s = serial ('COM1');
fopen (s);

%This gets data from text boxes
temp = str2num(get(handles.edit-Temp,'String'));
inter = str2num(get(handles.edit-Interval,'String'));
expo = str2num(get(handles.edit-exposure,'String'));
ttime = str2num(get(handles.edit-TotalTime,'String'));

% Setting the status bar and getting position from mouse fix
set(handles.static_status,'String','Program has started')
% x is a temporary variable to move data
```

```
x = getappdata(handles.pushbutton_start,'UserData');
xm = x(1);
ym = x(2);

%start the loop, begins in init, steps of inter and finish
    in final
for (i= 0:inter:ttime)
    if (get(handles.pushbutton_start,'UserData') ==2)
        %Close shutter
        fprintf(s,'A');
        set(handles.static-LeftTime,'String',0);
        set(handles.static-CurrentCapture,'String',0);
        fclose (s);
        clear s
    else
    set(handles.static-LeftTime,'String',ttime-i);
    set(handles.static-CurrentCapture,'String',i);
    %Pause for the interval
    pause(inter*60 - expo- 5)
    %Open shutter
    fprintf(s,'\');pause (2)javasetmouselocation( xm,
    ym);javaclickmouse([1
    0]);pause(expo+3)fprintf(s,'A');endendset(handles.static-status,'String','Program
    finished with no interruption')fclose (s);clear s
```

C.3 Import sequential data from IC tester

```

for foldercount = 1:numFolders;
    strFoldercount = int2str ( foldercount );
    eval (['Foldername = folder', strFoldercount, ';']);

    for device = 1:device_count;
        strDevicecount = int2str ( device );
        eval (['Devicename = device', strDevicecount, ';']);

        if(foldercount>1)
            splitDevice = regexp (Devicename, replaceString
    (1), 'split');
            part1 = char(splitDevice(1));
```

```
            part2 = char (splitDevice(2));
            eval(['Devicename = [part1, fold',
    strFoldercount, 'String, part2];']);
        end

        Filename = [Foldername,'\',Devicename, '.csv']
        M = csvread ( Filename, 1, 1 );
        cutName = regexp (Devicename, '_2015', 'split');
        shortName = char (cutName(1));
        cutName = regexp (shortName, 'TV1_', 'split');
        shortName = char (cutName(2));
        Devicename = shortName;
        RawDrain ( foldercount, : ) = mean (transpose(M(:,
    7:7+sweeps-1)));
        if (sweeps == 1)
            DrainI ( foldercount, : ) = ((transpose(M(:,
    7:7+sweeps-1)))-0.2)*10;
        else
            DrainI ( foldercount, : ) = (mean (transpose(M
    (:, 7:7+sweeps-1)))-0.2)*10;
        end
        eval(sprintf('DrainMatrix_%d = transpose(vec2mat(
    DrainI,1024));', device));
        RawNoise ( foldercount, : ) = std (transpose(M(:,
    7:7+sweeps-1)));
        NoiseI ( foldercount, : ) = DrainI.*RawNoise./
    RawDrain;
        eval(sprintf('NoiseMatrix_%d = transpose(vec2mat(
    NoiseI,1024));', device));
     end
end
```

C.4 Pixel-normalized analysis

```
%Plot Id Vg for averaged values
pHArray=str2num(input('Enter an array with test pH [a b ...]
    ','s'));

%Calculate slope
for (i=1:device_count-1)
```

```
    next=i+1;
    eval(sprintf('Diff_%d=DrainMatrix_%d-DrainMatrix_%d;', i
    ,i,next));
    eval(sprintf('PatCurrentSens_%d=Diff_%d/(pHArray(%d)-
    pHArray(%d));', i,i,next,i));
end

%Initialize matrix  with sens data
SensCurrent = zeros(size(DrainMatrix_1));
NoiseCurrent = ones(size(DrainMatrix_1));

%Add the difference matrixes
for (i=1:device_count-1)
    eval(sprintf('SensCurrent=SensCurrent+PatCurrentSens_%d;
    ', i));
end

for (i=1:device_count)
    eval(sprintf('NoiseCurrent= max(NoiseCurrent,
    NoiseMatrix_%d);', i));
end
NoiseCurrent(NoiseCurrent==0)=0.5;
SensCurrent = SensCurrent/(device_count-1);
Tam=size(SensCurrent);
if (Tam(1)==1024)
    ResolutionCurrent = ResolutionCeiling1K((3*NoiseCurrent)
    ./SensCurrent);
else
    ResolutionCurrent = ResolutionCeiling(NoiseCurrent./
    SensCurrent);
end
```

C.5 ESD routine for outlier elimination

```
function [FilteredArray,testT] =ESD_OutliersDelete(x,r,alpha
    )
xy =x;
%Calculate mean and standard deviation for array
for(i=1:r)
    aver = mean(xy);
```

```
    dev = std(xy);
    %Compute largest gap
    Gap_min = abs(aver-min(xy));
    Gap_max = abs(aver-max(xy));
    %Calculate the R stadistic for the largest difference
    R_value = max(Gap_max,Gap_min)/dev;

    %Obtain vector size and p_value (theorem shows equal to
    1-alpha/2n)
    totalN = max(size(xy));
    if(totalN<r)
        break
    end

    p_value = alpha/totalN;
    df = totalN-2;
    %Calculate t distribution
    t_crit = tinv(p_value,df);
    \%Compute lambda
    lambda_crit = (totalN-1)*t_crit/sqrt(totalN*(df+t_crit
    ^2));

    %Eliminate Outlier
    if(R_value>lambda_crit)
        if(Gap_max>Gap_min)
            xy(xy==max(xy))=[];
        else
            xy(xy==min(xy))=[];
        end
    end
end

FilteredArray = xy;
```

REFERENCES

[1] E. K. Sackmann, A. L. Fulton, and D. J. Beebe, "The present and future role of microfluidics in biomedical research," *Nature*, vol. 507, no. 7491, pp. 181–9, 2014. [Online]. Available: http://www.ncbi.nlm.nih.gov/pubmed/24622198

[2] C. Toumazou and P. Georgiou, "Piet Bergveld - 40 years of ISFET technology: From neuronal sensing to DNA sequencing," *Electronics Letters*, vol. 47, no. 26, 2011. [Online]. Available: http://digital-library.theiet.org/content/journals/10.1049/el.2011.3231

[3] M. U. Ahmed, I. Saaem, P. C. Wu, and A. S. Brown, "Personalized diagnostics and biosensors: a review of the biology and technology needed for personalized medicine," *Critical Reviews in Biotechnology*, vol. 34, no. 2, pp. 180–96, 2014. [Online]. Available: http://www.ncbi.nlm.nih.gov/pubmed/23607309

[4] Y. J. Chen, "Some new applications of MEMS in the biomedical and environmental fields," *Advanced Materials Research*, vol. 650, pp. 498–502, 2013. [Online]. Available: http://www.scientific.net/AMR.650.498

[5] M. Balconi and R. Fontana, "Entry and innovation: an analysis of the fabless semiconductor business," *Small Business Economics*, vol. 37, no. 1, pp. 87–106, 2009. [Online]. Available: http://link.springer.com/10.1007/s11187-009-9231-5

[6] B. Merriman, I. T. R&D Team, and J. M. Rothberg, "Progress in Ion Torrent semiconductor chip based sequencing," *Electrophoresis*, vol. 33, no. 23, pp. 3397–3417, 2012. [Online]. Available: http://doi.wiley.com/10.1002/elps.201200424

[7] N. P. Pai, C. Vadnais, C. Denkinger, N. Engel, and M. Pai, "Point-of-care testing for infectious diseases: diversity, complexity, and barriers in low- and middle-income countries," *PLoS Medicine*, vol. 9, no. 9, p. e1001306, 2012. [Online]. Available: http://www.pubmedcentral.nih.gov/articlerender.fcgi?artid=3433407

[8] M. Hamon, O. Oyarzabal, and J. W. Hong, "Nanoliter/picoliter scale fluidic systems for food safety," in *Advances in Applied Nanotechnology for Agriculture*. American Chemical Society, 2013, ch. 8, pp. 145–165. [Online]. Available: http://pubs.acs.org/doi/abs/10.1021/bk-2013-1143.ch008

[9] E. L. Lewandrowski, E. M. Van Cott, K. Gregory, I.-K. Jang, and K. B. Lewandrowski, "Clinical evaluation of the i-STAT kaolin activated clotting time (ACT) test in different clinical settings in a large academic urban medical center: Comparison with the Medtronic ACT Plus," *American Journal of Clinical Pathology*, vol. 135, no. 5, pp. 741–8, 2011. [Online]. Available: http://www.ncbi.nlm.nih.gov/pubmed/21502428

[10] M. A. Poritz, A. J. Blaschke, C. L. Byington, L. Meyers, K. Nilsson, D. E. Jones, S. A. Thatcher, T. Robbins, B. Lingenfelter, E. Amiott, A. Herbener, J. Daly, S. F. Dobrowolski, D. H.-F. Teng, and K. M. Ririe, "FilmArray, an automated nested multiplex PCR system for multi-pathogen detection: development and application to respiratory tract infection," *PloS One*, vol. 6, no. 10, p. e26047, 2011. [Online]. Available: http://www.pubmedcentral.nih.gov/articlerender.fcgi?artid=3198457

[11] GENEU, "Our Genomics Revolution," 2014. [Online]. Available: http://geneu.com/about-geneu/about-us/

[12] P. Craw and W. Balachandran, "Isothermal nucleic acid amplification technologies for point-of-care diagnostics: A critical review," *Lab on a Chip*, vol. 12, no. 14, pp. 2469–86, 2012. [Online]. Available: http://pubs.rsc.org/en/content/articlehtml/2012/lc/c2lc40100b

[13] F. Ahmad and S. A. Hashsham, "Miniaturized nucleic acid amplification systems for rapid and point-of-care diagnostics: A review," *Analytica Chimica Acta*, vol. 733, pp. 1–15, 2012. [Online]. Available: http://www.sciencedirect.com/science/article/pii/S0003267012006265

[14] R. D. Stedtfeld, D. M. Tourlousse, G. Seyrig, T. M. Stedtfeld, M. Kronlein, S. Price, F. Ahmad, E. Gulari, J. M. Tiedje, and S. A. Hashsham, "Gene-Z: a device for point of care genetic testing using a smartphone," *Lab on a Chip*, vol. 12, no. 8, pp. 1454–1462, 2012. [Online]. Available: http://pubs.rsc.org/en/content/articlehtml/2012/lc/c2lc21226a

[15] Y. Zhang and P. Ozdemir, "Microfluidic DNA amplification–a review," *Analytica Chimica Acta*, vol. 638, no. 2, pp. 115–25, 2009. [Online]. Available: http://www.ncbi.nlm.nih.gov/pubmed/19327449

[16] L. Jiang, M. Mancuso, Z. Lu, G. Akar, E. Cesarman, and D. Erickson, "Solar thermal polymerase chain reaction for smartphone-assisted molecular diagnostics," *Scientific Reports*, vol. 4, p. 4137, 2014. [Online]. Available: http://www.pubmedcentral.nih.gov/articlerender.fcgi?artid=3929917

[17] Y. Mori, H. Kanda, and T. Notomi, "Loop-mediated isothermal amplification (LAMP): recent progress in research and development," *Journal of Infection and Chemotherapy*, vol. 19, no. 3, pp. 404–411, 2013. [Online]. Available: http://linkinghub.elsevier.com/retrieve/pii/S1341321X13701223

[18] C. Guiducci and F. M. Spiga, "Another transistor-based revolution: on-chip qPCR," *Nature Methods*, vol. 10, no. 7, pp. 617–8, 2013. [Online]. Available: http://www.ncbi.nlm.nih.gov/pubmed/23807193

[19] E. Scallan, R. M. Hoekstra, F. J. Angulo, R. V. Tauxe, M. A. Widdowson, S. L. Roy, J. L. Jones, and P. M. Griffin, "Foodborne illness acquired in the United States-Major pathogens," *Emerging Infectious Diseases*, vol. 17, no. 1, pp. 7–15, 2011. [Online]. Available: http://www.ncbi.nlm.nih.gov/pmc/articles/PMC3375761/

[20] L. Zach, M. E. Doyle, V. Bier, and C. Czuprynski, "Systems and governance in food import safety: A U.S. perspective," *Food Control*, vol. 27, no. 1, pp. 153–162, 2012. [Online]. Available: http://linkinghub.elsevier.com/retrieve/pii/S0956713512001326

[21] A. Niemz, T. M. Ferguson, and D. S. Boyle, "Point-of-care nucleic acid testing for infectious diseases." *Trends in Biotechnology*, vol. 29, no. 5, pp. 240–50, 2011. [Online]. Available: http://www.ncbi.nlm.nih.gov/pubmed/21377748

[22] E. A. Vetter, J. D. C. Yao, N. L. Wengenack, F. R. Cockerill, and T. F. Smith, "Real-time PCR in clinical microbiology : Applications for routine laboratory testing," *Clinical Microbiology Reviews*, vol. 19, no. 1, pp. 165–256, 2006. [Online]. Available: http://cmr.asm.org/content/19/1/165

[23] M. D. Adams, J. M. Kelley, J. D. Gocayne, M. Dubnick, M. H. Polymeropoulos, H. Xiao, C. R. Merril, A. Wu, B. Olde, R. F. Moreno, A. R. Kerlavage, W. R. Mccombie, and J. C. Venter, "Complementary sequencing: expressed sequence tags and human genome project," *Science*, vol. 252, no. 1990, pp. 1651–1656, 1991.

[24] PRNewswire, "Polymerase chain reaction (PCR) technologies and global markets," BCC research, Wellesley, Tech. Rep., 2010.

[Online]. Available: http://www.bccresearch.com/market-research/biotechnology/polymerase-chain-reaction-markets-bio087a.html

[25] H. VanGuilder, K. Vrana, and W. Freeman, "Twenty-five years of quantitative PCR for gene expression analysis," *BioTechniques*, vol. 44, no. 4, pp. 619–626, 2008. [Online]. Available: http://www.biotechniques.com/article/000112776

[26] Y. Ho Kim, I. Yang, Y.-S. Bae, and S.-R. Park, "Performance evaluation of thermal cyclers for PCR in a rapid cycling condition," *BioTechniques*, vol. 44, no. 4, pp. 495–505, 2008. [Online]. Available: http://www.biotechniques.com/article/000112705

[27] T. Notomi, H. Okayama, H. Masubuchi, T. Yonekawa, K. Watanabe, N. Amino, and T. Hase, "Loop-mediated isothermal amplification of DNA," *Nucleic Acids Research*, vol. 28, no. 12, p. E63, 2000. [Online]. Available: http://nar.oxfordjournals.org/content/28/12/e63

[28] X.-J. Ma, Y.-L. Shu, K. Nie, M. Qin, D.-Y. Wang, R.-B. Gao, M. Wang, L.-Y. Wen, F. Han, S.-M. Zhou, X. Zhao, Y.-H. Cheng, D.-X. Li, and X.-P. Dong, "Visual detection of pandemic influenza A H1N1 Virus 2009 by reverse-transcription loop-mediated isothermal amplification with hydroxynaphthol blue dye," *Journal of Virological Methods*, vol. 167, no. 2, pp. 214–7, 2010. [Online]. Available: http://www.ncbi.nlm.nih.gov/pubmed/20381535

[29] S. Chen, F. Wang, J. C. Beaulieu, R. E. Stein, and B. Ge, "Rapid detection of viable salmonella in produce by coupling propidium monoazide with loop-mediated isothermal amplification," *Applied and Environmental Microbiology*, vol. 77, no. 12, pp. 4008–16, 2011. [Online]. Available: http://aem.asm.org/content/77/12/4008.long

[30] S. Endo, T. Komori, G. Ricci, A. Sano, K. Yokoyama, A. Ohori, K. Kamei, M. Franco, M. Miyaji, and K. Nishimura, "Detection of gp43 of Paracoccidioides brasiliensis by the loop-mediated isothermal amplification (LAMP) method," *FEMS Microbiology Letters*, vol. 234, no. 1, pp. 93–7, 2004. [Online]. Available: http://www.ncbi.nlm.nih.gov/pubmed/15109725

[31] Q.-M. Kong, S.-H. Lu, Q.-B. Tong, D. Lou, R. Chen, B. Zheng, T. Kumagai, L.-Y. Wen, N. Ohta, and X.-N. Zhou, "Loop-mediated isothermal amplification (LAMP): Early detection of toxoplasma gondii infection in mice," *Parasites & Vectors*, vol. 5, no. 1, p. 2, 2012. [Online]. Available: http://www.pubmedcentral.nih.gov/articlerender.fcgi?artid=3280158

[32] Eiken Chemical Co, "The principle of LAMP method About LAMP method," 2005. [Online]. Available: http://loopamp.eiken.co.jp/e/lamp/

[33] K. Nagamine, T. Hase, and T. Notomi, "Accelerated reaction by loop-mediated isothermal amplification using loop primers," *Molecular and Cellular Probes*, vol. 16, no. 3, pp. 223–229, 2002. [Online]. Available: http://www.sciencedirect.com/science/article/pii/S0890850802904159

[34] Z. K. Njiru, "Loop-mediated isothermal amplification technology: Towards point of care diagnostics," *PLoS Neglected Tropical Diseases*, vol. 6, no. 6, p. e1572, 2012. [Online]. Available: http://dx.plos.org/10.1371/journal.pntd.0001572

[35] M. M. Ali, F. Li, Z. Zhang, K. Zhang, D.-K. Kang, J. A. Ankrum, X. C. Le, and W. Zhao, "Rolling circle amplification: a versatile tool for chemical biology, materials science and medicine," *Chemical Society reviews*, vol. 43, no. 10, pp. 3324–41, 2014. [Online]. Available: http://www.ncbi.nlm.nih.gov/pubmed/24643375

[36] H. Zhou, K. Bouwman, M. Schotanus, C. Verweij, J. A. Marrero, D. Dillon, J. Costa, P. Lizardi, and B. B. Haab, "Two-color, rolling-circle amplification on antibody microarrays for sensitive, multiplexed serum-protein measurements," *Genome Biology*, vol. 5, no. 4, p. R28, 2004. [Online]. Available: http://www.pubmedcentral.nih.gov/articlerender.fcgi?artid=395787

[37] E. Cho, L. Yang, M. Levy, and A. Ellington, "Using a deoxyribozyme ligase and rolling circle amplification to detect a non-nucleic acid analyte, ATP," *Journal of American Chemical Society*, vol. 127, pp. 2022–2023, 2005. [Online]. Available: http://pubs.acs.org/doi/abs/10.1021/ja043490u

[38] W. Zhao, C. H. Cui, S. Bose, D. Guo, C. Shen, W. P. Wong, K. Halvorsen, O. C. Farokhzad, G. S. L. Teo, J. a. Phillips, D. M. Dorfman, R. Karnik, and J. M. Karp, "Bioinspired multivalent DNA network for capture and release of cells," *Proceedings of the National Academy of Sciences*, vol. 109, no. 48, pp. 19 626–31, nov 2012. [Online]. Available: http://www.pubmedcentral.nih.gov/articlerender.fcgi?artid=3511714

[39] B. Liu, X. Ouyang, J. Chao, H. Liu, Y. Zhao, and C. Fan, "Self-assembly of DNA origami using rolling circle amplification based DNA nanoribbons," *Chinese Journal of Chemistry*, vol. 32, no. 2, pp. 137–141, 2014. [Online]. Available: http://doi.wiley.com/10.1002/cjoc.201300827

[40] J. Inoue, Y. Shigemori, and T. Mikawa, "Improvements of rolling circle amplification (RCA) efficiency and accuracy using Thermus thermophilus SSB mutant protein," *Nucleic Acids Research*, vol. 34, no. 9, p. e69, 2006. [Online]. Available: http://www.pubmedcentral.nih.gov/articlerender.fcgi?artid=1463899

[41] O. Piepenburg, C. Williams, N. Armes, and D. Stemple, "Recombinase polymerase amplification," ASM Scientific Inc, assignee. Patent US7399590B2. 20 Mar. 2004. Print.

[42] M. Euler, Y. Wang, P. Otto, H. Tomaso, R. Escudero, P. Anda, F. T. Hufert, and M. Weidmann, "Recombinase polymerase amplification assay for rapid detection of Francisella tularensis," *Journal of Clinical Microbiology*, vol. 50, no. 7, pp. 2234–8, 2012. [Online]. Available: http://www.pubmedcentral.nih.gov/articlerender.fcgi?artid=3405570

[43] D. J. Arndt-Jovin, M. Robert-Nicoud, D. a. Zarling, C. Greider, E. Weimer, and T. M. Jovin, "Left-handed Z-DNA in bands of acid-fixed polytene chromosomes," *Proceedings of the National Academy of Sciences*, vol. 80, no. 14, pp. 4344–8, 1983. [Online]. Available: http://www.pubmedcentral.nih.gov/articlerender.fcgi?artid=384034

[44] Twist Dx Inc., "A Revolution in DNA Detection," 2014. [Online]. Available: http://www.twistdx.co.uk/

[45] F. L. Kiechle and C. a. Holland, "Point-of-care testing and molecular diagnostics: miniaturization required," *Clinics in laboratory medicine*, vol. 29, no. 3, pp. 555–60, 2009. [Online]. Available: http://www.ncbi.nlm.nih.gov/pubmed/19840687

[46] H. Ledford, "Life hackers," *Nature*, vol. 467, no. 7316, pp. 650–652, 2010. [Online]. Available: http://www.nature.com/news/2010/101006/full/467650a.html

[47] J. Love and R. Marquis-Nicholson, "Portable battery-operated rapid PCR amplification of the CAG repeat region of the Huntington disease locus," *Research Journal of Biology*, vol. 02, no. 06, pp. 191–196, 2012. [Online]. Available: https://www.yumpu.com/en/document/view/26128091/portable-battery-operated-rapid-pcr-scientific-journals

[48] OpenPCR, "Real-Time PCR Coming soon Your open-source PCR Thermocycler ," 2014. [Online]. Available: http://openpcr.org/

[49] BioFire, "FilmArray Panels," 2014. [Online]. Available: http://filmarray.com/the-panels/

[50] D. Matricardi, "The FilmArray System: A fire fueled by consumables," 2012. [Online]. Available: http://www.mdbuyline.com/blog/the-filmarray-system-a-fire-fueled-by-consumables/

[51] T. Abe, Y. Segawa, H. Watanabe, T. Yotoriyama, S. Kai, A. Yasuda, N. Shimizu, and N. Tojo, "Point-of-care testing system enabling 30 min detection of influenza genes," *Lab on a Chip*, vol. 11, no. 6, pp. 1166–7, 2011.

[52] S. C. K. Lam, K. L. Wong, K. O. Wong, W. Wong, and W. H. Mow, "A smartphone-centric platform for personal health monitoring using wireless wearable biosensors," in *7th International Conference on Information, Communications and Signal Processing, ICICS*, 2009. [Online]. Available: http://dx.doi.org/10.1109/ICICS.2009.5397628 pp. 1–7.

[53] D. Gallegos, K. D. Long, H. Yu, P. P. Clark, Y. Lin, S. George, P. Nath, and B. T. Cunningham, "Label-free biodetection using a smartphone," *Lab on a Chip*, vol. 13, no. 11, p. 2124, 2013. [Online]. Available: http://xlink.rsc.org/?DOI=c3lc40991k

[54] H. Yu, Y. Tan, and B. T. Cunningham, "Smartphone fluorescence spectroscopy," *Analytical Chemistry*, vol. 86, no. 17, pp. 8805–13, 2014. [Online]. Available: http://www.ncbi.nlm.nih.gov/pubmed/25098859

[55] E. J. Topol, "Individualized medicine from prewomb to tomb," *Cell*, vol. 157, no. 1, pp. 241–253, 2014. [Online]. Available: http://linkinghub.elsevier.com/retrieve/pii/S0092867414002049

[56] Biomeme Inc., "Biomeme device is a real-time PCR thermocycler that attaches to your iPhone 5," 2015. [Online]. Available: http://www.biomeme.com/

[57] P. R. Wakeley, J. Errington, S. Hannon, H. I. J. Roest, T. Carson, B. Hunt, J. Sawyer, and P. Heath, "Development of a real time PCR for the detection of Taylorella equigenitalis directly from genital swabs and discrimination from Taylorella asinigenitalis," *Veterinary Microbiology*, vol. 118, no. 3-4, pp. 247–54, 2006. [Online]. Available: http://www.ncbi.nlm.nih.gov/pubmed/16971068

[58] K. Sugawara, M. Himeno, T. Keima, Y. Kitazawa, K. Maejima, K. Oshima, and S. Namba, "Rapid and reliable detection of phytoplasma by loop-mediated isothermal amplification targeting a housekeeping gene," *Journal of General Plant Pathology*, vol. 78, no. 6, pp. 389–397, 2012. [Online]. Available: http://link.springer.com/10.1007/s10327-012-0403-9

[59] A. Bühlmann, J. F. Pothier, F. Rezzonico, T. H. M. Smits, M. Andreou, N. Boonham, B. Duffy, and J. E. Frey, "Erwinia amylovora loop-mediated isothermal amplification (LAMP) assay for rapid pathogen detection and on-site diagnosis of fire blight," *Journal of Microbiological Methods*, vol. 92, no. 3, pp. 332–339, 2013. [Online]. Available: http://dx.doi.org/10.1016/j.mimet.2012.12.017

[60] B. Y. Ng, E. J. Wee, N. P. West, and M. Trau, "Rapid DNA detection of Mycobacterium tuberculosis-towards single cell sensitivity in point-of-care diagnosis," *Scientific Reports*, vol. 5, p. 15027, 2015. [Online]. Available: http://www.nature.com/articles/srep15027

[61] C. Escadafal, O. Faye, A. A. Sall, O. Faye, M. Weidmann, O. Strohmeier, F. von Stetten, J. Drexler, M. Eberhard, M. Niedrig, and P. Patel, "Rapid molecular assays for the detection of yellow fever virus in low-resource settings," *PLoS Neglected Tropical Diseases*, vol. 8, no. 3, p. e2730, 2014. [Online]. Available: http://journals.plos.org/plosntds/article?id=10.1371/journal.pntd.0002730

[62] E. J. H. Wee, H. Y. Lau, J. R. Botella, and M. Trau, "Re-purposing bridging flocculation for on-site, rapid, qualitative DNA detection in resource-poor settings," *Chemical Communications*, vol. 51, no. 27, pp. 5828–5831, 2015. [Online]. Available: http://xlink.rsc.org/?DOI=C4CC10068A

[63] S. Lutz, P. Weber, M. Focke, B. Faltin, J. Hoffmann, C. Müller, D. Mark, G. Roth, P. Munday, N. Armes, O. Piepenburg, R. Zengerle, and F. von Stetten, "Microfluidic lab-on-a-foil for nucleic acid analysis based on isothermal recombinase polymerase amplification (RPA)," *Lab on a Chip*, vol. 10, no. 7, p. 887, 2010. [Online]. Available: http://xlink.rsc.org/?DOI=b921140c

[64] S. Purushothaman, C. Toumazou, and C.-P. Ou, "Protons and single nucleotide polymorphism detection: A simple use for the ion sensitive field effect transistor," *Sensors and Actuators B: Chemical*, vol. 114, no. 2, pp. 964–968, 2006. [Online]. Available: http://www.sciencedirect.com/science/article/pii/S0925400505007409

[65] C. Toumazou, L. M. Shepherd, S. C. Reed, G. I. Chen, A. Patel, D. M. Garner, C.-J. Wang, C.-P. Ou, K. Amin-Desai, P. Athanasiou, H. Bai, I. M. Q. Brizido, B. Caldwell, D. Coomber-Alford, P. Georgiou, K. S. Jordan, J. C. Joyce, M. La Mura, D. Morley, S. Sathyavruthan, S. Temelso, R. E. Thomas, and L. Zhang, "Simultaneous DNA amplification and detection using a pH-sensing semiconductor system," *Nature Methods*, vol. 10, no. 7, pp. 641–6, 2013. [Online]. Available: http://www.ncbi.nlm.nih.gov/pubmed/23749303

[66] P. Athanasiou, A. Patel, D. Witaker, H. Bai, and J. Palmer-felgate, "Biosensor Device And System," 2012, Dna Electronics Ltd, assignee. Patent WO2013144643A2. 03 Oct. 2013. Print.

[67] A. S. Patterson, K. Hsieh, H. T. Soh, and K. W. Plaxco, "Electrochemical real-time nucleic acid amplification: Towards point-of-care quantification of pathogens," *Trends in Biotechnology*, vol. 31, no. 12, pp. 704–12, 2013. [Online]. Available: http://www.ncbi.nlm.nih.gov/pubmed/24209384

[68] T. Deféver, M. Druet, M. Rochelet-Dequaire, M. Joannes, C. Grossiord, B. Limoges, and D. Marchal, "Real-time electrochemical monitoring of the polymerase chain reaction by mediated redox catalysis," *Journal of the American Chemical Society*, vol. 131, no. 32, pp. 11 433–11 441, 2009. [Online]. Available: http://pubs.acs.org/doi/abs/10.1021/ja901368m

[69] B. Y. Won, S. Shin, S. Baek, Y. L. Jung, T. Li, S. C. Shin, D.-Y. Cho, S. B. Lee, and H. G. Park, "Investigation of the signaling mechanism and verification of the performance of an electrochemical real-time PCR system based on the interaction of methylene blue with DNA," *Analyst*, vol. 136, no. 8, pp. 1573–9, 2011. [Online]. Available: http://www.ncbi.nlm.nih.gov/pubmed/21321686

[70] X. Luo, F. Xuan, and I. M. Hsing, "Real time electrochemical monitoring of PCR amplicons using electroactive hydrolysis probe," *Electrochemistry Communications*, vol. 13, no. 7, pp. 742–745, 2011. [Online]. Available: http://dx.doi.org/10.1016/j.elecom.2011.04.027

[71] N. T. Q. Nhu, D. Heemskerk, D. D. A. Thu, T. T. H. Chau, N. T. H. Mai, H. D. T. Nghia, P. P. Loc, D. T. M. Ha, L. Merson, T. T. V. Thinh, J. Day, N. v. V. Chau, M. Wolbers, J. Farrar, and M. Caws, "Evaluation of GeneXpert MTB/RIF for diagnosis of tuberculous meningitis," *Journal of Clinical Microbiology*, vol. 52, no. 1, pp. 226–233, 2014. [Online]. Available: http://jcm.asm.org/cgi/doi/10.1128/JCM.01834-13

[72] M. J. Binnicker, M. J. Espy, C. L. Irish, and E. a. Vetter, "Direct detection of influenza A/B in less than twenty minutes using a commercially-available rapid PCR assay," *Journal of Clinical Microbiology*, vol. 53, no. 7, pp. JCM.00 791–15, 2015. [Online]. Available: http://jcm.asm.org/lookup/doi/10.1128/JCM.00791-15

[73] P. Ruggiero, T. McMillen, Y. W. Tang, and N. E. Babady, "Evaluation of the BioFire FilmArray Respiratory Panel and the GenMark eSensor Respiratory Viral Panel on Lower Respiratory Tract Specimens," *Journal of Clinical Microbiology*, vol. 52, no. 1, pp. 288–290, 2014.

[74] DNA Electronics, "Genalysis," 2014. [Online]. Available: http://dnae.co.uk/platforms/genalysis/lab-free-dna-testing/

[75] F. Kivlehan, F. Mavré, L. Talini, B. Limoges, and D. Marchal, "Real-time electrochemical monitoring of isothermal helicase-dependent amplification of nucleic acids," *Analyst*, vol. 136, no. 18, pp. 3635–42, 2011. [Online]. Available: http://www.ncbi.nlm.nih.gov/pubmed/21792448

[76] S. Hakenberg, M. Hügle, M. Weidmann, F. Hufert, G. Dame, and G. A. Urban, "A phaseguided passive batch microfluidic mixing chamber for isothermal amplification," *Lab on a Chip*, vol. 12, p. 4576, 2012. [Online]. Available: http://pubs.rsc.org/en/content/articlehtml/2012/lc/c2lc40765e

[77] A. N. Mohon, R. Elahi, W. A. Khan, R. Haque, D. J. Sullivan, and M. S. Alam, "A new visually improved and sensitive loop mediated isothermal amplification (LAMP) for diagnosis of symptomatic falciparum malaria," *Acta Tropica*, vol. 134, pp. 52–57, 2014. [Online]. Available: http://linkinghub.elsevier.com/retrieve/pii/S0001706X1400062X

[78] J. McCormack, E. Harrington, J. O'Halloran, M. Solomon, D. Briggs, M. Andre, and M. Schuenemann, "Fabrication and use of a microfluidics multitemperature flexible reaction device," 2014, Quantumdx Group Limited, assignee. Patent US 14/159,219. 20 Jan. 2014. Print.

[79] Foodborne Diseases Active Surveillance Network (FoodNet), "Trends in foodborne illness in the United States, 2006-2013," pp. 1–8, 2014. [Online]. Available: http://www.cdc.gov/foodborneburden/trends-in-foodborne-illness.html

[80] L. A. Hanson, E. A. Zahn, S. R. Wild, D. Döpfer, J. Scott, and C. Stein, "Estimating global mortality from potentially foodborne diseases: an analysis using vital registration data," *Population Health Metrics*, vol. 10, no. 1, p. 5, 2012. [Online]. Available: http://www.pubmedcentral.nih.gov/articlerender.fcgi?artid=3341201

[81] Inspection and Safety Division of the Department of Food Safety, "Food Poisoning Statistics 2009," Pharmaceutical and Food Safety Bureau of Japan, Tech. Rep., 2009. [Online]. Available: http://www.mhlw.go.jp/english/topics/foodsafety/poisoning/

[82] E. C. Alocilja and S. M. Radke, "Market analysis of biosensors for food safety," *Biosensors and Bioelectronics*, vol. 18, no. 5-6, pp. 841–846, 2003. [Online]. Available: http://linkinghub.elsevier.com/retrieve/pii/S0956566303000095

[83] United States Deparment of Agriculture. Food Safety Inspection Service, "FSIS Accredited Laboratories," 2014. [Online]. Available: http://www.fsis.usda.gov/wps/portal/fsis/topics/science/laboratories-and-procedures/accredited-laboratories/accredited-laboratories

[84] L. Galli, E. Miliwebsky, K. Irino, G. Leotta, and M. Rivas, "Virulence profile comparison between LEE-negative Shiga toxin-producing Escherichia coli (STEC) strains isolated from cattle and humans," *Veterinary microbiology*, vol. 143, no. 2-4, pp. 307–13, 2010. [Online]. Available: http://www.ncbi.nlm.nih.gov/pubmed/20022185

[85] E. Gouin, J. Mengaud, and P. Cossart, "The virulence gene cluster of Listeria Monocytogenes is also present in Listeria Ivanovii , an animal pathogen , and Listeria Seeligeri , a nonpathogenic species," *Infection and Immunity*, vol. 62, pp. 3550–3553, 1994. [Online]. Available: http://iai.asm.org/content/62/8/3550.long

[86] C. G. Pfeifer, S. L. Marcus, O. Steele-mortimer, L. A. Knodler, and B. B. Finlay, "Salmonella typhimurium virulence genes are induced upon bacterial invasion into phagocytic and nonphagocytic cells," *Infection and Immunity*, vol. 67, pp. 5690–5698, 1999. [Online]. Available: http://iai.asm.org/content/67/11/5690.long

[87] Laboratory Quality Assurance Division (LQAD), "Detection, isolation and identification of Escherichia coli O157 : H7 from meat products," *USDA FSIS Laboratory Guidebook*, no. MLG 5.06, pp. 1–16, 2012. [Online]. Available: http://goo.gl/imDiKI

[88] R. F. Wang, W. W. Cao, and C. E. Cerniglia, "A universal protocol for PCR detection of 13 species of foodborne pathogens in foods," *Journal of Applied Microbiology*, vol. 83, no. 6, pp. 727–736, 1997. [Online]. Available: http://onlinelibrary.wiley.com/doi/10.1046/j.1365-2672.1997.00300.x/abstract

[89] P. Feng, "Rapid methods for the detection foofborne pathogens: Current and next-genetation technologies," in *Food Microbiology: Fundamental and Frontiers*, M. Doyle and L. Beuchat, Eds. Washington, D.C.: ASM Press, 2007, ch. 43, pp. 911–934.

[90] X. Li, E. Ximenes, M. A. R. Amalaradjou, H. B. Vibbert, K. Foster, J. Jones, X. Liu, A. K. Bhunia, and M. R. Ladisch, "Rapid sample processing for foodborne pathogen detection via crossflow microfiltration," *Applied and Environmental Microbiology*, vol. 79, no. 22, pp. AEM.02 587–13, 2013. [Online]. Available: http://aem.asm.org/content/early/2013/09/03/AEM.02587-13

[91] L. Yang, P. P. Banada, M. R. Chatni, K. Seop Lim, A. K. Bhunia, M. Ladisch, and R. Bashir, "A multifunctional micro-fluidic system for dielectrophoretic concentration coupled with immuno-capture of low numbers of Listeria monocytogenes," *Lab on a Chip*, vol. 6, no. 7, p. 896, 2006. [Online]. Available: http://xlink.rsc.org/?DOI=b607061m

[92] M.-J. Tang, S. Zhou, X.-Y. Zhang, J.-H. Pu, Q.-L. Ge, X.-J. Tang, and Y.-S. Gao, "Rapid and sensitive detection of Listeria monocytogenes by loop-mediated isothermal amplification," *Current Microbiology*, vol. 63, no. 6, pp. 511–6, 2011. [Online]. Available: http://link.springer.com/article/10.1007/s00284-011-0013-3

[93] F. Wang, L. Jiang, and B. Ge, "Loop-mediated isothermal amplification assays for detecting shiga toxin-producing Escherichia coli in ground beef and human stools," *Journal of Clinical Microbiology*, vol. 50, no. 1, pp. 91–7, 2012. [Online]. Available: http://jcm.asm.org/content/50/1/91.short

[94] W. Wang, H.-B. Wang, Z.-X. Li, and Z.-Y. Guo, "Silicon inhibition effects on the polymerase chain reaction: A real-time detection approach," *Journal of Biomedical Materials Research. Part A*, vol. 77, no. 1, pp. 28–34, 2006. [Online]. Available: http://www.ncbi.nlm.nih.gov/pubmed/16345097

[95] H. Wang, L. Wang, L. Yuan, W. Yang, J. L. Brash, and H. Chen, "Inhibitory effect of silicon nanowires on the polymerase chain reaction," *Nanotechnology*, vol. 23, no. 36, p. 365101, 2012. [Online]. Available: http://www.ncbi.nlm.nih.gov/pubmed/22914382

[96] C. Zhang and D. Xing, "Single-molecule DNA amplification and analysis using microfluidics," *Chemical Reviews*, vol. 110, no. 8, pp. 4910–47, 2010. [Online]. Available: http://www.ncbi.nlm.nih.gov/pubmed/20394378

[97] F. Ahmad, G. Seyrig, D. M. Tourlousse, R. D. Stedtfeld, J. M. Tiedje, and S. A. Hashsham, "A CCD-based fluorescence imaging system for real-time loop-mediated isothermal amplification-based rapid and sensitive detection of waterborne pathogens on microchips," *Biomedical Microdevices*, vol. 13, no. 5, pp. 929–37, 2011. [Online]. Available: http://link.springer.com/article/10.1007/s10544-011-9562-2/fulltext.html

[98] W. E. Tenhaeff and K. K. Gleason, "Initiated and oxidative chemical vapor deposition of polymeric thin films: iCVD and oCVD," *Advanced Functional Materials*, vol. 18, no. 7, pp. 979–992, 2008. [Online]. Available: http://doi.wiley.com/10.1002/adfm.200701479

[99] Y. Kimura, M. J. L. de Hoon, S. Aoki, Y. Ishizu, Y. Kawai, Y. Kogo, C. O. Daub, A. Lezhava, E. Arner, and Y. Hayashizaki, "Optimization of turn-back primers in isothermal amplification," *Nucleic Acids Research*, vol. 39, no. 9, p. e59, 2011. [Online]. Available: http://nar.oxfordjournals.org/content/39/9/e59.long

[100] E. Zubritsky, "Spotting a microarray system," *Analytical Chemistry*, vol. 72, no. 23, pp. 761A–767A, 2000. [Online]. Available: http://www.ncbi.nlm.nih.gov/pubmed/11128961

[101] T. J. Anchordoquy and M. C. Molina, "Preservation of DNA," *Cell Preservation Technology*, vol. 5, no. 4, pp. 180–188, 2007. [Online]. Available: http://www.liebertonline.com/doi/abs/10.1089/cpt.2007.0511

[102] M. D. C. Molina, T. K. Armstrong, Y. Zhang, M. M. Patel, Y. K. Lentz, and T. J. Anchordoquy, "The stability of lyophilized lipid/DNA complexes during prolonged storage," *Journal of Pharmaceutical Sciences*, vol. 93, no. 9, pp. 2259–73, 2004. [Online]. Available: http://www.ncbi.nlm.nih.gov/pubmed/15295787

[103] E. Scallan, "Foodborne illness acquired in the United States - major Pathogens," *Emerging Infectious Diseases*, vol. 17, no. 1, pp. 7–15, 2011.

[104] D. Werber, G. Krause, C. Frank, A. Fruth, A. Flieger, M. Mielke, L. Schaade, and K. Stark, "Outbreaks of virulent diarrheagenic Escherichia coli–are we in control?" *BMC Medicine*, vol. 10, no. 1, p. 11, 2012. [Online]. Available: http://www.pubmedcentral.nih.gov/articlerender.fcgi?artid=3350439

[105] F. Wang, L. Jiang, Q. Yang, W. Prinyawiwatkul, and B. Ge, "Rapid and specific detection of escherichia coli serogroups O26, O45, O103, O111, O121, O145, and O157 in ground beef, beef trim, and produce by loop-mediated isothermal amplification," *Applied and Environmental Microbiology*, vol. 78, no. 8, pp. 2727–36, 2012. [Online]. Available: http://aem.asm.org/content/early/2012/02/07/AEM.07975-11.short

[106] W. Wong, P. Georgiou, C.-P. Ou, and C. Toumazou, "PG-ISFET based DNA-logic for reaction monitoring," *Electronics Letters*, vol. 46, no. 5, p. 330, 2010. [Online]. Available: http://digital-library.theiet.org/content/journals/10.1049/el.2010.3463

[107] E. Salm, C. Duarte-Guevara, P. Dak, B. R. Dorvel, B. Reddy, M. A. Alam, and R. Bashir, "Ultralocalized thermal reactions in subnanoliter droplets-in-air," *Proceedings of the National Academy*

of Sciences, vol. 110, no. 9, pp. 1–6, 2013. [Online]. Available: http://www.pnas.org/content/110/9/3310.abstract

[108] N. Jokilaakso, E. Salm, A. Chen, L. Millet, C. Duarte-Guevara, B. Dorvel, B. Reddy, A. E. Karlstrom, Y. Chen, H. Ji, R. Sooryakumar, and R. Bashir, "Ultra-localized single cell electroporation using silicon nanowires," *Lab on a Chip*, vol. 13, no. 3, pp. 336–9, 2013. [Online]. Available: http://www.ncbi.nlm.nih.gov/pubmed/23179093

[109] P. Bergveld, "Development of an ion-sensitive solid-state device for neurophysiological measurements," *IEEE Transactions*, pp. 70–71, 1970. [Online]. Available: http://www.ncbi.nlm.nih.gov/pubmed/23785103

[110] P. Bergveld, "Thirty years of ISFETOLOGY: What happened in the past 30 years and what may happen in the next 30 years," *Sensors and Actuators B: Chemical*, vol. 88, pp. 1–20, 2003. [Online]. Available: http://www.sciencedirect.com/science/article/pii/S0925400502003015

[111] K. Balasubramanian, "Challenges in the use of 1D nanostructures for on-chip biosensing and diagnostics: A review," *Biosensors & Bioelectronics*, vol. 26, no. 4, pp. 1195–204, 2010. [Online]. Available: http://www.ncbi.nlm.nih.gov/pubmed/20692156

[112] Y. Cui, Q. Wei, H. Park, and C. M. Lieber, "Nanowire nanosensors for highly sensitive and selective detection of biological and chemical species," *Science*, vol. 293, no. 5533, pp. 1289–92, 2001. [Online]. Available: http://www.ncbi.nlm.nih.gov/pubmed/11509722

[113] B. R. Dorvel, B. Reddy, J. Go, C. Duarte-Guevara, E. Salm, M. A. Alam, and R. Bashir, "Silicon nanowires with high-k hafnium oxide dielectrics for sensitive detection of small nucleic acid oligomers," *ACS Nano*, vol. 6, no. 7, pp. 6150–64, 2012. [Online]. Available: http://www.ncbi.nlm.nih.gov/pubmed/22695179

[114] R. M. Penner, "Chemical sensing with nanowires," *Annual Review of Analytical Chemistry*, vol. 5, pp. 461–85, 2012. [Online]. Available: http://www.ncbi.nlm.nih.gov/pubmed/22524224

[115] Y. Chen, A. Star, and S. Vidal, "Sweet carbon nanostructures: carbohydrate conjugates with carbon nanotubes and graphene and their applications," *Chemical Society Reviews*, vol. 42, no. 11, pp. 4532–42, 2013. [Online]. Available: http://www.ncbi.nlm.nih.gov/pubmed/23247183

[116] J. Lei and H. Ju, "Nanotubes in biosensing," *Wiley Interdisciplinary Reviews. Nanomedicine and Nanobiotechnology*, vol. 2, no. 5, pp.

496–509, 2010. [Online]. Available: http://www.ncbi.nlm.nih.gov/pubmed/20803683

[117] T. Ahuja and D. Kumar, "Recent progress in the development of nano-structured conducting polymers/nanocomposites for sensor applications," *Sensors and Actuators B: Chemical*, vol. 136, no. 1, pp. 275–286, 2009. [Online]. Available: http://linkinghub.elsevier.com/retrieve/pii/S0925400508006357

[118] X. Li, E. Chin, H. Sun, P. Kurup, and Z. Gu, "Fabrication and integration of metal oxide nanowire sensors using dielectrophoretic assembly and improved post-assembly processing," *Sensors and Actuators B: Chemical*, vol. 148, no. 2, pp. 404–412, 2010. [Online]. Available: http://linkinghub.elsevier.com/retrieve/pii/S0925400510004703

[119] S. Pal, E. C. Alocilja, and F. P. Downes, "Nanowire labeled direct-charge transfer biosensor for detecting Bacillus species," *Biosensors & Bioelectronics*, vol. 22, no. 9-10, pp. 2329–36, 2007. [Online]. Available: http://www.ncbi.nlm.nih.gov/pubmed/17320373

[120] Y. Lung Khung and D. Narducci, "Synergizing nucleic acid aptamers with 1-dimensional nanostructures as label-free field-effect transistor biosensors," *Biosensors & Bioelectronics*, vol. 50, no. 2013, pp. 278–93, 2013. [Online]. Available: http://www.ncbi.nlm.nih.gov/pubmed/23872609

[121] M. S. Makowski and A. Ivanisevic, "Molecular analysis of blood with micro-/nanoscale field-effect-transistor biosensors," *Small*, vol. 7, no. 14, pp. 1863–75, 2011. [Online]. Available: http://www.pubmedcentral.nih.gov/articlerender.fcgi?artid=3876889

[122] D.-J. Kim, N.-E. Lee, J.-S. Park, I.-J. Park, J.-G. Kim, and H. J. Cho, "Organic electrochemical transistor based immunosensor for prostate specific antigen (PSA) detection using gold nanoparticles for signal amplification," *Biosensors & Bioelectronics*, vol. 25, no. 11, pp. 2477–82, 2010. [Online]. Available: http://www.ncbi.nlm.nih.gov/pubmed/20435461

[123] E. Stern, A. Vacic, C. Li, F. N. Ishikawa, C. Zhou, M. a. Reed, and T. M. Fahmy, "A nanoelectronic enzyme-linked immunosorbent assay for detection of proteins in physiological solutions," *Small*, vol. 6, no. 2, pp. 232–8, 2010. [Online]. Available: http://www.pubmedcentral.nih.gov/articlerender.fcgi?artid=2838924

[124] J.-Y. Kim, K. Choi, D.-I. Moon, J.-H. Ahn, T. J. Park, S. Y. Lee, and Y.-K. Choi, "Surface engineering for enhancement of sensitivity in an underlap-FET biosensor by control of wettability," *Biosensors*

& Bioelectronics, vol. 41, pp. 867–70, 2013. [Online]. Available: http://www.ncbi.nlm.nih.gov/pubmed/22985673

[125] J.-R. Gong, "Label-free attomolar detection of proteins using integrated nanoelectronic and electrokinetic devices," *Small*, vol. 6, no. 8, pp. 967–73, 2010. [Online]. Available: http://www.ncbi.nlm.nih.gov/pubmed/20209654

[126] A. Al-Ahdal and C. Toumazou, "High gain ISFET based νMOS chemical inverter," *Sensors and Actuators B: Chemical*, vol. 171-172, pp. 110–117, 2012. [Online]. Available: http://linkinghub.elsevier.com/retrieve/pii/S0925400511010720

[127] J. M. Rothberg, W. Hinz, T. M. Rearick, J. Schultz, W. Mileski, M. Davey, J. H. Leamon, K. Johnson, M. J. Milgrew, M. Edwards, J. Hoon, J. F. Simons, D. Marran, J. W. Myers, J. F. Davidson, A. Branting, J. R. Nobile, B. P. Puc, D. Light, T. A. Clark, M. Huber, J. T. Branciforte, I. B. Stoner, S. E. Cawley, M. Lyons, Y. Fu, N. Homer, M. Sedova, X. Miao, B. Reed, J. Sabina, E. Feierstein, M. Schorn, M. Alanjary, E. Dimalanta, D. Dressman, R. Kasinskas, T. Sokolsky, J. A. Fidanza, E. Namsaraev, K. J. McKernan, A. Williams, G. T. Roth, and J. Bustillo, "An integrated semiconductor device enabling non-optical genome sequencing," *Nature*, vol. 475, no. 7356, pp. 348–52, 2011. [Online]. Available: http://www.nature.com/nature/journal/v475/n7356/full/nature10242.html

[128] M. Kalofonou and C. Toumazou, "Semiconductor technology for early detection of DNA methylation for cancer: From concept to practice," *Sensors and Actuators B: Chemical*, vol. 178, pp. 572–580, 2013. [Online]. Available: http://linkinghub.elsevier.com/retrieve/pii/S0925400512013639

[129] J. Wang, "Electrochemical biosensors: Towards point-of-care cancer diagnostics," *Biosensors & Bioelectronics*, vol. 21, no. 10, pp. 1887–92, 2006. [Online]. Available: http://www.ncbi.nlm.nih.gov/pubmed/16330202

[130] J. Go, P. Nair, B. R. Jr, and B. Dorvel, "Coupled heterogeneous nanowire - nanoplate planar transistor sensors for giant ($>$ 10 V/pH) Nernst response," *ACS Nano*, vol. 6, no. 7, pp. 5972–5979, 2012. [Online]. Available: http://pubs.acs.org/doi/abs/10.1021/nn300874w

[131] O. Knopfmacher, A. Tarasov, W. Fu, M. Wipf, B. Niesen, M. Calame, and C. Schönenberger, "Nernst limit in dual-gated Si-nanowire FET sensors," *Nano Letters*, vol. 10, no. 6, pp. 2268–74, 2010. [Online]. Available: http://www.ncbi.nlm.nih.gov/pubmed/20499926

[132] M.-J. Spijkman, J. J. Brondijk, T. C. T. Geuns, E. C. P. Smits, T. Cramer, F. Zerbetto, P. Stoliar, F. Biscarini, P. W. M. Blom, and D. M. de Leeuw, "Dual-gate organic field-effect transistors as potentiometric sensors in aqueous solution," *Advanced Functional Materials*, vol. 20, no. 6, pp. 898–905, 2010. [Online]. Available: http://doi.wiley.com/10.1002/adfm.200901830

[133] B. Khamaisi, O. Vaknin, O. Shaya, and N. Ashkenasy, "Electrical performance of silicon-on-insulator field-effect transistors with multiple top-gate organic layers in electrolyte solution," *ACS Nano*, vol. 4, no. 8, pp. 4601–8, 2010. [Online]. Available: http://www.ncbi.nlm.nih.gov/pubmed/20731443

[134] H.-K. Lim and J. G. Fossum, "Threshold voltage of thin-film silicon-on-insulator," *IEEE Transactions*, vol. 30, no. 10, pp. 1244–1251, 1983. [Online]. Available: http://ieeexplore.ieee.org/stamp/stamp.jsp?arnumber=1483183

[135] J. Go, P. R. Nair, and M. A. Alam, "Theory of signal and noise in double-gated nanoscale electronic pH sensors," *Journal of Applied Physics*, vol. 112, no. 3, p. 34516, 2012. [Online]. Available: http://www.pubmedcentral.nih.gov/articlerender.fcgi?artid=3436503

[136] A. Tarasov, W. Fu, O. Knopfmacher, J. Brunner, M. Calame, and C. Schonenberger, "Signal-to-noise ratio in dual-gated silicon nanoribbon field-effect sensors," *Applied Physics Letters*, vol. 98, no. 1, p. 012114, 2011. [Online]. Available: http://scitation.aip.org/content/aip/journal/apl/98/1/10.1063/1.3536674

[137] Z. Gao, A. Agarwal, A. D. Trigg, N. Singh, C. Fang, C.-H. Tung, Y. Fan, K. D. Buddharaju, and J. Kong, "Silicon nanowire arrays for label-free detection of DNA," *Analytical Chemistry*, vol. 79, no. 9, pp. 3291–7, 2007. [Online]. Available: http://www.ncbi.nlm.nih.gov/pubmed/20563793

[138] N. K. Rajan, X. Duan, and M. A. Reed, "Performance limitations for nanowire/nanoribbon biosensors," *Wiley Interdisciplinary Reviews. Nanomedicine and Nanobiotechnology*, vol. 5, no. 6, pp. 629–45, 2013. [Online]. Available: http://www.ncbi.nlm.nih.gov/pubmed/23897672

[139] Y. Gu, T. Vu, and G. Li, "SOI material characterization using optical second harmonic generation," in *IEEE International SOI Conference*, no. 4, 1995. [Online]. Available: http://goo.gl/WhX5In pp. 94–95.

[140] A. Baldi, A. Bratov, R. Mas, and C. Dominguez, "Electrostatic discharge sensitivity tests for ISFET sensors," *Sensors and Actuators*

B: Chemical, vol. 80, no. 3, pp. 255–260, 2001. [Online]. Available: http://www.sciencedirect.com/science/article/pii/S0925400501009182

[141] Y. Liu, P. Georgiou, T. G. Constandinou, D. Garner, and C. Toumazou, "An auto-offset-removal circuit for chemical sensing based on the PG-ISFET," *2009 IEEE International Symposium on Circuits and Systems*, pp. 1165–1168, 2009. [Online]. Available: http://ieeexplore.ieee.org/lpdocs/epic03/wrapper.htm?arnumber=5117968

[142] C. Duarte, E. Salm, B. Dorvel, B. Reddy, and R. Bashir, "On-chip parallel detection of foodborne pathogens using loop-mediated isothermal amplification," *Biomedical microdevices*, vol. 15, no. 5, pp. 821–30, 2013. [Online]. Available: http://www.ncbi.nlm.nih.gov/pubmed/23620454

[143] Y. Liu, P. Georgiou, T. Prodromakis, T. G. Constandinou, and C. Toumazou, "An extended CMOS ISFET model incorporating the physical design geometry and the effects on performance and offset variation," *IEEE Transactions on Electron Devices*, vol. 58, no. 12, pp. 4414–4422, 2011. [Online]. Available: http://ieeexplore.ieee.org/stamp/stamp.jsp?arnumber=6058632

[144] N. K. Rajan, K. Brower, X. Duan, and M. A. Reed, "Limit of detection of field effect transistor biosensors: Effects of surface modification and size dependence," *Applied Physics Letters*, vol. 104, no. 8, p. 084106, 2014. [Online]. Available: http://scitation.aip.org/content/aip/journal/apl/104/8/10.1063/1.4867025

[145] G. M. Credo, X. Su, K. Wu, O. H. Elibol, D. J. Liu, B. Reddy, T.-W. Tsai, B. R. Dorvel, J. S. Daniels, R. Bashir, and M. Varma, "Label-free electrical detection of pyrophosphate generated from DNA polymerase reactions on field-effect devices," *Analyst*, vol. 137, no. 6, pp. 1351–62, 2012. [Online]. Available: http://www.pubmedcentral.nih.gov/articlerender.fcgi?artid=3367324

[146] J. B. Luchansky, C. S. Porto-Fett, B. A. Shoyer, J. Phillips, D. Eblen, P. Evans, and N. Bauer, "Thermal inactivation of a single strain each of serotype O26:H11, O45:H2, O103:H2, O104:H4, O111:H, O121:H19, O145:NM, and O157:H7 cells of Shiga toxin-producing Escherichia coli in wafers of ground beef," *Journal of Food Protection*, vol. 76, no. 8, pp. 1434–7, 2013. [Online]. Available: http://www.ncbi.nlm.nih.gov/pubmed/23905801

[147] K. K. Bradley, J. M. Williams, L. J. Burnsed, M. B. Lytle, M. D. McDermott, R. K. Mody, A. Bhattarai, S. Mallonee, E. W. Piercefield, C. K. McDonald-Hamm, and L. K. Smithee,

"Epidemiology of a large restaurant-associated outbreak of Shiga toxin-producing Escherichia coli O111:NM," *Epidemiology and Infection*, vol. 140, no. 9, pp. 1644–54, 2012. [Online]. Available: http://www.ncbi.nlm.nih.gov/pubmed/22117135

[148] E. W. Piercefield, K. K. Bradley, R. L. Coffman, and S. M. Mallonee, "Hemolytic uremic syndrome after an Escherichia coli O111 outbreak," *Archives of Internal Medicine*, vol. 170, no. 18, pp. 1656–1663, 2010. [Online]. Available: http://archinte.jamanetwork.com/article.aspx?articleid=226060

[149] I. Erill, S. Campoy, N. Erill, J. Barbé, and J. Aguiló, "Biochemical analysis and optimization of inhibition and adsorption phenomena in glasssilicon PCR-chips," *Sensors and Actuators B: Chemical*, vol. 96, no. 3, pp. 685–692, 2003. [Online]. Available: http://linkinghub.elsevier.com/retrieve/pii/S0925400503005227

[150] P. J. Asiello and A. J. Baeumner, "Miniaturized isothermal nucleic acid amplification, a review," *Lab on a Chip*, vol. 11, no. 8, pp. 1420–30, 2011. [Online]. Available: http://www.ncbi.nlm.nih.gov/pubmed/21387067

[151] F. B. Myers and L. P. Lee, "Innovations in optical microfluidic technologies for point-of-care diagnostics," *Lab on a Chip*, vol. 8, no. 12, pp. 2015–31, 2008. [Online]. Available: http://www.ncbi.nlm.nih.gov/pubmed/19023464

[152] Y.-H. Hsieh, M. T. Hogan, M. Barnes, M. Jett-Goheen, J. Huppert, A. M. Rompalo, and C. A. Gaydos, "Perceptions of an ideal point-of-care test for sexually transmitted infections–a qualitative study of focus group discussions with medical providers," *PloS One*, vol. 5, no. 11, p. e14144, 2010. [Online]. Available: http://www.pubmedcentral.nih.gov/articlerender.fcgi?artid=2994750

[153] S. Sze and K. Ng, "Sensors," in *Physics of Semiconductor Devices,*. John Wiley & Sons, Inc.,, 2006, ch. 14, pp. 743–769. [Online]. Available: http://www.wiley.com/WileyCDA/WileyTitle/productCd-0471143235.html

[154] A. Michalska, "All-solid-state ion selective and all-solid-state reference electrodes," *Electroanalysis*, vol. 24, no. 6, pp. 1253–1265, 2012. [Online]. Available: http://doi.wiley.com/10.1002/elan.201200059

[155] I.-Y. Huang and R.-S. Huang, "Fabrication and characterization of a new planar solid-state reference electrode for ISFET sensors," *Thin Solid Films*, vol. 406, no. 1-2, pp. 255–261, 2002. [Online]. Available: http://linkinghub.elsevier.com/retrieve/pii/S0040609001017837

[156] M. W. Shinwari, D. Zhitomirsky, I. A. Deen, P. R. Selvaganapathy, M. J. Deen, and D. Landheer, "Microfabricated reference electrodes and their biosensing applications," *Sensors*, vol. 10, no. 3, pp. 1679–715, 2010. [Online]. Available: http://www.mdpi.com/1424-8220/10/3/1679

[157] I.-Y. Huang, S.-H. Wang, C.-C. Chu, and C.-T. Chiu, "Improved solid-state planar Ti/Pd/ag/AgCl/KCl-gel microreference electrode by silicon cap sealing package," *Journal of Micro/Nanolithography, MEMS, and MOEMS*, vol. 8, no. 3, p. 033050, 2009. [Online]. Available: http://nanolithography.spiedigitallibrary.org/article.aspx?doi=10.1117/1.3196547

[158] B. J. Polk, A. Stelzenmuller, G. Mijares, W. MacCrehan, and M. Gaitan, "Ag/AgCl microelectrodes with improved stability for microfluidics," *Sensors and Actuators B: Chemical*, vol. 114, no. 1, pp. 239–247, 2006. [Online]. Available: http://linkinghub.elsevier.com/retrieve/pii/S0925400505004612

[159] E. S. McLamore, J. Shi, D. Jaroch, J. C. Claussen, A. Uchida, Y. Jiang, W. Zhang, S. S. Donkin, M. K. Banks, K. K. Buhman, D. Teegarden, J. L. Rickus, and D. M. Porterfield, "A self referencing platinum nanoparticle decorated enzyme-based microbiosensor for real time measurement of physiological glucose transport," *Biosensors & Bioelectronics*, vol. 26, no. 5, pp. 2237–45, 2011. [Online]. Available: http://goo.gl/wf7Zux

[160] J. Noh, S. Park, H. Boo, H. C. Kim, and T. D. Chung, "Nanoporous platinum solid-state reference electrode with layer-by-layer polyelectrolyte junction for pH sensing chip," *Lab on a Chip*, vol. 11, no. 4, pp. 664–71, 2011. [Online]. Available: http://www.ncbi.nlm.nih.gov/pubmed/21135953

[161] G. Inzelt, "Pseudo-reference electrodes," in *Handbook of Reference Electrodes*, G. Inzelt, A. Lewenstam, and F. Scholz, Eds. Berlin, Heidelberg: Springer Berlin Heidelberg, 2013, ch. 14, pp. 331–332. [Online]. Available: http://link.springer.com/10.1007/978-3-642-36188-3

[162] D.-S. Lee, S. H. Park, H. Yang, K.-H. Chung, T. H. Yoon, S.-J. Kim, K. Kim, and Y. T. Kim, "Bulk-micromachined submicroliter-volume PCR chip with very rapid thermal response and low power consumption," *Lab on a Chip*, vol. 4, no. 4, pp. 401–7, 2004. [Online]. Available: http://www.ncbi.nlm.nih.gov/pubmed/15269812

[163] E. Salm, Y. Zhong, B. Reddy Jr, C. Duarte-Guevara, V. Swaminathan, Y.-S. Liu, and R. Bashir, "Electrical detection of nucleic acid

amplification using an on-chip quasi-reference electrode and a PVC REFET," *Analytical Chemistry*, vol. 86, pp. 6968–6975, 2014. [Online]. Available: http://pubs.acs.org/doi/abs/10.1021/ac500897t

[164] J. Ghilane, P. Hapiot, and A. J. Bard, "Metal/polypyrrole quasi-reference electrode for voltammetry in nonaqueous and aqueous solutions," *Analytical Chemistry*, vol. 78, no. 19, pp. 6868–72, 2006. [Online]. Available: http://www.ncbi.nlm.nih.gov/pubmed/17007508

[165] Y. Yoshida, S. Yamaguchi, and K. Maeda, "Conducting polymer-coated electrode as a reference/counter electrode in an organic phase and its application to a two-electrode type thin-layer cell for voltammetry at the liquid / liquid Interface," *Analytical Sciences*, vol. 26, no. 2, pp. 137–139, 2010. [Online]. Available: http://joi.jlc.jst.go.jp/JST.JSTAGE/analsci/26.137?from=CrossRef

[166] D. Zhan, F.-R. Fan, and A. J. Bard, "The Kv channel blocker 4-aminopyridine enhances Ag+ uptake: a scanning electrochemical microscopy study of single living cells," *Proceedings of the National Academy of Sciences*, vol. 105, no. 34, pp. 12 118–22, 2008. [Online]. Available: http://www.pnas.org/content/105/34/12118.long

[167] L. E. Barrosse-Antle, A. M. Bond, R. G. Compton, A. M. O'Mahony, E. I. Rogers, and D. S. Silvester, "Voltammetry in room temperature ionic liquids: Comparisons and contrasts with conventional electrochemical solvents," *Chemistry - An Asian Journal*, vol. 5, pp. 202–230, 2010. [Online]. Available: http://onlinelibrary.wiley.com/doi/10.1002/asia.200900191/full

[168] B. Dorvel, B. Reddy, I. Block, P. Mathias, S. E. Clare, B. Cunningham, D. E. Bergstrom, and R. Bashir, "Vapor-phase deposition of monofunctional alkoxysilanes for sub-nanometer-level biointerfacing on silicon oxide surfaces," *Advanced Functional Materials*, vol. 20, no. 1, pp. 87–95, 2010. [Online]. Available: http://doi.wiley.com/10.1002/adfm.200901688

[169] C.-S. Lai, C.-M. Yang, and T.-F. Lu, "pH sensitivity improvement on 8 nm thick hafnium oxide by post deposition annealing," *Electrochemical and Solid-State Letters*, vol. 9, p. G90, 2006. [Online]. Available: http://esl.ecsdl.org/content/9/3/G90/F3.expansion.html

[170] K. A. Yusof, S. H. Herman, and W. F. H. Abdullah, "TiO 2 -based extended gate FET pH-sensor : Effect of annealing temperature on its sensitivity , hysteresis and stability," in *IEEE International Conference on Semiconductor Electronics (ICSE)*, 2014. [Online]. Available: http://ieeexplore.ieee.org/xpls/icp.jsp?arnumber=6920905 pp. 491–494.

[171] A. Ortiz-Conde, F. Garca Sánchez, J. Liou, A. Cerdeira, M. Estrada, and Y. Yue, "A review of recent MOSFET threshold voltage extraction methods," *Microelectronics Reliability*, vol. 42, no. 4-5, pp. 583–596, 2002. [Online]. Available: http://linkinghub.elsevier.com/retrieve/pii/S0026271402000276

[172] M. Zhou, M. Pagels, B. Geschke, and J. Heinze, "Electropolymerization of pyrrole and electrochemical study of polypyrrole. 5. Controlled electrochemical synthesis and solid-state transition of well-defined polypyrrole variants," *The Journal of Physical Chemistry B*, vol. 106, no. 39, pp. 10 065–10 073, 2002. [Online]. Available: http://pubs.acs.org/doi/abs/10.1021/jp0210778

[173] D. Quéré, "Wetting and roughness," *Annual Review of Materials Research*, vol. 38, no. 1, pp. 71–99, 2008. [Online]. Available: http://goo.gl/b0qKq2

[174] H. Suzuki, H. Ozawa, S. Sasaki, and I. Karube, "A novel thin-film Ag/AgCl anode structure for microfabricated Clark-type oxygen electrodes," *Sensors and Actuators B: Chemical*, vol. 53, no. 3, pp. 140–146, 1998. [Online]. Available: http://linkinghub.elsevier.com/retrieve/pii/S092540059900009X

[175] Y. Ma, S. Jiang, G. Jian, H. Tao, L. Yu, X. Wang, X. Wang, J. Zhu, Z. Hu, and Y. Chen, "CNx nanofibers converted from polypyrrole nanowires as platinum support for methanol oxidation," *Energy & Environmental Science*, vol. 2, p. 224, 2009.

[176] C. Duarte-Guevara, F.-L. Lai, C.-W. Cheng, B. Reddy, E. Salm, V. Swaminathan, Y.-K. Tsui, H. C. Tuan, A. Kalnitsky, Y.-S. Liu, and R. Bashir, "Enhanced biosensing resolution with foundry fabricated individually addressable dual-gated ISFETs," *Analytical Chemistry*, vol. 86, no. 16, pp. 8359–67, 2014. [Online]. Available: http://www.ncbi.nlm.nih.gov/pubmed/25072939

[177] X. Duan, Y. Li, N. K. Rajan, D. A. Routenberg, Y. Modis, and M. A. Reed, "Quantification of the affinities and kinetics of protein interactions using silicon nanowire biosensors," *Nature Nanotechnology*, vol. 7, no. 6, pp. 401–7, 2012. [Online]. Available: http://www.ncbi.nlm.nih.gov/pubmed/22635097

[178] S. J. Slattery, J. K. Blaho, J. Lehnes, and K. A. Goldsby, "pH-Dependent metal-based redox couples as models for proton-coupled electron transfer reactions," *Coordination Chemistry Reviews*, vol. 174, no. 1, pp. 391–416, jul 1998. [Online]. Available: http://linkinghub.elsevier.com/retrieve/pii/S001085459800143X

[179] A. Fog and R. P. Buck, "Electronic semiconducting oxides as pH sensors," *Sensors and Actuators*, vol. 5, no. 2, pp. 137–146, 1984. [Online]. Available: http://linkinghub.elsevier.com/retrieve/pii/0250687484800049

[180] L. Nyholm, "Electrochemical techniques for lab-on-a-chip applications," *Analyst*, vol. 130, no. 5, p. 599, 2005. [Online]. Available: http://xlink.rsc.org/?DOI=b415004j

[181] D. E. Tallman, C. Vang, G. G. Wallace, and G. P. Bierwagen, "Direct electrodeposition of polypyrrole on aluminum and aluminum alloy by electron transfer mediation," *Journal of the Electrochemical Society*, vol. 149, no. 3, p. C173, 2002. [Online]. Available: http://jes.ecsdl.org/cgi/doi/10.1149/1.1448820

[182] Y. Nishi, T. Sonehara, A. Hokazono, S. Kawanaka, S. Inaba, and A. Kinoshita, "Palladium incorporated nickel silicide for a cost effective alternative salicide technology for scaled CMOS," in *Proceedings of 2010 International Symposium on VLSI Technology, System and Application*, vol. 15. IEEE, 2010. [Online]. Available: http://ieeexplore.ieee.org/lpdocs/epic03/wrapper.htm?arnumber=5488921 pp. 120–121.

[183] B. Imbert, R. Pantel, S. Zoll, M. Gregoire, R. Beneyton, S. D. Medico, and O. Thomas, "Nickel silicide encroachment formation and characterization," *Microelectronic Engineering*, vol. 87, no. 3, pp. 245–248, 2010. [Online]. Available: http://linkinghub.elsevier.com/retrieve/pii/S0167931709004584

[184] E. De Giglio, M. Guascito, L. Sabbatini, and G. Zambonin, "Electropolymerization of pyrrole on titanium substrates for the future development of new biocompatible surfaces," *Biomaterials*, vol. 22, no. 19, pp. 2609–2616, oct 2001. [Online]. Available: http://linkinghub.elsevier.com/retrieve/pii/S014296120000449X

[185] Y. Liu, Z. Liu, N. Lu, E. Preiss, S. Poyraz, M. J. Kim, and X. Zhang, "Facile synthesis of polypyrrole coated copper nanowires: a new concept to engineered core-shell structures," *Chemical Communications*, vol. 48, no. 20, pp. 2621–3, 2012. [Online]. Available: http://www.ncbi.nlm.nih.gov/pubmed/22294152

[186] W.-Y. Chung, C.-H. Yang, D. Pijanowska, A. Krzyskow, and W. Torbicz, "ISFET interface circuit embedded with noise rejection capability," *Electronics Letters*, vol. 40, no. 18, p. 1115, 2004. [Online]. Available: http://ieeexplore.ieee.org/stamp/stamp.jsp?arnumber=1335005

[187] C. Laborde, F. Pittino, H. A. Verhoeven, S. G. Lemay, L. Selmi, M. A. Jongsma, and F. P. Widdershoven, "Real-time imaging of

microparticles and living cells with CMOS nanocapacitor arrays," *Nature Nanotechnology*, vol. 10, no. 9, pp. 791–795, 2015. [Online]. Available: http://www.nature.com/doifinder/10.1038/nnano.2015.163

[188] Y. Chen, C. C. Wong, T. S. Pui, R. Nadipalli, R. Weerasekera, J. Chandran, H. Yu, and A. R. Rahman, "CMOS high density electrical impedance biosensor array for tumor cell detection," *Sensors and Actuators, B: Chemical*, vol. 173, no. 2012, pp. 903–907, 2012. [Online]. Available: http://dx.doi.org/10.1016/j.snb.2012.07.024

[189] G. Nabovati, E. Ghafar-Zadeh, and M. Sawan, "A 64 pixel ISFET-based biosensor for extracellular pH gradient monitoring," in *Circuits and Systems (ISCAS), 2015*. IEEE, 2015. [Online]. Available: http://ieeexplore.ieee.org/xpls/icp.jsp?arnumber=7168995 pp. 1762–1765.

[190] T. Chen, C. Wen, J. Huang, Y. Peng, S. Liu, S. Su, L. Cheng, H. Lai, F. Lai, C. Cheng, C. Yang, J. Yang, Y. Hsieh, E. Salm, B. Reddy, F. Tsui, R. Bashir, and M. Chen, "A semiconductor bio-electrical platform with addressable thermal control circuits for accelerated bioassay development," in *Electron Devices Meeting (IEDM)*, 2014. [Online]. Available: http://ieeexplore.ieee.org/stamp/stamp.jsp?arnumber=7047058 pp. 390–393.

[191] S. Ingebrandt, "Bioelectronics: Sensing beyond the limit," *Nature Nanotechnology*, vol. 10, no. 9, pp. 734–735, 2015. [Online]. Available: http://www.nature.com/doifinder/10.1038/nnano.2015.199

[192] A. Bandiziol, P. Palestri, F. Pittino, D. Esseni, L. Selmi, and A. E. Model, "A TCAD-based methodology to model the site-binding charge at ISFET / electrolyte interfaces," *IEEE Transactions*, vol. 62, no. 10, pp. 3379–3386, 2015. [Online]. Available: http://ieeexplore.ieee.org/xpls/icp.jsp?arnumber=7202896

[193] C. Duarte-Guevara, V. V. Swaminathan, M. Burgess, B. Reddy, E. Salm, Y.-S. Liu, J. Rodriguez-Lopez, and R. Bashir, "On-chip metal/polypyrrole quasi-reference electrodes for robust ISFET operation," *Analyst*, vol. 140, no. 10, pp. 3630–3641, 2015. [Online]. Available: http://xlink.rsc.org/?DOI=C5AN00085H

[194] J. Go, P. R. Nair, B. Reddy, B. Dorvel, R. Bashir, and M. A. Alam, "Beating the Nernst limit of 59mV/pH with double-gated nano-scale field-effect transistors and its applications to ultra-sensitive DNA biosensors," *Technical Digest - International Electron Devices Meeting, IEDM*, vol. 2, pp. 202–205, 2010. [Online]. Available: http://ieeexplore.ieee.org/xpls/icp.jsp?arnumber=5703325

[195] P. De Boe and J.-C. Golinval, "Principal component analysis of a piezosensor array for damage localization," *Structural Health Monitoring*, vol. 2, no. 2, pp. 137–144, 2003. [Online]. Available: http://shm.sagepub.com/content/2/2/137.full.pdf

[196] R. G. Baraniuk, "Compressive sensing," *IEEE Signal Processing Magazine*, vol. 24, no. 4, p. 015023, 2007.

[197] M. Zhang, "Compressive acquisition CMOS image sensor: From algorithm to hardware implementation," *IEEE transactions on Very Large Scale Integration*, vol. 18, no. 3, p. 171, 2010. [Online]. Available: http://search.proquest.com/docview/1512627557?accountid=43623

[198] M. Ni, J. R. Stetter, and W. J. Buttner, "Orthogonal gas sensor arrays with intelligent algorithms for early warning of electrical fires," *Sensors and Actuators B: Chemical*, vol. 130, no. 2, pp. 889–899, 2008. [Online]. Available: http://linkinghub.elsevier.com/retrieve/pii/S0925400507009069

[199] J. L. Chiang, S. S. Jan, J. C. Chou, and Y. C. Chen, "Study on the temperature effect, hysteresis and drift of pH-ISFET devices based on amorphous tungsten oxide," *Sensors and Actuators, B: Chemical*, vol. 76, no. 1-3, pp. 624–628, 2001.

[200] S. Jamasb, "An analytical technique for counteracting drift in ion-selective field effect transistors (ISFETs)," *IEEE Sensors Journal*, vol. 4, no. 6, pp. 795–801, 2004. [Online]. Available: http://ieeexplore.ieee.org/xpls/icp.jsp?arnumber=1359841

[201] D. Y. Chen and P. K. Chan, "An intelligent ISFET sensory system with temperature and drift compensation for long-term monitoring," *IEEE Sensors Journal*, vol. 8, no. 12, pp. 1948–1959, 2008. [Online]. Available: http://ieeexplore.ieee.org/stamp/stamp.jsp?arnumber=4670986

[202] D.-H. Kwon, B.-W. Cho, C.-S. Kim, and B.-K. Sohn, "Effects of heat treatment on Ta2O5 sensing membrane for low drift and high sensitivity pH-ISFET," *Sensors and Actuators B: Chemical*, vol. 34, no. 1-3, pp. 441–445, 1996. [Online]. Available: http://www.sciencedirect.com/science/article/pii/S0925400596019387

[203] J. R. Castle, A. Pitts, K. Hanavan, R. Muhly, J. El Youssef, C. Hughes-Karvetski, B. Kovatchev, and W. K. Ward, "The accuracy benefit of multiple amperometric glucose sensors in people with type 1 diabetes," *Diabetes Care*, vol. 35, no. 4, pp. 706–10, 2012. [Online]. Available: http://care.diabetesjournals.org/content/35/4/706.long

[204] V. J. Hodge and J. Austin, "A survey of outlier detection methodoligies," *Artificial Intelligence Review*, vol. 22, no. 1969, pp. 85–126, 2004. [Online]. Available: http://link.springer.com/article/10.1007/s10462-004-4304-y

[205] N. Meratnia and P. Havinga, "Outlier detection techniques for wireless sensor networks: A survey," *IEEE Communications Surveys & Tutorials*, vol. 12, no. 2, pp. 159–170, 2010. [Online]. Available: http://ieeexplore.ieee.org/lpdocs/epic03/wrapper.htm?arnumber=5451757

[206] C. A. Mack, "Fifty years of Moore's law," *IEEE Transactions on Semiconductor Manufacturing*, vol. 24, no. 2, pp. 202–207, 2011. [Online]. Available: http://ieeexplore.ieee.org/xpls/icp.jsp?arnumber=5696765

[207] K.-I. Chen, B.-R. Li, and Y.-T. Chen, "Silicon nanowire field-effect transistor-based biosensors for biomedical diagnosis and cellular recording investigation," *Nano Today*, vol. 6, no. 2, pp. 131–154, apr 2011. [Online]. Available: http://linkinghub.elsevier.com/retrieve/pii/S1748013211000168

[208] M. Kalofonou, P. Georgiou, C. P. Ou, and C. Toumazou, "An ISFET based translinear sensor for DNA methylation detection," *Sensors and Actuators, B: Chemical*, vol. 161, no. 1, pp. 156–162, 2012. [Online]. Available: http://dx.doi.org/10.1016/j.snb.2011.09.089

[209] W. Sant, P. Temple-Boyer, J. Launay, and A. Martinez, "On-line monitoring of urea using enzymatic field effect transistors," *Sensors and Actuators B: Chemical*, vol. 160, no. 1, pp. 59–64, 2011. [Online]. Available: http://linkinghub.elsevier.com/retrieve/pii/S092540051100654X

[210] M. L. Pourciel-Gouzy, S. Assié-Souleille, L. Mazenq, J. Launay, and P. Temple-Boyer, "pH-ChemFET-based analysis devices for the bacterial activity monitoring," *Sensors and Actuators, B: Chemical*, vol. 134, no. 1, pp. 339–344, 2008. [Online]. Available: http://www.sciencedirect.com/science/article/pii/S092540050800289X

[211] A. Kauffmann and W. Huber, "Microarray data quality control improves the detection of differentially expressed genes," *Genomics*, vol. 95, no. 3, pp. 138–142, 2010. [Online]. Available: http://dx.doi.org/10.1016/j.ygeno.2010.01.003

[212] D. J. Cook, "Making sense of sensor data," *Pervasive Computing, IEEE*, vol. 6, no. 2, pp. 105–108, 2007. [Online]. Available: http://goo.gl/3q0T86

[213] M.-J. Spijkman, K. Myny, E. C. P. Smits, P. Heremans, P. W. M. Blom, and D. M. de Leeuw, "Dual-gate thin-film transistors, integrated circuits and sensors," *Advanced materials*, vol. 23, no. 29, pp. 3231–42, 2011. [Online]. Available: http://www.ncbi.nlm.nih.gov/pubmed/21671446

[214] P. Kainz, "The PCR plateau phase - towards an understanding of its limitations," *Biochimica et Biophysica Acta*, vol. 1494, no. 1-2, pp. 23–27, 2000. [Online]. Available: http://www.sciencedirect.com/science/article/pii/S0167478100002001

[215] K. Nagamine, K. Watanabe, K. Ohtsuka, T. Hase, and T. Notomi, "Loop-mediated isothermal amplification reaction using a nondenatured template," *Clinical Chemistry*, vol. 47, no. 9, pp. 1742–1743, 2001. [Online]. Available: http://www.clinchem.org/content/47/9/1742.full

[216] C. Sandalli, K. Singh, M. J. Modak, A. Ketkar, S. Canakci, I. Demir, and A. O. Belduz, "A new DNA polymerase I from Geobacillus caldoxylosilyticus TK4: Cloning, characterization, and mutational analysis of two aromatic residues," *Applied Microbiology and Biotechnology*, vol. 84, pp. 105–17, 2009. [Online]. Available: http://www.ncbi.nlm.nih.gov/pubmed/19365630

[217] R. Kodzius, K. Xiao, J. Wu, X. Yi, X. Gong, I. G. Foulds, and W. Wen, "Inhibitory effect of common microfluidic materials on PCR outcome," *Sensors and Actuators B: Chemical*, vol. 161, no. 1, pp. 349–358, 2012. [Online]. Available: http://linkinghub.elsevier.com/retrieve/pii/S0925400511009361

[218] G. L. Damhorst, C. Duarte-Guevara, W. Chen, T. Ghonge, B. T. Cunningham, and R. Bashir, "Smartphone-imaged HIV-1 reverse transcription loop-mediated isothermal amplification (RT-LAMP) on a chip from whole blood," *Engineering*, vol. 1, no. 3, pp. 324–335, 2015. [Online]. Available: http://engineering.org.cn/EN/10.15302/J-ENG-2015072

[219] H. B. Vibbert, S. Ku, X. Li, X. Liu, E. Ximenes, T. Kreke, M. R. Ladisch, A. J. Deering, and A. G. Gehring, "Accelerating sample preparation through enzyme-assisted microfiltration of Salmonella in chicken extract," *Biotechnology Progress*, pp. 1–12, 2015. [Online]. Available: http://doi.wiley.com/10.1002/btpr.2167

[220] M. A. Quail, M. Smith, P. Coupland, T. D. Otto, S. R. Harris, T. R. Connor, A. Bertoni, H. P. Swerdlow, and Y. Gu, "A tale of three next generation sequencing platforms: comparison of Ion Torrent,

Pacific Biosciences and Illumina MiSeq sequencers," *BMC Genomics*, vol. 13, no. 1, p. 341, 2012. [Online]. Available: http://bmcgenomics.biomedcentral.com/articles/10.1186/1471-2164-13-341

[221] G. López-Campos, J. V. Martínez-Suárez, M. Aguado-Urda, and V. López-Alonso, "DNA microarrays: Principles and technologies," in *Microarray Detection and Characterization of Bacterial Foodborne Pathogens*, 2012, pp. 33–47. [Online]. Available: http://link.springer.com/10.1007/978-1-4614-3250-0

[222] C. Zhang and D. Xing, "Miniaturized PCR chips for nucleic acid amplification and analysis: latest advances and future trends," *Nucleic Acids Research*, vol. 35, no. 13, pp. 4223–37, 2007. [Online]. Available: http://nar.oxfordjournals.org/content/35/13/4223.long

[223] D. E. Cohen, T. Schneider, M. Wang, and D. T. Chiu, "Self-digitization of sample volumes," *Analytical Chemistry*, vol. 82, no. 13, pp. 5707–5717, 2010. [Online]. Available: http://pubs.acs.org/doi/abs/10.1021/ac100713u

[224] M. Baker, "Digital PCR hits its stride," *Nature Methods*, vol. 9, no. 6, pp. 541–544, 2012. [Online]. Available: http://www.nature.com/doifinder/10.1038/nmeth.2027

[225] P. T. Desai, M. K. Walsh, and B. C. Weimer, "Solid-phase capture of pathogenic bacteria by using gangliosides and detection with real-time PCR," *Applied and Environmental Microbiology*, vol. 74, no. 7, pp. 2254–8, 2008. [Online]. Available: http://aem.asm.org/content/74/7/2254.long

[226] J. Bruno, "Application of DNA aptamers and quantum dots to lateral flow test strips for detection of foodborne pathogens with improved sensitivity versus colloidal gold," *Pathogens*, vol. 3, no. 2, pp. 341–355, 2014. [Online]. Available: http://www.mdpi.com/2076-0817/3/2/341/

[227] K. A. Curtis, D. L. Rudolph, and S. M. Owen, "Rapid detection of HIV-1 by reverse-transcription, loop-mediated isothermal amplification (RT-LAMP)," *Journal of Virological Methods*, vol. 151, no. 2, pp. 264–70, 2008. [Online]. Available: http://www.ncbi.nlm.nih.gov/pubmed/18524393